On the mathematical modeling of structurally complex polymerization systems: which modeling approach for what type of application?

Dimitrios Meimaroglou

On the mathematical modeling of structurally complex polymerization systems: which modeling approach for what type of application?

A Dissertation

by

Dimitrios Meimaroglou

Submitted to the University of Lorraine
in view of obtaining the authorization to

direct and supervise research

(HDR: Habilitation à Diriger les Recherches)

Members of the committee

Reviewers:	
Dr. Timothy McKENNA	Directeur de Recherche, CNRS, Lyon
Dr. Serge REBOUILLAT	IP & Innovation Strategist, DuPont, Geneva (CH)
Prof. Juan MARTINEZ VEGA	Professeur, Université Paul Sabatier, Toulouse
Examiners:	
Dr. Halima ALEM-MARCHAND	Maître des Conférences, Université de Lorraine, Nancy
Prof. Sophie DUQUESNE	Professeur, Université de Lille
Prof. Guo-Hua HU (sc. supervisor)	Professeur, Université de Lorraine, Nancy
Dr. Apostolos KRALLIS	Vice President, Innovation Centre, Borouge Pte
Dr. Nida SHEIBAT – OTHMAN	Directrice de Recherche, CNRS, Lyon
Invited:	
Prof. Costas KIPARISSIDES	Professor Emeritus, Aristotle University, Thessaloniki (GR)

Defense Date: July 5, 2021

Abstract

The present dissertation presents a synthesis of my research developments, in the field of mathematical modeling of polymerization systems, in view of obtaining the authorization of the University of Lorraine to autonomously direct and supervise scientific research. The presented work extends over a period of 17 years, starting from the early stages of my career in Greece and reaching until the latest developments, carried out in the Laboratory of Reactions and Process Engineering (LRGP) in Nancy. Throughout the chapters of this manuscript, several case studies are exposed in an attempt to illustrate different key-issues, related with the development of mathematical models for physicochemical systems. These issues, concern the selection of the most suitable modeling approach, in terms of both the specificities of the problem under study and the characteristics of the different modeling techniques. In this sense, the 'dilemma' between knowledge-based or data-driven modeling approaches, as well as that between stochastic and deterministic techniques, are directly addressed and analyzed through multiple viewpoints. At the same time, and in parallel to the technical modeling aspects, specific attention is also payed to the nature and the challenges posed by different systems. Finally, the guideline adopted throughout the presentation of these developments is extended to provide a projection towards future perspectives, capitalizing on previously acquired knowledge and opening towards new techniques and approaches.

Résumé Etendu [1]

Ce manuscrit présente un résumé de mes travaux de recherche, en vue de l'obtention de l'habilitation à diriger les recherches. La période de référence couvre les dernières 17 années écoulées et concerne les travaux que j'ai effectués d'abord en Grèce, avant mon arrivée en France puis, au sein du Laboratoire Réactions et Génie des Procédés (LRGP) de Nancy depuis 2010. Pendant la première période, j'ai pu acquérir des bases solides sur la modélisation de procédés de polymérisation, à travers une série d'applications sur différents systèmes. Ces bases m'ont ensuite permis, d'une part, de mettre en œvre, et d'étendre vers d'autres problématiques, des techniques de modélisation ainsi maîtrisées et, d'autre part, d'effectuer une ouverture vers de nouvelles techniques et des approches différentes. Ce manuscrit présente donc ce parcours, par le biais de plusieurs cas d'études, ainsi que la ligne directrice des travaux que je souhaite développer au cours des années à venir.

Les activités de recherche effectuées pendant la première partie de ce parcours ont donc principalement concerné la modélisation des procédés de polymérisation. Plus spécifiquement, il s'est agi de construire des modèles mathématiques, en grande partie basés sur l'application de techniques de modélisations phénoménologiques, à la fois déterministes et stochastiques, pour des systèmes et des applications variées, telles que les procédés industriels de synthèse de polymères, de copolymères et de biopolymères. L'objectif commun à ces travaux a été la description du comportement de ces systèmes, ainsi que la prédiction de l'évolution des différentes propriétés des chaînes macromoléculaires produites, en fonction des conditions opératoires de leur synthèse. La prédiction de ces propriétés vise à établir des relations entre les paramètres du procédé et certaines propriétés des produits obtenus, telles que leur comportement rhéologique, mécanique, thermique,

[1] An extended summary in French is required by the University of Lorraine for all dissertations written in a foreign language.

etc. Par conséquent, il est ainsi possible d'envisager à la fois le contrôle optimal des caractéristiques des produits synthétisés ainsi que la conception et la fabrication de produits à propriétés ciblées, et cela, dans le cadre de la maîtrise des relations entre la structure, les procédés et les propriétés.

Les produits qui présentent la plus grande polyvalence sont ceux dont la microstructure moléculaire est très complexe. C'est, en particulier, le cas des polymères et copolymères ramifiés ainsi que des polymères et des biopolymères multifonctionnels (polyesters, polysaccharides, etc.), dont la modélisation des caractéristiques macromoléculaires, voire de la topologie de la microstructure, n'est pas une tâche simple car elle implique la gestion d'une très grande dimensionnalité, au sens d'un nombre important de propriétés qui doivent être suivies en parallèle. Ceci, sous un formalisme de bilans de population, conduit à des bilans dits multidimensionnels.

Devant la multitude d'approches qui sont proposées dans la littérature pour la modélisation de systèmes de polymérisation, le chercheur se trouve souvent en plein dilemme. Le choix de l'approche la mieux adaptée au système étudié dépend typiquement de plusieurs paramètres, dont notamment la nature du système et l'état actuel de sa connaissance. Par ailleurs, le niveau de détail envisagé, concernant les propriétés ciblées, les ressources disponibles et la maîtrise des différentes techniques qui se présentent comme solutions éventuelles pour la modélisation du système, sont également des paramètres qui doivent influencer cette décision. Il existe des nombreuses catégories selon lesquelles on peut classer les approches de modélisation. Chacune d'elles présente ses propres avantages et inconvénients, jouant ainsi un rôle décisif dans le choix décrit précédemment. Un telle classification permet de distinguer les modèles phénoménologiques et les modèles basés sur les données (ou empiriques). Dans la première catégorie on trouve les modèles qui visent à décrire les phénomènes produits dans le système, en utilisant des lois physiques. En revanche, les modèles dont le but est simplement de construire, sur la base des données disponibles, une expression mathématique, capable à créer une liaison entre les entrées (par exemple, les conditions expérimentales du procédé) et les sorties (par exemple, les propriétés calculées) du système, sans pour autant que cette expression ait un rapport quelconque avec les mécanismes dirigeant le procédé, font partie de

la deuxième catégorie des modèles basés sur les données.

Une autre classification des modèles mathématiques est celle qui distingue les modèles déterministes et stochastiques. Dans la première catégorie se situent typiquement les modèles classiques du génie des procédés, qui comportent des systèmes d'équations différentielles ou algébriques, et qui définissent de façon explicite la(es) sortie(s) du système par rapport à ses entrées. Les modèles stochastiques, contrairement à la première catégorie, se basent sur la génération de nombres aléatoires afin de décrire la transition d'états consécutifs en fonction de probabilités de transition. De ce fait, la(e)s sorties du système est(sont) liée(s) à ses entrées par le biais d'une distribution de probabilités.

Ce manuscrit tente d'adresser et de répondre au dilemme présenté précédemment pour choisir l'approche de modélisation la mieux adaptée à la problématique étudiée, en s'appuyant principalement sur ces deux types de classification des modèles. Ainsi, à travers les différentes applications et études de cas qui seront exposées, les forces et les faiblesses des approches adoptées seront démontrées. Dans ce cadre, les études présentées contiennent aussi bien des cas où le choix d'une approche est plutôt imposée par la nature du système et le niveau de détail dans les propriétés calculées, ainsi que des cas où un choix, voire une combinaison des approches fondamentalement différentes, est envisageable. La structure du manuscrit se décline en cinq chapitres, dont trois dédiés à la présentation des différents développements. Ainsi, suite à un premier chapitre d'introduction générale du sujet et des problématiques traitées, les chapitres 2, 3 et 4 sont dédiés à la présentation de différentes études de cas. En même temps, chacun de ces chapitres est focalisé sur un point de vue différent, en liaison avec le dilemme présenté précédemment. Enfin, le dernier chapitre propose une synthèse des travaux présentés et une projection vers le futur.

Plus précisément, le chapitre 2 se focalise sur le choix entre des approches de modélisation déterministes et stochastiques. Dans ce cadre, l'accent est placé sur des développements de modèles pour des systèmes de polymérisation complexes, en utilisant principalement la méthode stochastique de Monte Carlo (MC). Il s'agit d'une approche de modélisation qui offre l'avantage d'une gestion plus efficace des problèmes qui sont caractérisés par une grande dimensionnalité

(du fait que le nombre de propriétés qui doivent être suivies est élevé). Ainsi, dans le cas, par exemple, d'un procédé de synthèse d'un polymère ramifié, il est nécessaire de suivre l'évolution, non seulement de la taille des chaînes de polymère, afin de pouvoir suivre l'évolution de la distribution des masses molaires, mais également du nombre de ramifications, à la fois longues et courtes (selon la nature du système), afin de pouvoir décrire les développements au niveau de la distribution de ces ramifications. Ceci est important car les comportements mécanique, thermique et rhéologique d'un polymère ne sont pas seulement affectés par sa masse molaire, mais aussi par sa nature linéaire ou ramifiée. En plus, dans le dernier cas d'un polymère non-linéaire, la structure des ramifications (ex., sous forme de peigne, étoile, etc.) affecte également ces propriétés d'usage. De la même façon, les fonctionnalités d'un copolymère ne dépendra pas seulement de la nature de ces co-monomères constitutifs, mais aussi de leur séquence relative au sein de chaînes macromoléculaires.

Ces systèmes sont des exemples typiques de problèmes de modélisation de dimensionnalité élevée, pour lesquels il est nécessaire de mettre en œuvre des approches de modélisation avancées, comme la méthode stochastique de MC, ou comme des techniques déterministes qui se basent sur la discrétisation du domaine d'étude et sur la transformation du système d'équations différentielles par de méthodes numériques poussées. Malgré le fait que ces deux approches ont été excessivement testées sur différentes applications, pendant toutes ces dernières années, la méthode de MC a été plus employée à cause du nombre des qualités qu'elle présente par rapport aux méthodes déterministes. Notamment, le fait que la méthode de MC s'adapte parfaitement au caractère inhérent stochastique des procédés de polymérisation étudiés, ainsi qu'à sa capacité de gérer une dimensionnalité accrue sans augmenter la complexité de la formulation mathématique du modèle, rendent cette approche très attractive pour ce type de problèmes.

De ce fait, la première étude qui est présentée dans le chapitre 2, est un article de revue qui décrit, de façon succincte, une série d'applications de la méthode de MC sur différents systèmes de polymérisation, qui portent à la fois sur l'échelle des gouttelettes/particules, dans des systèmes dispersés (ex. polymérisation en suspension), et sur l'échelle de macromolécules contenues dans

ces gouttelettes/particules. Ces développements ont été effectuées pendant la période avant mon arrivée en France et constituent la base sur laquelle les développements suivants ont été grandement appuyés. Parmi les applications présentées dans cet article, un accent important est placé sur le système de polymérisation radicalaire de l'éthylène, pour la production du polyéthylène de basse densité (LDPE), dans des réacteurs tubulaires sous haute pression. En effet, à travers cette étude, la capacité de la méthode de MC de traiter des problèmes de très grande dimensionnalité est clairement démontrée.

La problématique traitée au sein de cette application concerne la prédiction de l'évolution de la topologie de la microstructure des chaînes macromoléculaires du LDPE en fonction des conditions opératoires de synthèse de ce dernier. Cette nécessité provient du fait que, comme mentionné précédemment, ce n'est pas seulement le nombre de ramifications qui affecte les propriétés d'usage d'un polymère fortement ramifié, mais aussi sa forme topologique concernant la position de rattachement ainsi que la taille de chacune de ces ramifications. De ce fait, la seule approche de modélisation capable de suivre simultanément tous les paramètres décrivant en détail la microstructure de chaque molécule, comme la taille et la position de chacune des ramifications le long des chaînes macromoléculaires, ainsi que la polydispersité des longueurs (ou des masses molaires) du très grand nombre de macromolécules formées en cours de synthèse, est la modélisation stochastique sur la base d'un algorithme de MC topologique. Ce développement a permis, par la suite, la liaison directe entre les conditions de synthèse du LDPE et son comportement rhéologique. Il a également ouvert tout un domaine d'applications de cette approche de MC topologique à d'autres systèmes similaires.

La deuxième étude de cas qui est présentée dans ce chapitre concerne encore l'application de la méthode de MC à un système de copolymérisation de l'acide acrylique, dans un réacteur tubulaire, équipé des mélangeurs statiques. Il s'agit d'une étude qui a été effectuée dans le cadre d'un projet européen, portant sur la conception de procédés industriels intensifiés et modulables, avec la participation d'un grand nombre de partenaires industriels et académiques. L'implémentation de la méthode de MC pour la modélisation de ce système, a permis de mettre en évidence l'importance

de pouvoir suivre en détail les distributions bivariées, en termes des masses molaires du copolymère et de sa composition en co-monomères, ainsi que de la distribution des longueurs de séquence des deux co-monomères. En effet, ce suivi détaillé a clairement révélé des effets indésirables, par rapport à ces propriétés, qui n'ont pas pu être détectés par le suivi des propriétés respectives moyennes. Par ailleurs, dans le cadre de cette étude, un simulateur hybride a été développé, sur la base de la combinaison de la méthode stochastique de MC avec une méthode déterministe, à savoir la méthode des moments. Le but de cette combinaison a été de donner, à l'utilisateur de ce simulateur, la possibilité de pouvoir choisir la méthode à appliquer selon le niveau de détail recherché dans les propriétés calculées. Ainsi, le dilemme du choix de la méthode est directement adressé sur la base de l'objectif de la modélisation du système, montrant que le choix d'une méthode avancée, comme la méthode de MC, n'est pas toujours indispensable. La dernière application de la méthode de MC de ce chapitre porte sur la modélisation d'un système de polycondensation des sucres. Il s'agit d'un problème de modélisation qui présente également une dimensionnalité élevée, qui est due, cette fois, au caractère multifonctionnel de l'unité constitutive des macromolécules, à savoir la molécule de glucose. Cette molécule possède cinq groupements OH libres, qui sont tous susceptibles à participer dans la formation de liaisons avec d'autres groupements, appartenant à la même ou à d'autres molécules. L'approche de modélisation qui a été développée pour ce système, permet de simuler des systèmes réactifs des polysaccharides allant jusqu'à des degrés de polymérisation très élevés. En même temps, les différents types de polysaccharides de même longueur sont distingués dans le modèle par leur nombre et leur type de groupements OH, ainsi que par la nature des différentes unités constitutives, qui peuvent comporter, en plus des unités d'anhydroglucose, des molécules d'autres oses. Dans cette étude, une deuxième approche de modélisation du système, par la méthode des moments, a également été démontrée. En revanche, contrairement à l'application précédente du système de copolymère de l'acide acrylique, cette approche n'est pas du tout adaptée à la modélisation de ce système, à cause de la forme finale des équations des moments qui ne permet pas une solution numérique robuste. De ce fait, ce système est un exemple représentatif où le choix de l'approche de modélisation est limitée par la formulation du modèle,

selon les caractéristiques du système étudié.

Le troisième chapitre, porte sur ne autre type de classification des modèles mathématiques, à savoir celle qui distingue les modèles phénoménologiques (ou de connaissances), des modèles basés sur des données. La première catégorie de ces modèles offre une meilleure compréhension des effets observés et est, en général, applicable dans un grand domaine de variation des variables d'entrée. En revanche, ces modèles nécessitent souvent un temps de développement significatif. Par ailleurs, les modèles basés sur des données, sont plus rapides à développer et à mettre en œuvre, mais sont limités au domaine d'application, qui doit être couvert, de façon représentative, par les données utilisées lors du développement du modèle. Au vu de ces avantages et inconvénients, le choix des modèles basés sur les données est souvent plus judicieux dans de cas où l'état des connaissances du système, et/ou les ressources disponibles (ex., le temps et/ou le budget alloué(s)), sont limitées. Par ailleurs, le développement explosif que connait, depuis ces dernières années, le domaine des techniques d'apprentissage automatique (*machine learning*), a beaucoup privilégié cette deuxième catégorie de modèles, dont elles font partie.

En effet, ces méthodes sont devenues de plus en plus importantes dans l'industrie, dans le cadre d'un nouveau mode opérationnel souvent appelé "industrie 4.0" ou "industrie du futur" ou encore "industrie numérique". Dans ce cadre, l'opération de l'usine du futur repose, en grande partie, sur l'acquisition et l'exploitation efficace et exhaustive de données, voire de données massives (*Big Data*), afin de monter en capacité pour mieux prédire le comportement des systèmes. Le processus typique passe par les étapes de collection des données, de leur visualisation statistique (analyse descriptive), de l'identification de motifs (analyse prédictive) et, enfin, de la prise de décisions (analyse prescriptive). Des modèles statistiques adaptés, qui peuvent analyser des grandes quantités de données afin d'identifier des liens et des motifs entre elles, sans pour autant donner ou nécessiter des informations sur les phénomènes des systèmes, jouent un rôle principal dans ce processus. C'est là où les modèles d'apprentissage automatique, comme par exemple les réseaux des neurones, commencent à devenir essentiels pour l'industrie qui décide de suivre et de s'adapter à ce mode de fonctionnement.

Plus particulièrement, ces techniques d'apprentissage automatique sont couramment employées pour la modélisation de systèmes complexes (ex., dans la robotique), présentant des nombreux avantages et des performances très élevées. Certaines, comme les réseaux de neurones artificiels, ont déjà trouvé des applications dans des systèmes physico-chimiques, mais il existe également toute une série d'autres techniques qui restent encore relativement sous-exploitées dans le domaine du génie des procédés et des produits. Ces méthodes sont, elles mêmes, classées en quatre catégories principales, à savoir les catégories d'apprentissage supervisé, non-supervisé, semi-supervisé ainsi que la catégorie d'apprentissage renforcé.

Dans la première catégorie on trouve les méthodes qui utilisent, dans leur apprentissage, des données composées à la fois des entrées et des réponses, appelées également étiquettes. De ce fait, elles 'apprennent' à créer un lien entre les nouvelles entrées et les réponses cherchées, sur la base de ce qu'elles ont déjà 'vu' dans les données d'apprentissage. Les problèmes qui sont typiquement traités par ces méthodes sont des problèmes de régression, où la réponse prend la forme d'une fonction continue, et des problèmes de classification, où les réponses sont des classes distinctes.

La deuxième catégorie comporte des méthodes qui sont employées pour l'identification de motifs dans des séries de données pour lesquelles les étiquettes ne sont pas disponibles. Dans ce cas, on parle de problèmes de *clustering*, où les données sont regroupées dans des groupes (*clusters*), sur la base d'un ou plusieurs critères de similarité. Des applications typiques de cette catégorie de méthodes portent sur le diagnostic et la détection des dérives des procédés ainsi que sur la réduction de la dimensionnalité.

La troisième catégorie est intermédiaire entre les deux premières, et concerne de problèmes où les données comportent à la fois de données étiquettées et non étiquettées, les premières étant souvent limitées en quantité par rapport aux secondes. Enfin, la dernière catégorie concerne principalement la procédure de prise de décision, sur la base de l'apprentissage de règles et est employée plutôt dans des applications du domaine de l'automatisme.

L'étude de cas qui est présentée dans ce chapitre montre le développement d'un modèle basé sur

des données pour un système de photocatalyse, en vue de la destruction de contaminants présents dans l'eau. Dans ce cas, deux réseaux de neurones consécutifs et inter-connectés ont été mis en œvre pour la modélisation de deux étapes critiques du procédé, celle de la synthèse du photocatalyseur et celle de la dégradation du contaminant. Ainsi, il a été possible de relier les conditions opératoires de la synthèse du catalyseur à celles des essais de dégradation du contaminant et d'évaluer alors la performance finale du catalyseur. Ceci a permis par la suite, via une étude d'optimisation, d'identifier les conditions de synthèse et de dégradation qui maximisent la quantité du contaminant dégradé. A travers cette application est démontré l'intérêt de l'utilisation des techniques basées sur des données, dans le cas où la complexité du système étudié, en combinaison avec la durée envisagée de l'étude, ne permettent pas le développement d'un modèle des connaissances. Par ailleurs, la capacité prédictive accrue de ces techniques, dans des systèmes très complexes, a également été mise en évidence par cette étude.

Le quatrième chapitre met plus l'accent sur le type d'application que sur le choix de la technique de modélisation. Il s'agit d'une étude qui vise à répondre à la problématique de la suraccumulation de pneumatiques usagés, qui est devenue un enjeu majeur en écologie au cours des dernières années à l'échelle mondiale. Parmi les approches de traitement et/ou de réutilisation de ces déchets des pneumatiques, la méthode de leur recyclage par granulation est particulièrement intéressante. Elle consiste à broyer mécaniquement ces pneumatiques en granulés de caoutchouc de tailles micrométriques, commercialisés sous le terme de GTR (*Ground Tire Rubber*), qui conservent les propriétés élastomères du caoutchouc et qui peuvent être utilisés en tant que charge pour renforcer des polymères.

Dans ce cadre, des travaux de recherche ont été entamés pendant les dernières années, au sein de l'axe Génie des Produits du LRGP. Ses travaux, qui ont fait l'objet de deux thèses de doctorat consécutives, portent sur l'amélioration des propriétés mécaniques (e.g., déformation à la traction et résistance aux chocs) du polystyrène (PS) grâce à l'ajout de GTR. Etant donné l'intérêt de ce système pour l'industrie du recyclage, du transport et des polymères, ces travaux ont également conduit au dépôt d'un dossier de brevet auprès de la SATT SAYENS.

Un verrou principal de ce concept est que le GTR et la matrice de PS présentent une faible adhérence de par la nature différente de leurs phases. Afin de surmonter cet obstacle, les chaînes de PS ont été greffées sur la surface du GTR via une polymérisation radicalaire *in situ*. Cependant, la présence du GTR dans le système peut aussi altérer le mécanisme et/ou la cinétique de la polymérisation radicalaire, présentant, selon les conditions, un effet accélérateur, retardateur ou même inhibiteur. Un enjeu majeur de ces travaux est alors de maximiser la quantité de PS qui est greffé sur les particules de pneumatiques, tout en utilisant un rapport de GTR/styrène élevé, afin de promouvoir d'avantage le recyclage de GTR et de limiter la production de PS libre (non-greffé) dans le système. Parmi les paramètres qui affectent l'évolution du système, se trouvent notamment la nature de l'agent amorceur, la quantité et la composition du GTR ainsi que la température de synthèse. L'objectif principal de cette étude a alors été d'élucider et de comprendre l'effet de ces paramètres sur l'évolution de la polymérisation de greffage. Le but a été de pouvoir contrôler les conditions opératoires afin de maximiser à la fois le taux de conversion du styrène et le taux de greffage sur le GTR. Pour ce faire, un schéma réactionnel étendu a été adopté, permettant de décrire à la fois les mécanismes de polymérisation du styrène libre, ainsi que ceux du greffage de ce dernier sur les particules de GTR. Ce modèle phénoménologique a été formulé en utilisant la méthode des moments, qui est largement adéquate pour décrire l'évolution du taux de conversion et du taux de greffage du système.

Le dernier chapitre résume les développements et les études citées, dont la présentation dans ce manuscrit a été faite à travers :

- Le choix entre les méthodes de modélisation stochastiques et déterministes,
- le choix entre des techniques de modélisation phénoménologiques et celles basées sur des données, et
- les différents domaines d'application, en liaison avec les enjeux majeurs industriels et sociétaux.

Suivant la même ligne directrice, les développements qui sont envisagés pour le futur portent sur les mêmes axes. Ainsi, les approches stochastiques et, notamment, les modèles de MC topologique, seront d'avantage développées pour la modélisation d'autres systèmes multi-dimensionnels, comme c'est le cas des polysaccharides. Par ailleurs, une montée en puissance des compétences sur des techniques d'apprentissage automatique sera également poursuivie, notamment par une thèse de doctorat qui vient de démarrer sous ma supervision sur cette thématique. Tous ces développements seront appliqués, autant que possible, sur des problématiques qui répondront à la demande pour une production industrielle moderne et durable, dans le cadre d'une économie circulaire.

L'ensemble de ces travaux de recherche, au cours de ces années depuis ma soutenance de thèse, ont conduit à la production d'une totalité de 22 articles à comité de lecture, dont 4 actes de colloques. J'ai également participé, depuis 2011, à 24 conférences, dont 22 avec actes, 18 internationales et 14 en communication orale. Une grande partie de ces travaux a été effectuée dans le cadre de l'encadrement des travaux de recherche de 14 étudiant(e)s, dont 7 en thèse et 7 en stage de Master. Une présentation analytique de ces travaux et productions est donnée en Annexe **??**.

To the loving memory of my parents.

To Maria, Eleni and Ioannis who are my constant point of equilibrium.

Acknowledgements

I would like to extend my gratitude to professor Costas Kiparissides and my colleagues from Greece who played a crucial role in my first steps in the field of mathematical modeling and have remained constantly present in a series of later collaborations that make an important part of my developments. I am also deeply grateful to Fernand Pla, Sandrine Hoppe, Christian Fonteix and Guo-Hua Hu who have welcomed me in the group and have immensely facilitated my integration, both professionally and personally, by making me part of a number of research projects and of the different actions of the group. A specific word of gratitude is also addressed to Gabriel Wild and Michael Matlosz for accepting me in LRGP and ENSIC and for helping me navigate through the administrative procedures and difficulties of my recruitment. I would like to thank the different colleagues and friends for the collaborative and friendly environment they have created around me, as well as the numerous students and young researchers who have contributed to my different developments. Finally, I would like to thank the members of the examining committee for accepting to evaluate this dissertation and to share their valuable knowledge and experience with me.

Table of Contents

Page

1. Introduction

Mathematical modeling is very much an art...

W. L. Luyben

1.1 A journey in the notions of mathematical modeling

The present dissertation aims in providing a synthetic overview of a journey in the notions of mathematical modeling of polymerization systems, which has begun about 17 years ago in Aristotle University of Thessaloniki. Throughout this journey, several modeling techniques and approaches have been tested and implemented to various types of problems. In this respect, different versions of the method of moments, advanced discretization techniques, stochastic Monte Carlo algorithms and, lately, machine learning techniques have been employed for the modeling of polymerization and other physicochemical systems.

In the course of the different developments that have been realized throughout these years, some of the aforementioned techniques have been preferably utilized over other alternatives. This preference was often driven by the specific characteristics of the problems under study and the associated envisaged modeling outcomes, which made these techniques more *fitted* in comparison to others. This question of *fitness* has been a continuous interrogation along the different developments and a constant reference point for the presented applications in the rest of this dissertation.

To address this issue, a series of representative case studies are presented in the following chapters, in an attempt to illustrate the strengths and the shortcomings of different modeling approaches. Accordingly, the suitability of their implementation is considered in direct conjunction

with the characteristics of each problem, mainly in terms of the complexity of its formulation, as well as in terms of the required level of detail in the sought properties or responses. Besides this methodological motivation, and in parallel to the analysis of the applied modeling techniques, the presented developments share a common application domain, related to the evolution of the scientific and societal challenges in the field of polymers. Accordingly, the covered application spectrum extends from the prediction of the topological properties of structurally complex polymers and copolymers to the sustainability issues related to the production and the end-of-life treatment of the produced polymers.

1.2 Different types of modeling approaches

Mathematical model(ing) is a term that finds extremely widespread use in all domains of science, ranging from mathematics to astronomy, marketing and finance. As such, it is extremely difficult to clearly define the outline of a modeling work, without providing additional relevant details. And quite often, even the additional definition of the targeted application domain, as in *mathematical modeling of polymerization systems*, is not enough to clarify things as the different forms and types of such modeling studies are still numerous. For example, a simple literature search in the Web of Science, using the keywords 'model*' and 'polymer*' returns more than 262000 records. As a result, a rather more detailed description is required before one can comprehend the meaning and the objectives of a modeling work. In addition, it is important that the adopted terminology is clarified and some basic notions are agreed upon.

Mathematical models can be loosely defined as the ensemble of mathematical expressions that can be employed to describe a system or a process. They can be broadly classified into several categories with respect to different characteristics or criteria. For example, it is quite frequent to distinguish linear from non-linear mathematical models, depending on their structural form, or dynamic from steady-state models, depending on whether they refer to the transitional state or the steady-state of a process. Several other categories exist, or can be defined, that are more or less commonly encountered in scientific reports and studies [1]. Note that, the classification of a given mathematical model can follow several of these categories in a non-exclusive manner, in the sense

that a model can be both non-linear and dynamic.

In the present work, the modeling developments will be primarily distinguished according to the following two categories:

- Knowledge-based vs data-driven models.
- Deterministic vs stochastic models.

A mathematical model falls within the category of knowledge-based models when it is composed of basic principle laws and equations. In the field of chemical engineering, this would reflect, for example, the models that incorporate basic conservation or transfer equations for the mass, energy and momentum. These models describe the underlying phenomena of a process on the basis of prior knowledge and, as such, possess significant predictive capacity in a very large domain of application. On the downside, they demand a rather laborious development procedure and may result in an overall difficult-to-solve form (i.e., in terms of mathematical solution), especially when implemented to describe complex systems.

Data-driven models, on the other hand, are exactly the opposite; they are not employed to describe the mechanisms and phenomena of the process, but rather in an attempt to create a connection between some selected input(s) and response(s). The form of the equations can be any mathematical expression, whose terms have no physical meaning. A typical example of such models are the polynomial expressions derived from an experimental design. These models are typically very fast to develop and simple in structure but, at the same time, suffer from limited applicability (i.e., restricted to the domain represented by the data) and poor understanding of the mechanisms.

The above two categories may also be encountered under slightly different definitions and with various names. Accordingly, knowledge-based models are also known as phenomenological models (i.e., describing the phenomena), mechanistic models (i.e., describing the mechanisms) or glass-box models (i.e., where the process is transparent in terms of the underlying phenomena). On the opposite side, one finds the so-called empirical or behavioural models, where the model

expression(s) are not entirely disconnected from the mechanisms but are based on empirical observations, or the black-box models (i.e., in contrast to the glass-box), where the mechanisms of the process are completely unknown and their description remains out of scope.

The second category of reference in this work is that distinguishing mathematical models in either deterministic or stochastic. In a deterministic model, the output(s) are uniquely defined by the input(s), typically via a set of algebraic and/or differential equations, in such a way that consecutive executions of the model, under the same parameters, will always result to the exact same output. Inversely, stochastic models are based on the generation of sequences of random numbers that are employed for the determination of the different state transitions. The output(s) are subject to the input(s) and to state transition probabilities that dictate the most probable outcome of the model, which varies from one execution to the other, even under identical parameter values.

Deterministic models are the general rule when it comes to classical chemical engineering problems, which are typically formulated through systems of differential equations. These models are often very powerful and robust (i.e., perform well under a wide range of conditions) and provide the advantage of absolute traceability of the calculations. However, they fail to capture the inevitable uncertainties of the process and the inherently stochastic nature of many physicochemical systems. They also tend to assume highly-complex mathematical forms when a multivariate description of a system is in order. In this respect, stochastic modeling techniques, commonly grouped under the general term Monte Carlo (MC), find increasing applicability in an ever-growing spectrum of applications that spans from numerical integration and finance to molecular biology and engineering. Stochastic models provide the benefit of scaling extremely well in multidimensional problems while keeping a very simple mathematical form. On the other hand, their applicability is somewhat hindered by their increased computational demands, with respect to their deterministic counterparts, when it comes to low-dimensional problems, as well by their incompatibility with deterministic optimization algorithms.

To illustrate the importance and the expansion of MC methods in scientific research, Figure 1.1 shows the number of publications appearing annually on the Web of Science database, containing

the keyword 'Monte Carlo' in the topic. An analysis of the corresponding scientific domains, shows that around 43% of a total count of more than 287000 records refers to the domain of physics, 22% in the domains of engineering and materials and 11% in the domain of chemistry.

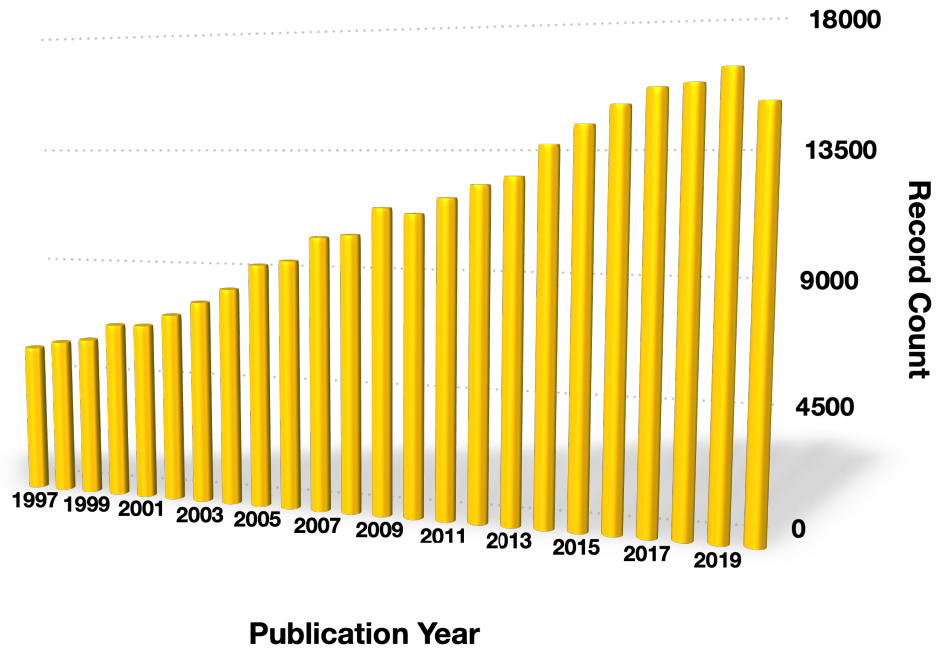

Figure 1.1: Annual publication records in the topic Monte Carlo on the Web of Science database.

1.3 The modeling dilemma

Any researcher that is faced with the dilemma of developing a mathematical model for the system (s)he is studying, is inevitably confronted with a series of questions raising from the multitude of model types (and not only). More specifically, the principal questions that need to be addressed within this procedure are the following:

- What is the reason (if any) for developing a mathematical model for this system?
- What will be the inputs and, more importantly, what are the envisaged responses of such a model?

- Which type/form/category of model is best suited to this problem?
- What is the required know-how and effort, in terms of resources and temporal horizon, for developing this model?

The answers to the above questions are not always evident and may depend on many factors. In addition, the questions themselves are not independent from one another and the eventual responses are correlated. More precisely, the type of the model that will be most suitable to a problem, depends both on the type of information that is sought from the model and on the available resources. And inversely, the type of information that can be retrieved by the mathematical model of a process, depends on the available know-how and on the type of modeling approach. This situation may quickly lead to frustration and to the adoption of a sub-optimal approach. It is, for example, very common to employ a modeling technique on the basis of previous experience rather than on the basis of the characteristics of the problem.

The landscape of modeling methods and approaches is extremely vast, even for very narrow and well-identified application domains. The further one proceeds into the analysis of the different aspects of various modeling techniques, new routes unravel before him, exposing unknown aspects and techniques (as is, besides, the case for any domain of scientific research). This is further amplified when taking into account the different aspects associated with the development of mathematical models, such as those related to the estimation of the parameters of the model, to the data acquisition procedures, to the model validation process, etc.

In view of these elements, a driving force for the developments realized over the last years has been the attempt to tackle the above questions in a systematic way. There is no doubt that there is not one modeling technique that is superior to all the rest and that certain approaches are more pertinent than others on specific problems. It is also obvious that, even though it is important to understand a method in order to apply it efficiently and correctly, the selection of the most fitted approach to a problem cannot be based solely on one's previous knowledge and/or habits, even though the latter is inevitable to some extent.

1.4 Outline of this report

The rest of the content of the present report is organized into four chapters (i.e., not including the present general introduction), following the aforementioned viewpoint. Accordingly, Chapter 2 is dedicated to a series of stochastic modeling developments, on the basis of the MC method, to tackle complex problems in the field of polymer reaction engineering. The presented applications are representative examples of the capacity of the MC method to handle the increased complexity of the systems under study. At the same time, they demonstrate the interest in resorting to the implementation of a stochastic modeling framework through a comparative study with other commonly employed deterministic modeling techniques. This section is more extensive than the rest, due to the wider range of relative developments over all these years.

Chapter 3, contains a case study that has been based on the use of a data-driven modeling approach, on the basis of a method that belongs to the family of machine learning techniques. Coupled to this modeling approach is also an optimization study that employs an alternative technique, with respect to the most widespread deterministic optimization algorithms, via the use of an evolutionary algorithm. Finally, Chapter 4 focuses on the modeling of a polymer recycling process of great industrial and societal interest. Through this case study, the attention is focused more on the associated difficulty in describing the observed phenomena of the process, rather than on the employed modeling technique.

The presentation of the selected case studies is made principally through the use of articles, either published or in the form of submitted works. The fifth and final chapter of the report is dedicated to providing a conclusion and a discussion of the perspectives of continuation of the presented developments.

The adopted structure of Chapters 2-4 aims in addressing the following key-issues that underpin both previous developments and future perspectives:

1. Deterministic vs stochastic modeling approaches; what type of information is accessible by each technique and what are the relative limitations? In which cases one or the other

approach is imposed and in which cases there is a choice?

2. Knowledge-based vs data-driven approaches; what are the benefits and drawbacks of each technique in the framework of the treated problems? In what type of problems it is more interesting to select one over the other approach and what are the relevant limitations?

3. Domains of application. The presented developments were not solely driven by purely technical aspects in terms of the modeling techniques but also by the nature of the applications and their relevant characteristics. In this sense, some of the presented applications display a well-established industrial interest, as is the case of high-commodity polyolefins, while others display an increased interest within a more sustainable production of polymeric products, as is the case of biopolymers. The recyclability and, in a general sense, the end-of-life treatment of polymeric products is also addressed via the application presented in Chapter 4.

Although the first two issues, listed above, are clearly related to the first two sections of applications (i.e., Chapters 2 and 3), the third one is more transverse as it is addressed in all three application Chapters. A schematic representation of the above is depicted in Figure 1.2.

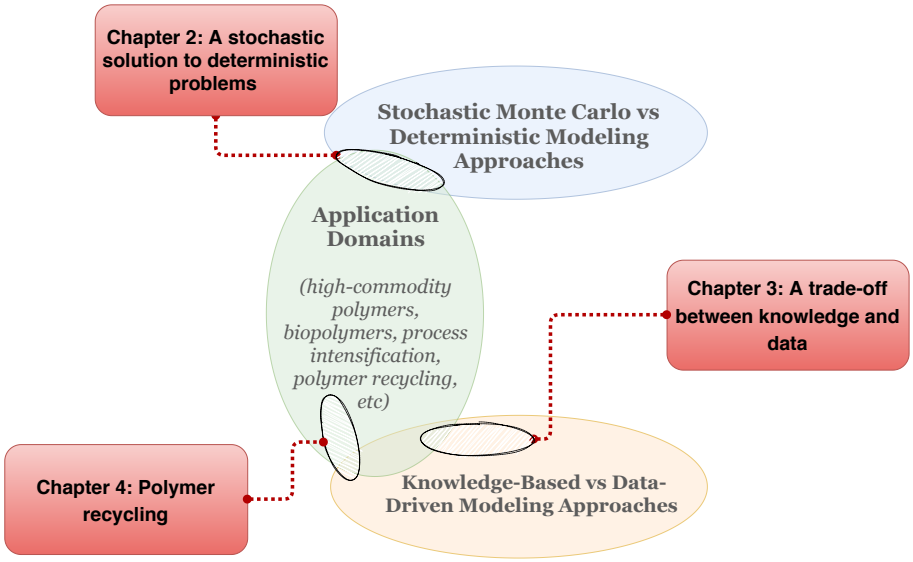

Figure 1.2: Outline of the application chapters and their relevance to the addressed subjects.

2. A Stochastic Solution to Deterministic Problems

A likely impossibility is always preferable to an unconvincing possibility...

Aristotle

2.1 Monte Carlo methods in Population Balance Modeling

Among the different case studies presented in this report, stochastic MC algorithms possess the lion's share. Indeed, although several modeling techniques have been tested throughout these years, notably within the framework of the kinetic modeling of different (co)polymerization systems, the MC method has been shown to display a series of comparative advantages over deterministic approaches, especially when it comes to complex modeling formulations. As such, it has been employed for the modeling of polymerization systems that display an increased dimensionality, either in terms of their macromolecular structure, or in terms of their reactive functionality.

Polymers are, by nature, molecules that present a high degree of structural complexity as they are composed of smaller constituting units, whose exact number and, in certain systems, arrangement vary between each macromolecule. The sole fact that the most basic molecular property characterizing a polymer, namely their molar mass, is defined via a distribution, is evidence of their inherent complexity. In addition to this, many polymerization systems present characteristics that further complicate their description, such as a non-linear macromolecular form, the presence of more than one types of monomer units or even the existence of multiple reacting centers on the molecules.

A very powerful tool that is commonly employed for the description of complex systems, com-

posed of multiple constituting units, are population balances. Population Balance Modeling (PBM) is typically employed for the description of the evolution of selected characteristics or properties (also known as internal coordinates) of the entities of a population, under the action of different mechanisms. Typical examples are systems of droplets or particles, dispersed in an heterogeneous medium, where the coordinates of interest may be their size (i.e., expressed via their volume or diameter) in a 1-dimensional formulation and, eventually, their concentration (i.e., in terms of a specific substance), or their porosity (i.e., in the case of solid particles, such as catalyst particles), in a 2-dimensional framework. The Population Balance Equation (PBE) describes the evolution of these properties under the actions of various mechanisms, such as coagulation, breakage, growth and nucleation [2, 3, 4].

Once the system of equations has been established, under a population balance perspective, a number of different numerical approaches can be employed for their solution. The form and the associated complexity of the resulting system of equations depends directly on the considered dimensionality of the problem (i.e., in terms of the number of accounted internal coordinates) as well as on the considered mechanisms, governing the system. The above display also a dramatic effect on the computational effort required for the numerical solution of the resulting system of Integro-Differential Equations (IDEs), whose number typically rises to several hundreds or even thousands of equations that need to be solved simultaneously at every point (or node) of the integration domain. As a result, although several very powerful deterministic techniques have been developed and reported for solving the PBE [5, 6], their implementation is constrained by the considered dimensionality of the problem.

On the other hand, MC provides a viable alternative to these approaches as its formulation is completely different than that of the deterministic methods. In general, instead of discretizing the considered coordinates in a number of elements and then establishing the complete system of IDEs on each node of the discretization grid, MC considers a representation of the system in the form of a finite sample of virtual entities. These entities are characterized in terms of the considered internal coordinates and are allowed to interact with each other in a representation of the simulated

mechanisms. Accordingly, the mathematical formulation of the model remains extremely simple, irrespective of the number of considered coordinates. Of course, several issues of different nature need to be addressed in this type of modeling framework as well, notably concerning the characteristics of the sample and the sequence of the simulated events. Hence, many different types of MC algorithms have been reported to deal with each of the above issues [7, 8, 9, 10, 11].

PBM is commonly employed in the modeling of polymer systems. Depending on the considered scale of the system, different modeling problems can be formulated. Accordingly, a typical application domain concerns the evolution of the Particle Size Distribution (PSD) in dispersed polymerization systems, such as emulsion and suspension polymerization processes [12, 13, 14, 15, 16, 17, 18]. However, by descending on a lower scale in the consideration of the system, it is possible to formulate an equivalent PBM problem in a polymer reaction engineering perspective. In this case, instead of tracking the evolution of the size of droplets or particles under the actions of nucleation, growth, coalescence and breakage, it is possible to track the size of polymer chains that exist within these droplets/particles, under the actions of initiation, propagation, termination and scission, respectively. As a result, the Number Chain Length Distribution (NCLD) of the polymer can be tracked throughout the duration of the polymerization, instead of the PSD [5].

As is the case of problems formulated within a one-dimensional PBM framework, where a single internal coordinate is considered (i.e., the size of the particles or the polymer chains), a great number of numerical techniques can be employed for the solution of the model equations, including methods based on the calculation of the moments, advanced discretization deterministic techniques (e.g., OCFE, discrete weighted Galerkin, Fixed Pivot, Moving Pivot, Moving Grid, etc.), Radial Basis methods, and stochastic MC algorithms. Each one of these approaches can be very efficient in this type of problems, although under some limitations in terms of their predictive capabilities and associated computational effort [19, 20, 21, 22, 23, 24, 25, 26, 27].

However, in some cases, the nature of the system dictates the necessity to include more than one internal coordinates in the modeling formulation. More specifically, when it comes to polymerization systems containing more than one types of monomer units, or resulting in non-linear

polymers, or even containing multi-functional reacting units, there is a great wealth of information that resorts in these additional properties (i.e., besides the chain length of the polymer) and that can only be accessed by considering additional internal coordinates in the formulation of the PBM. These coordinates will represent, for example, the copolymer composition or the number of branches of the produced macromolecules in a copolymerization or a non-linear system, respectively. Several numerical techniques can perform well in treating such two-dimensional modeling formulations, although the computational burden of the class of advanced discretization techniques increases significantly, with respect to the one-dimensional case, as a result of the geometrical increase of the computational nodes of the formed two-dimensional discretization grid.

The interest in accessing the analytical information about these properties lies within the fact that they are directly related to the so-called end-use properties (or functionalities) of the formed polymers, such as their thermal, mechanical or rheological properties. For example, the volume occupied by a linear polymer chain in a solvent or in melt, will not be the same as the one occupied by another polymer chain of the same length but of highly-branched form, with direct implications in their viscoelastic behavior. In the same way, the use of different types of comonomers, in view of imparting specific mechanical characteristics to the formed copolymer, depends on the sequential arrangement of these comonomers (or blocks of them) on the formed macromolecules. As such, even though two copolymers may present the same average value of copolymer composition, defined in terms of the relative amounts of the two comonomers, their mechanical properties may be completely different as a result of different arrangements of these comonomers along the chains of the copolymer.

Although this two-dimensional modeling formulation can provide important additional information about the form of the produced polymer chains, in comparison to the simplest one-dimensional case, in some systems, this information is still not sufficient to describe in detail their important characteristics. For instance, in the example a branched polymer chain, it is not sufficient to know the number of branches of each polymer to be able to predict with accuracy its rheological behavior. In fact, the branching structure of two macromolecules, possessing the same number of

branches, can be very different, depending on whether these branches are more or less of the same size, or not, as well as on their relevant position, with respect to the backbone of the polymer. For example, a star-shaped polymer and a comb-shaped one (cf. Figure 2.1), of the same overall size and number of branches, will display different rheological behavior [28, 29, 30].

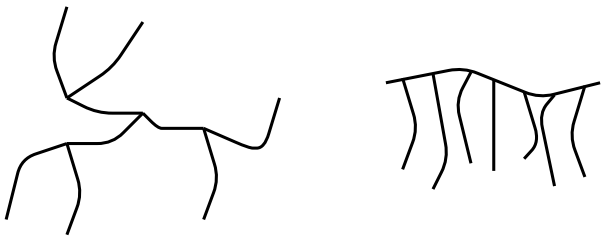

Figure 2.1: Different configurations of branched polymers.

To access this information, it is necessary to formulate a completely different modeling approach where, besides the overall size of the polymer chain and its total number of branches, the exact size and position of every single branch is also monitored. Such a *topological* modeling formulation can only be conceivable in the framework of a stochastic MC algorithm, coupled with a detailed book-keeping algorithm for the characteristics of each polymer chain. The different modeling approaches that are associated with the different levels of problem complexity are presented in Figure 2.2.

On the basis of the above, the present section presents a series of developed stochastic MC modeling approaches, employed in the framework of different case studies. The common objective of these developments has been the prediction of the macromolecular properties, of different levels of complexity, in terms of the conditions of the polymerization, towards the targeted conception and synthesis of polymers with tailored properties and functionalities. Such modeling formulations fall within an overall product design perspective, on the basis of the control of the structure-property relationship.

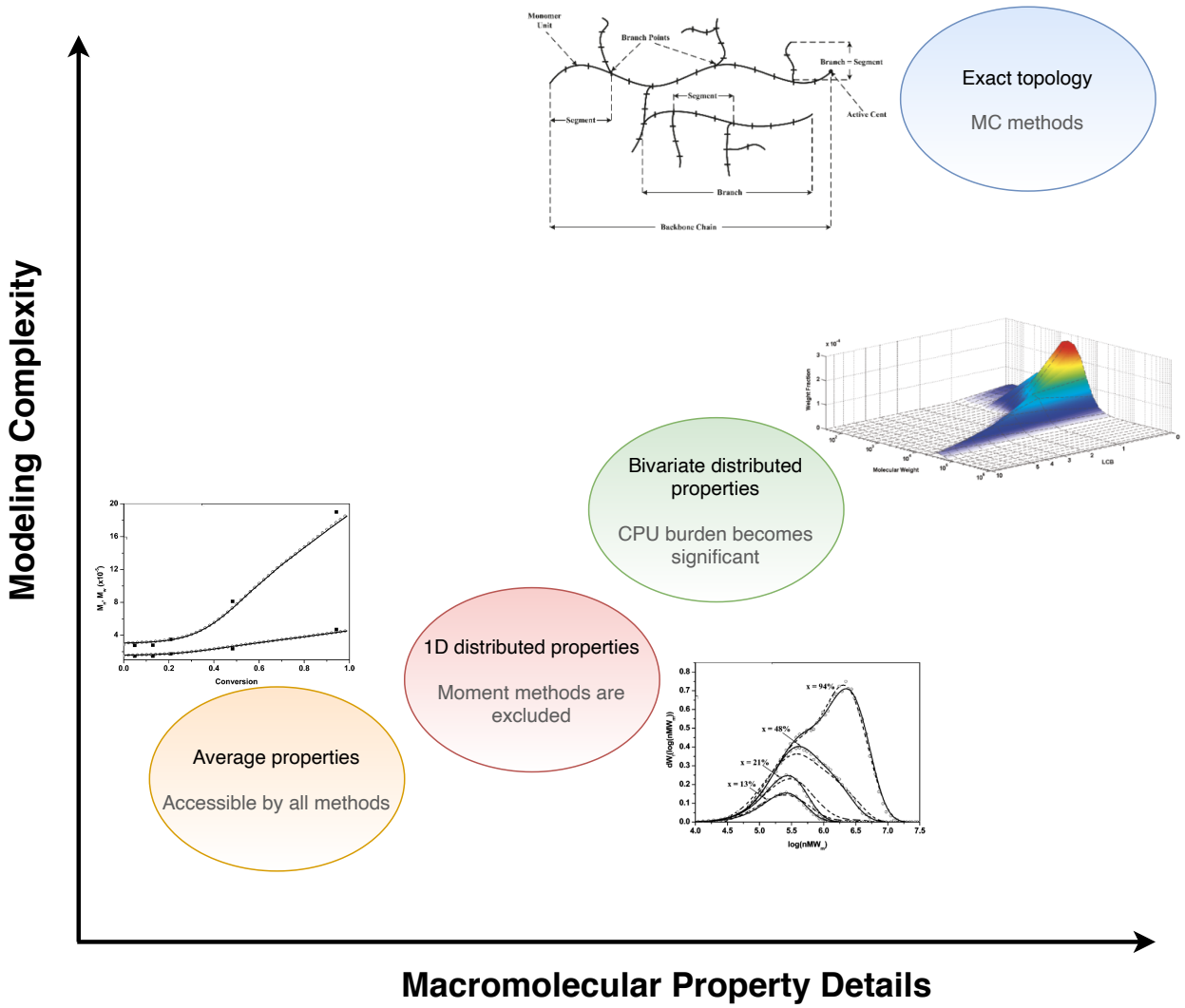

Figure 2.2: Qualitative correlation between the level of detail in the calculated macromolecular properties and the respective complexity of the required modeling approach.

2.2 Stochastic models in polymer science

The first article that has been selected for this section, concerning the implementation of the MC technique to polymerization systems, is in fact a review of several different case studies. It allows, in this way, to present a synthesis of the most representative early-stage developments that relate mainly to the period of my PhD dissertation and post-Doctoral work, both carried out in Greece. Within this review, different applications are presented that cover both the particulate and macromolecular modeling scales.

More precisely, after a general overview of the MC method and a short introduction of its implementation for the solution of the PBE in particulate systems, a specific application is presented on the suspension polymerization of methylmethacrylate (MMA). At a second stage, the implementation of the MC method is demonstrated at a lower scale of the PBM formulation, for the modeling of several macromolecular properties of different polymerization systems, on the basis of their kinetic developments. Special emphasis is placed on two-dimensional modeling formulations, where the required information extends in more dimensions than the simple case of the exclusive consideration of the polymer chain length. In this respect, the calculation of the bivariate molecular weight - copolymer composition (MW-CC) and the chain sequence-length (CSL) distributions is presented for the styrene-methylmethacrylate (St-MMA) copolymerization system.

The final part of this publication is dedicated to the modeling of the industrial process of production of low-density polyethylene (LDPE) in high-pressure tubular reactors. This process represents one of the two typical production processes of polyethylene via radical polymerization (i.e., polyethylene is also produced industrially in low-pressure catalytic processes), displaying an extended kinetic scheme that combines chain-branching and scission reactions. The overall process runs in an non-isothermal mode, comprising a series of characteristic temperature peaks, combined with side injections of the mixture of initiators along the tubular reactor, which reaches several hundreds of meters in length. All the above synthesize a picture of a process that, although has been used in industrial practice and has been extensively studied for over 50 years [31, 32, 33], it remains quite challenging to model in view of predicting with accuracy the macromolecular characteristics of the produced polyethylene chains.

The article presents the results of a series of modeling studies on the system that demonstrate the capacity of the MC method to predict the evolution of not only the bivariate chain branching-molecular weight (CB-MW) distributions but also of a series of topological characteristics of the produced polymer chains. These latter were obtained by a novel topological MC modeling framework that has been developed on the basis of this system and that has eventually lead to the connection of the process conditions with the rheological properties of the polyethylene melt, through

an integrated multi-scale stochastic modeling framework [34, 35]. The continuation of the last part of this work, on the viscoelastic properties, has also been published in a subsequent article [30], that is not presented here in detail.

I&EC research
Industrial & Engineering Chemistry Research

Review

pubs.acs.org/IECR

Review of Monte Carlo Methods for the Prediction of Distributed Molecular and Morphological Polymer Properties

Dimitrios Meimaroglou[†,‡] and Costas Kiparissides*[,§,⊥,∥]

[†]CNRS, LRGP, UMR 7274, Nancy, F-54001, France

[‡]Université de Lorraine, LRGP, UMR 7274, Nancy, F-54001, France

[§]Chemical Process & Energy Resources Institute, Centre for Research and Technology Hellas and [⊥]Department of Chemical Engineering, Aristotle University of Thessaloniki, P.O. Box 472, Thessaloniki, Greece 541 24

[∥]Department of Chemical Engineering, The Petroleum Institute, Abu Dhabi, UAE

ABSTRACT: Monte Carlo (MC) is a term quite common in the research community but, quite surprisingly, it may possess a different meaning among researchers in different areas. This paradox is derived from the potential of the method to serve as a modeling tool of systems that belong to a very wide range of different areas in science, such as mathematics, biology, economics, and physics. Thus, depending on the nature of the system under study and the type of the calculated properties, a different variation of the MC method may be encountered. In the present work, an attempt is made to provide a short overview of some of the most important MC techniques and their applications. Special emphasis is placed on problems related to the polymer science, with a more persistent presentation of a specific class of MC methods that can be implemented to the different scales of a polymerization process in order to predict the dynamic evolution of key properties of the polymer in terms of the varying process conditions. The latest developments in this field have made it possible to relate the macroscopic characteristics of a process to the end-use properties and functionalities of the produced polymeric products, via a detailed tracking of the evolution of the microstructural characteristics of the polymer chains. The presentation of these MC techniques is accompanied by specific illustrative examples from the literature.

1. INTRODUCTION

The real world consists of innumerous many-body systems and subsystems of a vast range of length and time scales. Such systems may constitute our surrounding natural environment, the materials of everyday use, food or medicines, and even the very human organism. In an effort to understand or predict the properties and the behavior of such systems, it is necessary to elucidate their structure and the interactions that take place among their building units, either in a dynamic or an equilibrium state. Computer simulations can serve this purpose in terms of two principal simulation techniques, namely the molecular dynamics (MD) and the Monte Carlo (MC).

Molecular dynamics simulations consist of the numerical, step-by-step, solution of the classical equations of motion of a set of interacting atoms.[1] In this context, it is a deterministic technique that is based on the principles of classical mechanics.[2] On the other hand, the term Monte Carlo describes a collection of probability-based methods with its name directly evoking gambling (via the famous casino of the French city) where any event is considered unpredictable, but the averages over many events can be considered certain.[3] In general, the Monte Carlo method can be loosely defined as a technique for the solution of models via the use of random numbers[4] or as a numerical method of solving mathematical problems by random sampling.[5]

An extremely rich collection of books describing the different principles and the various "versions" of MD and MC algorithms is already available and such a description certainly exceeds the subject of this work. An attempt to cover all the major recent developments of the MC method is also far from the scope of this paper. The present work will only be focused on the application of the MC method to very specific problems related to the polymer science and, in particular, to the fields of polymer chemistry and polymer reaction engineering.

Accordingly, the following outline is followed: initially, and for reasons of consistency, a very short introduction of the MD and MC methods is presented, including their most important variations and their common applications spectra, mainly in relation to polymers. Specific attention is paid to some of the latest MC developments, which are not covered by previous review publications. In the second, main part, the interest is focused on the problem of predicting a series of polymer properties via the implementation of the MC method on dynamically evolving polymerization systems. The major contributions in the area are presented in terms of the different length scales of the system on which the method may be applied. Finally, a number of illustrative examples are presented for each case concerning different polymerization processes of industrial interest.

1.1. Origins and Applications of the Two Techniques.

The use of statistical methods to provide exact answers to mathematical problems goes back many years, a characteristic example being the estimation of the value of π by the notorious

Special Issue: Massimo Morbidelli Festschrift

Received: October 3, 2013
Revised: December 13, 2013
Accepted: December 16, 2013
Published: January 24, 2014

"Buffon's needle problem" of the 18th century. Monte Carlo methods where officially born in 1944 within an effort to simulate the diffusion of neutrons in fissionable materials.[6] A few years later, in 1953, N. Metropolis, A. W. Rosenbluth, M. N. Rosenbluth, A. H. Teller, and E. Teller[7] presented the *Metropolis Rule for Monte Carlo*, also known as the *Metropolis algorithm*, which is considered as one of the greatest intellectual achievements of the 20th century,[8] with a great influence on the development and practice of science and engineering.[9] This algorithm is an instance of a large class of sampling algorithms, known as *Markov chain Monte Carlo (MCMC)* that have been proven to be excellent tools in statistics, econometrics, physics, and computing science.[10] It also served as the basis of the simulated annealing algorithm.[11] A variation of the Metropolis algorithm was later proposed by Barker[12] while the most notable generalization was introduced by Hastings[13] and studied further by Peskun.[14] Another famous generalization, also known as *the hit-and-run algorithm*, was proposed by Smith[15] and Schmeiser and Chen.[16,17]

In the years that followed, and as a result of the great potential of the technique, MC has found application in virtually every field of scientific research including biology, chemistry, computer science, economics and finance, engineering, material science and physics, while modern MC methods have been implemented to problems from numerical quadrature, to random walks, polymer and crystal growth, statistical physics, molecular simulation, bioinformatics, dynamic system analysis, statistical hypothesis testing, and many others.[2,3,18]

Molecular dynamics was first introduced as a method by Alder and Wainwright,[19,20] who studied the dynamics of an assembly of hard spheres.[21] Later, the group of Vineyard[22] implemented the technique to simulate radiation damage in crystalline Cu, which is reported as the first MD simulation of a real material, while the technique was applied for the simulation of a real liquid (argon) only four years later by Rahman.[23] Since then, MD simulations have become very powerful in treating complex physical systems with important applications to chemical physics, materials science, biochemistry, and biophysics.[2]

The obvious advantage of MD over MC is that it provides a route to dynamical properties of the system: transport coefficients, time-dependent responses to perturbations, rheological properties, and spectra.[1] On the other hand, MC is preferable in cases where one is interested in the study of the static properties of a system or in cases where detailed dynamics cannot feasibly approach the fully equilibrated behavior of a system, due to its long time behavior. As an intermediate solution, hybrid Monte Carlo (HMC) techniques have also been proposed that combine the advantages of both MC and MD.[24] For a more analytical description of MC and MD, the reader is encouraged to consult the excellent books[2−5,25−27] and review articles[1,8,21,28−32] that are available in the literature.

2. MONTE CARLO APPLICATIONS IN POLYMER SCIENCE

According to the above, a general assumption could be drawn that virtually any property of a many-body system—no matter how complex—that can be inferred via the description of a series of states occurring in a stochastic manner and under specific transition probabilities can be calculated by the implementation of the MC method. Considering the plethora of such systems and properties, the extremely powerful potential of the MC method is easily understood and its widespread penetration in all these different scientific fields is clearly justified. Some illustrative applications of the method include the predictions of a system's compositional and structural characteristics, thermodynamic properties, phase diagrams and free energies, diffusion and relaxation behavior and even the testing and modification of molecular-based theories. More significantly, MC methods are implemented in terms of a multiscale modeling framework as a tool to analyze the dependence of macro- or mesoscopic properties of the simulated systems on their molecular-level architecture and interactions.[8,33]

Polymer science has particularly profited by the potential of the MC method since the complexity of the chemical architecture and geometrical structure of the polymer macromolecules and the huge variability of their physical properties constitute their study a very difficult, if not impossible, task to accomplish by the use of conventional theoretical methods. Another great difficulty is imposed by the enormous spread of length and time scales involved in the study of polymers, which is mainly due to their macromolecular nature and may reach several orders of magnitude.[34]

Hence, the MC method has been extensively used in polymer science to study the structure and elastic response of polymer networks, the forces acting between polymer brushes, phase diagrams of polymer blends, etc.[34] It has also been employed for the study of the effect of the macromolecular chain nonlinearities (i.e., chain branching) on the structural, thermodynamic, conformational, and topological properties of polymers. This specific area has attracted considerable interest over the past two decades as it provides an insight to the "structure−property relationship" problem, a problem of profound and constantly increasing interest for the polymer industry. In this area, MC offers an approach that overcomes the difficulties of the commonly employed MD simulations, associated with the long relaxation times of the polymer chain segments. Such MC algorithms have been introduced since the 1980s[35] and have significantly improved since, with a range of different variations and novelties, mainly concerning the possible "moves" of the algorithm. They have been extensively applied for the simulation of linear chains of increasing size as well as for the simulation of nonlinear polymers containing either long- or short-chain branches and forming different types of shape (i.e., H-shape, star, pom-pom, etc.).[33,36−45]

Another important class of MC algorithms with specific application on dense polymer systems are the so-called lattice models, which are used to construct the possible configurations (e.g., of a polymer chain) on the specific coordinates of a lattice, thus simplifying the problem. A significant number of such algorithms has been based on the pioneering works of Verdier and Stockmayer[46] and Rosenbluth and Rosenbluth.[47] The latter is also known as the configurational bias MC (CBMC) method. These algorithms were very rapidly explored and upgraded by numerous researchers to deal with various problems of polymer physics. Details on the origins and the evolution of these methods can be found elsewhere.[8,34,48]

A MC method, based on the dynamic lattice liquid model (DLL), was recently implemented by Polanowski and coworkers[49] to simulate the synthesis of star polymers and subsequent gelation in ATRP living copolymerization. The same model (DLL) was previously applied by the same group to model the branching and gelation phenomena in

copolymerization of mono- and bifunctional monomers using ATRP, in bulk[50] and in diluted systems.[51] Hsu and Grassberger demonstrated the performance of a modification of the CBMC, known as the pruned-enriched Rosenbluth method (PERM), when applied to a series of significant problems of polymer physics.[52] Their study involved, among others, polymers in good solvents and at the Θ point, semistiff polymers, polymers in confining geometries, stretched polymers, star, bottle brush and randomly branched polymer models. The same group also tested two well-established lattice models to study the relation between the chemical architecture and the geometrical structure of bottle brush polymers.[53]

In earlier works, Binder and Paul,[54] provided an extensive review of lattice MC algorithms for the calculation of static equilibrium properties of polymers, placing the emphasis on the relatively novel developments on the field, while a comprehensive review of stochastic lattice models implemented for the description of the dynamics of linear polymers was also provided by van Leeuwen and Drzewiński.[55]

In similar indicative applications, MC has also been employed for the modeling of the hierarchical structure and phase behavior of polymer nanocomposites,[56,57] for the simulation of the glass transition of polymers,[58] for the study of the effects of the polydispersity of grafted polymers on nanoparticle surfaces,[59] for the investigation of the effect of the length of blocks in a grafted monomer sequence on the shape, size and structure of assembled nanoparticle clusters,[60] for the study of the structural and topological developments in step-growth polymerization systems[61] and for the simulation of the performance of polymer solar cells for photovoltaic applications.[62] Finally, stochastic-nature approaches have also been reported for the rheological behavior of polymer melts[63−65] and for the scheduling and optimal control of polymerization reactors.[66]

The majority of the studies mentioned above focus on the prediction of some properties of a system of macromolecular polymer chains of known characteristics (e.g., size, branching characteristics, etc.). Another important field of research, related rather to polymer chemistry than polymer physics, is concerned with the prediction of certain properties of a polymer product on the basis of its production procedure (i.e., the polymerization process) and the governing conditions. Naturally, stochastic MC methods have become an invaluable tool in this research area as well, especially in cases where the complexity or the dimensionality of the treated problem becomes a prohibitive factor for alternative, deterministic approaches.

In the remainder of the present work, this field of research will be highlighted via a presentation of the major contributions and of the most commonly employed stochastic approaches. This discussion will be subdivided according to the class of properties under investigation since, in the different length scales of a polymerization system (i.e., meso-, micro-, or nanoscale), the most important properties of interest are related to the number and size of the entities that are characteristic of the scale under investigation. Such entities may be the polymer particles in dispersed-phase polymerization or, in a lower scale of the same system, the monomer units that comprise the backbone and the branches of a single polymer chain. Finally, the calculated properties may be either average or distributed over one or more dimensions.

2.1. Particulate Processes−Prediction of the Particle Size Distribution. Particulate or dispersed-phase systems are very commonly encountered in various physicochemical processes of significant industrial importance, such as crystallization, combustion, polymerization and catalytic chemical processes. These systems are generally characterized by the particle size distribution (PSD), a property of paramount importance that controls key aspects of the process and affects the end-use properties of the product. PSDs are generally time-variant with respect to the mean particle size as well as with respect to their form (i.e., broadness or/and skewness, unimodal or/and bimodal character, etc.), due to the influence of different possible dynamic events or mechanisms. Such acting mechanisms may include coagulation/aggregation, breakage, growth, nucleation, deposition (settling), etc.

The most common approach for the calculation of the dynamic evolution of the PSD, under the actions of such events, is via the solution of the general population balance equation (PBE) of the process.[67] This approach is typically referred to as population balance modeling (PBM) and has initially appeared on diverse applications, including crystallization,[68] microbial cell population[69] and fluidized bed reactors.[70,71] In the general case, the system is commonly considered to be spatially homogeneous thus simplifying the form of the (spatially averaged) PBE. On the other hand, depending on the specific application, the PBE may be expressed in terms of one or more internal coordinates (i.e., properties of the entities/particles such as size, porosity, concentration, etc.) thus resulting in a mono- or multidimensional PSD.

Following the original developments of Hulburt and Katz and Ramkrishna, one can write a general form of a spatially averaged macroscopic PBE as:[72,73]

$$\frac{\partial n_v(V,t)}{\partial t} + \frac{\partial (G_v(V) n_v(V,t)}{\partial V} = (B_{agg}(V) + B_{br}(V)) - (D_{agg}(V) + D_{br}(V)) + S(V,t) \quad (1)$$

where n(V,t) dV denotes the number of particles per unit volume in the size range [V,V+dV], G(V) and S(V,t) are the particle volume growth and nucleation rates, respectively and the terms B(V) and D(V) represent the corresponding particle "birth" and "death" rates due to aggregation (indexed *agg*) and breakage (indexed *br*). These rates are expressed in terms of an integral form containing the respective mechanism kernels. Hence, key issues of the PBM are the mathematical expressions of the kernels that describe the dynamics of the acting mechanisms and, in turn, affect the final form of the partial integro-differential PBE and, hence, its numerical (or, in simplified cases, analytical) solution. Finally, in the multivariate form of the PBE, the particle number density function, n(V,t), and the respective rates are expressed in terms of one or more additional internal properties (i.e., n(V,x,...,t)).

In principle, one can distinguish different classes of numerical solution methods for the PBE. Under a very general perspective, these methods can be broadly classified into deterministic and stochastic or, more specifically, into the direct discretization methods (DDM), the moment methods (MM) and the Monte Carlo (MC) methods.[74] Evidently different classifications can also be proposed. Since the numerical solution of the PBE often requires the discretization of both time and, most importantly, the internal property domains,[75] the class of DDMs employ traditional discretization techniques

(e.g., finite elements, finite differences, etc.) directly for this purpose. A number of very well-known and powerful techniques belong in this category such as the sectional grid methods,[76] the finite elements methods[77,78] and the fixed pivot,[79] moving pivot[80] and moving grid[81] techniques.

The methods of moments, on the other hand, simply track the evolution of the PSD through a number of selected moments of the distribution. The MMs are characterized by minimum computational requirements and were the first to be applied for the solution of the PBE.[72] They can be further classified according to the closure technique and the selection of moments (e.g., generalized MMs, interpolative closure methods, etc.). For the above methods (i.e., DDMs and MMs), reviews and comparative studies are available in the literature.[74,82−88]

The alternative class of solution of the PBE is the probabilistic approach provided by the MC methods.[89−92] The simplest and most commonly employed MC method for PBM problems is the Direct Simulation Monte Carlo (DSMC) method, which was initially employed for the treatment of problems in gas dynamics.[93] The discrete and stochastic nature of the DSMC helps it adapt perfectly to the nature of the treated problems and overcomes the inconveniency of directly discretizing the solution domain.

During the application of the method, the simulated system is represented by a smaller sample subsystem whose size is crucial to the accuracy and efficiency of the simulation. This assignment of a number of physical particles to a single simulation particle, resulting from this sample selection, is an indirect discretization of the solution domain that naturally entrains an error. This error is inversely proportional to the computational demands of the simulation and becomes especially important in the most 'infrequent' areas of the domain (i.e., related to the rarest particles that commonly characterize the tail(s) of the PSD). This inherent disadvantage of the method becomes less important with the constant increase in computational power and is an acceptable weakness in comparison to the significant advantages of the method, mainly in terms of its simple and straightforward applicability to multivariate/multidimensional problems.[94−96]

The use of a sample population during the simulation is the source of another important issue on the application of the MC method to problems that are dominated either by particle formation (e.g., by nucleation or breakage) or by particle elimination (e.g., by coalescence), thus resulting in the net increase or decrease of the total size of the sample population and the corresponding decrease in the simulation efficiency or accuracy, respectively. To deal with this issue, it is necessary to perform adjusting actions on the size of the sample population in order to maintain it within a certain range. Hence, several techniques have been proposed to this end, which can be distinguished on the basis of whether these adjusting actions occur in a stepwise manner or continuously, as is the case in the constant volume MC (CVMC)[97,98] and the constant number MC,[99−101] respectively. Other similar techniques have also been proposed to deal with this issue.[102−112]

Another common classification of the MC techniques that are implemented for the simulation of dynamic particulate systems is based on the calculation of the time-step with respect to the occurring events. Accordingly, the DSMC can be distinguished into time-driven and event- driven. In time-driven MC techniques,[102,107] the time step is explicitly specified at each step of the simulation and is followed by the occurrence of all possible events that can take place within this time interval. Evidently, the selection of this time step is directly related to the time-scale of the events. On the other hand, in event-driven MC techniques[91,95,97,113−115] single events occur consecutively in the simulation, each being followed by the calculation of the time step that was required for its occurrence, on the basis of the known event probabilities. A connection between event-driven and time-driven techniques has been presented by Rajamani et al.[116] while comparative reviews for all the above techniques are also available.[98,117]

Often, the above methods of numerical solution of the PBE (i.e., both deterministic and stochastic) are evaluated in terms of accuracy and efficiency through their implementation to purely theoretical problems for which analytical solutions of the PBE exist.[118,119] In this case, theoretical models are used to describe the kernels of the acting particle mechanisms (i.e., aggregation, breakage, growth, etc.) while the initial PSD is arbitrary set to follow a statistical distribution (i.e., Gauss, exponential, etc.). Accordingly, the performance of different methods can be assessed for univariate or multivariate PBE problems.[86,99,102,120−127]

As an example, in Figure 1, the dynamic evolution of the univariate PSD is depicted under the action of Brownian-type

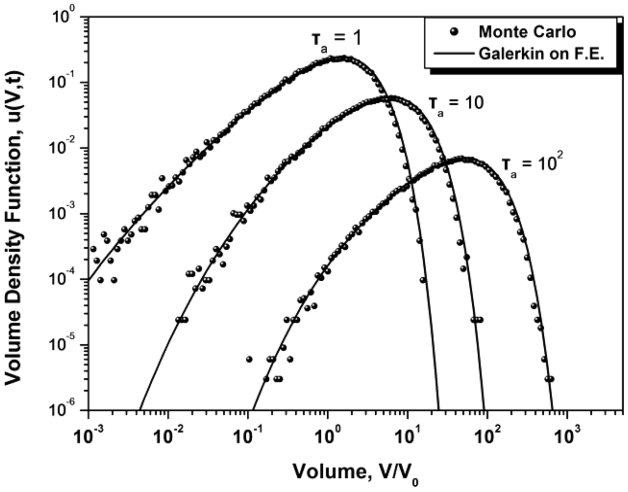

Figure 1. Dynamic evolution of the PSD under Brownian particle aggregation kernel, as calculated by the MC and Galerkin methods. Reprinted with permission from ref 125. Copyright 2006 Elsevier.

aggregation as calculated by the MC method and by the Galerkin on finite elements method for different aggregation times, τ_a (i.e., describing the extent of aggregation in the process).[125] In Figure 2, the corresponding bivariate PSD is depicted for constant particle aggregation.[126] Through these examples, the aforementioned issue of poor sampling of the edges of the PSD becomes evident, especially in the case of the bivariate PSD.

The MC method, in its different variations, has been extensively applied to a wide range of PSD problems and applications including aerosols,[107,113] aggregation/coalescence systems,[97,103,90,128] colloids and suspensions,[129] crystallization,[94,130] microbial systems,[131] liquid−liquid extraction,[111] and soot particle formation.[132−134]

In more recent studies, Khalili et al.[135] from the group of Matsoukas implemented the constant-number MC to a system that includes nucleation, coagulation, and surface deposition

dx.doi.org/10.1021/ie4033044 | Ind. Eng. Chem. Res. 2014, 53, 8963−8979

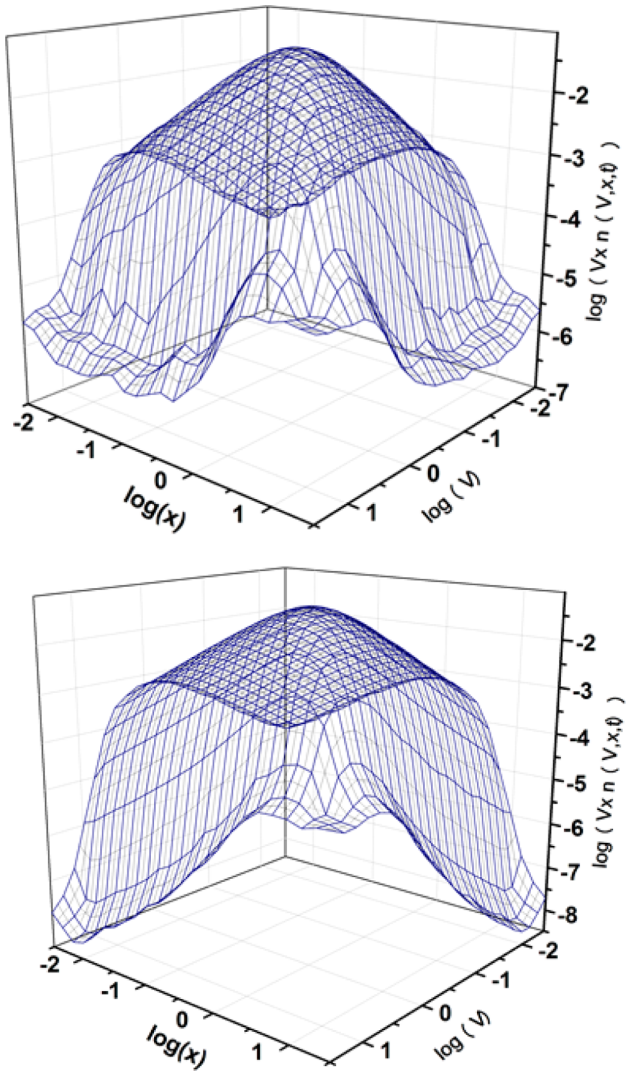

Figure 2. Bivariate PSDs under constant particle aggregation kernel ($\tau_\alpha = 1$): (a) Monte Carlo and (b) analytical solution. Reprinted with permission from ref 126. Copyright 2007 Elsevier.

coupled to a chemical reaction, in order to account for the multiple growth mechanisms. Irizarry[136] proposed a hybrid strategy for the stochastic simulation of systems in which the acting mechanisms display a substantial difference in terms of their rates (i.e., rates that are different by orders of magnitude). The group of Zhao, in 2009, proposed a new event-driven constant-volume (EDCV) MC algorithm for the description of the time evolution of the PSD in dispersed systems under the combined actions of several particle mechanisms and on the basis of a differentially weighting procedure of the simulation particles. Among the advantages of their proposed method are the increased efficiency and precision, with respect to other MC techniques,[137] as well as the reduction of the statistical noise produced in coagulation dominated processes.[138] The same group recently also proposed a novel MC method to simulate the evolution of the PSD in spatially inhomogeneous systems, by coupling the differentially weighted MC method with Eulerian−Lagrangian hydrodynamic models.[139]

A selection of stochastic weighted particle methods for the PBE under the actions of coagulation and growth was also presented by Patterson[140] while, in a similar approach, DeVille et al.[141] proposed the weighted flow algorithm (WFA) for particle coagulation problems. Terrazas-Velarde introduced in 2009 the concept of positions (CoP) in a study of agglomerate growth during fluidized bed spray agglomeration[142] in which a methodology is presented that includes continuous binder addition and drying. The CoP was later extended by the same group who also introduced a novel 3D structure algorithm for the description of spatial particle structures during spray fluidized bed agglomeration processes.[143] It should be noted that the idea of weighting particles in numerous variations has been explored by other researchers as well,[105−107,144−148] characteristic examples being the mass flow algorithm (MFA)[106] and the multi Monte Carlo (MMC) method.[108−110]

The evolution of the PSD is a subject of profound importance for dispersed polymerization processes as well, since many important properties of the produced polymer are directly related to this phase of the production. Thus, population balance modeling of polymerization reactors has been the subject of many studies since the 1970s,[149] with an emphasis clearly placed on the modeling of emulsion processes, mainly due to its industrial importance and increased complexity.[150−159] Reviews are available.[82,160,161]

Case study—MC Calculation of the PSD in Suspension Polymerization. Despite the vast amount of studies on the field, there is a surprising lack of MC approaches on the modeling of the PSD in dispersed polymerization systems. An exception is the publication of Saliakas and co-workers[162] who employed two different approaches, namely the fixed pivot technique and an event-driven MC method, for the prediction of the dynamic evolution of the droplet/particle size distribution (DSD/PSD) in both nonreactive liquid−liquid dispersions and the free-radical liquid(solid)−liquid suspension polymerization of methyl methacrylate (MMA), in terms of a comprehensive population balance model. The model predictions were compared with experimental measurements in the framework of a study of the effect of the various process conditions (i.e., agitation speed, temperature, surfactant concentration, and initial monomer volume fraction) on the evolution of the size of the polymerizing droplets/particles. The breakage and coalescence rate kernels of the dispersed monomer droplets/particles were expressed via the use of semiempirical and phenomenological expressions, in terms of the type and concentration of suspending agent, quality of agitation and evolution of the physical, thermodynamic, and transport properties of the polymerization system.[152] The effects of the mixture viscosity on the kinetic rate constants were also considered. As an example of this work, three characteristic results are presented here.

In Figure 3, the effect of agitation speed (i.e., 220, 300, and 500 rpm) on the Sauter mean diameter, D32, is depicted for the reactive free-radical polymerization case where the three different phases of polymerization (i.e., in terms of the average droplet/particle size) are presented; i.e., the initial phase of significant droplet breakage leading to a decrease in the mean size of the droplets, the second sticky phase where the viscosity of the dispersed phase increases and particle coalescence becomes the dominant mechanism (thus increasing the average particle size) and the final equilibration phase. It is also shown that an increase in the agitation speed results in an increase of the droplet breakage rate thus overall decreasing the average particle size.

In Figure 4, the effect of the surfactant concentration on the Sauter mean diameter, D32, is illustrated. It is shown that, in

dx.doi.org/10.1021/ie4033044 | Ind. Eng. Chem. Res. 2014, 53, 8963−8979

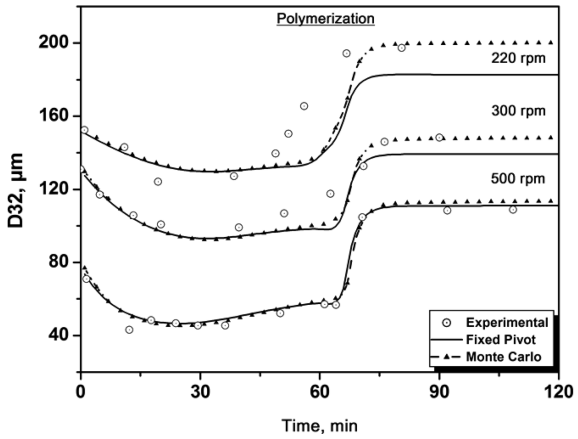

Figure 3. Effect of the agitation speed on the Sauter mean particle diameter in suspension polymerization of MMA. Reprinted with permission from ref 162. Copyright 2008 John Wiley and Sons.

both nonreactive liquid–liquid (lower curves) and reactive (upper curves) dispersions, higher stabilizer coverage results in a reduction of the coalescence rate and a subsequent decrease of the mean particle size. Finally, in Figure 5, an overview of the calculated PSDs at different instances of the polymerization is depicted in relation to the Sauter mean diameter, D32.

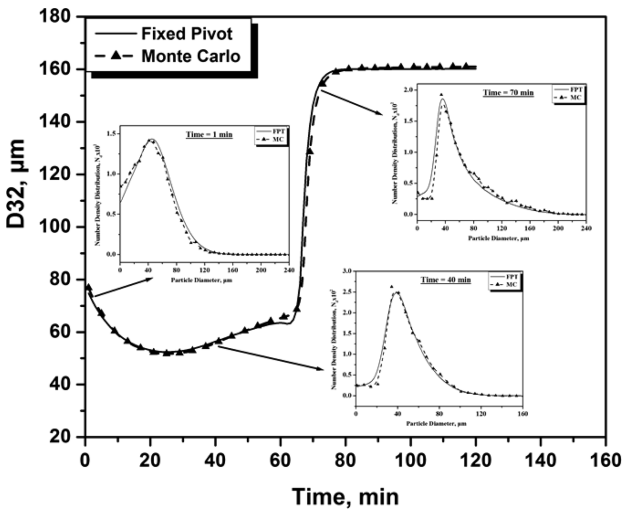

Figure 5. Model predictions and experimental measurements on the Sauter mean diameter and the dynamic evolution of the PSD in suspension polymerization of MMA. Reprinted with permission from ref 162. Copyright 2008 John Wiley and Sons.

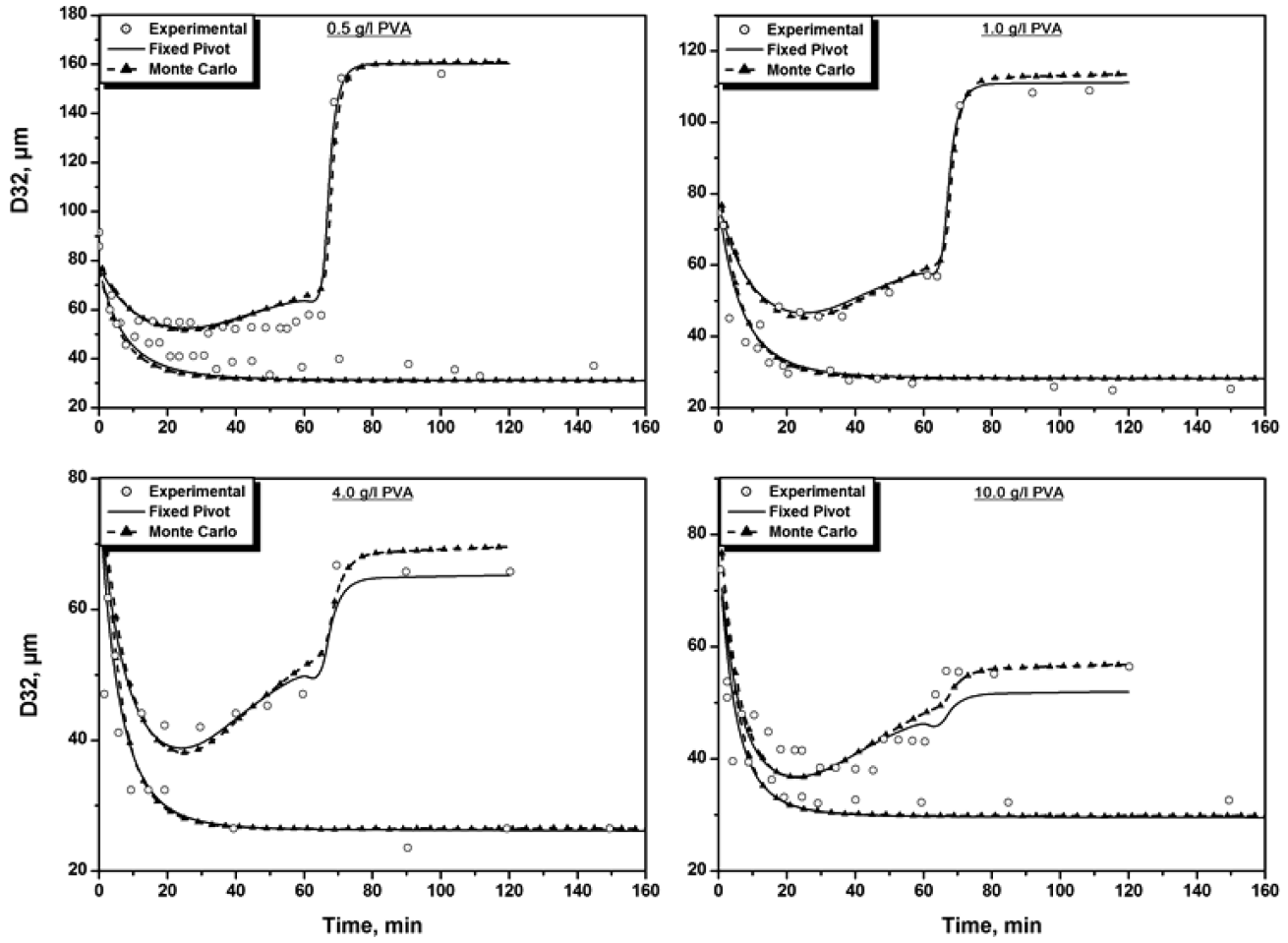

Figure 4. Effect of the stabilizer concentration (PVA) on the Sauter mean droplet/particle diameter for both nonreactive (lower curves) and reactive (upper curves) dispersions. Reprinted with permission from ref 162. Copyright 2008 John Wiley and Sons.

dx.doi.org/10.1021/ie4033044 | Ind. Eng. Chem. Res. 2014, 53, 8963–8979

2.2. Reactive Systems—Prediction of the Molecular Properties. Within the same framework, the MC method can be implemented on a lower scale (i.e., nanoscale) of a reactive system to predict the influence of the different process conditions (i.e., temperature, concentrations of the reactive species, etc.) on the molecular properties and characteristics of the final product. Such a study displays an evident interest for the polymer science due to the complex macromolecular character of the polymer chains that may possess a variety of compositional, architectural, topological, and conformational characteristics, which, in turn, influence significantly the end-use properties and application domain of the produced polymeric product.

A population balance approach can be implemented in this case as well. Accordingly, the corresponding PBE is expressed in terms of the number of polymer chains that are present in the reactive system, using as internal coordinates the size of the polymer chains (i.e., the degree of polymerization), the comonomer content (i.e., in the case of a copolymerization system), the number of branches, etc.[82] As a result, most of the numerical approaches that were mentioned in the previous section can be properly adjusted for the solution of this population balance problem as well. Among them, MC has gradually become the method of choice for an increasing number of researchers on the field.

The pioneering works of Gillespie[163] and Tobita[164] consist the two principal approaches for the stochastic simulation of the polymerization kinetics, on which the vast majority of existing stochastic simulation studies in this specific area of polymer science is based. Gillespie was the first to introduce an exact method for the stochastic simulation of spatially homogeneous chemical systems, also known as the *stochastic simulation algorithm (SSA)*, on the basis of the reaction probability density function.[163,165] It consists of an event-driven MC method where the different events (i.e., the chemical reactions) occur according to their instantaneous reaction probabilities, while the duration of each time-step, Δt, is calculated on the basis of the cumulative reaction rate of the system:

$$\Delta t = \left(\sum_{i=1}^{N_R} R_i\right)^{-1} \ln(\mathrm{rn}^{-1}) \tag{2}$$

In the above expression, rn is a randomly generated number from a uniform distribution in the range of [0, 1] and R_i denotes the stochastic reaction rate of the chemical reaction "i", calculated in terms of the corresponding kinetic rate constant, k_i, and the total number of possible combinations of the molecules involved in a reaction step, h_i:

$$R_i = k_i h_i; \qquad i = 1, 2, ..., N_R \tag{3}$$

N_R being the total number of chemical reactions of the system. Accordingly, the instantaneous reaction probability of the chemical reaction i will be calculated by the following expression:

$$P_i = R_i / \sum_{j=1}^{N_R} R_j \tag{4}$$

On the basis of this algorithm, Lu[166] studied the kinetics of polymerization systems that do not comply with the stationary state assumption, in a work that has been a reference point for later stochastic modeling studies of pulsed laser polymerization (PLP) systems. A few years later, Gillespie proposed a variation of the SSA, called the *τ-leap* method, which consists of an approximate procedure that can, in certain cases, significantly lower the computational demands of the simulation under acceptable losses in accuracy.[167]

The SSA has been used by numerous researchers for the simulation of various polymerization systems. Typical examples include PLP,[168,169] living free-radical polymerization,[170] cross-linking systems,[171] microemulsion polymerization,[172] and hyperbranched copolymerization systems in the presence of multifunctional initiators.[173,174] In more recent studies, Cai[175] extended Gillespie's SSA to account for chemical reaction in systems with delays, such as gene transcription and translation in living cells and Salami-Kalajahi et al.[176] studied the polymerization of ethylene over Ziegler−Natta catalysts and the molecular weight distribution (MWD) developments in terms of the active catalyst sites.

On the basis of Gillespie's formulation, the group of Soares has also made significant contribution in the area. Notably, Soares and Hamielec[177] used a dynamic MC simulation algorithm to validate an analytical solution of the description of the chain length distribution developments of polyolefins, produced by coordination catalysts at very short polymerization times. The same group also published a series of studies for the stochastic simulation of the polymerization kinetics and the successful prediction of the structural characteristics of polymers and copolymers produced in free-radical (FRP) or atom transfer radical polymerization (ATRP) systems, with the use of monofunctional or bifunctional initiators.[178−181]

Finally, Schutte and Wulkow presented a hybrid model, on the basis of a combination of a variation of the SSA with the Galerkin method, to exploit the advantages of both approaches in the solution of higher-dimensional population balances in polymerization systems.[182] The proposed approach is a pioneering work, in terms of actually integrating the two methods in a unique model, but, although simplified, still entails a high level of mathematical sophistication and complexity as well as certain inevitable assumptions in its application.

A characteristic example of the potential of the SSA can be illustrated via an application on the prediction of the bivariate properties of copolymerization systems. An MC method, based on the SSA, makes it possible to efficiently keep track of the dynamic evolution of the bivariate molecular weight−copolymer composition (MW−CC) characteristics of the growing copolymer chains in a copolymerization system in transient state. It can also directly track the chain sequence-length (CSL) characteristics of the copolymers without making use of expressions based on the kinetic rate constants and subject to assumptions. In Figure 6, the bivariate MW−CC distributions, as calculated by the MC method for the free-radical copolymerization system of styrene−methylmethacrylate (St−MMA)[183] are depicted for two different values of the initial comonomer content (i.e., 0.3 and 0.7) and a total monomer conversion of 93%. In Figure 7, the dynamic evolution of the MC calculated CSL distributions are depicted for eight different cases (i.e., four for each monomer type). This type of distributions can reveal very valuable information regarding the evolution of the copolymer composition characteristics in terms of the reactivity ratios and of the instantaneous comonomer content of the reaction mixture.

In a completely different approach, Tobita proposed a general method for the prediction of the macromolecular characteristics of the polymer chains in a polymerization

dx.doi.org/10.1021/ie4033044 | Ind. Eng. Chem. Res. 2014, 53, 8963−8979

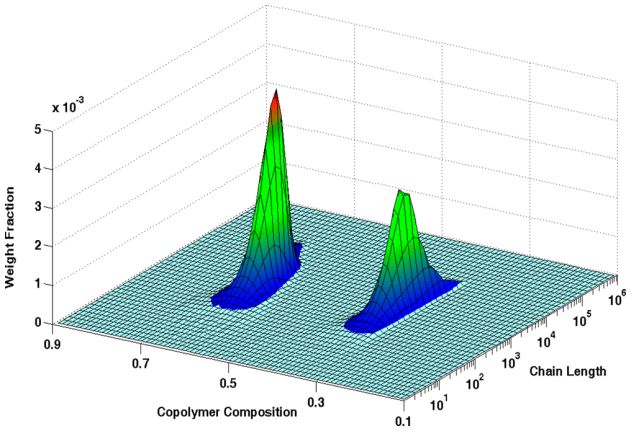

Figure 6. MC calculated bivariate (MW−CC) distribution at 93% converson of the St−MMA free-radical copolymerization system. Reprinted with permission from ref 183. Copyright 2008 Elsevier.

system, on the basis of the MC sampling and the use of appropriate density functions.[164] In fact, Tobita proposed a technique that takes into account the history-dependent structural characteristics of the macromolecular chains in a reacting system (i.e., on the basis of the monomer conversion), thus correcting this omission of the statistical model of Flory.[184] Accordingly, the polymer macromolecules are constructed in a stepwise manner, via the successive connection of linear polymer chain segments, called *primary polymer molecules*, whose structural characteristics are defined on the basis of distributional expressions (e.g., the most probable distribution for the chain length, the branching density distribution for the branches, etc.). Hence, any property related to the structural characteristics of the macromolecules can be directly inferred by this powerful technique, given that the required distribution functions can be accurately described for the system under study.

The exploitation of this technique, initially by Tobita and later by other researchers, has resulted in a massive production of studies and publications covering different cases and problems of polymer reaction engineering. These include the primary studies of Tobita on the branching and cross-linking in batch[164,185,186] and continuous[187] reactors, emulsion polymerization[188,189] and copolymerization,[190] studies on the degradation of polymer chains due to random scission,[191] cross-linked network formation,[192] and investigation of SEC (i.e., size exclusion chromatography) elution curves.[193−195] Later, Tobita updated his proposed random sampling technique by coupling it with the use of matrices and applying it to systems containing branching, cross-linking, and scission phenomena.[196−199] Another noteworthy extension was proposed by the same author to account for the general case of controlled/living radical polymerization systems in emulsified systems[200] with major applications on atom transfer radical polymerization (ATRP)[201] and reversible addition−fragmentation chain transfer polymerization (RAFT)[202,203] systems. Finally, in a most recent publication, the same MC technique is extended to account for simultaneous long-chain branching and scission reactions in a CSTR.[204]

Naturally, a number of researchers have used the MC technique proposed by Tobita in a number of studies of relevant polymerization systems. Notably, the group of Iedema has coupled this technique with the Galerkin method and the graph theory to predict the branching architectures of polymer chains produced in radical[205] and catalyzed polymerization systems.[206] After an extended series of related publications the same group recently presented a semianalytical approach on the basis of the MC sampling technique, to model simultaneous chain scission and branching, by assuming the separation of the scission and the branching problem as well as by considering known properties and identical branching and scission history

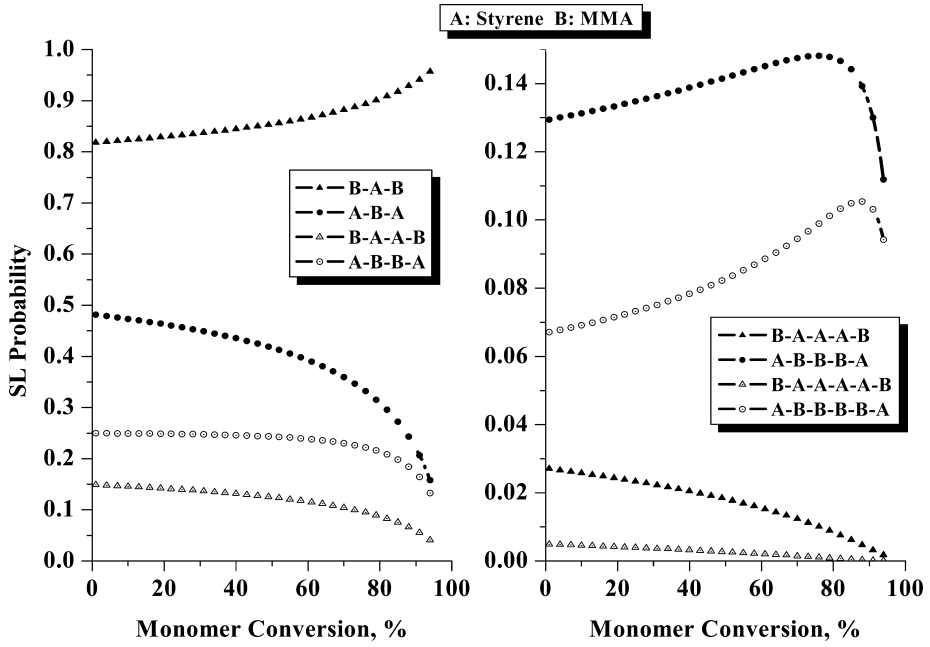

Figure 7. Evolution of the MC calculated (CSL) distributions of eight different comonomer sequences of the produced pSt−MMA copolymer. Reprinted with permission from ref 183. Copyright 2008 Elsevier.

dx.doi.org/10.1021/ie4033044 | *Ind. Eng. Chem. Res.* 2014, 53, 8963−8979

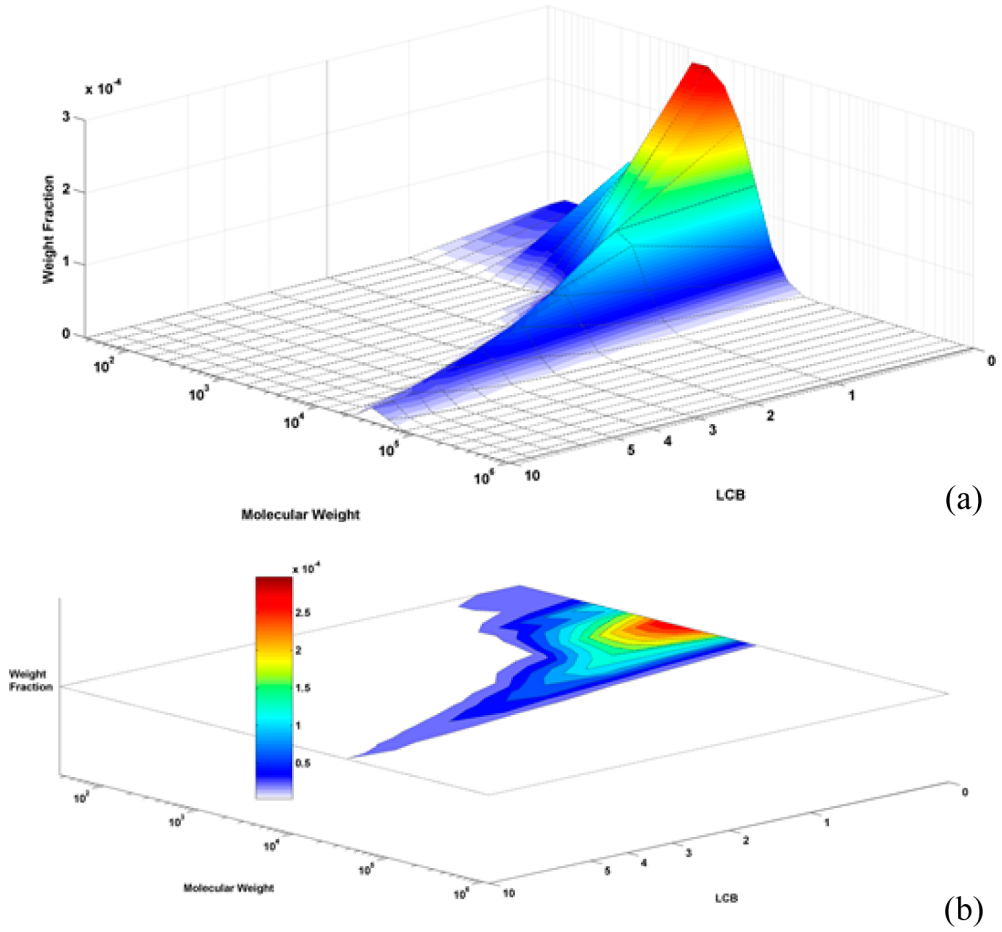

Figure 8. Calculated (a) 2D joint (LCB-MW) distribution and (b) respective contour plots of LDPE at the reactor exit, using a sample population of 4.9×10^4 branched polymer chains. Reprinted with permission from ref 224. Copyright 2010 American Chemical Society.

for all primary polymer chain segments.[207] A variation of this MC technique was also recently proposed by the same author for the study of the reactive processing of high-density polyethylene (HDPE).[208] Other researchers applied the MC algorithm of Tobita on different polymer problems, most notably emulsion systems[209−211] and ATRP copolymerization systems.[212]

Different MC approaches have also been proposed for the modeling of polymerization systems, notably the works of O'Driscoll and Manders on the simulation of PLP[213,214] and the studies that followed on their basis[215] as well as the combinatorial MC method of Platkowski and Reichert.[216] Soares also proposed a MC technique to model the fractionation process in crystallization analysis fractionation (CRYSTAF) experiments.[217,218] Finally, it should be mentioned that significant developments have also been reported on the increase of the efficiency of the stochastic simulation of reacting systems.[219,220]

Case Study—MC Calculation of the Molecular Properties of LDPE. In a number of studies (e.g., the works of Iedema[221] and Wulkow[182]), it is claimed that the calculation of the architectural characteristics of the polymer chains (i.e., the branching and connection point details), via the MC method, becomes prohibitive in the case of large polymer chains, due to the excessive number of required simulation chains that significantly slows down the computer simulation to infeasible levels. As a result, they resort to alternative solutions based on the combination of the MC method with deterministic approaches, commonly under several assumptions regarding the distributed forms of the various chain length fragments of the polymer chains. These approaches, although novel and, in many cases, effective, virtually abolish one of the primary advantages of the use of the MC method, i.e., its simplicity and generality in application to complex multivariate problems. In fact, the proposed methods are usually mathematically complicated, tailored to a specific kinetic scheme and strongly dependent on the adopted distributional and discretizational assumptions.

It should also be kept in mind that the relative advantage of such approaches (i.e., the increased computational efficiency) is actually based on a defect of the MC method that is not invariant but increasingly improving in parallel to the continuous increase of the computational capacity of modern computers. In fact, it has been shown, in a series of recent publications, that the MC method can be implemented in a way that will provide the complete architectural characteristics of highly branched and extremely long polymer chains with high accuracy and under absolutely tolerable computational times, without making use of any kind of additional assumptions or simplifications.[183,222,223]

Such a kinetic/topological MC algorithm was implemented for the calculation of the complete molecular weight−branching number−branching position−branching size distribution of low-density polyethylene (LDPE) polymer chains produced in

dx.doi.org/10.1021/ie4033044 | *Ind. Eng. Chem. Res.* 2014, 53, 8963−8979

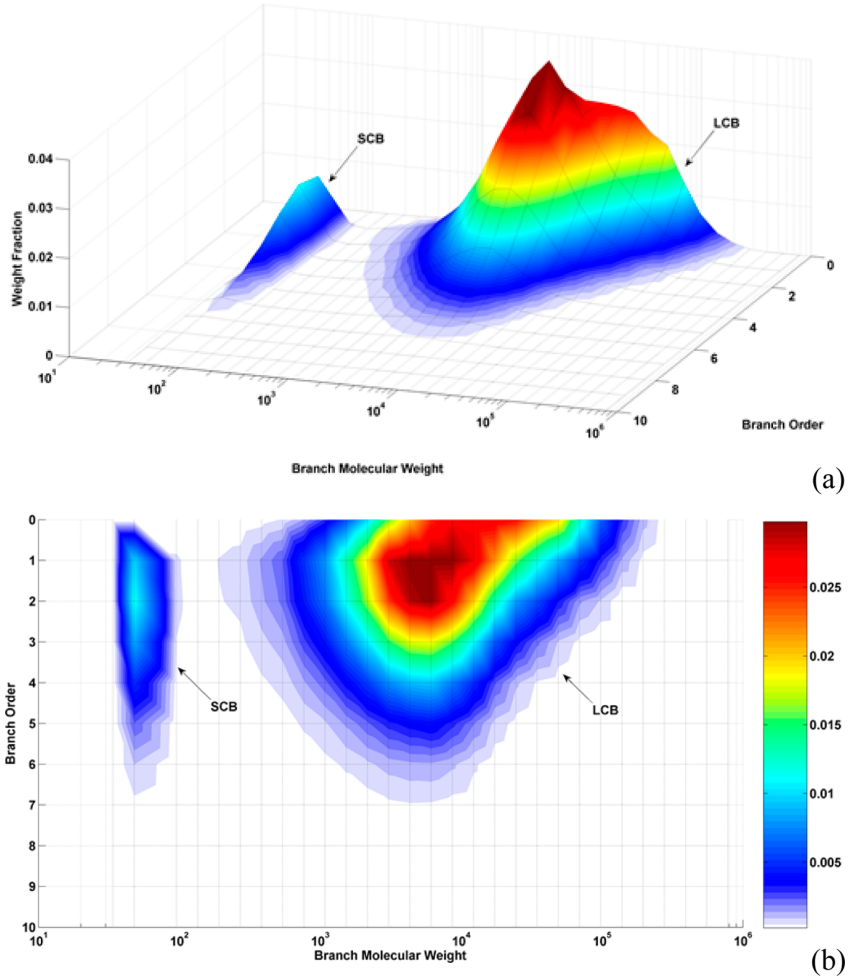

Figure 9. Calculated (a) bivariate (BO-BMW) distribution and (b) respective contour plots of LDPE at the reactor exit, using a sample population of 4.9×10^4 branched polymer chains. Reprinted with permission from ref 224. Copyright 2010 American Chemical Society.

industrial high-pressure tubular reactors.[224−226] These polymer chains are known to be extremely branched and of high molecular weight. Accordingly, for the successful prediction of the analytical topological characteristics of a population of 67×10^3 polymer chains of a maximum chain length of approximately 113×10^3 monomer units and a maximum branching degree (i.e., number of branches on a unique polymer chain) that exceeded 2850 branches, a typical personal computer (2.21 GHz dual-core AMD processor) required a simulation time of 111 min. The exact same simulation, on a slightly more powerful personal computer (2.4 GHz dual-CPU quad-core Intel Xeon processor), presented a reduction in the simulation time of the order of 40% (i.e., 67 min). Clearly, a simulation time of this order for the prediction of the exact topological characteristics of such a large sample of highly branched polymer chains cannot be considered prohibitive for any type of off-line simulation purposes, especially taking into account that the test was performed on personal computers and not on more powerful processing units (i.e., servers or clusters), which are expected to further improve the simulation efficiency.

The proposed MC approach was based on the SSA of Gillespie[163] for the simulation of the kinetic developments of the polymerization, coupled with a novel, simple and very powerful algorithm for the simulation of the topological developments in terms of the architecture of the polymer chains. This novel topological algorithm was based on the very simple principle of mimicking the topological changes produced by the stochastically occurring chemical reactions of randomly selected polymer chains, always in complete conjunction with the polymerization kinetic scheme and mechanism and without the prerequisite of any type of distributional expressions. At the same time, the simulation remains completely flexible and modular in terms of the number and type of chemical reactions that participate in the kinetic scheme as well as in terms of the level of detailed molecular information that is provided by the model. Some representative results of this work are presented next.

In Figure 8, the 2D long-chain branching-molecular weight (LCB-MW) distribution of LDPE is depicted, as calculated at the exit of an industrial reactor of length of 1040 m.[224] This type of distribution provides detailed information on the number of long-chain branches of the polymer chains with respect to their molecular weight. The contour plots of the distribution, depicted right below it, provide an alternative representation of this distribution that reveals very useful information in terms of the size and the branching density of the polymer chains.

In Figure 9, the respective bivariate branching order-branch molecular weight (BO-BMW) distribution[224] is depicted for the same population of LDPE chains. This type of distribution

dx.doi.org/10.1021/ie4033044 | Ind. Eng. Chem. Res. 2014, 53, 8963−8979

provides complementary information with respect to the "branching order levels" of the long- and short-chain branches of the polymer chains, which are clearly distinguished on the graph in terms of their different molecular weight.

The detailed topological information provided by this MC approach, can be further exploited in terms of a simple stochastic random walk algorithm to calculate additional properties related to the spatial configurations of the polymer chains (e.g., the radius of gyration, the hydrodynamic radius, the branching factor *g*, etc.).[224] As an example, in Figure 10, the

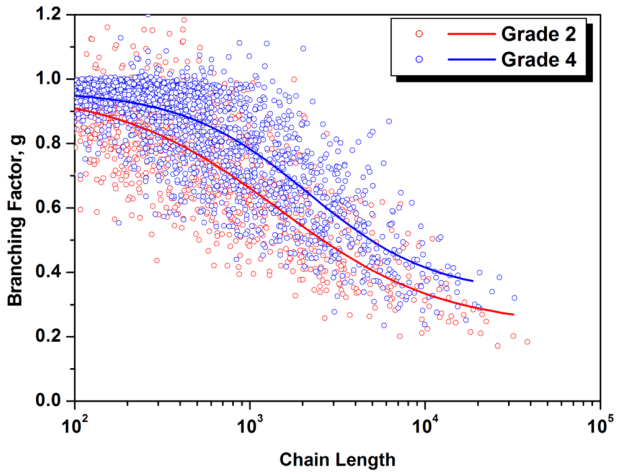

Figure 10. Variation of the average branching factor, *g*, with respect to PE chain length, calculated at the reactor exit for two industrial grades, using a sample population of 8.98 × 10^4 and 1.18 × 10^5 branched polymer chains, respectively. Reprinted with permission from ref 226. Copyright 2011 Elsevier.

variation of the branching factor, g, is depicted for two different LDPE grades, with respect to the polymer chain length and in terms of the polymerization temperature (i.e., a difference in the respective temperature pick of approximately 60 °C).[226] The continuous curves represent an average of the MC simulation discrete points. It is shown that an increase in the temperature (red points and curve) results in an increase in the LCB content of the polymer chains that results in a respective decrease of the average branching factor, *g*.

2.3. Extension to Rheology—Prediction of the Viscoelastic Properties of Polymers. The topological characteristics of branched polymer chains are directly related to the rheological behavior of the produced polymer, with significant implications on its processability and applicability. Hence, the accurate prediction of these characteristics in terms of the process conditions, as shown in the previous section, becomes even more important, as it can be directly utilized in an attempt to predict and control the rheology of highly branched polymers.

In the open literature, a number of publications deal with the mathematical modeling of the viscoelastic behavior of polymers in terms of the polymer molecular weight[227−229] or the branched chain microstructure.[230−234] Among them, the so-called "branch-on-branch" model of Das and co-workers[234] is specifically suitable for the simulation of the rheological behavior of randomly branched polymer chains, as is the case of LDPE. Evidently, the main drawback of these studies is the lack of information on the exact topological characteristics of polymers produced in nontrivial, complex polymerization processes.

In 2010, the viscosity−frequency curves of a series of three industrial LDPE grades (see Figure 11) have been successfully

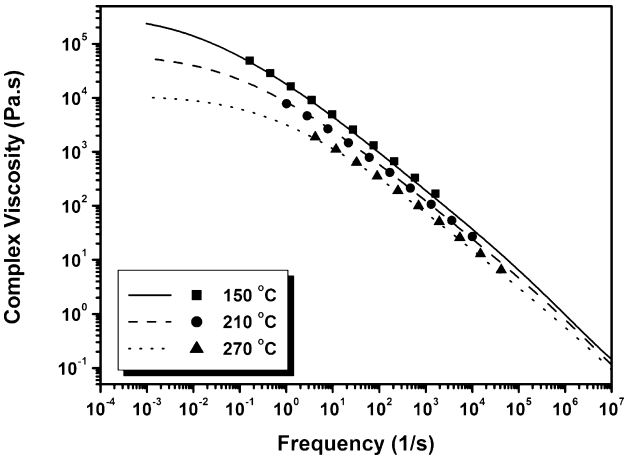

Figure 11. Predicted and experimental (viscosity−frequency) curves of LDPE produced in an industrial high-pressure tubular reactor (curves: simulation, points: experimental). Reprinted with permission from ref 225. Copyright 2010 John Wiley and Sons.

predicted by simply feeding the results of the aforementioned kinetic/topological MC simulation algorithm[224] on the rheological model of Das[234] and using the rheological model parameters provided for the system in the open literature.[225] An extension of this work is also under publication.[235] As can be seen in Figure 11, the predictions of the model where in excellent agreement with the respective industrial data, for all three studied temperatures.[225]

One year later, Read and his co-workers[236] published a similar approach for the prediction of the rheological behavior of LDPE. A good agreement was presented between simulation and experiment for the linear rheological response and nonlinear transient viscosity growth curves in uniaxial extension and shear. However, their MC model, which was based on the technique of Tobita, did not account for the topological developments of the polymer chains in terms of the actual industrial process conditions. Instead, a fitting procedure was followed in terms of the experimental MWD and branching index, *g*, by considering a weighted sum of different batch reactor simulations. In this respect, the predictive capabilities of their model were directly dependent on an a-priori knowledge of these polymer properties, a drawback that is completely absent from the proposed combined approach presented previously.[225]

3. CONCLUDING REMARKS

Almost 60 years have already passed since the invention and initial applications of the Monte Carlo method, during which it has undoubtedly evolved to an extremely powerful tool in the hands of many researchers of very different fields. The solution of important problems in mathematics, material science, biology or economics is just a small evidence of the potential of the MC method which is under continuous development and expansion of its application span.

Polymer science has especially profited by this class of stochastic techniques that is perfectly adaptable to the discrete

dx.doi.org/10.1021/ie4033044 | Ind. Eng. Chem. Res. 2014, 53, 8963−8979

and stochastic nature characterizing the majority of the treated problems. The individual macromolecular nature of the polymer molecules and the extreme spread of length and time scales that may be encountered in a single polymer system, often pose such modeling difficulties that would be impossible to handle via nonstochastic approaches.

In the present work, an emphasis has been given in the presentation of specific MC techniques that can be applied for the successful modeling of a dynamically evolving polymerization process in order to track the evolution of key particle-size or molecular-size properties of the produced polymer in terms of the process conditions and characteristics. When applied to the molecular nanoscale, the MC method can be used to accurately follow the topological developments that occur on the microstructure of the growing polymer macromolecules, due to their participation in the chemical reactions that constitute the polymerization kinetic scheme.

The latest developments in the area have made it possible to establish a clear theoretical connection between the polymer chain microstructure and the viscoelastic behavior of the produced polymer, thus revealing new paths toward the design and control of the end-use properties of polymeric products via an optimal selection/regulation of the macroscopic production process characteristics.

The MC method has played a catalytic role toward the developments that are briefly described in this work (as well as toward innumerous others) and, by following its evolution over its relatively short lifetime, it is safe to assume that many new breakthroughs are yet to be expected by the use of this powerful technique.

AUTHOR INFORMATION

Corresponding Author

*Tel.: + 30 2310 996211. Fax: +30 2310 996198. E-mail: cypress@cperi.certh.gr.

Notes

The authors declare no competing financial interest.

REFERENCES

(1) Allen, M. P. Introduction to Molecular Dynamics Simulation. *Comput. Soft Matter—Synth. Polym. Proteins* **2004**, *23*, 1−28.

(2) Liu, J. S. *Monte Carlo Strategies in Scientific Computing*; Springer: Cambridge, MA, 2001.

(3) Lim, C.; Nebus, J. *Vorticity, Statistical Mechanics, and Monte Carlo Simulation*; Springer: New York, 2007.

(4) Rubinstein, R. Y. *Simulation and the Monte Carlo Method*; John Wiley & Sons: New York, 2009.

(5) Sobol', I. M. *A Primer for the Monte Carlo Method*; CRC Press: Boca Raton, 1994.

(6) Hammersley, J. M.; Handscomb, D. C. *Monte Carlo Methods*; John Wiley & Sons: New York, 1964.

(7) Metropolis, N.; Rosenbluth, A. W.; Rosenbluth, M. N.; Teller, A. H.; Teller, E. Equation of State Calculations by Fast Computing Machines. *J. Chem. Phys.* **1953**, *21*, 1087−1092.

(8) Theodorou, D. N. Progress and Outlook in Monte Carlo Simulations. *Ind. Eng. Chem. Res.* **2010**, *49*, 3047−3058.

(9) Beichl, I.; Sullivan, F. The Metropolis Algorithm. *Comput. Sci. Eng.* **2000**, *2*, 65−69.

(10) Andrieu, C.; De Freitas, N.; Doucet, A.; Jordan, M. I. An Introduction to MCMC for Machine Learning. *Mach. Learn.* **2003**, *50*, 5−43.

(11) Kirkpatrick, S.; Gelatt, C. D.; Vecchi, M. P. Optimization by Simulated Annealing. *Science* **1983**, *220*, 671−680.

(12) Barker, A. A. Monte Carlo Calculations of the Radial Distribution Functions for a Proton-electron Plasma. *Aust. J. Phys.* **1965**, *18*, 119−133.

(13) Hastings, W. K. Monte Carlo Sampling Methods Using Markov Chains and Their Applications. *Biometrika* **1970**, *57*, 97−109.

(14) Peskun, P. H. Optimum Monte-Carlo Sampling Using Markov Chains. *Biometrika* **1973**, *60*, 607−612.

(15) Smith, R. L. Efficient Monte Carlo Procedures for Generating Points Uniformly Distributed over Bounded Regions. *Oper. Res.* **1984**, *32*, 1296−1308.

(16) Schmeiser, B. W.; Chen, M.-H. *On Hit-and-Run Monte Carlo Sampling for Evaluating Multidimensional Integrals*; Technical Report 91-39; Purdue University, Department of Statistics, 1991.

(17) Chen, M.-H.; Schmeiser, B. W. General Hit-and-Run Monte Carlo Sampling for Evaluating Multidimensional Integrals. *Oper. Res. Lett.* **1996**, *19*, 161−169.

(18) Dagpunar, J. S. *Simulation and Monte Carlo: With Applications in Finance and MCMC*; John Wiley & Sons, Ltd: Chichester, UK, 2007.

(19) Alder, B. J.; Wainwright, T. E. Phase Transition for a Hard Sphere System. *J. Chem. Phys.* **1957**, *27*, 1208−1209.

(20) Alder, B. J.; Wainwright, T. E. Studies in Molecular Dynamics. I. General Method. *J. Chem. Phys.* **1959**, *31*, 459−466.

(21) Frenkel, D. Introduction to Monte Carlo Methods. *Comput. Soft Matter Synth. Polym. Proteins* **2004**, *23*, 29−60.

(22) Gibson, J. B.; Goland, A. N.; Milgram, M.; Vineyard, G. H. Dynamics of Radiation Damage. *Phys. Rev.* **1960**, *120*, 1229−1253.

(23) Rahman, A. Correlations in the Motion of Atoms in Liquid Argon. *Phys. Rev.* **1964**, *136*, A405−A411.

(24) Duane, S.; Kennedy, A. D.; Pendleton, B. J.; Roweth, D. Hybrid Monte Carlo. *Phys. Lett. B* **1987**, *195*, 216−222.

(25) Chen, M.-H.; Shao, Q.-M.; Ibrahim, J. G. *Monte Carlo Methods in Bayesian Computation*; Springer: New York, 2000.

(26) Gilks, W.; Richardson, S.; Spiegelhalter, D. *Markov Chain Monte Carlo in Practice*; Chapman & Hall: London, 1995.

(27) Robert, C. P.; Casella. *Monte Carlo Statistical Methods*; Springer: New York, 2004.

(28) Tierney, L. Markov-Chains for Exploring Posterior Distributions. *Ann. Stat.* **1994**, *22*, 1701−1728.

(29) Besag, J.; Green, P.; Higdon, D.; Mengersen, K. Bayesian Computation and Stochastic-Systems. *Stat. Sci.* **1995**, *10*, 3−41.

(30) Brooks, S. Markov Chain Monte Carlo Method and Its Application. *J. R. Stat. Soc. Ser. Stat.* **1998**, *47*, 69−100.

(31) Diaconis, P.; Saloff-Coste, L. What Do We Know About the Metropolis Algorithm? *J. Comput. Syst. Sci.* **1998**, *57*, 20−36.

(32) Gubbins, K. E.; Moore, J. D. Molecular Modeling of Matter: Impact and Prospects in Engineering. *Ind. Eng. Chem. Res.* **2010**, *49*, 3026−3046.

(33) Baig, C.; Alexiadis, O.; Mavrantzas, V. G. Advanced Monte Carlo Algorithm for the Atomistic Simulation of Short- and Long-Chain Branched Polymers: Implementation for Model H-Shaped, A_3AA_3 Multiarm (Pom-Pom), and Short-Chain Branched Polyethylene Melts. *Macromolecules* **2010**, *43*, 986−1002.

(34) Binder, K. *Monte Carlo and Molecular Dynamics Simulations in Polymer Science*; Oxford University Press: New York, 1995.

(35) Olaj, O. F.; Lantschbauer, W. Simulation of Chain Arrangement in Bulk Polymer, 1. Chain Dimensions and Distribution of the End-to-end Distance. *Makromol. Chem. Rapid Commun.* **1982**, *3*, 847−858.

(36) De Pablo, J. J.; Laso, M.; Suter, U. W. Simulation of Polyethylene Above and Below the Melting Point. *J. Chem. Phys.* **1992**, *96*, 2395−2403.

(37) Siepmann, J. I.; Frenkel, D. Configurational Bias Monte Carlo: a New Sampling Scheme for Flexible Chains. *Mol. Phys.* **1992**, *75*, 59−70.

(38) Dodd, L. R.; Boone, T. D.; Theodorou, D. N. A Concerted Rotation Algorithm for Atomistic Monte Carlo Simulation of Polymer Melts and Glasses. *Mol. Phys.* **1993**, *78*, 961−996.

(39) Leontidis, E.; de Pablo, J. J.; Laso, M.; Suter, U. W. A Critical Evaluation of Novel Algorithms for the Off-lattice Monte Carlo Simulation of Condensed Polymer Phases. In *Atomistic Modeling of*

Physical Properties; Monnerie, P. D. L., Suter, P. D. U. W., Eds.; Advances in Polymer Science; Springer: Berlin Heidelberg, 1994; pp 283−318.
(40) Pant, P. V. K.; Theodorou, D. N. Variable Connectivity Method for the Atomistic Monte Carlo Simulation of Polydisperse Polymer Melts. *Macromolecules* **1995**, *28*, 7224−7234.
(41) Karayiannis, N. C.; Mavrantzas, V. G.; Theodorou, D. N. A Novel Monte Carlo Scheme for the Rapid Equilibration of Atomistic Model Polymer Systems of Precisely Defined Molecular Architecture. *Phys. Rev. Lett.* **2002**, *88*, 105503-1−105503-4.
(42) Daoulas, K. C.; Harmandaris, V. A.; Mavrantzas, V. G. Detailed Atomistic Simulation of a Polymer Melt/Solid Interface: Structure, Density, and Conformation of a Thin Film of Polyethylene Melt Adsorbed on Graphite. *Macromolecules* **2005**, *38*, 5780−5795.
(43) Alexiadis, O.; Daoulas, K. C.; Mavrantzas, V. G. An Efficient Monte Carlo Algorithm for the Fast Equilibration and Atomistic Simulation of Alkanethiol Self-Assembled Monolayers on a Au(111) Substrate. *J. Phys. Chem. B* **2008**, *112*, 1198−1211.
(44) Cortés, J.; Carrión, S.; Curcó, D.; Renaud, M.; Alemán, C. Relaxation of Amorphous Multichain Polymer Systems Using Inverse Kinematics. *Polymer* **2010**, *51*, 4008−4014.
(45) Ivanov, V. A.; Martemyanova, J. A.; Rodionova, A. S.; Stukan, M. R. Computer Simulation of Stiff-chain Polymers. *Polym. Sci. Ser. C* **2013**, *55*, 4−22.
(46) Verdier, P. H.; Stockmayer, W. H. Monte Carlo Calculations on the Dynamics of Polymers in Dilute Solution. *J. Chem. Phys.* **1962**, *36*, 227−235.
(47) Rosenbluth, M. N.; Rosenbluth, A. W. Monte Carlo Calculation of the Average Extension of Molecular Chains. *J. Chem. Phys.* **1955**, *23*, 356−359.
(48) Vanderzande, C. *Lattice Models of Polymers*; Cambridge University Press, 1998.
(49) Polanowski, P.; Jeszka, J. K.; Matyjaszewski, K. Star Polymer Synthesis and Gelation in ATRP Copolymerization: Monte Carlo Simulations. *Polymer* **2013**, *54*, 1979−1986.
(50) Polanowski, P.; Jeszka, J. K.; Matyjaszewski, K. Modeling of Branching and Gelation in Living Copolymerization of Monomer and Divinyl Cross-linker Using Dynamic Lattice Liquid Model (DLL) and Flory−Stockmayer Model. *Polymer* **2010**, *51*, 6084−6092.
(51) Polanowski, P.; Jeszka, J. K.; Li, W.; Matyjaszewski, K. Effect of Dilution on Branching and Gelation in Living Copolymerization of Monomer and Divinyl Cross-linker: Modeling Using Dynamic Lattice Liquid Model (DLL) and Flory−Stockmayer (FS) Model. *Polymer* **2011**, *52*, 5092−5101.
(52) Hsu, H.-P.; Grassberger, P. A Review of Monte Carlo Simulations of Polymers with PERM. *J. Stat. Phys.* **2011**, *144*, 597−637.
(53) Hsu, H.-P.; Paul, W.; Binder, K. Understanding the Multiple Length Scales Describing the Structure of Bottle-brush Polymers by Monte Carlo Simulation Methods. *Macromol. Theory Simul.* **2011**, *20*, 510−525.
(54) Binder, K.; Paul, W. Recent Developments in Monte Carlo Simulations of Lattice Models for Polymer Systems. *Macromolecules* **2008**, *41*, 4537−4550.
(55) Van Leeuwen, J. M. J.; Drzewiński, A. Stochastic Lattice Models for the Dynamics of Linear Polymers. *Phys. Rep.* **2009**, *475*, 53−90.
(56) Zeng, Q. H.; Yu, A. B.; Lu, G. Q. Multiscale Modeling and Simulation of Polymer Nanocomposites. *Prog. Polym. Sci.* **2008**, *33*, 191−269.
(57) Jayaraman, A.; Nair, N. Integrating PRISM Theory and Monte Carlo Simulation to Study Polymer-functionalised Particles and Polymer Nanocomposites. *Mol. Simul.* **2012**, *38*, 751−761.
(58) Baschnagel, J. The Glass Transition in Polymer Melts: a Review of Recent Monte Carlo Results. *J. Phys.: Condens. Matter* **1996**, *8*, 9599−9603.
(59) Dodd, P. M.; Jayaraman, A. Monte Carlo Simulations of Polydisperse Polymers Grafted on Spherical Surfaces. *J. Polym. Sci., Part B: Polym. Phys.* **2012**, *50*, 694−705.
(60) Martin, T. B.; McKinney, C.; Jayaraman, A. Effect of Blockiness in Grafted Monomer Sequences on Assembly of Copolymer Grafted Nanoparticles: a Monte Carlo Simulation Study. *Soft Matter* **2013**, *9*, 155−169.
(61) Hillegers, L. T.; Kapnistos, M.; Nijenhuis, A.; Slot, J. J. M.; Steeman, P. A. M. Monte Carlo Simulation of Randomly Branched Step-Growth Polymers: Generation and Analysis of Representative Molecular Ensembles. *Macromol. Theory Simul.* **2011**, *20*, 219−229.
(62) Meng, L.; Shang, Y.; Li, Q.; Li, Y.; Zhan, X.; Shuai, Z.; Kimber, R. G. E.; Walker, A. B. Dynamic Monte Carlo Simulation for Highly Efficient Polymer Blend Photovoltaics. *J. Phys. Chem. B* **2010**, *114*, 36−41.
(63) Xu, F.; Denn, M. M.; Schieber, J. D. A Full-chain Stochastic Tube Model for Entangled Melts and Solutions of Linear Polymers. *J. Rheol.* **2006**, *50*, 477−494.
(64) Xu, F.; Denn, M. M.; Schieber, J. D. Stochastic Chain Simulation of Wall Slip in Entangled Polymer Melts. *J. Rheol.* **2007**, *51*, 451−464.
(65) Park, J.; Mead, D. W.; Denn, M. M. Stochastic Simulation of Entangled Polymeric Liquids in Fast Flows: Microstructure Modification. *J. Rheol.* **2012**, *56*, 1057−1081.
(66) Terrazas-Moreno, S.; Flores-Tlacuahuac, A.; Grossmann, I. E. Simultaneous Design, Scheduling, and Optimal Control of a Methyl-methacrylate Continuous Polymerization Reactor. *AIChE J.* **2008**, *54*, 3160−3170.
(67) Ramkrishna, D. *Population Balances: Theory and Applications to Particulate Systems in Engineering*; Academic Press: San Diego, CA, 2000.
(68) Randolph, A. D.; Larson, M. A. Transient and Steady State Size Distributions in Continuous Mixed Suspension Crystallizers. *AIChE J.* **1962**, *8*, 639−645.
(69) Fredrickson, A. G.; Tsuchiya, H. M. Continuous Propagation of Microorganisms. *AIChE J.* **1963**, *9*, 459−468.
(70) Behnken, D. W.; Horowitz, J.; Katz, S. Particle Growth Processes. *Ind. Eng. Chem. Fundam.* **1963**, *2*, 212−216.
(71) Randolph, A. D. A Population Balance for Countable Entities. *Can. J. Chem. Eng.* **1964**, *42*, 280−281.
(72) Hulburt, H. M.; Katz, S. Some Problems in Particle Technology: A Statistical Mechanical Formulation. *Chem. Eng. Sci.* **1964**, *19*, 555−574.
(73) Ramkrishna, D. The Status of Population Balances. *Rev. Chem. Eng.* **1985**, *3*, 49−95.
(74) Su, J.; Gu, Z.; Xu, X. Y. Advances in Numerical Methods for the Solution of Population Balance Equations for Disperse Phase Systems. *Sci. China Ser. B Chem.* **2009**, *52*, 1063−1079.
(75) Kumar, J.; Peglow, M.; Warnecke, G.; Heinrich, S. An Efficient Numerical Technique for Solving Population Balance Equation Involving Aggregation, Breakage, Growth and Nucleation. *Powder Technol.* **2008**, *182*, 81−104.
(76) Lister, J. D.; Smit, D. J.; Hounslow, M. J. Adjustable Discretized Population Balance for Growth and Aggregation. *AIChE J.* **1995**, *41*, 591−603.
(77) Villadsen, J. V.; Stewart, W. E. Solution of Boundary-value Problems by Orthogonal Collocation. *Chem. Eng. Sci.* **1967**, *22*, 1483−1501.
(78) Gelbard, F.; Seinfeld, J. H. Numerical Solution of the Dynamic Equation for Particulate Systems. *J. Comput. Phys.* **1978**, *28*, 357−375.
(79) Kumar, S.; Ramkrishna, D. On the Solution of Population Balance Equations by discretization—I. A Fixed Pivot Technique. *Chem. Eng. Sci.* **1996**, *51*, 1311−1332.
(80) Kumar, S.; Ramkrishna, D. On the Solution of Population Balance Equations by discretization—II. A Moving Pivot Technique. *Chem. Eng. Sci.* **1996**, *51*, 1333−1342.
(81) Kumar, S.; Ramkrishna, D. On the Solution of Population Balance Equations by discretization—III. Nucleation, Growth and Aggregation of Particles. *Chem. Eng. Sci.* **1997**, *52*, 4659−4679.
(82) Kiparissides, C. Challenges in Particulate Polymerization Reactor Modeling and Optimization: A Population Balance Perspective. *J. Process Control* **2006**, *16*, 205−224.

(83) Meimaroglou, D.; Roussos, A. I.; Kiparissides, C. Part IV: Dynamic Evolution of the Particle Size Distribution in Particulate Processes. A Comparative Study Between Monte Carlo and the Generalized Method of Moments. *Chem. Eng. Sci.* **2006**, *61*, 5620−5635.
(84) Barrett, J. C.; Webb, N. A. A Comparison of Some Approximate Methods for Solving the Aerosol General Dynamic Equation. *J. Aerosol Sci.* **1998**, *29*, 31−39.
(85) Kostoglou, M.; Karabelas, A. J. An Assessment of Low-order Methods for Solving the Breakage Equation. *Powder Technol.* **2002**, *127*, 116−127.
(86) Roussos, A. I.; Alexopoulos, A. H.; Kiparissides, C. Dynamic Evolution of PSD in Continuous Flow Processes: A Comparative Study of Fixed and Moving Grid Numerical Techniques. *Chem. Eng. Sci.* **2006**, *61*, 124−134.
(87) Rigopoulos, S. Population Balance Modelling of Polydispersed Particles in Reactive Flows. *Prog. Energy Combust. Sci.* **2010**, *36*, 412−443.
(88) Christofides, P. D.; Li, M.; Mädler, L. Control of Particulate Processes: Recent Results and Future Challenges. *Powder Technol.* **2007**, *175*, 1−7.
(89) Spielman, L. A.; Levenspiel, O. A Monte Carlo Treatment for Reacting and Coalescing Dispersed Phase Systems. *Chem. Eng. Sci.* **1965**, *20*, 247−254.
(90) Gillespie, D. T. The Stochastic Coalescence Model for Cloud Droplet Growth. *J. Atmos. Sci.* **1972**, *29*, 1496−1510.
(91) Shah, B. H.; Ramkrishna, D.; Borwanker, J. D. Simulation of Particulate Systems Using the Concept of the Interval of Quiescence. *AIChE J.* **1977**, *23*, 897−904.
(92) Ramkrishna, D. Analysis of Population balance—IV: The Precise Connection Between Monte Carlo Simulation and Population Balances. *Chem. Eng. Sci.* **1981**, *36*, 1203−1209.
(93) Bird, G. A. *Molecular Gas Dynamics*; Clarendon Press: New York, 1976.
(94) Van Peborgh Gooch, J. R.; Hounslow, M. J. Monte Carlo Simulation of Size-enlargement Mechanisms in Crystallization. *AIChE J.* **1996**, *42*, 1864−1874.
(95) Tandon, P.; Rosner, D. E. Monte Carlo Simulation of Particle Aggregation and Simultaneous Restructuring. *J. Colloid Interface Sci.* **1999**, *213*, 273−286.
(96) Rosner, D. E.; McGraw, R.; Tandon, P. Multivariate Population Balances via Moment and Monte Carlo Simulation Methods. *An Important Sol Reaction Engineering Bivariate Example and "Mixed" Moments for the Estimation of Deposition, Scavenging, and Optical Properties for Populations of Nonspherical Suspended Particles. Ind. Eng. Chem. Res.* **2003**, *42*, 2699−2711.
(97) Kruis, F. E.; Maisels, A.; Fissan, H. Direct Simulation Monte Carlo Method for Particle Coagulation and Aggregation. *AIChE J.* **2000**, *46*, 1735−1742.
(98) Maisels, A.; Einar Kruis, F.; Fissan, H. Direct Simulation Monte Carlo for Simultaneous Nucleation, Coagulation, and Surface Growth in Dispersed Systems. *Chem. Eng. Sci.* **2004**, *59*, 2231−2239.
(99) Smith, M.; Matsoukas, T. Constant-number Monte Carlo Simulation of Population Balances. *Chem. Eng. Sci.* **1998**, *53*, 1777−1786.
(100) Lee, K.; Matsoukas, T. Simultaneous Coagulation and Break-up Using constant-N Monte Carlo. *Powder Technol.* **2000**, *110*, 82−89.
(101) Lin, Y.; Lee, K.; Matsoukas, T. Solution of the Population Balance Equation Using Constant-number Monte Carlo. *Chem. Eng. Sci.* **2002**, *57*, 2241−2252.
(102) Liffman, K. A Direct Simulation Monte-Carlo Method for Cluster Coagulation. *J. Comput. Phys.* **1992**, *100*, 116−127.
(103) Garcia, A. L.; van den Broeck, C.; Aertsens, M.; Serneels, R. A Monte Carlo Simulation of Coagulation. *Phys. Stat. Mech. Its Appl.* **1987**, *143*, 535−546.
(104) Eibeck, A.; Wagner, W. An Efficient Stochastic Algorithm for Studying Coagulation Dynamics and Gelation Phenomena. *SIAM J. Sci. Comput.* **2000**, *22*, 802−821.
(105) Eibeck, A.; Wagner, W. Approximative Solution of the Coagulation−fragmentation Equation by Stochastic Particle Systems. *Stoch. Anal. Appl.* **2000**, *18*, 921−948.
(106) Babovsky, H. On a Monte Carlo Scheme for Smoluchowski's Coagulation Equation. *Monte Carlo Methods Appl.* **1999**, *5*, 1−18.
(107) Debry, E.; Sportisse, B.; Jourdain, B. A Stochastic Approach for the Numerical Simulation of the General Dynamics Equation for Aerosols. *J. Comput. Phys.* **2003**, *184*, 649−669.
(108) Haibo, Z.; Chuguang, Z.; Minghou, X. Multi-Monte Carlo Approach for General Dynamic Equation Considering Simultaneous Particle Coagulation and Breakage. *Powder Technol.* **2005**, *154*, 164−178.
(109) Zhao, H.; Zheng, C.; Xu, M. Multi-Monte Carlo Method for Coagulation and Condensation/evaporation in Dispersed Systems. *J. Colloid Interface Sci.* **2005**, *286*, 195−208.
(110) Zhao, H.; Zheng, C.; Xu, M. Multi-Monte Carlo Method for Particle Coagulation: Description and Validation. *Appl. Math. Comput.* **2005**, *167*, 1383−1399.
(111) Goodson, M.; Kraft, M. Simulation of Coalescence and Breakage: An Assessment of Two Stochastic Methods Suitable for Simulating Liquid−liquid Extraction. *Chem. Eng. Sci.* **2004**, *59*, 3865−3881.
(112) Sabelfeld, K. K.; Rogasinsky, S. V.; Kolodko, A. A.; Levykin, A. I. Stochastic Algorithms for Solving Smolouchovsky Coagulation Equation and Applications to Aerosol Growth Simulation. *Monte Carlo Methods Appl.* **1996**, *2*, 41−87.
(113) Efendiev, Y.; Zachariah, M. R. Hybrid Monte Carlo Method for Simulation of Two-Component Aerosol Coagulation and Phase Segregation. *J. Colloid Interface Sci.* **2002**, *249*, 30−43.
(114) Laurenzi, I. J.; Bartels, J. D.; Diamond, S. L. A General Algorithm for Exact Simulation of Multicomponent Aggregation Processes. *J. Comput. Phys.* **2002**, *177*, 418−449.
(115) Goodson, M.; Kraft, M. An Efficient Stochastic Algorithm for Simulating Nano-particle Dynamics. *J. Comput. Phys.* **2002**, *183*, 210−232.
(116) Rajamani, K.; Pate, W. T.; Kinneberg, D. J. Time-driven and Event-driven Monte Carlo Simulations of Liquid-liquid Dispersions: a Comparison. *Ind. Eng. Chem. Fundam.* **1986**, *25*, 746−752.
(117) Zhao, H.; Maisels, A.; Matsoukas, T.; Zheng, C. Analysis of Four Monte Carlo Methods for the Solution of Population Balances in Dispersed Systems. *Powder Technol.* **2007**, *173*, 38−50.
(118) Scott, W. T. Analytic Studies of Cloud Droplet Coalescence I. *J. Atmospheric Sci.* **1968**, *25*, 54−65.
(119) Ramabhadran, T. E.; Peterson, T. W.; Seinfeld, J. H. Dynamics of Aerosol Coagulation and Condensation. *AIChE J.* **1976**, *22*, 840−851.
(120) Zhao, H.; Maisels, A.; Matsoukas, T.; Zheng, C. Analysis of Four Monte Carlo Methods for the Solution of Population Balances in Dispersed Systems. *Powder Technol.* **2007**, *173*, 38−50.
(121) Alexopoulos, A. H.; Roussos, A. I.; Kiparissides, C.; Part, I. Dynamic Evolution of the Particle Size Distribution in Particulate Processes Undergoing Combined Particle Growth and Aggregation. *Chem. Eng. Sci.* **2004**, *59*, 5751−5769.
(122) Alexopoulos, A. H.; Kiparissides, C. A. Part II: Dynamic Evolution of the Particle Size Distribution in Particulate Processes Undergoing Simultaneous Particle Nucleation, Growth and Aggregation. *Chem. Eng. Sci.* **2005**, *60*, 4157−4169.
(123) Roussos, A. I.; Alexopoulos, A. H.; Kiparissides, C. Part III: Dynamic Evolution of the Particle Size Distribution in Batch and Continuous Particulate Processes: A Galerkin on Finite Elements Approach. *Chem. Eng. Sci.* **2005**, *60*, 6998−7010.
(124) Alexopoulos, A. H.; Kiparissides, C. Solution of the Bivariate Dynamic Population Balance Equation in Batch Particulate Systems: Combined Aggregation and Breakage. *Chem. Eng. Sci.* **2007**, *62*, 5048−5053.
(125) Meimaroglou, D.; Roussos, A. I.; Kiparissides, C. Part IV: Dynamic Evolution of the Particle Size Distribution in Particulate Processes. A Comparative Study Between Monte Carlo and the

Generalized Method of Moments. *Chem. Eng. Sci.* **2006**, *61*, 5620−5635.
(126) Meimaroglou, D.; Kiparissides, C. Monte Carlo Simulation for the Solution of the Bi-variate Dynamic Population Balance Equation in Batch Particulate Systems. *Chem. Eng. Sci.* **2007**, *62*, 5295−5299.
(127) Friesen, W. I.; Dabros, T. Constant-number Monte Carlo Simulation of Aggregating and Fragmenting Particles. *J. Chem. Phys.* **2003**, *119*, 2825−2839.
(128) Gillespie, D. T. An Exact Method for Numerically Simulating the Stochastic Coalescence Process in a Cloud. *J. Atmospheric Sci.* **1975**, *32*, 1977−1989.
(129) Chen, J. C.; Kim, A. S. Brownian Dynamics, Molecular Dynamics, and Monte Carlo Modeling of Colloidal Systems. *Adv. Colloid Interface Sci.* **2004**, *112*, 159−173.
(130) Falope, G. O.; Jones, A. G.; Zauner, R. On Modelling Continuous Agglomerative Crystal Precipitation via Monte Carlo Simulation. *Chem. Eng. Sci.* **2001**, *56*, 2567−2574.
(131) Shah, B. H.; Borwanker, J. D.; Ramkrishna, D. Monte Carlo Simulation of Microbial Population Growth. *Math. Biosci.* **1976**, *31*, 1−23.
(132) Balthasar, M.; Kraft, M. A Stochastic Approach to Calculate the Particle Size Distribution Function of Soot Particles in Laminar Premixed Flames. *Combust. Flame* **2003**, *133*, 289−298.
(133) Singh, J.; Balthasar, M.; Kraft, M.; Wagner, W. Stochastic Modeling of Soot Particle Size and Age Distributions in Laminar Premixed Flames. *Proc. Combust. Inst.* **2005**, *30*, 1457−1465.
(134) Violi, A. Modeling of Soot Particle Inception in Aromatic and Aliphatic Premixed Flames. *Combust. Flame* **2004**, *139*, 279−287.
(135) Khalili, S.; Lin, Y.; Armaou, A.; Matsoukas, T. Constant Number Monte Carlo Simulation of Population Balances with Multiple Growth Mechanisms. *AIChE J.* **2010**, *56*, 3137−3145.
(136) Irizarry, R. Stochastic Simulation of Population Balance Models with Disparate Time Scales: Hybrid Strategies. *Chem. Eng. Sci.* **2011**, *66*, 4059−4069.
(137) Zhao, H.; Zheng, C. A New Event-driven Constant-volume Method for Solution of the Time Evolution of Particle Size Distribution. *J. Comput. Phys.* **2009**, *228*, 1412−1428.
(138) Zhao, H.; Kruis, F. E.; Zheng, C. Reducing Statistical Noise and Extending the Size Spectrum by Applying Weighted Simulation Particles in Monte Carlo Simulation of Coagulation. *Aerosol Sci. Technol.* **2009**, *43*, 781−793.
(139) Zhao, H.; Zheng, C. A Population balance-Monte Carlo Method for Particle Coagulation in Spatially Inhomogeneous Systems. *Comput. Fluids* **2013**, *71*, 196−207.
(140) Patterson, R. I. A.; Wagner, W.; Kraft, M. Stochastic Weighted Particle Methods for Population Balance Equations. *J. Comput. Phys.* **2011**, *230*, 7456−7472.
(141) DeVille, R. E. L.; Riemer, N.; West, M. Weighted Flow Algorithms (WFA) for Stochastic Particle Coagulation. *J. Comput. Phys.* **2011**, *230*, 8427−8451.
(142) Terrazas-Velarde, K.; Peglow, M.; Tsotsas, E. Stochastic Simulation of Agglomerate Formation in Fluidized Bed Spray Drying: A Micro-scale Approach. *Chem. Eng. Sci.* **2009**, *64*, 2631−2643.
(143) Dernedde, M.; Peglow, M.; Tsotsas, E. A Novel Structure-Tracking Monte Carlo Algorithm for Spray Fluidized Bed Agglomeration. *AIChE J.* **2012**, *58*, 3016−3029.
(144) Kolodko, A.; Sabelfeld, K. Stochastic Particle Methods for Smoluchowski Coagulation Equation: Variance Reduction and Error Estimations. *Monte Carlo Methods Appl.* **2003**, *9*, 315−339.
(145) Shima, S.; Kusano, K.; Kawano, A.; Sugiyama, T.; Kawahara, S. The Super-droplet Method for the Numerical Simulation of Clouds and Precipitation: A Particle-based and Probabilistic Microphysics Model Coupled with a Non-hydrostatic Model. *Q. J. R. Meteorol. Soc.* **2009**, *135*, 1307−1320.
(146) Irizarry, R. Fast Monte Carlo Methodology for Multivariate Particulate systems—I: Point Ensemble Monte Carlo. *Chem. Eng. Sci.* **2008**, *63*, 95−110.
(147) Irizarry, R. Fast Monte Carlo Methodology for Multivariate Particulate systems-II: -PEMC. *Chem. Eng. Sci.* **2008**, *63*, 111−121.
(148) Wells, C. G.; Kraft, M. Direct Simulation and Mass Flow Stochastic Algorithms to Solve a Sintering-Coagulation Equation. *Monte Carlo Methods Appl.* **2005**, *11*, 175−197.
(149) Min, K. W.; Ray, W. H. On the Mathematical Modeling of Emulsion Polymerization Reactors. *J. Macromol. Sci. Part C Polym. Rev.* **1974**, *11*, 177−255.
(150) Kiparissides, C.; Ponnuswamy, S. R. Application of Population Balance Equations to Latex Reactors. *Chem. Eng. Commun.* **1981**, *10*, 283−291.
(151) Kiparissides, C. Challenges in Particulate Polymerization Reactor Modeling and Optimization: A Population Balance Perspective. *J. Process Control* **2006**, *16*, 205−224.
(152) Kotoulas, C.; Kiparissides, C. A Generalized Population Balance Model for the Prediction of Particle Size Distribution in Suspension Polymerization Reactors. *Chem. Eng. Sci.* **2006**, *61*, 332−346.
(153) Crowley, T. J.; Meadows, E. S.; Kostoulas, E.; Doyle Iii, F. J. Control of Particle Size Distribution Described by a Population Balance Model of Semibatch Emulsion Polymerization. *J. Process Control* **2000**, *10*, 419−432.
(154) Maggioris, D.; Goulas, A.; Alexopoulos, A. H.; Chatzi, E. G.; Kiparissides, C. Use of CFD in Prediction of Particle Size Distribution in Suspension Polymer Reactors. *Comput. Chem. Eng.* **1998**, *22*, S315−S322.
(155) Immanuel, C. D.; Cordeiro, C. F.; Sundaram, S. S.; Meadows, E. S.; Crowley, T. J.; Doyle, F. J., III Modeling of Particle Size Distribution in Emulsion Co-polymerization: Comparison with Experimental Data and Parametric Sensitivity Studies. *Comput. Chem. Eng.* **2002**, *26*, 1133−1152.
(156) Immanuel, C. D.; Doyle, F. J., III Computationally Efficient Solution of Population Balance Models Incorporating Nucleation, Growth and Coagulation: Application to Emulsion Polymerization. *Chem. Eng. Sci.* **2003**, *58*, 3681−3698.
(157) Sood, A. Modeling of the Particle Size Distribution in Emulsion Polymerization. *J. Appl. Polym. Sci.* **2008**, *109*, 1403−1419.
(158) Araujo, P. H. H.; de la Cal, J. C.; Asua, J. M.; Pinto, J. C. Modeling Particle Size Distribution (PSD) in Emulsion Copolymerization Reactions in a Continuous Loop Reactor. *Macromol. Theory Simulations* **2001**, *10*, 769−779.
(159) Sajjadi, S. Population Balance Modeling of Particle Size Distribution in Monomer-starved Semibatch Emulsion Polymerization. *AIChE J.* **2009**, *55*, 3191−3205.
(160) Gao, J.; Penlidis, A. Mathematical Modeling and Computer Simulator/database for Emulsion Polymerizations. *Prog. Polym. Sci.* **2002**, *27*, 403−535.
(161) Vale, H. M.; McKenna, T. F. Modeling Particle Size Distribution in Emulsion Polymerization Reactors. *Prog. Polym. Sci.* **2005**, *30*, 1019−1048.
(162) Saliakas, V.; Kotoulas, C.; Meimaroglou, D.; Kiparissides, C. Dynamic Evolution of the Particle Size Distribution in Suspension Polymerization Reactors: A Comparative Study on Monte Carlo and Sectional Grid Methods. *Can. J. Chem. Eng.* **2008**, *86*, 924−936.
(163) Gillespie, D. T. A General Method for Numerically Simulating the Stochastic Time Evolution of Coupled Chemical Reactions. *J. Comput. Phys.* **1976**, *22*, 403−434.
(164) Tobita, H. Molecular Weight Distribution in Free Radical Polymerization with Long-chain Branching. *J. Polym. Sci., Part B: Polym. Phys.* **1993**, *31*, 1363−1371.
(165) Gillespie, D. T. Exact Stochastic Simulation of Coupled Chemical Reactions. *J. Phys. Chem.* **1977**, *81*, 2340−2361.
(166) Lu, J.; Zhang, H.; Yang, Y. Monte-Carlo Simulation of Kinetics and Chain-Length Distribution in Radical Polymerization. *Makromol. Chem.-Theory Simulations* **1993**, *2*, 747−760.
(167) Gillespie, D. T. Approximate Accelerated Stochastic Simulation of Chemically Reacting Systems. *J. Chem. Phys.* **2001**, *115*, 1716−1733.
(168) He, J.; Zhang, H.; Yang, Y. Monte Carlo Simulation of Chain Length Distribution in Radical Polymerization with Transfer Reaction. *Macromol. Theory Simulations* **1995**, *4*, 811−819.

(169) Arzamendi, G.; Plessis, C.; Leiza, J. R.; Asua, J. M. Effect of the Intramolecular Chain Transfer to Polymer on PLP/SEC Experiments of Alkyl Acrylates. *Macromol. Theory Simulations* **2003**, *12*, 315−324.
(170) He, J.; Zhang, H.; Chen, J.; Yang, Y. Monte Carlo Simulation of Kinetics and Chain Length Distributions in Living Free-radical Polymerization. *Macromolecules* **1997**, *30*, 8010−8018.
(171) Wen, M.; Scriven, L. E.; McCormick, A. V. Kinetic Gelation Modeling: Structural Inhomogeneity During Cross-Linking Polymerization. *Macromolecules* **2003**, *36*, 4140−4150.
(172) Nie, L.; Yang, W.; Zhang, H.; Fu, S. Monte Carlo Simulation of Microemulsion Polymerization. *Polymer* **2005**, *46*, 3175−3184.
(173) He, X. H.; Liang, H. J.; Pan, C. Y. Monte Carlo Simulation of Hyperbranched Copolymerizations in the Presence of a Multifunctional Initiator. *Macromol. Theory Simulations* **2001**, *10*, 196−203.
(174) He, X.; Liang, H.; Pan, C. Self-condensing Vinyl Polymerization in the Presence of Multifunctional Initiator with Unequal Rate Constants: Monte Carlo Simulation. *Polymer* **2003**, *44*, 6697−6706.
(175) Cai, X. Exact Stochastic Simulation of Coupled Chemical Reactions with Delays. *J. Chem. Phys.* **2007**, *126*, 124108−8.
(176) Salami-Kalajahi, M.; Najafi, M.; Haddadi-Asl, V. Application of Monte Carlo Simulation Method to Polymerization Kinetics over Ziegler-Natta Catalysts. *Int. J. Chem. Kinet.* **2009**, *41*, 45−56.
(177) Soares, J. B. P.; Hamielec, A. E. Chain Length Distributions of Polyolefins Made with Coordination Catalysts at Very Short Polymerization Times − Analytical Solution and Monte Carlo Simulation. *Macromol. React. Eng.* **2007**, *1*, 53−67.
(178) Al-Harthi, M.; Soares, J. B. P.; Simon, L. C. Dynamic Monte Carlo Simulation of ATRP with Bifunctional Initiators. *Macromol. React. Eng.* **2007**, *1*, 95−105.
(179) Maafa, I. M.; Soares, J. B. P.; Elkamel, A. Prediction of Chain Length Distribution of Polystyrene Made in Batch Reactors with Bifunctional Free-Radical Initiators Using Dynamic Monte Carlo Simulation. *Macromol. React. Eng.* **2007**, *1*, 364−383.
(180) Al-Harthi, M. A.; Masihullah, J. K.; Abbasi, S. H.; Soares, J. B. P. Dynamic Monte Carlo Simulation of ATRP in a Batch Reactor. *Macromol. Theory Simul.* **2009**, *18*, 307−316.
(181) Al-Harthi, M.; Khan, M. J.; Abbasi, S. H.; Soares, J. B. P. Gradient Copolymers by ATRP in Semibatch Reactors: Dynamic Monte Carlo Simulation. *Macromol. React. Eng.* **2009**, *3*, 148−159.
(182) Schütte, C.; Wulkow, M. A Hybrid Galerkin-Monte-Carlo Approach to Higher-Dimensional Population Balances in Polymerization Kinetics. *Macromol. React. Eng.* **2010**, *4*, 562−577.
(183) Krallis, A.; Meimaroglou, D.; Kiparissides, C. Dynamic Prediction of the Bivariate Molecular Weight−copolymer Composition Distribution Using Sectional-grid and Stochastic Numerical Methods. *Chem. Eng. Sci.* **2008**, *63*, 4342−4360.
(184) Flory, P. J. *Principles of Polymer Chemistry*; Cornell University Press: Ithaka, NY, 1953.
(185) Tobita, H. A Simulation Model for Long-chain Branching in Vinyl Acetate Polymerization: 1. Batch Polymerization. *J. Polym. Sci., Part B: Polym. Phys.* **1994**, *32*, 901−910.
(186) Tobita, H.; Hatanaka, K. Long-chain Branching in Free-radical Polymerization Due to Chain Transfer to Polymer. *J. Polym. Sci., Part B: Polym. Phys.* **1995**, *33*, 841−853.
(187) Tobita, H. A Simulation Model for Long-chain Branching in Vinyl Acetate Polymerization: 2. Continuous Polymerization in a Stirred Tank Reactor. *J. Polym. Sci., Part B: Polym. Phys.* **1994**, *32*, 911−919.
(188) Tobita, H. Kinetics of Long-Chain Branching in Emulsion Polymerization 0.1. Chain Transfer to Polymer. *Polymer* **1994**, *35*, 3023−3031.
(189) Tobita, H. Kinetics of Long-Chain Branching in Emulsion Polymerization 0.2. Vinyl-Acetate Polymerization. *Polymer* **1994**, *35*, 3032−3038.
(190) Tobita, H.; Yamamoto, K. Network Formation in Emulsion Crosslinking Copolymerization. *Macromolecules* **1994**, *27*, 3389−3396.
(191) Tobita, H. Random Degradation of Branched Polymers. 2. Multiple Branches. *Macromolecules* **1996**, *29*, 3010−3021.
(192) Tobita, H. Structural Requirements for Gel Formation. *J. Polym. Sci., Part B: Polym. Phys.* **1998**, *36*, 2015−2018.
(193) Tobita, H.; Hamashima, N. Monte Carlo Simulation of Size Exclusion Chromatography for Branched Polymers Formed through Free-radical Polymerization with Chain Transfer to Polymer. *Macromol. Theory Simulations* **2000**, *9*, 453−462.
(194) Tobita, H.; Hamashima, N. Monte Carlo Simulation of Size Exclusion Chromatography for Randomly Branched and Crosslinked Polymers. *J. Polym. Sci., Part B: Polym. Phys.* **2000**, *38*, 2009−2018.
(195) Tobita, H. Dimensions of Branched Polymers Formed in Simultaneous Long-chain Branching and Random Scission. *J. Polym. Sci., Part B: Polym. Phys.* **2001**, *39*, 2960−2968.
(196) Tobita, H. Markovian Approach to Nonlinear Polymer Formation: Free-radical Polymerization with Chain Transfer to Polymer. *J. Polym. Sci., Part B: Polym. Phys.* **1998**, *36*, 357−371.
(197) Tobita, H. Simultaneous Long-chain Branching and Random Scission. II. Analytic Expression for the Weight-average Molecular Weights. *J. Polym. Sci., Part B: Polym. Phys.* **2001**, *39*, 404−414.
(198) Tobita, H. Molecular Weight Development During Simultaneous Chain Scission, Long-Chain Branching and Crosslinking, 1. General Matrix Formula. *Macromol. Theory Simulations* **2003**, *12*, 24−31.
(199) Tobita, H. Molecular Weight Development During Simultaneous Chain Scission, Long-Chain Branching and Crosslinking, 2. Free-Radical Polymerization. *Macromol. Theory Simulations* **2003**, *12*, 32−41.
(200) Tobita, H.; Yanase, F. Monte Carlo Simulation of Controlled/Living Radical Polymerization in Emulsified Systems. *Macromol. Theory Simulations* **2007**, *16*, 476−488.
(201) Tobita, H. Effects of Fluctuation and Segregation in the Rate Acceleration of ATRP Miniemulsion Polymerization. *Macromol. Theory Simulations* **2011**, *20*, 179−190.
(202) Tobita, H. RAFT Miniemulsion Polymerization Kinetics, 1 - Polymerization Rate. *Macromol. Theory Simulations* **2009**, *18*, 108−119.
(203) Tobita, H. RAFT Miniemulsion Polymerization Kinetics, 2 - Molecular Weight Distribution. *Macromol. Theory Simulations* **2009**, *18*, 120−126.
(204) Tobita, H. Free-Radical Polymerization with Long-Chain Branching and Scission in a Continuous Stirred-Tank Reactor. *Macromol. React. Eng.* **2013**, *7*, 181−192.
(205) Iedema, P. D.; Hoefsloot, H. C. J. Synthesis of Branched Polymer Architectures from Molecular Weight and Branching Distributions for Radical Polymerisation with Long-chain Branching, Accounting for Topology-controlled Random Scission. *Macromol. Theory Simul.* **2001**, *10*, 855−869.
(206) Hoefsloot, H. C. J.; Iedema, P. D. A Conditional Monte Carlo Method to Determine the Architectures of Metallocene Catalyzed Polyethylene. *Macromol. Theory Simul.* **2003**, *12*, 484−498.
(207) Iedema, P. D. Predicting MWD and Branching Distribution of Terminally Branched Polymers Undergoing Random Scission. *Macromol. Theory Simul.* **2012**, *21*, 166−186.
(208) Iedema, P. D.; Remerie, K.; van der Ham, M.; Biemond, E. Development of MWD and Branching During Peroxide Modification of High-Density Polyethylene by SEC-MALS and Monte Carlo Simulation. *Polymer* **2013**, *54*, 4093−4104.
(209) Jabbari, E. Monte Carlo Simulation of Tri-functional Branching and Tetra-functional Crosslinking in Emulsion Polymerization of Butadiene. *Polymer* **2001**, *42*, 4873−4884.
(210) Arzamendi, G.; Leiza, J. R. Molecular Weight Distribution (Soluble and Insoluble Fraction) in Emulsion Polymerization of Acrylate Monomers by Monte Carlo Simulations. *Ind. Eng. Chem. Res.* **2008**, *47*, 5934−5947.
(211) Stubbs, J.; Carrier, R.; Sundberg, D. C. Monte Carlo Simulation of Emulsion Polymerization Kinetics and the Evolution of Latex Particle Morphology and Polymer Chain Architecture. *Macromol. Theory Simul.* **2008**, *17*, 147−162.
(212) Bannister, I.; Billingham, N. C.; Armes, S. P. Monte Carlo Modelling of Living Branching Copolymerisation of Monovinyl and

Divinyl Monomers: Comparison of Simulated and Experimental Data for ATRP Copolymerisation of Methacrylic Monomers. *Soft Matter* **2009**, *5*, 3495−3504.
(213) O'Driscoll, K. F.; Kuindersma, M. E. Monte Carlo Simulation of Pulsed Laser Polymerization. *Macromol. Theory Simul.* **1994**, *3*, 469−478.
(214) Manders, B. G.; van Herk, A. M.; German, A. L. Monte Carlo Simulation of the Chain Length Distribution in Pulsed-laser Polymerization Experiments in Microemulsion. *Macromol. Theory Simul.* **1995**, *4*, 325−333.
(215) Liang, H.; Jiang, W.; He, X. Monte Carlo Simulation of Pulsed-laser Polymerization in Emulsion. *Eur. Polym. J.* **2000**, *36*, 2527−2530.
(216) Platkowski, K.; Reichert, K. H. Application of Monte Carlo Methods for Modelling of Polymerization Reactions. *Polymer* **1999**, *40*, 1057−1066.
(217) Beigzadeh, D.; Soares, J. B. P.; Duever, T. A. Modeling of Fractionation in CRYSTAF Using Monte Carlo Simulation of Crystallizable Sequence Lengths: Ethylene/1-octene Copolymers Synthesized with Single-site−type Catalysts. *J. Appl. Polym. Sci.* **2001**, *80*, 2200−2206.
(218) Costeux, S.; Anantawaraskul, S.; Wood-Adams, P. M.; Soares, J. B. P. Distribution of the Longest Ethylene Sequence in Ethylene/alpha-olefin Copolymers Synthesized with Single-site-type Catalysts. *Macromol. Theory Simul.* **2002**, *11*, 326−341.
(219) Lukkien, J. J.; Segers, J. P. L.; Hilbers, P. a. J.; Gelten, R. J.; Jansen, A. P. J. Efficient Monte Carlo Methods for the Simulation of Catalytic Surface Reactions. *Phys. Rev. E* **1998**, *58*, 2598−2610.
(220) Gibson, M. A.; Bruck, J. Efficient Exact Stochastic Simulation of Chemical Systems with Many Species and Many Channels. *J. Phys. Chem. A* **2000**, *104*, 1876−1889.
(221) Iedema, P. D.; Hoefsloot, H. C. J. Computing the Trivariate Chain Length/Degree of Branching/Number of Combination Points Distribution for Radical Polymerization with Transfer to Polymer and Recombination Termination. *Macromol. Theory Simul.* **2005**, *14*, 505−518.
(222) Meimaroglou, D.; Krallis, A.; Saliakas, V.; Kiparissides, C. Prediction of the Bivariate Molecular Weight - Long Chain Branching Distribution in Highly Branched Polymerization Systems Using Monte Carlo and Sectional Grid Methods. *Macromolecules* **2007**, *40*, 2224−2234.
(223) Meimaroglou, D.; Krallis, A.; Kiparissides, C. A. Prediction of Bivariate Molecular Property Distributions in Free-radical Polymerization Systems Using Monte Carlo and Sectional Grid Methods. *Chem. Prod. Process Model.* **2008**, *3*, 1−29.
(224) Meimaroglou, D.; Kiparissides, C. A Novel Stochastic Approach for the Prediction of the Exact Topological Characteristics and Rheological Properties of Highly-Branched Polymer Chains. *Macromolecules* **2010**, *43*, 5820−5832.
(225) Kiparissides, C.; Krallis, A.; Meimaroglou, D.; Pladis, P.; Baltsas, A. From Molecular to Plant-Scale Modeling of Polymerization Processes: A Digital High-Pressure Low-Density Polyethylene Production Paradigm. *Chem. Eng. Technol.* **2010**, *33*, 1754−1766.
(226) Meimaroglou, D.; Pladis, P.; Baltsas, A.; Kiparissides, C. Prediction of the Molecular and Polymer Solution Properties of LDPE in a High-pressure Tubular Reactor Using a Novel Monte Carlo Approach. *Chem. Eng. Sci.* **2011**, *66*, 1685−1696.
(227) De Gennes, P. G. Reptation of a Polymer Chain in the Presence of Fixed Obstacles. *J. Chem. Phys.* **1971**, *55*, 572−579.
(228) Tsenoglou, C. Molecular Weight Polydispersity Effects on the Viscoelasticity of Entangled Linear Polymers. *Macromolecules* **1991**, *24*, 1762−1767.
(229) Wasserman, S. H.; Graessley, W. W. Effects of Polydispersity on Linear Viscoelasticity in Entangled Polymer Melts. *J. Rheol.* **1992**, *36*, 543−572.
(230) McLeish, T. C. B.; Larson, R. G. Molecular Constitutive Equations for a Class of Branched Polymers: The Pom-pom Polymer. *J. Rheol.* **1998**, *42*, 81−110.
(231) Inkson, N. J.; McLeish, T. C. B.; Harlen, O. G.; Groves, D. J. Predicting Low Density Polyethylene Melt Rheology in Elongational and Shear Flows with "pom-pom" Constitutive Equations. *J. Rheol.* **1999**, *43*, 873−896.
(232) Blackwell, R. J.; Harlen, O. G.; McLeish, T. C. B. Theoretical Linear and Nonlinear Rheology of Symmetric Treelike Polymer Melts. *Macromolecules* **2001**, *34*, 2579−2596.
(233) Park, S. J.; Shanbhag, S.; Larson, R. G. A Hierarchical Algorithm for Predicting the Linear Viscoelastic Properties of Polymer Melts with Long-chain Branching. *Rheol. Acta* **2005**, *44*, 319−330.
(234) Das, C.; Inkson, N. J.; Read, D. J.; Kelmanson, M. A.; McLeish, T. C. B. Computational Linear Rheology of General Branch-on-branch Polymers. *J. Rheol.* **2006**, *50*, 207−234.
(235) Pladis, P.; Meimaroglou, D.; Kiparissides, C. Prediction of the Viscoelastic Bevaviour of Low-density Polyethylene Produced in High-pressure Tubular Reactors. *J. Rheol.* **2014**.
(236) Read, D. J.; Auhl, D.; Das, C.; den Doelder, J.; Kapnistos, M.; Vittorias, I.; McLeish, T. C. B. Linking Models of Polymerization and Dynamics to Predict Branched Polymer Structure and Flow. *Science* **2011**, *333*, 1871−1874.

2.3 Coupling stochastic and deterministic techniques

The second article, reported in this work, concerns the development of a stochastic MC model for an intensified modular reactor system, developed in the framework of a European project, entitled Fast Flexible Future Factory (F^3Factory). The referenced period is that of the early years of my integration in the Laboratory of Reactions and Process Engineering (LRGP) in Nancy. This application shows the transposition of the tools developed previously to a copolymerization system of industrial interest. Several academic and industrial partners were involved in this project, while this specific work included the collaboration between Solvay (ex Rhodia), LRGP, BASF and the Technical University of Dortmund.

The objective of this work was to be able to produce high added-value copolymers, in industrial scale, using intensified modular tubular reactors, equipped with static mixers. A major challenge that was faced during the project concerned the control of the properties of the produced copolymer, with respect to the reaction conditions. In fact, depending on the relative reactivity of the two comonomers, as well as on the temperature and velocity profiles in the reactor, the properties of the produced copolymer could vary significantly. The present study shows how the implementation of the MC algorithm allows to demonstrate the existence of a drift in the copolymer composition and the sequence length of the copolymer chains, under certain polymerization conditions, that was not detectable by the sole monitoring of the relative average properties.

Another interesting aspect of this reported work, concerns the development of an integrated simulator for the process, on the basis of the combination of a deterministic and a stochastic modeling approach. In fact, instead of developing a standalone MC model for the process, a choice was made to combine this latter with the well established method of moments (MoM). This provides flexibility to the developed simulator, as the MC module can be implemented *à la carte*, only when the need is presented for obtaining more detailed information on the macromolecular properties of the copolymer. Inversely, in cases where a rapid prediction of the average molar mass properties suffices, the simulator can run exclusively on the basis of the MoM, without activating the MC module, thus saving computational effort and time.

On the Modeling of Acrylic Acid Copolymerization in an Aqueous Solution: A Modular, Integrated Approach

Dimitrios Meimaroglou,* Marie-Claire Chevrel, Sandrine Hoppe, Alain Durand, Laurent Falk, James Wilson, Patrick Ferlin

A complete mathematical model of the free-radical copolymerization of acrylic acid in an aqueous solution, taking place in a pilot-scale tubular reactor equipped with static mixers, is presented. The developed kinetic/reactor model is numerically integrated in terms of a coupled deterministic–stochastic numerical approach that combines the advantages of speed, efficiency, and increased predictive capabilities. A series of experimental measurements on the monomer conversion and the molecular weight characteristics of the produced copolymer, under a wide range of process conditions, are used for the identification of the kinetic model parameters while a thorough analysis of the compositional characteristics of the produced copolymers is also carried out in terms of a series of bivariate distributed properties.

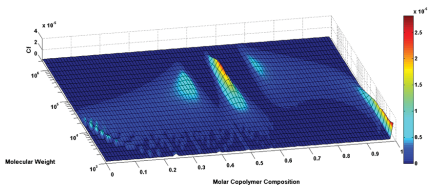

1. Introduction

Water soluble polymers and copolymers constitute an important part of the polymer industry products portfolio as they are used in a broad range of applications (e.g., pharmaceuticals, cosmetics, inks, construction materials, adhesives, etc.). Among the most important key functionalities of these polymers is their ability to increase the viscosity of solutions, form physical gels, and stabilize dispersions and emulsions.[1] More specifically, water-soluble polymers and copolymers of acrylic acid (AA) are commonly used for the synthesis of super-absorbent materials, paints, membranes, flocculants, solid detergents and dishwashing powders, cement additives, textile sizing agents, and many more.[2–4]

The polymerization of AA is commonly carried out in aqueous solutions with the elevated heat of reaction being the primary and most common drawback of the process in terms of process design and intensification. As in most polymerization systems, the final end-use properties of the produced polymers or copolymers, which dictate the application functionalities of the product, are greatly affected by the chemical composition and the molecular weight characteristics of the polymer.[5] Hence, one current challenge is to design models that conveniently describe the process parameters (heat exchange, hydrodynamics, pressure drop, etc.) and have the ability to accurately predict the influence of the various process conditions on these macromolecular characteristics. Taking up this challenge is of paramount importance for the chemical industry.

D. Meimaroglou, M.-C. Chevrel, S. Hoppe, L. Falk
CNRS
LRGP
UMR 7274, 1 Rue Grandville, Nancy F-54001, France
E-mail: dimitrios.meimaroglou@univ-lorraine.fr
D. Meimaroglou, M.-C. Chevrel, S. Hoppe, L. Falk
Université de Lorraine
LRGP
UMR 7274, Nancy F-54001, France
A. Durand
CNRS
LCPM
FRE 3564, Nancy F-54001, France
A. Durand
Université de Lorraine
LCPM
FRE 3564, Nancy F-54001, France
J. Wilson, P. Ferlin
SOLVAY Group
Aubervilliers, France

DOI: 10.1002/mren.201500036

Despite the existence of numerous studies on the aqueous free-radical solution polymerization of AA, it remains a system that can certainly not be considered trivial since a great number of factors (i.e., most notably the solution pH, the degree of ionization of AA, and the monomer concentration) may influence dramatically the kinetics of polymerization.[2,6–12] As a result, very few relative modeling studies have been presented in the literature. These studies were exclusively focused on the homopolymerization case and, at the same time, displayed significant differences among them (i.e., consideration of different kinetic schemes and polymerization rate expressions, etc.).[9,13] In addition, these published models displayed limited predictive capabilities when it comes to distributed molecular properties of interest, such as the molecular weight distribution of the polymer chains. A notable exception is a recent publication of Wittenberg et al.,[14] which presents a complete comprehensive kinetic model of the aqueous polymerization system of AA.

In order to acquire more detailed information that can be associated with/translated into a series of distributed molecular properties of the produced macromolecules, it becomes imperative to use advanced numerical methods for the resolution of a mathematical model that will describe the evolution of the chain length and/or the compositional or the branching characteristics of the polymer along the polymerization. In fact, such properties become especially interesting in the case of copolymerization or nonlinear systems. In this respect, the commonly employed approaches can be broadly classified into stochastic (i.e., Monte Carlo, MC) or deterministic, with the latter category containing a number of powerful techniques, such as the fixed pivot technique, the Galerkin on finite elements, the orthogonal collocation on finite elements, etc. The implementation of these techniques for the simulation of polymerization systems has already been widely demonstrated in the relevant literature.[15–18] Despite their undisputed capabilities, these methods commonly display increased complexity in terms of mathematical formulations, especially when applied to nonlinear or to copolymer systems, as well as dependence of their accuracy on the discretization of the chain length and/or copolymer composition domains.[19]

On the other hand, a very simple stochastic algorithm with increased predictive capabilities can be easily applied to any polymerization system, no matter how complex it may be (i.e., in terms of nonlinearity or of multiple types of monomers), on the principal cost of increased computational demands.[20,21] Hence, the stochastic approach may be considered as the optimal choice in cases where the time required for a simulation is of less significance (e.g., in off-line simulators designed to provide detailed information on the polymer chain characteristics).

A combination of the advantages of the deterministic and stochastic modeling approaches is possible on the basis of the development of either hybrid or coupled models, containing elements of these two principal modeling techniques. A pioneering hybrid model, for the solution of higher-dimensional population balances in polymerization systems, was presented by Schütte and Wulkow.[22] On the other hand, a coupled deterministic–stochastic modeling approach (i.e., based on the individual implementation of each of the two techniques to acquire different information of the same model) was proposed by the group of Kiparissides for the simulation of industrial high-pressure polymerization reactor[23] and was subsequently adopted by other researchers on similar problems.[24]

In the present work, a comprehensive detailed copolymerization model is presented for the simulation of the chemically initiated free-radical copolymerization of AA (henceforth denoted as M_1) with an industrial comonomer (henceforth denoted as M_2). The polymerization takes place in an aqueous solution, in a pilot-scale tubular reactor that is equipped with static mixers. In the framework of the proposed mathematical model, the evolution of the concentrations of the "live" and "dead" copolymer chains is described by a set of coupled population balance equations, which are numerically solved in terms of a modular integrated deterministic/stochastic approach on the basis of the method of double moments (DMoM) and an MC stochastic kinetic algorithm. The DMoM provides a fast, reliable, and efficient route for the calculation of the key indexes of the polymerization along the reactor, such as the evolution of monomer conversion and the average molecular properties of the polymer, while the MC method is optionally implemented to provide additional information on the chain length and compositional developments of the formed copolymer chains.

2. Reactor Configuration and Materials

The experimental setup was comprised of a tubular reactor of the Contiplant technology (Fluitec) containing static mixers of type CSE-X (Scheme 1). The reactor was divided in eight consecutive insulated sections of a length of 0.5 m each. The four initial sections (i.e., sections 1–4) had an internal diameter of 12 mm while sections 5–8 had an internal diameter of 21 mm. The length of each of the connecting elements was equal to 72 mm and their internal diameter was identical and equal to 8 mm. They were also equipped with static mixers of the same type (i.e., CSE-X). All parts were in 316L stainless-steel. The design of the static-mixers produced a near plug-flow behavior even at laminar conditions as well as improved mixing and heat transfer under a broad range of viscosity values.

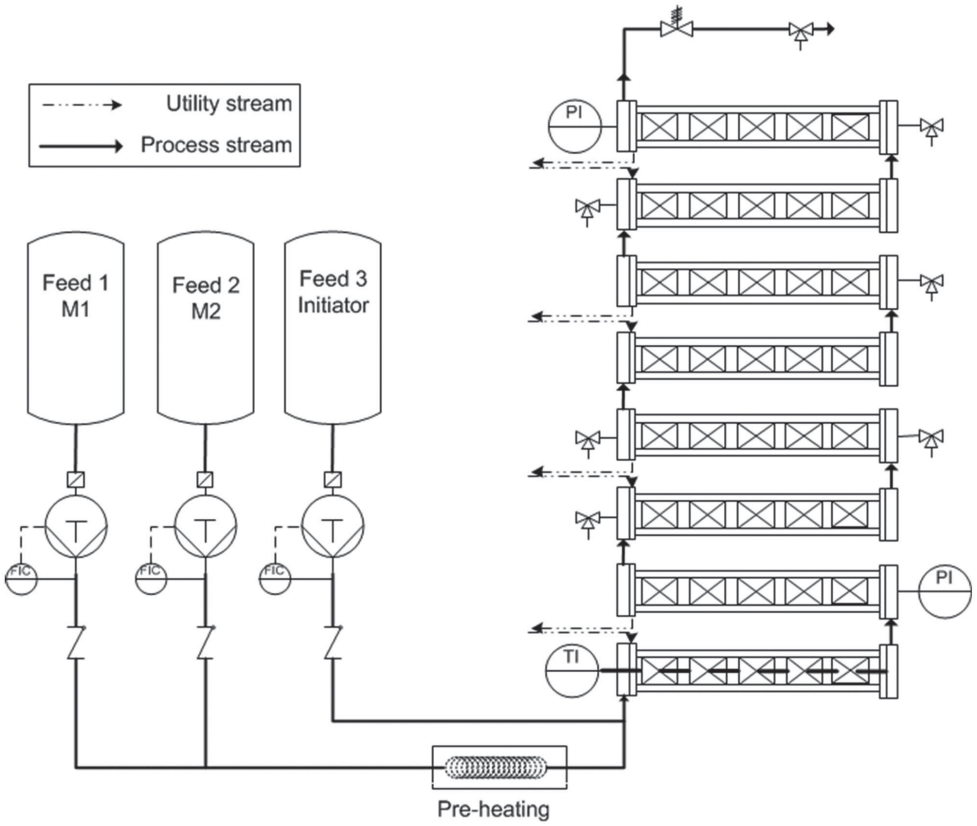

Scheme 1. Flowchart of the experimental setup.

Flanges were placed at both ends of each section, along with monitoring instrumentation (i.e., temperature and pressure sensors), sampling-valves, and interconnectors. The standardization of the flange points greatly facilitated the flexibility, scalability, and modularity of the setup.

Besides the temperature measurement at specific flanges, a measurement of the temperature profile along any of the reactor sections was possible via a movable axial temperature sensor. The overall reactor pressure drop was controlled by means of a back-pressure regulator placed at the outlet of the reactor. Temperature control was achieved by the use of a utility fluid (i.e., therminol oil) flowing within a tubular jacket along the main reactor sections (i.e., excluding the connecting parts). The jacket was comprised of four consecutive sections with individual inlet/outlet, all connected to the main heat exchanger that provided a high flow rate of the utility fluid (up to 10 L min^{-1}). Liquid double-piston pumps coupled with Coriolis flow controllers were used for feeding the two comonomer solutions, which were preheated and mixed with the initiator solution just before the reactor inlet. A "labview" environment was utilized for the control of the flow rates and for data acquisition, at a frequency of one measurement per 5 s.

AA (monomer grade) and sodium persulfate (reagent grade) were furnished by Aldrich. M_2 comonomer is a proprietary molecule of Solvay and was not available on the market. Both monomers and initiator were used in solutions after the necessary dilution and without any further purification. Monomer conversion was determined in terms of ^1H NMR analysis performed in a Bruker 300 MHz spectrometer and using D_2O as solvent. For the characterization of the copolymer molecular weight characteristics, aqueous size-exclusion chromatography was used including refractive index (Merck) and light scattering (MALLS from Wyatt Technologies) detectors. The calibration was performed on the basis of known samples of the specific system, using the MALLS detector.

3. Kinetic Mechanism

The following comprehensive kinetic mechanism was employed to describe the formation of copolymers in a chemically initiated free-radical copolymerization system, on the basis of the terminal copolymerization model.

Initiator decomposition

$$I \xrightarrow{k_d} 2\,PR^{\bullet} \quad (1)$$

Chain initiation

$$PR^{\bullet} + M_j \xrightarrow{k_{Ij}} P^j_{2-j,j-1} \quad (2)$$

Propagation

$$P^i_{n,m} + M_j \xrightarrow{k_{pij}} P^j_{n+2-j,m+j-1} \quad (3)$$

Chain transfer to monomer

$$P^i_{n,m} + M_j \xrightarrow{k_{fmij}} P^j_{2-j,j-1} + D_{n,m} \quad (4)$$

Termination by combination

$$P^i_{n,m} + P^j_{r,q} \xrightarrow{k_{tcij}} D_{n+r,m+q} \quad (5)$$

Termination by disproportionation

$$P^i_{n,m} + P^j_{r,q} \xrightarrow{k_{tdij}} D_{n,m} + D_{r,q} \quad (6)$$

The above kinetic scheme includes the typical initiation and propagation reactions, termination by combination and disproportionation as well as molecular weight control reactions via transfer to monomer. I, $PR^{\bullet}$, and M_j, (j = 1, 2) denote the initiator, the primary radicals, and the two monomers, respectively, while $P^i_{n,m}$ and $D_{n,m}$ represent the "live" and "dead" copolymer chains. Finally, the subscripts "n" and "m" represent the corresponding degrees of polymerization for M_1 and M_2 monomers and the superscript "i" refers to the final monomer unit (of either type M_1 or M_2) in a "live" copolymer chain. It should be noted that, contrary to evidences of different published studies,[9,25–27] exhibiting the existence of backbiting reactions in the kinetic scheme of the polymerization of AA, leading to the formation of mid-chain radicals that propagate with different rate than the typical end-chain radicals and producing a significant effect on the overall rate of polymerization and the polymer properties, such reactions were considered negligible in this study. The reason was that no experimental evidence was found for the present copolymerization system and the recipes that were tested to support the necessity of including such phenomena in the developed model. In addition, all the kinetic rate constants were considered constant throughout the polymerization (i.e., the effects of monomer content, monomer conversion, and ionization degree on the kinetic rate constants were not included in the present model) since it was found that the present system was modeled with sufficient accuracy without including additional complexity. Besides, the solution pH was kept constant throughout the polymerization, equal to a value around 2.2, thus justifying the consideration of nonionized AA at all stages of the polymerization process.

4. Model Developments

4.1. Copolymerization Rate Functions

Based on the postulated kinetic mechanism, the corresponding net production rates for the "live," $r_{P^i_{n,m}}$, and "dead," $r_{D_{n,m}}$, copolymer chains can be derived via the combination of their respective production/consumption rates in all the elementary reactions of the adopted kinetic scheme.[28]

Net formation rate of "live" copolymer chains ending in monomer "i"

$$r_{P^i_{n,m}} = \left(k_{Ii}[PR^{\bullet}][M_i] + \sum_{j=1}^{2} k_{fmji}[M_i] P^j_{o,o} \right) \delta(n+i-2, m+1-i) + \sum_{j=1}^{2} k_{pji}[M_i]\left[P^j_{n+i-2,m+1-i}\right] - \sum_{j=1}^{2} k_{pij}[M_j]\left[P^i_{n,m}\right] - A_i\left[P^i_{n,m}\right] \quad (7)$$

Net formation rate of "dead" copolymer chains

$$r_{D_{n,m}} = \sum_{i=1}^{2}\left(A_i - \sum_{j=1}^{2} k_{tcij} P^j_{o,o} \right)\left[P^i_{n,m}\right] + \frac{1}{2}\sum_{i=1}^{2}\sum_{j=1}^{2} k_{tcij} \sum_{r=1}^{n-1}\sum_{q=1}^{m-1}\left[P^i_{r,q}\right]\left[P^j_{n-r,m-q}\right] \quad (8)$$

with

$$A_i = \sum_{j=1}^{2}\left(k_{fmij} M_j + \left(k_{tcij} + k_{tdij}\right) P^j_{o,o}\right); \quad P^j_{o,o} = \sum_{n=o}^{\infty}\sum_{m=o}^{\infty}\left[P^j_{n,m}\right] \quad (9)$$

$\delta(n,m)$ is the Kronecker's delta function, given by

$$\delta(n,m) = \delta(n)\delta(m); \quad \delta(z) = \begin{cases} 1 & \text{for } z = o \\ o & \text{for } z \neq o \end{cases} \quad (10)$$

4.2. The Method of Double Moments

As the system of molecular species balances, resulting from the implementation of Equations (7–10), would be of prohibitively large order, the DMoM[29] was implemented in order to reduce the system into a new, low order system of differential moment equations. According to the DMoM, the respective double moments of the "live" and "dead" copolymer chain populations are defined by the following expressions

$$\lambda^i_{k,l} = \sum_{n=1}^{\infty}\sum_{m=1}^{\infty} n^k m^l \left[P^i_{n,m}\right]; \quad \mu_{k,l} = \sum_{n=1}^{\infty}\sum_{m=1}^{\infty} n^k m^l \left[D_{n,m}\right]; \; n+m \geq 1 \quad (11)$$

By assigning to k, l, values between 0 and 2, the leading moments of the chain length distribution are obtained.

The respective rate functions of the moments are obtained by the previously described "live" and "dead" copolymer rate functions, Equations (7)–(10), after multiplication with the term $n^k\ m^l$ and summation over the variation range of n and m.

Net formation rate of the moments of the "live" copolymer chains

$$r_{\lambda^i_{k,l}} = \left(k_{Ii}\left[\mathrm{PR}^\bullet\right][M_i] + \sum_{j=1}^{2} k_{\mathrm{fm}ji}[M_i]\lambda^j_{\mathrm{o,o}}\right)\left(\delta(l)\right)^{2-i}\left(\delta(k)\right)^{i-1} - \sum_{j=1}^{2} k_{\mathrm{p}ij}\left[M_j\right]\lambda^i_{k,l} - B_i\ \lambda^i_{k,l} + \sum_{j=1}^{2} k_{\mathrm{p}ji}\left[M_i\right]\left((2-i)\sum_{r=0}^{k}\binom{k}{r}\lambda^j_{k-r,l} + (i-1)\sum_{r=0}^{l}\binom{l}{r}\lambda^j_{k,l-r}\right) \tag{12}$$

Net formation rate of the moments of the "dead" copolymer chains

$$r_{\mu_{k,l}} = \sum_{i=1}^{2}\left(B_i - \sum_{j=1}^{2} k_{\mathrm{tc}ij}\lambda^j_{\mathrm{o,o}}\right)\lambda^i_{k,l} + \frac{1}{2}\sum_{i=1}^{2}\sum_{j=1}^{2} k_{\mathrm{tc}ij}\sum_{r=0}^{k}\sum_{q=0}^{l}\binom{k}{r}\binom{l}{q}\lambda^i_{r,q}\lambda^j_{k-r,l-q} \tag{13}$$

with

$$B_i = \sum_{j=1}^{2}\left(k_{\mathrm{fm}ij}\left[M_j\right] + \left(k_{\mathrm{tc}ij} + k_{\mathrm{td}ij}\right)\lambda^j_{\mathrm{o,o}}\right);\quad \binom{n}{m} = \frac{n!}{(n-m)!\,m!} \tag{14}$$

4.3. Reactor Design Equations

The overall mathematical model of the polymerization reactor is comprised of a set of differential material and energy balances. This set of coupled ordinary differential equations (ODEs) was numerically integrated with respect to the reactor length in order to provide information on the evolution of the compositional and molecular weight developments of the copolymer along the reactor and under steady-state conditions. For the derivation of the model, the following assumptions were made: (i) the reaction medium is considered as a one-phase system, (ii) the heat produced by the polymerization is exclusively produced by the propagation reactions, and (iii) the reaction medium flows within the different segments of the reactor under plug-flow conditions. Note that the last assumption has been experimentally verified via residence time distribution measurements.

Accordingly, the generalized species balance of the model can be expressed as

$$\frac{\mathrm{d}F_\mathrm{S}}{\mathrm{d}z} = A_\mathrm{c}\ r_\mathrm{S};\quad \mathrm{S}: \lambda^i_{n,m};\mu_{n,m};\ M_i; I \tag{15}$$

where F_S and r_S denote the molar flow rate and rate function of the species S, respectively, A_c is the free cross-sectional area of the reactor tube, and z denotes the reactor length. The rate functions of the rest of the species (i.e., besides the moments of the chain length distribution of the copolymer chains (see Equations (12)–(14)) are typically described by the following expressions.

Monomers

$$r_{M_i} = -\left(k_{Ii}\left[\mathrm{PR}^\bullet\right] + \left(k_{\mathrm{p}1i} + k_{\mathrm{fm}1i}\right)\lambda^1_{\mathrm{o,o}} + \left(k_{\mathrm{p}2i} + k_{\mathrm{fm}2i}\right)\lambda^2_{\mathrm{o,o}}\right)[M_i] \tag{16}$$

Initiator

$$r_I = -k_\mathrm{d}[I] \tag{17}$$

Primary radicals

$$r_{\mathrm{PR}^\bullet} = 2f\ k_\mathrm{d}[I] - \left(\sum_{i=1}^{2} k_{Ii}[M_i]\right)\left[\mathrm{PR}^\bullet\right] \tag{18}$$

The following energy balances describe the evolution of the temperature, T, of the reaction medium as well as the evolution of the temperature of the medium that flows in the reactor jacket, T_J.

Reactor energy balance

$$\frac{\mathrm{d}T}{\mathrm{d}z} = \frac{1}{puC_p}\left[-\Delta H_\mathrm{R}\left(\sum_{i=1}^{2}\left(k_{\mathrm{p}1i}\lambda^1_{\mathrm{o,o}}\right) + \left(k_{\mathrm{p}2i}\lambda^2_{\mathrm{o,o}}\right)[M_i]\right) - 4U/D_i\left(T - T_J\right)\right] \tag{19}$$

Jacket energy balance

$$\frac{\mathrm{d}T_J}{\mathrm{d}z} = \frac{\pi D_i U}{p_J Q_J C_{pJ}}\left(T - T_J\right) \tag{20}$$

In the above expressions, p, p_J, C_p, and C_{pJ} denote the density and the heat capacity of the reacting mixture and the jacket fluid, respectively, u and Q_J are the fluid velocity and the volumetric flow rate inside the reactor and the jacket, respectively, D is the internal tube diameter, and U is the overall heat transfer coefficient. For the calculation of U, the following expression was implemented[30]

$$\frac{1}{U} = \frac{1}{h_i} + \frac{D_i \ln\left(D_o / D_i\right)}{2k_w} + \frac{D_i}{D_o h_o} \tag{21}$$

Here h_i and h_o are the respective internal and external heat transfer coefficients, calculated in terms of the commonly employed expressions involving the Nusselt numbers of the two flows, D_o is the external diameter of the reactor tube and k_w denotes the thermal conductivity of the reactor metal wall (value reported in Table 1). It must be noted that, at the parts of the reactor that were not covered by the jacket (i.e., the connectors between the

Table 1. Physical and transport properties and constants of the reacting mixture and the service fluid.

Property	Value	Units
Service fluid[a)] density	974.0	kg m^{-3}
Service fluid[a)] viscosity	7.77×10^{-3}	Pa s
Service fluid[a)] heat capacity	1740.0	J kg^{-1} K^{-1}
Service fluid[a)] thermal conductivity	1.152×10^{-1}	W m^{-1} K^{-1}
Reacting mixture heat capacity	3.0×10^{3}	J kg^{-1} K^{-1}
Reacting mixture thermal conductivity	0.50	W m^{-1} K^{-1}
Metal wall thermal conductivity	18.0	W m^{-1} K^{-1}
External (air + insulation) thermal conductivity[b,c)]	20.0	W m^{-1} K^{-1}

[a)]Therminol oil; [b)]Used only for the connecting elements of the reactor; [c)]From ref. [30].

sections), h_i was not modeled by the incorporation of a specific environmental heat loss model but instead was considered constant (see Table 1). This approximation was implemented for reasons of simplicity of the overall model as well as on the basis of the expected minor effect of the produced temperature oscillations on the calculated polymer properties. The values of the physical and transport properties of the reaction mixture and the service fluid as well as the values of the various heat-transfer constants are presented in Table 1. Note also that the above expression does not account for the possible effects of reactor fouling. This is due to the fact that the reactor was operated within a region of operating conditions where no fouling was present in the reactor, defined in terms of a set of preliminary experiments (detailed results reported in an upcoming publication). All the experiments presented in this work were carried out within this region.

Finally, for the calculation of the monomer conversion and the average copolymer properties, the following expressions were used.

Monomer conversion

$$X_i = \frac{F_{M_i}^{\circ} - F_{M_i}}{F_{M_i}^{\circ}}; \quad X = \sum_{i=1}^{2} \frac{F_{M_i}^{\circ} - F_{M_i}}{F_{M_i}^{\circ}} \tag{22}$$

Average molecular weights, M_n, M_w

$$M_n = \frac{F_{\mu_{1,o}} \mathrm{MW}_1 + F_{\mu_{o,1}} \mathrm{MW}_2}{F_{\mu_{o,o}}} \tag{23}$$

$$M_w = \frac{F_{\mu_{2,o}} \mathrm{MW}_1^2 + 2F_{\mu_{1,1}} \mathrm{MW}_1 \mathrm{MW}_2 + F_{\mu_{o,2}} \mathrm{MW}_2^2}{F_{\mu_{1,o}} \mathrm{MW}_1 + F_{\mu_{o,1}} \mathrm{MW}_2} \tag{24}$$

Average molar copolymer composition in terms of M_1, cc

$$\mathrm{cc} = \frac{F_{\mu_{1,o}}}{F_{\mu_{1,o}} + F_{\mu_{o,1}}} \tag{25}$$

where MW_i is the molecular weight of the monomer unit of type "*i*."

4.4. The MC Module

The MC method has been widely implemented for the simulation of free-radical polymerization systems[19,21,22,31,32] due to its discrete stochastic nature that perfectly reflects the nature of such processes.[33] Besides, the constant increase of processing power in modern computer systems gradually depresses the disadvantages associated with the increased processing and memory demands of the method.

Among the various approaches that share common stochastic characteristics and, thus, typically fall under the general category of MC methods, the approach of Gillespie[20] has been proven to be very efficient in the stochastic simulation of homogeneous polymerization systems. His proposed formulation, also known as the "stochastic kinetic algorithm," provides a simple base for tracking the time evolution of a homogeneous multicomponent reacting system on the basis of the stochastic chemical reactions rates, R_j, defined as

$$R_j = k_j X^c; \qquad j = 1,2,\ldots,N_R \tag{26}$$

where k_j is the kinetic rate constant of the "*j*th" reaction and X^c is the total number of possible combinations of the molecules involved in a reaction step. The basic principles, governing the proposed stochastic formulation, have been thoroughly described in a previous publication.[21]

On the basis of this event-driven stochastic approach, the copolymerization process was dynamically simulated through a series of variable-duration time steps, providing detailed information on the evolution of all the key molecular properties of the individual copolymer chains of the reacting mixture (i.e., the exact number and the sequential arrangements of the two comonomer

units within each copolymer chain). Apparently, once these chain characteristics are known, it is relatively trivial to infer any average or distributed polymer property of interest (e.g., average molecular weights, molecular weight distribution, copolymer composition distribution, etc.).

From the above it becomes evident that a significant amount of information must be stored during the MC simulation, thus creating the need for an efficient bookkeeping of this information. For this reason, a number of vectors and arrays are created by the program and utilized in different ways. The main arrays of the system, P (i, j = 1:3) and D (i, j = 1:2), are used to store the number of monomer units of comonomer 1 or 2 (i.e., for j = 1 or 2, respectively), with a terminal monomer unit of type 1 or 2 (i.e., for j = 3), of the respective ith "live" or "dead" polymer chain. Accordingly, two additional vectors, L_{n1} and L_{n2}, serve as "pools" of the "live" polymer chains of the respective type of ending monomer unit (i.e., either 1 or 2), containing pointers to the actual position of each polymer chain in the overall array of the "live" chains, L_n. These vectors are required in order to avoid the redundancy that would be produced by the selection/rejection procedure that would be otherwise (i.e., if a unique pool of "live" chains were used) necessary for the selection of "live" polymer chains of a prespecified terminal unit type. Finally, a number of scalar variables indicate the instantaneous size of all the above vectors and arrays as well as the instantaneous size of the population of the rest of the reacting species (i.e., the monomers, M_1 and M_2, the initiator, I, as well as possible solvents, chain-transfer agents, etc.).

Among the different properties acquired by the implementation of the MC module exist all the polymer molecular properties also provided by the DMoM (i.e., M_n and M_w, cc) as well as a series of distributed molecular properties of interest, such as the overall weight chain length distribution (WCLD), the bivariate weight chain length distribution (2D-WCLD), and the molecular weight–copolymer composition distribution (MW-CCD). All these properties were calculated by the MC module using the following expressions.

Number average molecular weight (M_n)

$$M_n = \frac{\sum_{i=1}^{\mu_{oo}} \left(n_i^1 MW_1 + n_i^2 MW_2 \right)}{\mu_{oo}} \tag{27}$$

Weight average molecular weight (M_w)

$$M_w = \frac{\sum_{i=1}^{\mu_{oo}} \left(n_i^1 MW_1 + n_i^2 MW_2 \right)^2}{\sum_{i=1}^{\mu_{oo}} \left(n_i^1 MW_1 + n_i^2 MW_2 \right)} \tag{28}$$

Total molar fraction of monomer M_1 in the copolymer chains (cc)

$$cc = \frac{\sum_{i=1}^{\mu_{oo}} \left(n_i^1 / \left(n_i^1 + n_i^2 \right) \right)}{\mu_{oo}} \tag{29}$$

where n_i^j denotes the total number of monomer units of type "j" (j = 1, 2) for the "ith" "dead" copolymer chain and μ_{00}

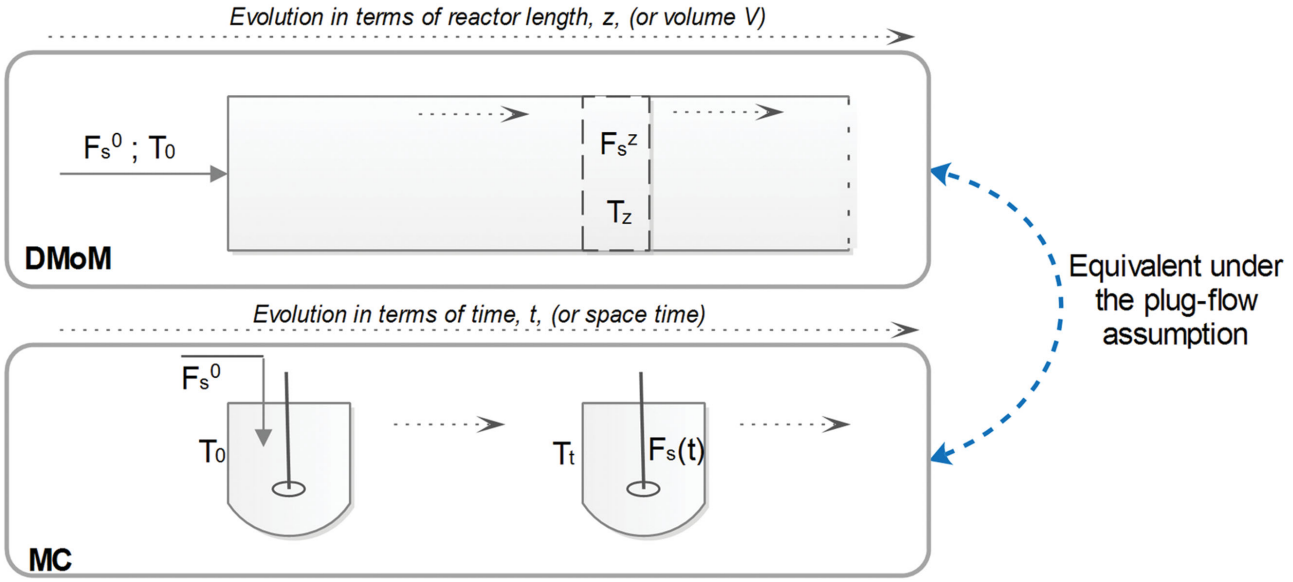

Figure 1. Schematic description of the connection between the DMoM and MC simulation algorithms.

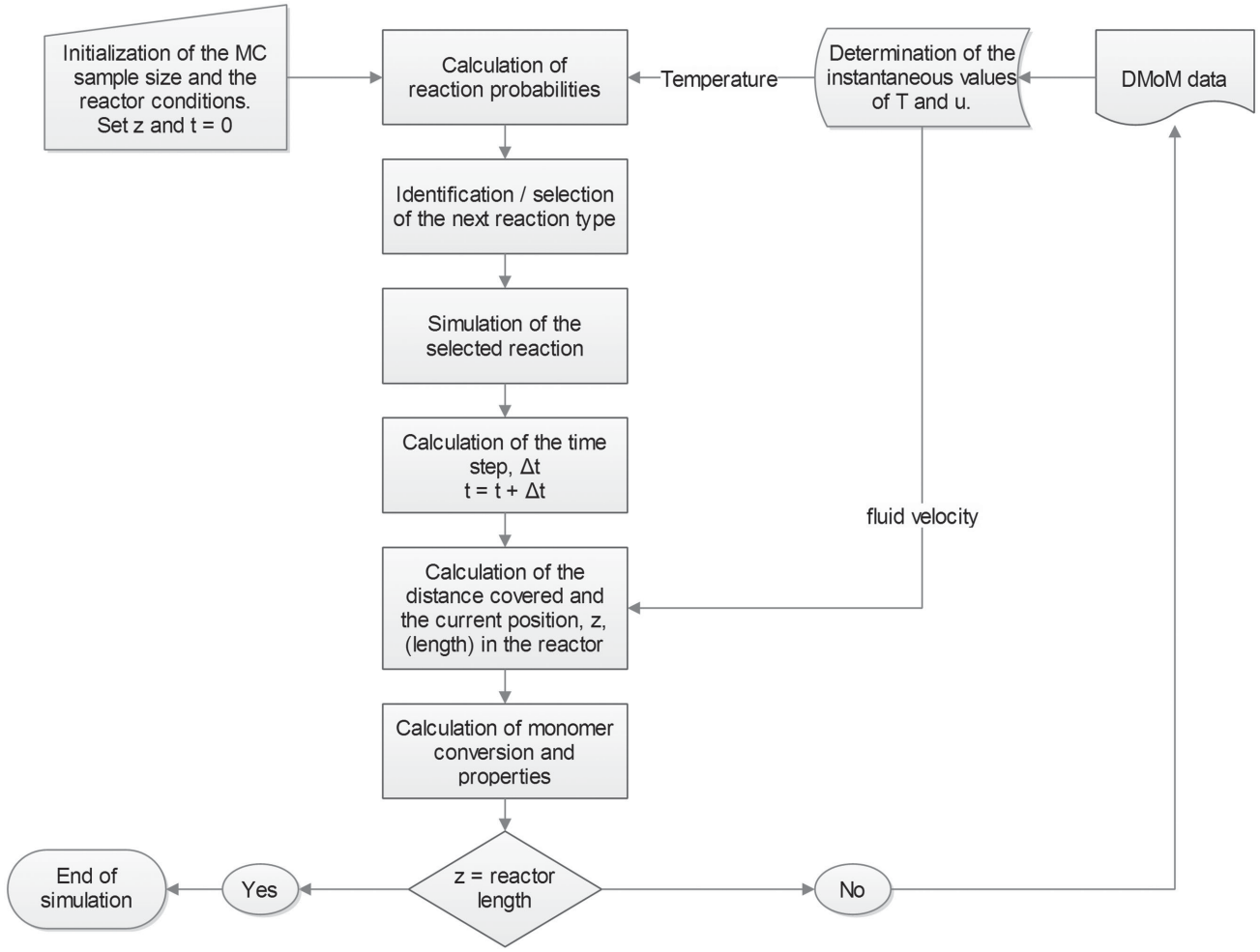

Figure 2. Schematic description of the MC algorithm.

is the total number of "dead" polymer chains in the sample population. For the reconstruction of the distributed molecular properties, the respective property domains (i.e., the chain length or the copolymer composition domains) must be discretized into a number of elements (i.e., $N_{e,N}$ and $N_{e,c}$ for the chain length and copolymer composition domains, respectively), denoted by $u_N(i); i = 1, 2, .., N_{e,N} + 1$ and $u_c(j); j = 1, 2, .., N_{e,c} + 1$. Accordingly, the respective normalized distributions were calculated by the following expressions.

Table 2. Kinetic rate constants of the model. The kinetic rate constants considering M_2 are not disclosed due to confidentiality reasons. The kinetic rate constants considering M_1 that do not appear in this table (i.e., k_{fm11}, k_{fm21}, k_{td11}, and k_{td21}) are set equal to 0.

Reaction	Pre-exponential factor, k_0	Activation energy, E	Units
Initiator decomposition, k_d	3.3×10^{11}	105.0	s^{-1}/kJ mol^{-1}
Propagation, k_{p11}	3.96×10^{7}	15.4	L mol^{-1} s^{-1}/kJ mol^{-1}
Termination by Comb., k_{tc11}	1.0×10^{11}	15.1	L mol^{-1} s^{-1}/kJ mol^{-1}
	r_{12}	r_{21}	
Reactivity ratio[a)]	0.42	0.28	–
Initiator efficiency, f	0.55	–	

[a)]Identified experimentally by the Laboratory of Polymer Engineering for High Technologies (LIPHT), Strasbourg, France.

Table 3. Outline of the experimental conditions of the cases presented in this work. The solution pH was kept constant around the value of 2.2.

Experiment ID	A1	A2	A3	B1	B2
Solid content[a)]	0.215	0.215	0.215	0.215	0.215
Initial initiator molar ratio[b)]	1.64×10^{-2}	3.28×10^{-3}	1.64×10^{-3}	1.64×10^{-2}	3.28×10^{-3}
Oil temperature, [°C]	70	70	70	80	80
Inlet temperature[c)], [°C]	60	60	60	70	70
Total flow rate[d)], [kg h^{-1}]	2	2	2	2	2

[a)]Solid content (SC) is defined as the initial weight fraction of both comonomers in the solution (w/w); [b)]Defined in terms of the total initial molar concentration of both comonomers; [c)]Denotes the temperature of preheating of the initial solutions of the comonomers and the initiator; [d)]Considered constant due to the low value of SC.

Weight chain length distribution (WCLD)

$$W_f(i)=\frac{\sum_{j=1\ ;\ u_N(i)\le\left(n_j^1+n_j^2\right)<u_N(i+1)}^{\mu_{00}}\left(n_j^1+n_j^2\right)}{\left(u_N(i+1)-u_N(i)\right)\left(\mu_{10}+\mu_{01}\right)};\quad i=1,2,.,N_{e,N} \tag{30}$$

Normalized bivariate weight chain length distribution (2D-WCLD)

$$\mathrm{WW}_f(i,j)=\frac{\sum_{z=1;\ u_N(i)\le n_z^1<u_N(i+1);\ u_N(j)\le n_z^2<u_N(j+1)}^{\mu_{00}}\left(n_z^1+n_z^2\right)}{\left(\left(u_N(i+1)-u_N(i)\right)\left(u_N(j+1)-u_N(j)\right)\right)\left(\mu_{10}+\mu_{01}\right)};\quad i,j=1,2,.,N_{e,N} \tag{31}$$

Normalized weight chain length–copolymer composition distribution (MW-CCD)

$$\mathrm{WC}_f(i,j)=\frac{\sum_{z=1;u_N(i)\le\left(n_z^1+n_z^2\right)<u_N(i+1);u_c(j)\le cc_z<u_c(j+1)}^{\mu_{00}}\left(n_z^1+n_z^2\right)}{\left(\left(u_N(i+1)-u_N(i)\right)\left(u_c(j+1)-u_c(j)\right)\right)\left(\mu_{10}+\mu_{01}\right)};\quad \begin{cases} i=1,2,.,N_{e,N} \\ j=1,2,.,N_{e,c} \end{cases} \tag{32}$$

where μ_{10} and μ_{01} denote the (one-zero) and (zero-one) moments of the bivariate distribution, respectively. These moments represent the total numbers of M_1 and M_2 monomer units in the "dead" polymer chains, respectively. Finally, cc_j denotes the molar fraction of monomer M_1 in the jth "dead" polymer chain.

Since the MC approach that is implemented in this work follows the evolution of the polymerization in terms of the molecular developments of each "live" or "dead" polymer chain existing in the sample population, it was also straightforward to acquire information on the sequence length distribution (SLD) of the formed copolymer chains (i.e., the length of the sequences of consecutive monomer units of comonomer 1 or 2 in the copolymer macromolecules). One, relatively simple approach to acquire this information is by keeping record of two additional characteristics of each growing macromolecule (i.e., besides the total number of monomer units of each comonomer and the identity of the final monomer unit of the chain) corresponding to the current sequence length of M_1 and M_2 in the respective chain (by definition one of these two values will always be equal to 0). As soon as the growing chain under consideration undergoes a chemical reaction that terminates this sequence, the total achieved sequence length is recorded for the respective type of comonomer. Such a reaction might be: (i) a propagation reaction of type $P_{n,m}^i + M_j$, with $i \neq j$, or any termination reaction, including transfer to monomer. Note that in the case of termination by combination of type $P_{n,m}^i + P_{r,q}^i$, the overall sequence length of type "i" will be equal to the summation of the respective lengths of the two participating chains. Since this tracking takes place from the moment of the creation (i.e., initiation) of a "live" polymer chain to the moment of its deactivation (i.e., by one of the mentioned chemical reactions) and throughout its growth (i.e., by the propagation chemical reactions), the sequence-length characteristics of the complete population are monitored. Hence, at any point during the polymerization, the total number of sequences (or segments) of different size and type, which form the entire length of all the "live" and "dead" chains of the mixture, is known. The cumulative sequence length distribution, SLD_c, can then be defined as the number of these sequences divided by the total (current) size of the polymer chains

$$\mathrm{SLD_c}(I,j)=\frac{\sum(\text{segments of type } I \text{ and size } j)}{m_{10}+m_{01}};\ I=1,2 \tag{33}$$

5. Structure of the Simulator

In the present approach, an integrated modular simulation approach was implemented in order to take full advantage

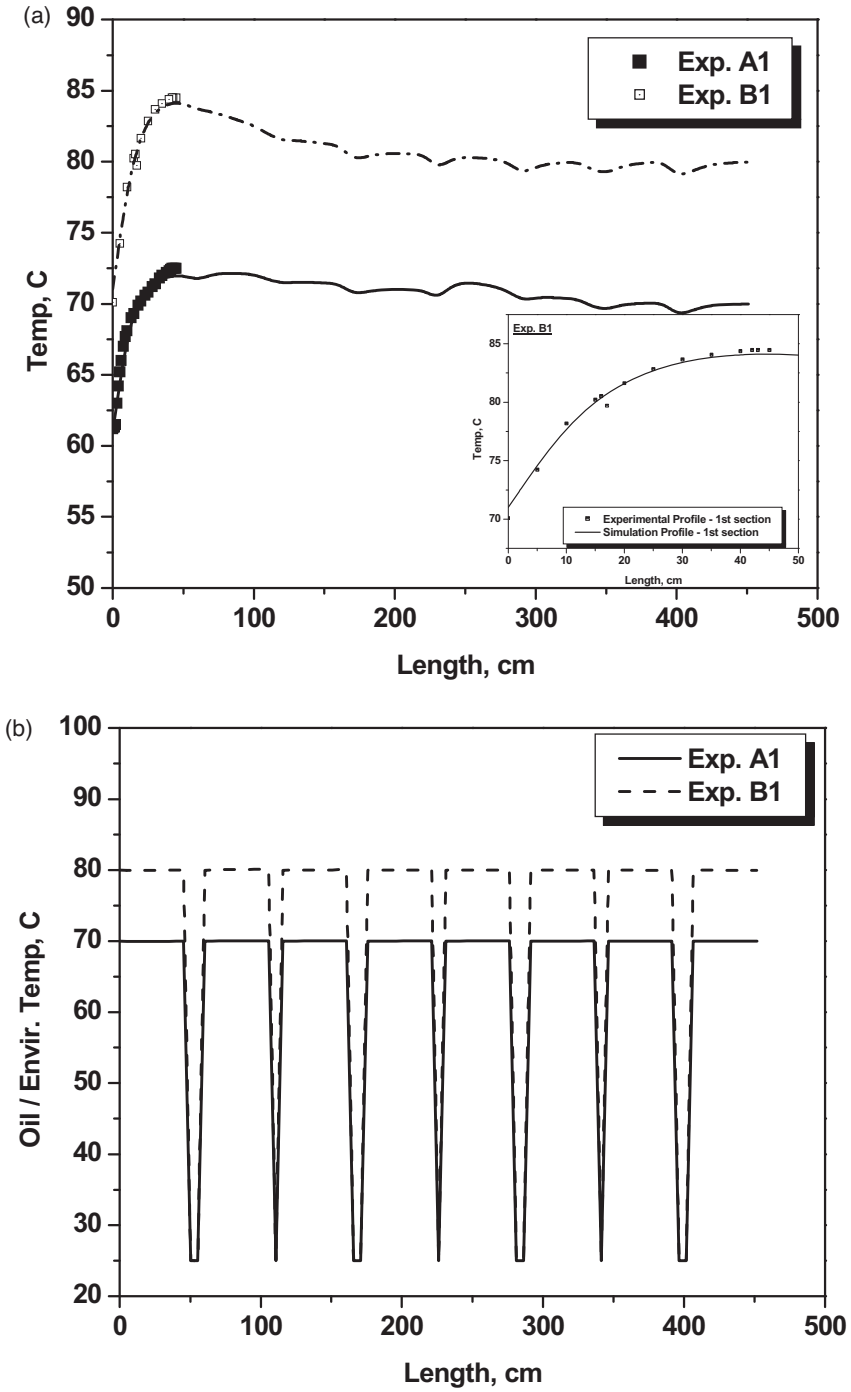

Figure 3. a) Evolution of the reactor temperature along the reactor length. Inset: Evolution of the reactor temperature in section 1; b) evolution of the external temperature along the reactor length (points: experimental measurements; curves: model predictions).

of the different capabilities of the two methods (i.e., the DMoM and the MC). More precisely, the integration of the ODEs of the reactor/kinetic model with respect to the reactor length results in the pseudo-dynamic profiles of (i) the reactor and jacket temperatures, (ii) the concentration of all the reactor species (i.e., monomers, initiator, and leading moments of the chain-length distribution of the copolymer), as well as of (iii) all the average properties of the copolymer (i.e., average molecular weights and composition) and conversion indexes (i.e., partial conversion in terms of each comonomer and total monomer conversion), calculated in terms of the leading moments with the use of Equations (22)–(29). The simulation can terminate at this point or it may be completed by the activation of the MC module.

The MC module can be utilized "at-will" to provide additional information on the molecular characteristics of the produced copolymer chains, most notably, the different chain length and/or copolymer composition distributed properties (Equations (30)–(33)). To this end, a dynamic kinetic MC simulation was run for a homogeneous differential volume (i.e., considered as a "slice" of the reactor volume), on the basis of the different profiles provided by the precedent DMoM simulation. This approach has been previously successfully applied to a high-pressure industrial low density polyethylene tubular reactor.[23] It should be emphasized at this point that the plug-flow assumption has been experimentally verified for the range of interest of operational conditions of the process.

More specifically, the kinetic MC module was run as a partially standalone simulation, starting from the same initial conditions as the DMoM simulation and making use of the profiles of the reactor temperature and fluid velocity with respect to the reactor length, issued by the previous reactor simulation. The MC simulation ran dynamically providing the time evolution of the polymer average and distributed properties of interest and conversion indexes. By making use of the fluid velocity, u, (as provided by the DMoM) at each instant of the MC simulation, it was possible to establish the connection between the process time elapsed within the MC simulation and the current point of the total reactor length, thus converting the dynamic character of the MC simulation to pseudo-dynamic. Via this procedure, the temperature profile

was accurately followed by the kinetic MC simulation. A schematic description of the connection of the kinetic MC algorithm with the reactor, as applied in the present study, is depicted in Figure 1 while in Figure 2, an overall algorithm of the MC module is presented.

The developed integrated modular approach combines the speed and accuracy of the DMoM with the detailed molecular information provided by the MC kinetic module in a single, very powerful, and flexible simulator. Since the MC method is significantly more CPU-demanding (i.e., requires higher simulation times), this module was optionally utilized each time additional polymer properties were of interest, while the DMoM simulation sufficed for a rapid acquisition of all the typical simulation results of interest (e.g., conversion and temperature profiles, average copolymer properties, etc.). It is characteristic that, while a DMoM simulation required a simulation time in the order of five to ten seconds (5–10 s), the MC module demanded an additional simulation time of one to twenty minutes (1–20 min), depending on the selection of the sample size (additional information on the selection of the initial sample size is provided elsewhere[21]). Typical initial MC sample sizes in the present work consisted of 10^8–10^{12} monomer molecules and 10^6–10^{10} initiator molecules. All simulations were carried out on a 2.4 GHz dual-CPU (Intel Xeon E5620) PC unit. The totality of the program was written in Fortran 90.

It should be noted at this point that the required CPU times, even for the more demanding MC module, are by no means prohibitive (i.e., contrary to the common belief of previous years), even for industrial use of the simulator in terms of an advanced process monitoring and control system that would operate on the basis of the molecular properties of the produced (co)polymer. If such an application was to be envisaged, the execution time could be even more decreased, at the cost of a minor decrease in accuracy, acceptable for such applications, by further decreasing the size of the simulation sample. This is an important development, mainly attributed to the impressive evolution of modern CPU systems (i.e., even of

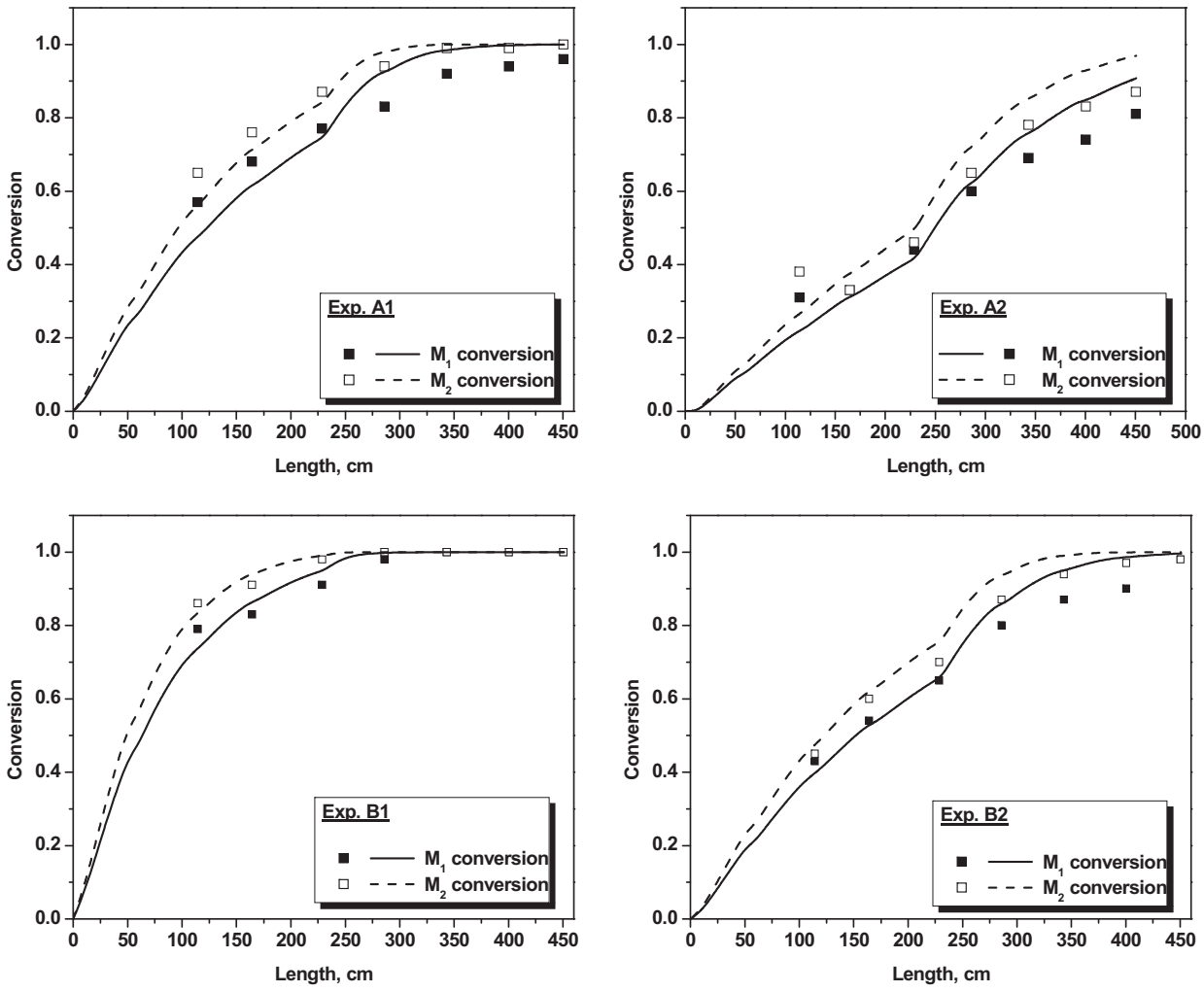

Figure 4. Evolution of the monomer conversion along the reactor length (points: experimental measurements; curves: model predictions).

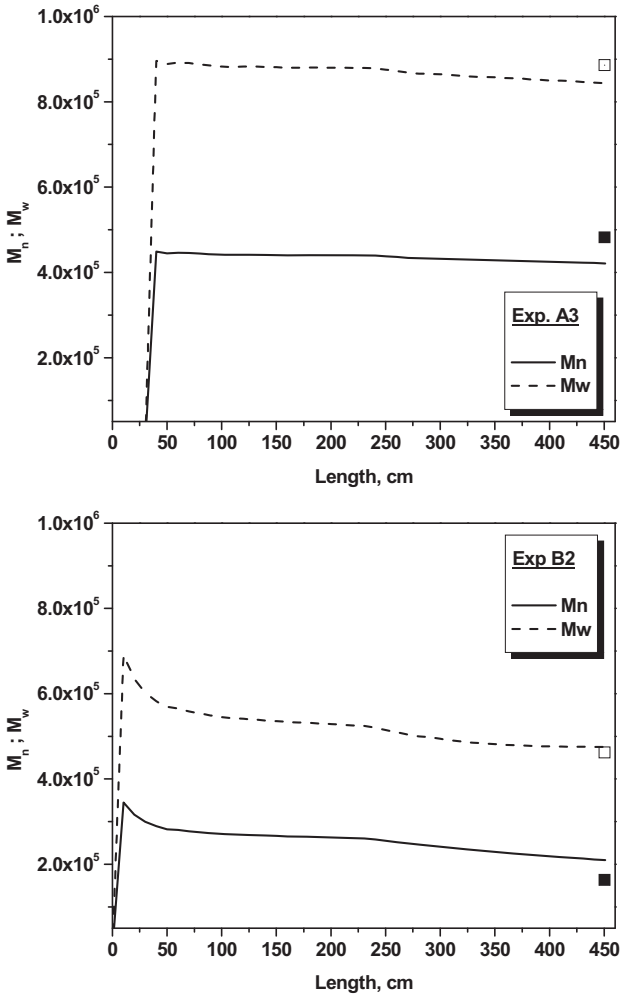

Figure 5. Evolution of the average molecular weights along the reactor length (curves: model predictions) and experimental measurements (points) of their final values.

personal computers) that can greatly facilitate and motivate a more widespread industrial applicability of comprehensive mechanistic models.

6. Results and Discussion

A series of experimental measurements under different conditions, in terms of the initial initiator flow rate and reactor temperature, were utilized to regulate the kinetic rate constants of the model. Note that the kinetic rate constants of the initiator decomposition as well as those of the propagation and termination reactions between AA species were based on the most recent literature data for AA homopolymerization.[25,34–36] The unknown values of the kinetic parameters of the model were fitted on the basis of the available experimental measurements. The propagation rate constants were fitted in terms of the monomer conversion measurements while the rest of the kinetic rate constants (i.e., the transfer and termination rate constants) were fitted on the basis of the molar mass measurements (i.e., M_n, M_w, and MWD). The final values of the parameters of the model are presented in Table 2. Since all the experiments were carried out under low percentage of solid content (see Table 3), the kinetic rate constants were considered to be chain length independent. Nevertheless, if necessary, such an effect could be very easily incorporated into the proposed model. The recipes and the conditions of the experiments presented in this study are shown in Table 3. The comonomer molar composition of the reactor feed for all the experiments was equal to 0.665.

In Figure 3a,b, the temperature curves corresponding to experiments A1 and B1 are presented. More specifically, in Figure 3a, the evolution of the reactor temperature is depicted along the reactor length for the two experiments. The curves correspond to the model predictions while the discrete points correspond to experimental measurements carried out in the first section of the reactor via the use of the movable thermocouple (see Section 2—"Reactor Configuration and Materials"). This part of the curves is more clearly depicted in the enlarged inset of this figure. A series of characteristic fluctuations of the reactor temperature, over a range of ≈2–3 °C, are easily observed in this figure and are attributed to the connecting parts (i.e., between the reactor sections) that are not covered by the reactor jacket and are, thus, exposed to a much lower external temperature (i.e., the environmental temperature). This is also demonstrated in Figure 3b, where the evolution of the external temperature of the reactor is depicted along the reactor length. Finally, a large fluctuation that is observed around the middle of the reactor length is the result of both the connector element and the increase of the internal reactor diameter.

In Figure 4a–d, the experimental measurements (i.e., points) of the conversion of both monomers are compared to the respective model predictions (i.e., curves) at different positions along the reactor, for experiments A1, A2, B1, and B2, respectively. Accordingly, in Figure 5a,b, the theoretically predicted evolution of the number and weight average molecular weights along the reactor is presented and compared to the respective experimental measurements at the reactor exit, for experiments A3 and B2, respectively. It can be seen that, despite some minor deviations, the proposed model is capable of describing with good accuracy the evolution of the polymerization under different conditions. It must be noted at this point that the DMoM and the MC predictions of all the average molecular properties of the produced copolymer are virtually identical, hence there is no need for a specific distinction with regard to the above presented results (i.e., Figures 4 and 5).

By making use of the MC module, it is possible to calculate the full WCLD developments of the copolymer at

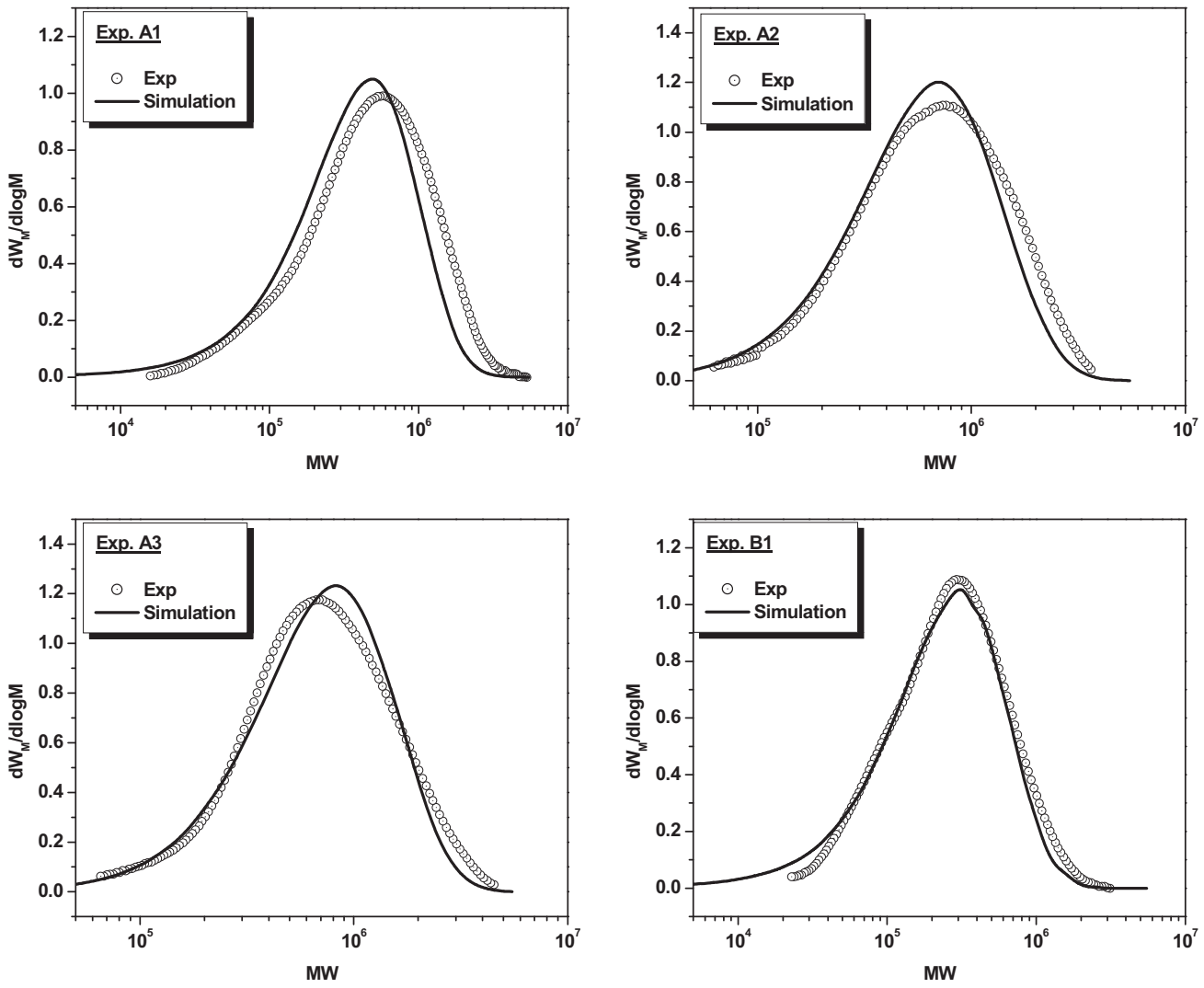

Figure 6. Comparison of the theoretical predictions (curves) with the experimentally measured molecular weight distribution of the copolymer at the exit of the reactor.

any point in the reactor. In Figure 6a–d, the molecular weight distribution of the final copolymer, as determined by size-exclusion chromatography (see Section 2—"Reactor Configuration and Materials") at the exit of the reactor, is compared to the respective theoretical predictions by the MC module, for experiments A1, A2, A3, and B1, respectively. This comparison verifies the validity of the model and clearly demonstrates the advantages in the use of this extra MC module.

The predictive capabilities of the MC module are not limited to the prediction of the WCLD but can be further exploited for the calculation of additional distributed properties of interest that cannot be provided by the DMoM. An example is the calculation of the bivariate molecular weight–copolymer composition distribution (MW-CCD) of the copolymer. Figure 7 depicts the MW-CCD as calculated by the MC module at the exit of the reactor, using the experimental conditions of experiment A1, with three different values of the initial comonomer feed molar composition (i.e., $F^{\circ}_{M_1}/\left(F^{\circ}_{M_1}+F^{\circ}_{M_2}\right)$ equal to 0.350, 0.554, and 0.750). According to the reactivity ratios of the system (see Table 2), the azeotropic feed composition of the system is equal to 0.554.[37] This is also verified in Figure 8, where the evolution of the molar copolymer compositions along the reactor is shown for the same experimental conditions. Accordingly, one can observe in Figure 7 that the MW-CCD corresponding to the azeotropic feed composition is a very narrow distribution, in terms of the CC domain, especially at the high-MW domain. On the other hand, the distribution of the copolymer produced with the initial comonomer feed molar composition equal to 0.35 is extremely broad, which is a result of the constant decrease of the average copolymer composition during the polymerization (see Figure 8), accompanied by the constant creation of new copolymer chains of lower MW and CC at the same time.

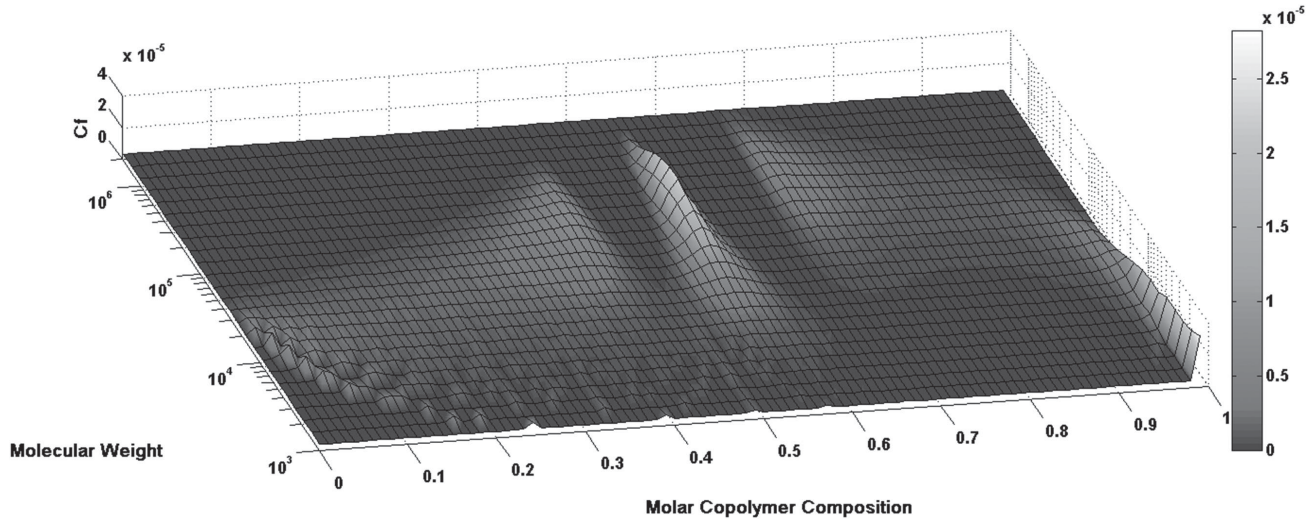

Figure 7. MC calculated MW-CCD at the exit of the reactor for three different values of the initial comonomer feed molar composition (0.350, 0.554, and 0.750).

Finally, the distribution corresponding to the initial comonomer feed molar composition of 0.75 displays an unconventional form as it seems to be comprised of two interconnected, individual distributions: one relatively broad, in terms of the CC domain, at the high-MW domain and another one extremely narrow close to a molar composition equal to 1, located at the low-MW domain. Although it would be expected that the form of this distribution would be similar (but reverse) to that of the second distribution (i.e., the one located at the low cc domain), this is not the case. It seems that the dominant factor determining the form of this distribution is the early depletion of the reacting mixture from M_2 (i.e., conversion of M_2 reaches 100% at a length of 3 m), which results in the formation of a quasi-individual population of homopolymer chains of M_1, of low MW, and of cc = 1. Hence, although the overall average copolymer composition of the final product is equal to 0.75, the distribution of the copolymer chains in terms of the copolymer composition is extremely irregular, which is expected to greatly influence the final properties of the product and which would not be easily detected without the implementation of the MC module.

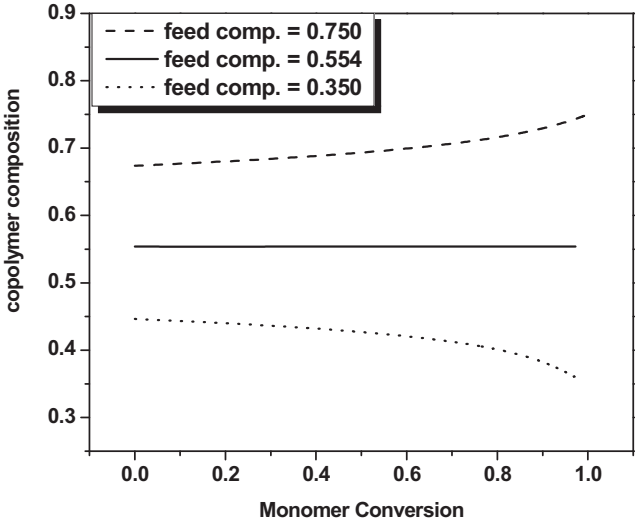

Figure 8. Evolution of the average copolymer composition of the copolymer, along the reactor length, for three different values of the initial comonomer feed molar composition (0.350, 0.554, and 0.750).

The same phenomenon can be observed in Figure 9, where the 2D projection of the bivariate weight chain length distribution (2D-WCLD) is depicted, as calculated by the MC module, under the same experimental conditions (i.e., experiment A1, comonomer feed molar composition equal to 0.75) and at four different positions along the reactor length (i.e., at 0.5, 1.5, 2.5 m, and at the reactor end). It can be seen that, as the polymerization progresses, the copolymer chains constantly increase their content in M_1 monomer units, especially the chains that remain relatively short (i.e., in the low CL domain of M_2), a phenomenon that is in complete agreement with the previous results.

In order to acquire a general picture of the evolution of the compositional characteristics of the polymer chains along the reactor, it is also possible to calculate via the MC module the bivariate distribution corresponding to the evolution of the instantaneous copolymer composition distribution with respect to the overall monomer conversion. Such a distribution is depicted in Figure 10 for the same experimental conditions used in Figure 7. As expected, the general form of these bivariate distributions is similar to that shown in Figure 8. The instantaneous

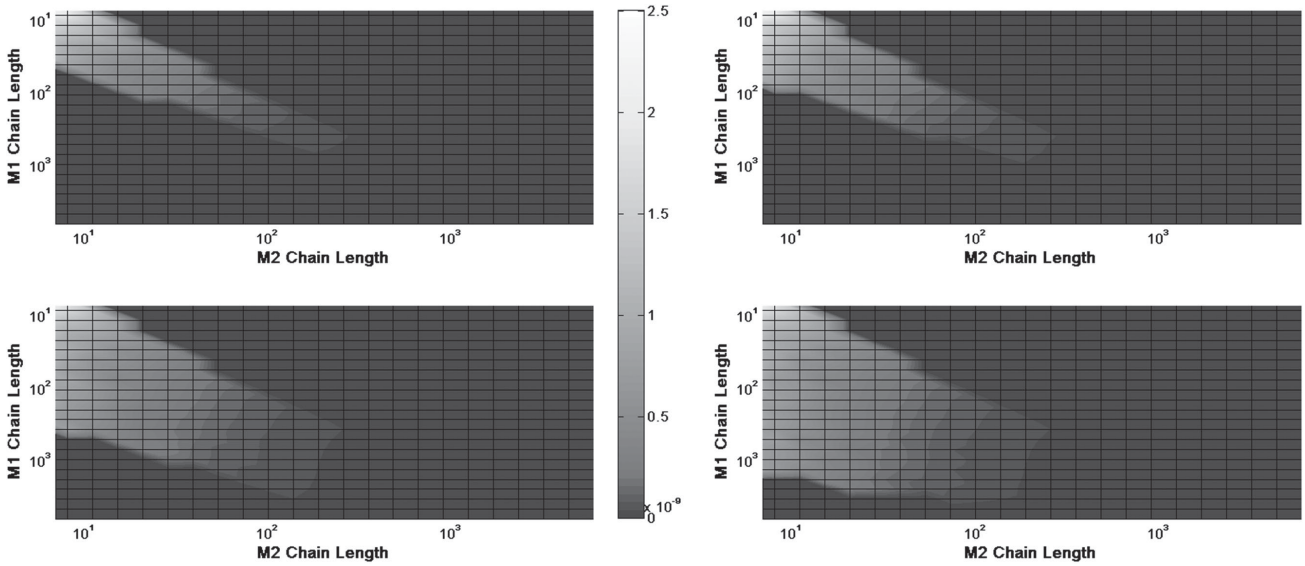

Figure 9. 2D projection of the bivariate weight chain length distribution, as calculated by the MC module at four different positions in the reactor (upper left: 0.5 m; upper right: 1.5 m; lower left: 2.5 m; and lower right: 4.5 m), for an initial comonomer feed molar composition of 0.750.

copolymer composition distribution produced at different instances in the reactor seems to remain relatively constant in terms of polydispersity (i.e., broadness) and simply drifts with respect to its median value. In complete accordance with the previous results, the distribution corresponding to the initial comonomer feed molar composition of 0.75 displays a more dramatic drift which, close to an overall conversion of 1, reaches a composition of pure M_1.

Finally, in Figure 11a,b, the MC calculated evolution of the cumulative sequence length distributions (SLD_c) of both comonomers is depicted along the reactor length, for size up to eight consecutive units and for a feed molar composition of 0.75. Note that the SLD_c represents the number fraction (i.e., in terms of m_1) of the segments of consecutive monomer units that are bound by monomer units of different type and/or by a chain end. As expected (according to the above observations), the SLDs of monomer 1 and of a larger size (i.e., the ones corresponding to seven and eight consecutive monomer units, marked with open symbol) display a gradual increase while the shorter ones continuously decrease. At the same time, the SLDs of comonomer

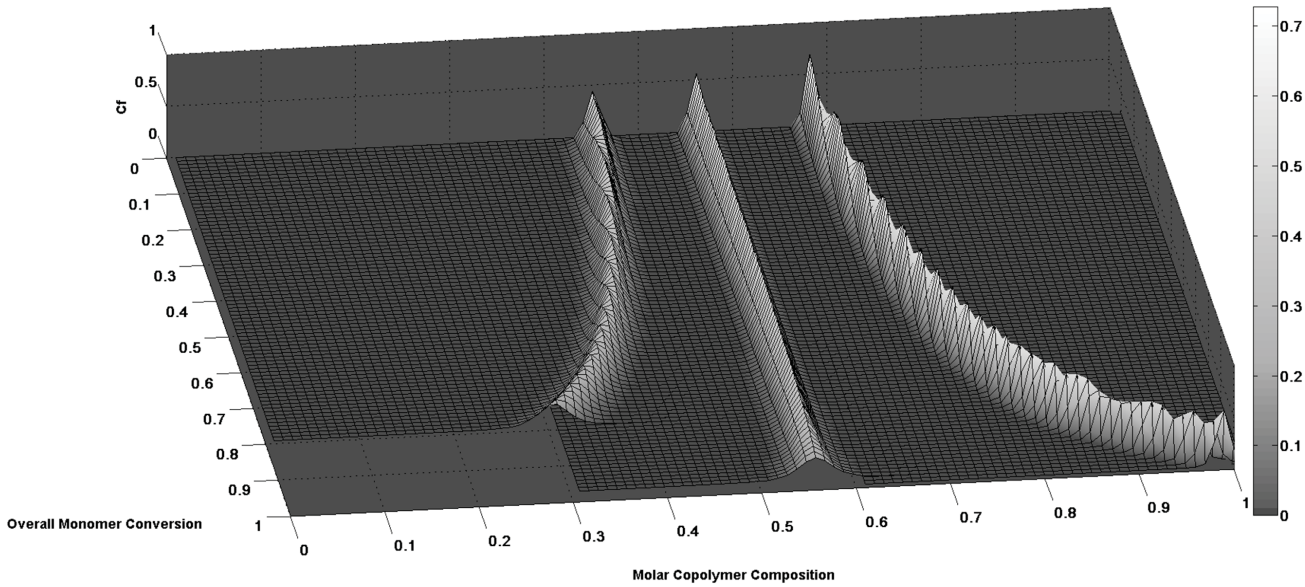

Figure 10. Evolution of the instantaneous copolymer composition distribution with respect to the overall monomer conversion, as calculated by the MC module for an initial comonomer feed molar composition of 0.750.

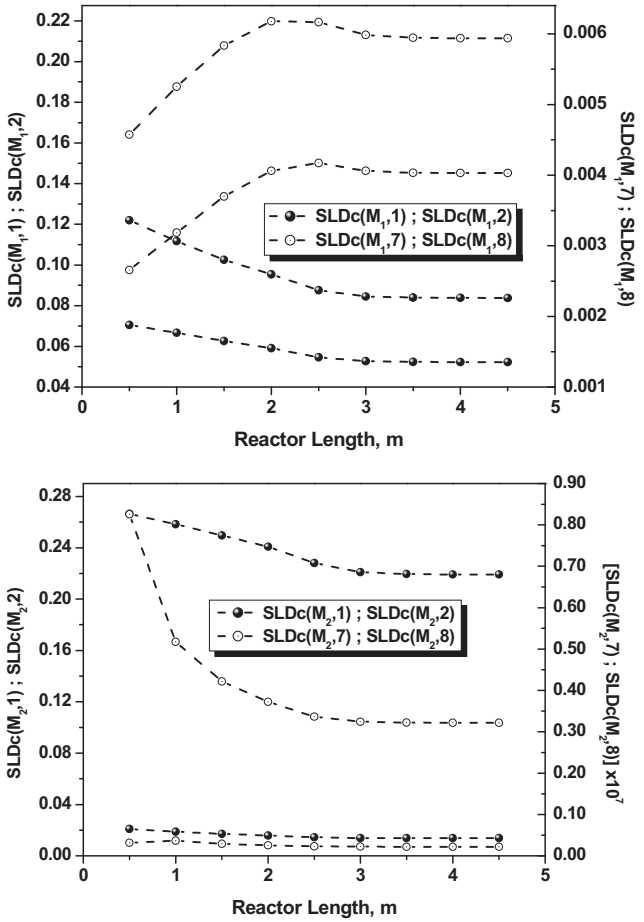

Figure 11. Evolution of the SLDc(*i*,*j*), for $j = 1,2,7,8$, as calculated by the MC module, for a feed molar composition of 0.75; a) $i = 1$, b) $i = 2$.

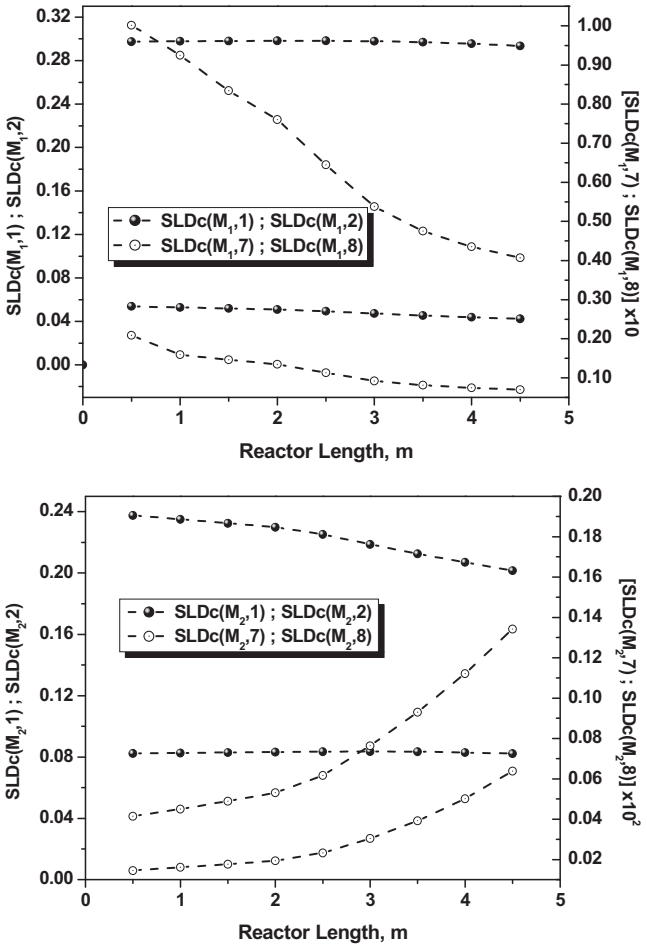

Figure 12. Evolution of the SLDc(*i*,*j*), for $j = 1,2,7,8$, as calculated by the MC module, for a feed molar composition of 0.35; a) $i = 1$, b) i = 2.

2 are all decreasing, irrespective of their size. Note also the relative difference in the values of these properties that extends several orders of magnitude (note the difference in scales between the right and left axes). The situation is reversed in Figure 12a,b, where the respective plots are drawn for the feed molar composition of 0.35. In this case, always in complete agreement with the previous results, the long M_1 sequences decrease while the long M_2 sequences increase, as a result of the continuous incorporation of less M_1 monomer units in the copolymer chains due to the gradual decrease of the copolymer composition.

7. Concluding Remarks

In the present work, a complete mathematical model of the free-radical copolymerization of AA in an aqueous solution was presented for a pilot-scale tubular reactor, equipped with static mixers. On the basis of the proposed model, an integrated, modular simulator was also developed in terms of the implementation of two different numerical approaches, namely, the DMoM and the MC method, in order to combine the advantages of speed, efficiency, and increased predictive capabilities. The parameters of the proposed model were fixed through a direct comparison of its predictions with available experimental measurements on the monomer conversion, the average molecular properties, and the molecular weight distribution of the produced copolymer, under different conditions. At a second stage, the effect of the initial comonomer molar ratio on the compositional characteristics of the copolymer chains was also investigated under varying comonomer feed ratios and via the implementation of the MC module.

This study has provided clear evidence of the necessity to develop efficient tools, capable of describing the influence of the process conditions on the macromolecular and compositional characteristics of the produced polymer macromolecules, within the context of process intensification and of acquiring deeper knowledge as well as control over the final properties of the synthesized polymers.

Acknowledgements: This work was funded by the European Community's Seventh Framework Program: F3Factory—Fast, Flexible, Future Factory.

Received: May 18, 2015; Revised: July 7, 2015; Published online: March 7, 2016; DOI: 10.1002/mren.201500036

Keywords: acrylic acid; method of double moments; Monte Carlo; polymerization; polymer properties

[1] P. A. Williams, *Handbook of Industrial Water Soluble Polymers*, Blackwell Publishing; Blackwell Publishing: Oxford; Ames, Iowa, **2007**.
[2] K. S. Anseth, R. A. Scott, N. A. Peppas, *Macromolecules* **1996**, *29*, 8308.
[3] F. L. Buchholz, *Encycl. Polym. Sci. Technol.* **2002**, *8*, 106.
[4] G. Swift, *Encycl. Polym. Sci. Technol.* **2002**, *1*, 79.
[5] C. Kiparissides, *J. Process Control* **2006**, *16*, 205.
[6] H. Catalgil-Giz, A. Giz, A. M. Alb, W. F. Reed, *J. Appl. Polym. Sci.* **2004**, *91*, 1352.
[7] V. A. Kabanov, D. A. Topchiev, T. M. Karaputadze, L. A. Mkrtchian, *Eur. Polym. J.* **1975**, *11*, 153.
[8] V. A. Kabanov, D. A. Topchiev, T. M. Karaputadze, *J. Polym. Sci. Polym. Symp.* **1973**, *42*, 173.
[9] R. J. Minari, G. Caceres, P. Mandelli, M. M. Yossen, M. Gonzalez-Sierra, J. R. Vega, L. M. Gugliotta, *Macromol. React. Eng.* **2011**, *5*, 223.
[10] I. Rintoul, C. Wandrey, *Macromolecules* **2005**, *38*, 8108.
[11] R. A. Scott, N. A. Peppas, *AIChE J.* **1997**, *43*, 135.
[12] H. Ito, A. Shimizu, S. Suzuki, *J. Chem. Soc. Jpn.* **1955**, *58*, 194.
[13] S. S. Cutie, P. B. Smith, D. E. Henton, T. L. Staples, C. Powell, *J. Polym. Sci. Part B : Polym. Phys.* **1997**, *35*, 2029.
[14] N. F. G. Wittenberg et al., *Macromol. React. Eng.* **2015**, DOI: 10.1002/mren.201500017.
[15] P. D. Iedema, H. C. J. Hoefsloot, *Macromol. Theory Simul.* **2005**, *14*, 505.
[16] A. Krallis, D. Meimaroglou, C. Kiparissides, *Chem. Eng. Sci.* **2008**, *63*, 4342.
[17] V. Saliakas, C. Chatzidoukas, A. Krallis, D. Meimaroglou, C. Kiparissides, *Macromol. React. Eng.* **2007**, *1*, 119.
[18] M. Wulkow, *Macromol. Theory Simul.* **1996**, *5*, 393.
[19] D. Meimaroglou, A. Krallis, C. A. Kiparissides, *Chem. Prod. Process Model.* **2008**, *3*, 1.
[20] D. T. Gillespie, *J. Phys. Chem.* **1977**, *81*, 2340.
[21] D. Meimaroglou, A. Krallis, V. Saliakas, C. Kiparissides, *Macromolecules* **2007**, *40*, 2224.
[22] C. Schütte, M. Wulkow, *Macromol. React. Eng.* **2010**, *4*, 562.
[23] D. Meimaroglou, P. Pladis, A. Baltsas, C. Kiparissides, *Chem. Eng. Sci.* **2011**, *66*, 1685.
[24] E. Neuhaus, T. Herrmann, I. Vittorias, D. Lilge, G. Mannebach, A. Gonioukh, M. Busch, *Macromol. Theory Simul.* **2014**, *23*, 415.
[25] J. Barth, W. Meiser, M. Buback, *Macromolecules* **2012**, *45*, 1339.
[26] C. Preusser, R. A. Hutchinson, *Macromol. Symp.* **2013**, *333*, 122.
[27] M. Buback, P. Hesse, I. Lacík, *Macromol. Rapid Commun.* **2007**, *28*, 2049.
[28] C. Kiparissides, D. Meimaroglou, P. Pladis, A. Baltsas, *Ind. Eng. Chem. Res.* **2005**, *44*, 2592.
[29] C. Kiparissides, G. Verros, J. F. Macgregor, *J. Macromol. Sci. Part C: Polym. Rev.* **1993**, *33*, 437.
[30] W. L. McCabe, J. C. Smith, P. Harriott, **1993**.
[31] M. A. Al-Harthi, J. K. Masihullah, S. H. Abbasi, J. B. P. Soares, *Macromol. Theory Simul.* **2009**, *18*, 307.
[32] H. Tobita, *J. Polym. Sci. Part B: Polym. Phys.* **1993**, *31*, 1363.
[33] D. Meimaroglou, C. Kiparissides, *Ind. Eng. Chem. Res.* **2014**, *53*, 8963.
[34] D. E. Henton, C. Powell, R. E. Reim, *J. Appl. Polym. Sci.* **1997**, *64*, 591.
[35] I. Lacík, S. Beuermann, M. Buback, *Macromolecules* **2003**, *36*, 9355.
[36] I. Lacík, S. Beuermann, M. Buback, *Macromolecules* **2001**, *34*, 6224.
[37] G. G. Odian, *Principles of Polymerization*; Wiley: Hoboken, N.J. **2004**.

2.4 On the modeling of multi-functional biopolymers

The third and final article of this section reports a modeling framework for the system of polycondensation of sugars. More specifically, the same two methods, namely the MoM and the MC method, were employed in this work to describe the kinetic developments of the reactive system of saccharides. It is a system of high interest to the industrial sectors of food and health products. The hydrolysis of cellulosic biomass for the derivation of oligosaccharides as intermediates for the synthesis of various platform chemicals has made the subject of numerous studies for many years. However, the inverse route of polycondensation of the oligosaccharides for the controlled synthesis of polysaccharides of high degree of polymerization (DP) in anhydrous conditions has received much less attention, especially in terms of the kinetic modeling of the system. The reported work, presents a modeling framework that is based on a classical polymerization paradigm, capable of describing the evolution of the system up to the formation of saccharides of high DP.

The implementation of the MoM on this system displays some interesting characteristics, as different key-indexes of the reacting system can be directly represented by some of the moments of the different populations. The formulation of the rate functions of the moments is also of interest, as the kinetic scheme of the system includes some reactions that are not commonly encountered in classical polymerization systems. However, through the analysis of the characteristics of the method and its respective equations, as derived for this system, it is demonstrated that its application is not suitable due to its severe limitations in terms of its predictive capacity and its inherent closure problem. Accordingly, the kinetic MC formulation is selected as the only viable approach (i.e., between the two) for the modeling of the system. The results of the model are validated through a comparison with available experimental data, under four different values of the reaction temperature.

An important characteristic of this work, that makes it different from the previously presented ones, lies within the fact that glucose, which acts as the monomer unit of the formed polysaccharides, is multifunctional. In fact, the molecule of D-glucose possesses a total of five hydroxyl groups, attached to the carbon atoms forming its cyclic form, at the positions 1, 2, 3, 4 and 6 (i.e.,

relative to the anomeric carbon atom that acts as a stereocenter for this molecule). The glycosidic bonds that are formed by the polycondensation reaction between two glucose units, involve the carbon atom at position 1 (i.e., the anomeric carbon atom) and a hydroxyl group that is attached at any of the aforementioned five positions of the second glucose unit. Adding to this the fact that the formed bonds may assume different stereoisomeric positions (i.e., α or β), as well as that intramolecular bonds can also be formed within the same glucose unit, it becomes evident that the modeling of the system is not as trivial as that of a typical polymerization system.

The developed MC algorithm tracks simultaneously the DP of the sugar molecules, their number and type of hydroxyl groups, as well as their eventual bonds with anhydrosugars or other types of molecules that are present in the system. It is the capacity of the MC method to follow all these properties (or coordinates, in a PBM perspective), without the necessity to resort to complicated mathematical forms or to heavy and unstable numerical solutions, that makes it a more suitable choice for the modeling of the system, over eventual deterministic alternatives. Finally, as will be described later, in the concluding chapter of this report (Chapter 5), the MC method provides also the possibility for an eventual extension towards a more complete topological description of the system.

processes

MDPI

Article

A Novel Kinetic Modeling Framework for the Polycondensation of Sugars Using Monte Carlo and the Method of Moments

Dimitrios Meimaroglou [1,*], Sandrine Hoppe [1] and Baptiste Boit [2]

[1] Laboratoire Réactions et Génie des Procédés, Université de Lorraine, CNRS UMR7274, LRGP, F-54000 Nancy, France; sandrine.hoppe@univ-lorraine.fr
[2] ROQUETTE Frères, 62136 Lestrem, France; baptiste.boit@roquette.com
* Correspondence: dimitrios.meimaroglou@univ-lorraine.fr; Tel.: +33-3-72-74-38-41

Abstract: The kinetics of the hydrolysis and polycondensation reactions of saccharides have made the subject of numerous studies, due to their importance in several industrial sectors. The present work, presents a novel kinetic modeling framework that is specifically well-suited to reacting systems under strict moisture control that favor the polycondensation reactions towards the formation of high-degree polysaccharides. The proposed model is based on an extended and generalized kinetic scheme, including also the presence of polyols, and is formulated using two different numerical approaches, namely a deterministic one in terms of the method of moments and a stochastic kinetic Monte Carlo approach. Accordingly, the most significant advantages and drawbacks of each technique are clearly demonstrated and the most fitted one (i.e., the Monte Carlo method) is implemented for the modeling of the system under different conditions, for which experimental data were available. Through these comparisons it is shown that the model can successfully follow the evolution of the reactions up to the formation of polysaccharides of very high degrees of polymerization.

Keywords: saccharides; hydrolysis; reversion reactions; polycondensation; kinetic modeling; Monte Carlo; method of moments; population balances; glucose

Citation: Meimaroglou, D.; Hoppe, S.; Boit, B. A Novel Kinetic Modeling Framework for the Polycondensation of Sugars Using Monte Carlo and the Method of Moments. *Processes* **2021**, *9*, 745. https://doi.org/10.3390/pr9050745

Academic Editor: Giannis Penloglou

Received: 15 March 2021
Accepted: 17 April 2021
Published: 22 April 2021

1. Introduction

Saccharides are biomolecules of great importance to our society, displaying significant market potential for several industrial sectors, such as cosmetics, pharmaceutics and food-related products. Saccharides of low degree of polymerization (DP), such as C5 and C6 monosaccharides, are typically obtained via the hydrolysis of starch or lignocellulosic biomass. These may be subsequently converted to glucose syrup, maltodextrin, polyols, organic acids, biofuels or other platform chemicals, such as fructose, sorbitol, citric acid, furfural, 5–(hydroxymethyl) furfural (HMF), formic acid and levulinic acid [1–6]. The hydrolysis of starch or lignocellulosic biomass can be carried out in acidic conditions or via the use of enzymes, with each route presenting different advantages and drawbacks in terms of the selectivity and the productivity of the process [7,8]. More precisely, in the presence of acid catalysts, several side-reactions may occur, in parallel to the hydrolysis of the sugars, such as decomposition and polymerization reactions. The polymerization reactions, which are also known as reversion reactions, are considered undesirable as they consume the monosaccharides to form disaccharides or low-DP oligosaccharides. However, under strict control of the humidity levels of the reaction medium, the polymerization of monosaccharides can be utilized for the synthesis of natural-origin products, presenting a direct interest to the food, nutrition and health industrial sectors.

The polycondensation of sugars under controlled temperature and humidity, in order to achieve sugars of high degree of polymerization, has been a subject of research interest since the early 50's and the pioneering works of [9,10] and later [11]. A clear industrial interest has also been expressed very early for the synthesis of the so-called polyglucoses (or polydextroses), via the anhydrous melt polymerization of glucose and sorbitol in the

presence of acid catalysts [12,13]. These reports have clearly shown the importance of several factors on the productivity and the quality indexes of the produced polysaccharides. More precisely, they have demonstrated that the type and concentration of the acid catalyst displays a direct effect on the presence of degradation side-reactions while the effective elimination of the water produced during the polycondensation reactions is crucial to achieve high degrees of polymerization by limiting the rate of hydrolysis [10]. Since then, several studies have been carried out in an attempt to better understand these reactions, either in view of suppressing them from the hydrolysis system as undesirable side effects, either in the framework of better controlling the characteristics of the produced polysaccharides within an optimized biorefinery viewpoint [14–17].

Mathematical modeling is a tool that has been traditionally implemented to describe the evolution of reactive systems and, in this sense, contribute to the understanding of the underlying phenomena (i.e., in the case of phenomenological models) and/or provide a predictive capability on key indexes of interest, in terms of the process conditions. Given the complexity characterizing the reactive system of biomass hydrolysis, several studies have proposed different reaction schemes in an attempt to encompass the various reaction routes leading to the observed variety of produced saccharides. One of the first kinetic models to be published for the hydrolysis of cellulose under dilute acidic conditions was that of [18], already in 1945. Since then, many new studies have been reported that modify the proposed kinetic scheme either to extend its application to a wider range of conditions or to focus on specific reaction routes and products (e.g., the decomposition reactions) [8,19–24]. However, in most of these studies, the polymerization reactions are commonly considered again as side reactions resulting only in oligosaccharides, on the basis of oversimplified kinetic schemes. For example, ref. [22] studied the reaction kinetics of glucose in mildly acidic aqueous solutions, under different temperatures and glucose concentrations. In that study, the different disaccharides (i.e., in terms of the type of glycosidic bond), as well as various anhydrosugars that were formed in the system, were clearly identified and considered as individual species in a kinetic model that was proposed for the relevant glucose conversion. However, such a model can only be applied to systems containing solely monosaccharides and disaccharides, since the identification of all possible types of sugar molecules of higher DP would require the consideration of a prohibitively large amount of species and equations. Ref. [23] proposed a comprehensive kinetic model for the decomposition of glucose in acidic solutions, taking into account the concentration of protons in the medium, but the considered species were limited to glucose and its dehydration products. A similar model was proposed by [24], starting from sucrose and including the consideration of different conversion reaction paths, but without taking into account possible formation routes of higher saccharides. Finally, ref. [8] proposed a more detailed kinetic model, within a population balance perspective, including formation and decomposition reactions of glucose and cellulose oligomers, under varying acid concentrations and temperatures. Their work took into account several scission reactions of cellulose to form lower-DP saccharides and glucose, as well as glucose degradation mechanisms. Although this model was not limited to monosaccharides and disaccharides, the considered oligomers were limited, in terms of their degree of polymerization, to a maximum value of six.

In the present work, a novel mathematical modeling framework is proposed for the polycondensation of sugars in the presence of polyols (polyalcohols), under controlled concentration of water to promote the formation of high-DP saccharides. The proposed model is based on a general kinetic scheme that is formulated in terms of a classical polymerization system, taking into account the chain length of the various species that participate in the reactions. The rate functions of the different saccharides are expressed within a population balance perspective, thus allowing the consideration of the formation of polysaccharides without limitation in the maximum considered DP. Two different numerical approaches are presented, namely a deterministic one, on the basis of the method of moments, and a stochastic Monte Carlo algorithm. Through the derivation of the model equations, the limitations and the advantages of these two approaches are

clearly demonstrated for this system, and the most suitable one is implemented for the prediction of the evolution of the polymerization under different reaction conditions, for which experimental data were available.

2. Polymerization Mechanism and Rate Functions

2.1. General Kinetic Scheme

The kinetic modeling developments, presented in this work, were based on the following generalized kinetic scheme for the description of the different chemical reactions taking place in the system:

- Intermolecular bond formation/hydrolysis reactions
  - Addition of a reducing saccharide (bonds: 1-2, 1-3, 1-4 or 1-6):

$$P_n + P_m \underset{k_{A1r}}{\overset{k_{A1}}{\longleftrightarrow}} P_{n+m} + H_2O \tag{1}$$

  - Addition of a reducing saccharide (bond: 1-1):

$$P_n + P_m \underset{k_{A2r}}{\overset{k_{A2}}{\longleftrightarrow}} D_{n+m} + H_2O \tag{2}$$

  - Addition of a non-reducing saccharide (bonds: 1-2, 1-3, 1-4 or 1-6):

$$P_n + D_m \underset{k_{A3r}}{\overset{k_{A3}}{\longleftrightarrow}} D_{n+m} + H_2O \tag{3}$$

$$P_n + D_m X \underset{k_{A3r}}{\overset{k_{A3}}{\longleftrightarrow}} D_{n+m} X + H_2O \tag{4}$$

  - Addition of a polyol:

$$P_n + PO \underset{k_{A4r}}{\overset{k_{A4}}{\longleftrightarrow}} D_n PO + H_2O \tag{5}$$

  - Addition of 1-6-anhydrosugars (bonds: 1-2, 1-3 or 1-4):

$$P_n + AG \underset{k_{A5r}}{\overset{k_{A5}}{\longleftrightarrow}} D_n AG + H_2O \tag{6}$$

  - Addition of HMF (bond: 1-4):

$$P_n + HMF \underset{k_{A6r}}{\overset{k_{A6}}{\longleftrightarrow}} D_n HMF + H_2O \tag{7}$$

- Internal Ring-Closure Reactions
  - Formation of 1-6-anhydrosugars:

$$P_n \underset{k_{D1r}}{\overset{k_{D1}}{\longleftrightarrow}} \begin{cases} AG + H_2O & \text{for } n = 1 \\ D_{n-1}AG + H_2O & \text{for } n \geq 2 \end{cases} \tag{8}$$

  - Formation of HMF:

$$P_1 \xrightarrow{k_{D2}} HMF + 3H_2O \tag{9}$$

- Degradation Reactions
  - Formation of Humins:

$$P_1 \xrightarrow{k_{D3}} H + 3H_2O \tag{10}$$

$$HMF \xrightarrow{k_{D4}} H \tag{11}$$

In the above kinetic scheme, the reducing saccharides, possessing a free anomeric hydroxyl group, are denoted as P_n, n designating their respective degree of polymerization in terms of their number of constituting glucose units. The notation used for non-reducing saccharides of DP n is D_n or D_nX, the latter denoting the sugar molecules possessing a non-glucose end-group, X (i.e., $X : PO, AG$ or HMF). Other species participating in the reactions of the postulated kinetic scheme are 1-6-anhydrosugars (e.g., 1,6-anhydro-β-D-glucopyranose and 1,6-anhydro-β-D-glucofuranose), denoted as AG, and 5-hydroxymethylfurfural, denoted as HMF. The present work also considers the presence of polyols in the reacting mixture, which may react with a reducing sugar via their numerous pending hydroxyl groups. They are denoted as PO. Finally, the different products of the degradation reactions (10) and (11), also referred to as Humin-like substancies or Humins in the relevant literature [25], are denoted here as H.

The chemical reactions of the postulated kinetic scheme have been grouped into three main categories. The first category includes the chemical reactions that lead to the formation of intermolecular bonds, via the addition of a hydroxyl group of a sugar molecule or polyol to the carbocation at the C1 carbon atom of a reducing saccharide (Equations (1)–(7)). These reactions are reversible by the respective hydrolysis reactions. To add flexibility to the model, the free hydroxyl groups of anhydrosugars have also been considered susceptible to participate in these reactions (Equations (6) and (7)). More precisely, the reactions between two reducing saccharides have been considered to result in the formation of another reducing saccharide, as shown in Equation (1), only in the case of the formation of a bond in positions 1-2, 1-3, 1-4 or 1-6. An example of such a reaction for the formation of a 1-6 bond is depicted in Scheme 1. If the glycosidic bond between two reducing saccharides is formed in position 1-1, then the resulting saccharide is a non-reducing one as it no longer possesses a free anomeric hydroxyl group, as shown in Equation (2) and in Scheme 2.

On the other hand, the formation of a glycosidic bond between a reducing and a non-reducing saccharide, will always result in the formation of a non-reducing saccharide, irrespective of the position of the bond (the formation of a 1-1 bond is not possible in this case). This is illustrated in Equations (3) and (4), as well as in Scheme 3.

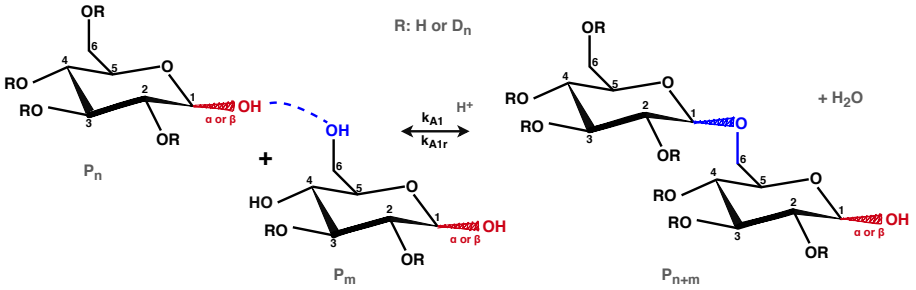

Scheme 1. Schematic representation of Reaction (1). The anomeric hydroxyl groups are marked in red and the formed linkages in blue.

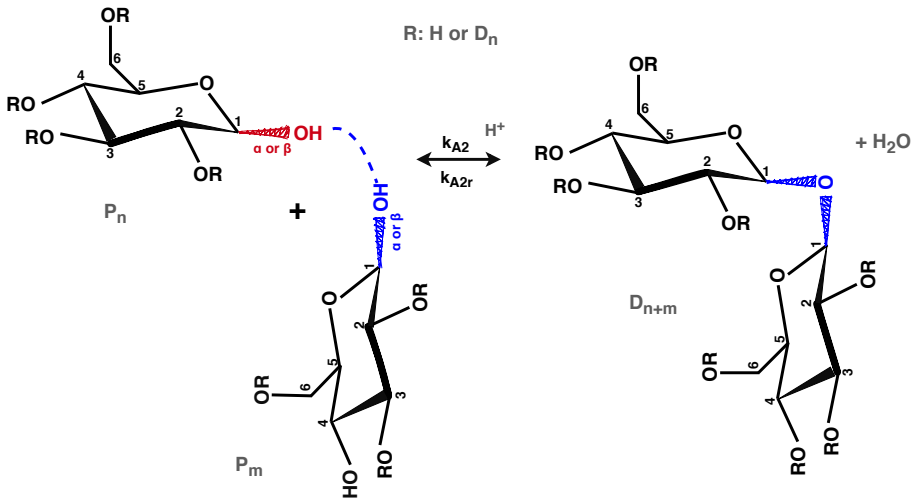

Scheme 2. Schematic representation of Reaction (2). The anomeric hydroxyl groups are marked in red and the formed linkages in blue.

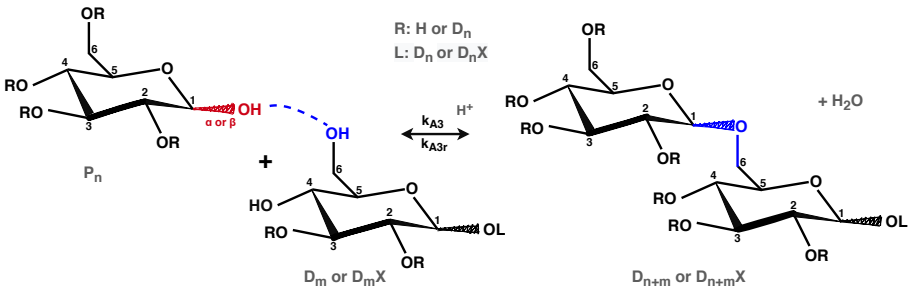

Scheme 3. Schematic representation of Reactions (3) and (4). The anomeric hydroxyl groups are marked in red and the formed linkages in blue.

Note that, a non-reducing saccharide can also be formed, besides the aforementioned mechanisms, by the reaction of a reducing saccharide with a polyol (Equation (5)) or with another anhydrosugar (Equations (6) and (7)). Accordingly, the second category of reactions contains the spontaneous formation of these anhydrosugars, via the creation of intramolecular linkages, as shown in Equations (8) and (9). In the present modeling work, it has been considered that these reactions may take place both on single glucose molecules (i.e., Equations (8) for $n = 1$ and (9)), as well as on the chain-end glucose units of higher-DP saccharides (i.e., Equation (8) for $n \geq 2$). An example of Reaction (8) is illustrated in Scheme 4. Finally, the last category includes the degradation reactions that lead to the formation of Humins.

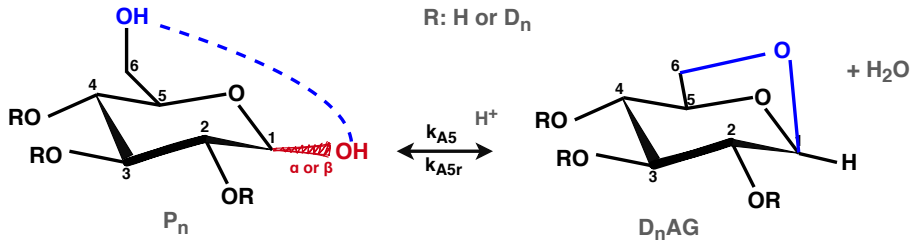

Scheme 4. Schematic representation of Reaction (8). The anomeric hydroxyl groups are marked in red and the formed linkages in blue.

Attention should be paid to the fact that the form of reaction (4) reduces to that of reactions (5)–(7), for $m = 0$ and for $X : PO, AG$ or HMF, respectively. However, the kinetic mechanisms described by these reactions is not the same. In fact, reaction (4) describes the formation/hydrolysis of the glycosidic bonds between the glucose units of the participating saccharides (i.e., between the units 1 to n of a saccharide of type D_nX), as shown in Scheme 3, while reactions (5)–(7) concern exclusively the bonds between the penultimate glucose unit and the end-group of type X, that are not covered by reaction (4) (i.e., the bond between the nth glucose unit and X, of a saccharide of type D_nX).

Note that, the above kinetic scheme contains only lumped reactions, without detailing the elementary mechanisms, as is the commonly adopted strategy in the relevant literature. Note also that, despite the multifunctional character of the glucose units that leads to the formation of branched saccharides, the fact that not all possible combinations of hydroxyl groups can lead to the formation of glycosidic bonds (i.e., since the participation of the carbocation at the C1 carbon atom of a reducing saccharide is required), as well as the significant extent of hydrolysis in the reaction medium, makes the formation of irreversible crosslinked networks unlikely.

2.2. Structural Characteristics of the Sugar Molecules

The development of the model equations describing the evolution of the concentration and the properties of the different sugar molecules necessitates the consideration of the individual structural characteristics of each species, such as their number of hydroxyl groups and bonds, with respect to their DP. In the present work, the hydroxyl groups of the saccharides are distinguished into two types, namely the anomeric and the *susceptible* hydroxyl groups. The first type refers to the hydroxyl groups that are attached to the anomeric carbon atom located at position 1 of reducing saccharides and are denoted in the model equations as OH_1. The second type describes the rest of the hydroxyl groups that are susceptible to create a bond with an anomeric carbon, without considering eventual steric limitations. These are denoted as OH_s. Note that, the number of anomeric and susceptible hydroxyl groups, found on a single individual sugar molecule, depends on the latter's type, DP and end-unit. Accordingly, each sugar molecule possesses a number of OH_s that is proportional to its DP and to its end-group, but may only posses one (or none) anomeric hydroxyl group, irrespective of its DP. For example, a saccharide ending in a polyol group is a non-reducing saccharide that contains only susceptible hydroxyl groups. Furthermore, the total number of these groups is higher than the respective number of susceptible hydroxyl groups of a reducing saccharide, of the same DP, due to the presence of the polyol group on the chain-end of the former. These differences must be reflected in the respective rate functions of the different types of sugar molecules. Table 1, shows the structural characteristics of the different types of saccharides, in terms of the total number of hydroxyl groups and bonds (per molecule) found on each type of molecule.

Table 1. Structural characteristics of the different species.

Type of Sugar Molecule	OH_1	OH_s	Bonds between Glucose Units (Equations (1)–(4))	Bonds between Glucose Units and X (Equations (5)–(7))	Internal Ring Closure Bonds (Equations (8) and (9))
P_n	1	$3+1$	$n-1$	0	0
D_n	0	$3+2$	$n-1$	0	0
D_nPO	0	$3+p$	$n-1$	1	0
P_nAG	0	$3+3$	$n-1$	1	1
P_nHMF	0	$3+1$	$n-1$	1	3

In Table 1, p denotes the number of hydroxyl groups of the free polyol units, PO.

2.3. Rate Functions

On the basis of the postulated kinetic scheme for the system (Equations (1)–(11)), it is possible to derive the rate functions describing the net rates of production of the different sugar molecules that are present in the reacting system. Concerning the macromolecular sugars, these expressions are defined in terms of the respective chain-length of each molecule (i.e., in terms of its number of glucose units). Accordingly, the rate function of the reducing sugar molecules of size n, P_n takes the following form:

$$\begin{aligned} r_{P_n} = & -k_{A1}\left([P_n]\cdot\sum_{m=1}^{\infty}[OH_s^{P_m}] + [OH_s^{P_n}]\cdot\sum_{m=1}^{\infty}[P_m]\right) - k_{A1r}\cdot[B^{P_n}]\cdot[H_2O] \\ & + 2k_{A1r}\cdot[H_2O]\cdot\sum_{m=n+1}^{\infty}[P_m] + k_{A1}\cdot\sum_{m=1}^{n-1}[OH_s^{P_m}]\cdot[P_{n-m}] - 2k_{A2}\cdot[P_n]\cdot\sum_{m=1}^{\infty}[P_m] \\ & + k_{A3r}\cdot[H_2O]\cdot\sum_{m=n+1}^{\infty}([D_m]+[D_mX]) + k_{A2r}\cdot[H_2O]\cdot\sum_{m=n+1}^{\infty}[D_m] \\ & - k_{A3}\cdot[P_n]\cdot\sum_{m=1}^{\infty}([OH_s^{D_m}]+[OH_s^{D_mX}]) - k_{D1}\cdot[P_n] + k_{D1r}\cdot[H_2O]\cdot[D_{n-1}AG] \\ & - \left(k_{A4}\cdot[OH_s^{PO}] + k_{A5}\cdot[OH_s^{AG}] + k_{A6}\cdot[OH_s^{HMF}]\right)\cdot[P_n] \\ & + (k_{A4r}\cdot[D_nPO] + k_{A5r}\cdot[D_nAG] + k_{A6r}\cdot[D_nHMF])\cdot[H_2O] \\ & + (k_{D1r}\cdot[H_2O]\cdot[AG] - (k_{D2}+k_{D3})\cdot[P_n])\cdot\delta(n-1) \end{aligned} \tag{12}$$

The rate, r_{P_n}, is expressed in units of molar concentration over time (i.e., mol L^{-1} min^{-1}), while the molar concentrations of the different species (i.e., in mol L^{-1}) are denoted with the use of brackets [ ]. Finally, B^{P_n} designates the number of bonds of the reducing saccharides of DP equal to n and $\delta(n-1)$ is the Kroenecker's delta, given by:

$$\delta(n-i) = \begin{cases} 1 & \text{for } n = i \\ 0 & \text{for } n \neq i \end{cases} \tag{13}$$

The rate functions for the rest of the polysaccharides can be defined accordingly, in terms of their respective DP. Besides the macromolecular species, the system contains also different types of monosaccharides, polyol molecules and water. The evolution of the quantities of these species is described by similar rate functions, always defined on the basis of the postulated kinetic scheme. Accordingly, the net rate of formation of free polyol molecules in the reacting mixture is described by the following expression:

Polyol molecules, *PO*

$$r_{PO} = -k_{A4}\cdot[OH_s^{PO}]\cdot\sum_{n=1}^{\infty}P_n + k_{A4r}\cdot[H_2O]\cdot[D_nPO] \tag{14}$$

The analytical expressions of the rate functions of the rest of the macromolecular and non-macromolecular species are given in Appendix A (Equations (A1)–(A9)).

2.4. Reactor Design Equations

Once the rate functions of the species are defined, it is possible to derive the design equations for a batch reactor, in the form of a system of ordinary differential equations (ODEs):

$$\frac{1}{V}\frac{d(V\cdot[MS_n])}{dt} = r_{MS_n} \quad ; \quad n = 1, 2, \ldots \tag{15}$$

$$\frac{1}{V}\frac{d(V\cdot[S])}{dt} = r_S \tag{16}$$

In the above expressions, $[MS_n]$ and $[S]$ denote respectively the molar concentration of the different macromolecular and non-macromolecular species of interest, appearing in the established rate functions, n being the DP of the former. V is the volume of the reacting mixture, which also varies according to:

$$\frac{dV}{dt} = \frac{K_w \cdot A \cdot (x_W - x_W^*)}{d_W} \tag{17}$$

where d_W denotes the molar density of water, K_W is the water evaporation constant and A is the evaporation surface. x_W and x_W^* denote the respective instantaneous and equilibrium molar fractions of water in the reactor. For the calculation of x_W^*, an activity coefficient thermodynamic model was employed, whose coefficients have been adjusted by the company ROQUETTE on the basis of the experimental data.

3. Model Developments

3.1. Method of Moments

The formulation of the rate functions in terms of the DP of the different molecules results in a system of coupled material balances that need to be solved simultaneously. Since the number of equations of the system is dictated by the maximum considered DP of each type of sugar molecule, one needs to presuppose its value and constrain the solution to this assumption. Several techniques have been proposed for the numerical solution of such systems, in view of calculating key properties of the produced polymers, such as the average molecular weights or the complete distributions. A relevant detailed discussion of such approaches can be found elsewhere [26,27]. Among them, one of the most commonly employed approaches to reduce the size of the system is the method of moments [28]. It is a widely-used technique, especially in the modeling studies of polymerization systems, that is based on the statistical representation of the average molecular properties of the macromolecular species in terms of the leading moments of their number-chain-length distribution. Accordingly, the moment of order k, for the reducing sugar molecules, P_n, can be defined as:

$$\lambda_k = \sum_{n=1}^{\infty} n^k P_n \tag{18}$$

The moments for the other types of sugar molecules can be defined accordingly. On the basis of the above definition of the moments, the rate functions of the different saccharides can be readily transformed to express the rate functions of their respective moments. All these expressions are presented in detail in Appendix A (Equations (A10)–(A20)). Accordingly, the reactor design equations, describing the evolution of the quantities of the different macromolecular species in a batch reactor (Equation (15)), are also transformed to describe the evolution of the respective leading moments of these species, thus significantly reducing the size of the system of ODEs:

$$\frac{1}{V}\frac{d(V\cdot[MMS_k])}{dt} = r_{MMS_k} \quad ; \quad k = 0,1,2 \tag{19}$$

where $[MMS_k]$ denotes the moment of the macromolecular species, S, of order k. The implementation of the method of moments provides the advantage that certain moments can be directly related to specific magnitudes and properties of the system. As such, the zeroth moment of the reducing sugars, λ_0, corresponds directly to the number of anomeric hydroxyl groups that are present, at any moment, in the reacting mixture. This

provides a useful indication of the capacity of the system to continue reacting towards higher DP. Similarly, the total amount of glucose units, that are present on the different sugar molecules, can be calculated by Equation (20). Since this quantity remains constant throughout the process, it can also be used to validate the correct implementation of the moment rate functions of the model (i.e., by verifying its value throughout the duration of the simulation):

$$[G] = \lambda_1 + \phi_0 + \omega_0 + \mu_1 + [AG] + [HMF] \tag{20}$$

where the moments λ_k, ϕ_k and ω_k correspond respectively to the macromolecular species P_n, D_nAG and D_nHMF (see Appendix A) and μ_1 is the 1st order moment of all the non-reducing sugar molecules (i.e., in general: $\mu_k = \xi_k + \psi_k + \phi_k + \omega_k$).

The calculation of the average molecular weights of the sugars, at any given moment in the system, is straightforward from their respective moments, according to the following expressions:

$$M_n = \frac{\lambda_1 + \mu_1}{\lambda_0 + \mu_0} \cdot (M_G - M_{H_2O}) \quad ; \quad M_w = \frac{\lambda_2 + \mu_2}{\lambda_1 + \mu_1} \cdot (M_G - M_{H_2O}) \tag{21}$$

in the above expressions, M_G and M_{H_2O} denote the molecular weights of a glucose molecule and a water molecule, respectively. Note that the above calculation of the average molecular weights is only approximate as it does not take into account the type of end-unit of each molecule.

Despite its aforementioned advantages, the method of moments presents a significant drawback. As can be seen in the postulated moment rate functions of the macromolecular saccharides (Equations (A10)–(A14)), some terms of the expressions create a dependency of a moment of order k on a moment of order $k+1$ (i.e., the so-called moment-closure problem). To overcome this problem and close the mass balances of the system, several closure techniques have been reported in the literature for different polymerization systems [29,30]. However, as these closure techniques depend on the form of the chain-length distribution of the produced macromolecular species, they are not directly transferable to different systems, as is the case of sugars. Indeed, the multimodal character of the chain-length distributions of the polysaccharides does not allow a direct implementation of the reported techniques. At the same time, other closure techniques that do not depend on the form of the chain-length distribution and take advantage of the quantitative difference between moments of different species, as is the technique proposed by [31], are also not applicable to this system, due to the absence of such quantitative difference between the sugar species.

To overcome this problem for this system, different solutions could be envisaged. The first one would be to couple the system of ODEs of the model (Equations (16), (17) and (19)) with Equation (20) in order to estimate, within each step of the integration, the values of the terms related to the closure problem. However, this approach is computationally complex and prone to numerical instabilities. A different approach would be to adopt simplifying assumptions that would allow the consideration of a simpler kinetic scheme, thus eliminating these terms from the model equations altogether.

3.2. The Kinetic Monte Carlo Algorithm

An alternative to the implementation of any deterministic approach, such as the method of moments, for the modeling of reactive systems, is to implement a stochastic modeling approach. Monte Carlo (MC) techniques provide this alternative via the use of random sampling (i.e., in terms of a pseudo-random number generator) and their fields of application include problems varying from numerical quadrature to statistical physics and finance [32–35]. In the modeling of polymerization reaction kinetics, two principal MC techniques have found the most widespread application, namely the Stochastic Simulation Algorithm (SSA) of [36] and the approach of [37], on the basis of primary polymer molecules. In general, MC is particularly suitable for the description of dynamically-evolving multi-

body systems that are characterized by stochastic state transitions and a relative complexity in the definition of the constituting elements of the system. These characteristics are typical of batch polymerization systems where the formed polymer displays structural complexity, such as non-linearity, multi-functionality, etc. In this respect, the polycondensation of sugars presents an excellent system for such a stochastic modeling approach.

Following the original developments of the SSA of [36], the reactive system, that is considered spatially homogeneous, is represented by a finite sample of molecules of all the participating species. These are subsequently subject to a series of stochastically occurring interaction steps, according to a set of dynamically varying instantaneous probabilities. These interaction steps represent the different reactions of the system's kinetic scheme, while their occurrence probabilities reflect their respective rates, depending on the kinetic constants and on the instantaneous molecular quantities of the different species in the simulation sample. The general expressions dictating the application of the SSA on polymerization systems, concerning the stochastic selection of the reaction event to be simulated in a given time step, as well as the calculation of the corresponding time-step duration, have been extensively presented in other studies [38,39] and, as such, are omitted from the present work. On the other hand, the details concerning the implementation of the MC algorithm to this specific system are presented in the following paragraphs.

The implementation of the MC formulation to the present system is based on the straightforward application of the above basic principles of the SSA. In this respect, a series of different species, indexes and properties are monitored throughout the temporal evolution of the reacting system. These species include the different types of reducing and non-reducing sugar molecules, as defined in the postulated kinetic scheme, water molecules and polyol molecules. All these constitute the reacting units of the simulated sample, whose quantity and properties are monitored by the developed kinetic MC algorithm, throughout the polymerization. More precisely, among the properties that are monitored, are the chain length of the different sugar molecules, in terms of their constituting number of glucose units, their exact number of glycosidic bonds, as well as their number of hydroxyl groups, both anomeric and susceptible ones.

The monitoring of the above quantities serves for the calculation of the instantaneous values of the reaction probabilities, as well as for the continuous tracking of the key properties of interest of the produced saccharides. Accordingly, at any given instant during the reaction, it is possible to infer detailed information about the molar mass of any molecule that is present in the system, via the tracking of their chain length and type (i.e., end-unit). It is also possible to follow the capacity of the system to continue creating new glycosidic bonds, via the evolution of the hydroxyl groups, as well as its hydrolysis rates, via the tracking of the formed bonds and the quantity of water molecules. The analytical expressions of the instantaneous rates of the different chemical reactions of the kinetic scheme, as transformed on the basis of the previously established rate functions (see Section 2.3), are presented in Table 2.

Table 2. Reaction rates for the kinetic MC algorithm.

Reaction Type	Rate of Bond Formation $\mathbf{min^{-1}}$	Hydrolysis Rate $\mathbf{min^{-1}}$
$P_n + P_m \underset{k_{A1r}}{\overset{k_{A1}}{\longleftrightarrow}} P_{n+m} + H_2O$	$k_{A1} \cdot OH_1 \cdot OH_s^P \cdot f$	$k_{A1r} \cdot W \cdot B^P \cdot f$
$P_n + P_m \underset{k_{A2r}}{\overset{k_{A2}}{\longleftrightarrow}} D_{n+m} + H_2O$	$k_{A2} \cdot OH_1 \cdot (OH_1 - 1) \cdot f$	$k_{A2r} \cdot W \cdot D \cdot f$
$P_n + D_m \underset{k_{A3r}}{\overset{k_{A3}}{\longleftrightarrow}} D_{n+m} + H_2O$	$k_{A3} \cdot OH_1 \cdot OH_s^D \cdot f$	$k_{A3r} \cdot W \cdot B^D \cdot f$
$P_n + D_mX \underset{k_{A3r}}{\overset{k_{A3}}{\longleftrightarrow}} D_{n+m}X + H_2O$	$k_{A3} \cdot OH_1 \cdot OH_s^{DX} \cdot f$	$k_{A3r} \cdot W \cdot B^{DX} \cdot f$
$P_n + PO \underset{k_{A4r}}{\overset{k_{A4}}{\longleftrightarrow}} D_nPO + H_2O$	$k_{A4} \cdot OH_1 \cdot OH_s^{PO} \cdot f$	$k_{A4r} \cdot W \cdot DPO \cdot f$
$P_n + AG \underset{k_{A5r}}{\overset{k_{A5}}{\longleftrightarrow}} D_nAG + H_2O$	$k_{A5} \cdot OH_1 \cdot OH_s^{AG} \cdot f$	$k_{A5r} \cdot W \cdot DAG \cdot f$
$P_n + HMF \underset{k_{A6r}}{\overset{k_{A6}}{\longleftrightarrow}} D_nHMF + H_2O$	$k_{A6} \cdot OH_1 \cdot OH_s^{HMF} \cdot f$	$k_{A6r} \cdot W \cdot DHMF \cdot f$
$P_n(/P_1) \underset{k_{D1r}}{\overset{k_{D1}}{\longleftrightarrow}} D_{n-1}AG(/AG) + H_2O$	$k_{D1} \cdot OH_1$	$k_{D1r} \cdot W \cdot DAG \cdot f$
$P_1 \xrightarrow{k_{D2}} HMF + 3H_2O$	$k_{D2} \cdot P_1$	-
$P_1 \xrightarrow{k_{D3}} H + 3H_2O$	$k_{D3} \cdot P_1$	-
$HMF \xrightarrow{k_{D4}} H$	$k_{D4} \cdot HMF$	-

$f = 1/(V \cdot N_A)$ [38].

In the expressions appearing in Table 2, OH_s^S is the total number of susceptible hydroxyl groups of the molecules of type S, in the simulation sample, and B^S represents the respective total glycosidic bonds between the glucose units of the molecules of type S. Finally, W denotes the number of water molecules in the sample. These quantities are calculated on the basis of the information that is tracked, in the MC algorithm, for every single molecule of the simulation sample, as well as on the basis of the instantaneous water evaporation rate (see Equation (17)).

A significant advantage of the MC formulation, over commonly employed deterministic approaches (i.e., such as the previously presented moments formulation), is that the different characteristics of the various species are tracked in detail, for every single saccharide, thus avoiding the necessity to use approximate expressions or simplifications to calculate the properties of interest. This becomes evident, for example, in the calculation of the average molecular weights that are directly inferred by their definition expressions:

$$M_n = \frac{\sum_{i=1}^{N_{MM}} MM_i}{N_{MM}} \quad ; \quad M_w = \frac{\sum_{i=1}^{N_{MM}} MM_i^2}{\sum_{i=1}^{N_{MM}} MM_i} \tag{22}$$

where MM_i is the exact molecular weight of molecule 'i', and N_{MM} is the total number of molecules taken into account for the calculation of the corresponding property, including reducing and non-reducing saccharides with different chain-end groups. For example, the molecular weight of two polysaccharides, each composed of n glucose units, the first one being a reducing polysaccharide and the second one being a non-reducing polysaccharide ending in a polyol unit, will be respectively:

$$\begin{aligned} MM_i^{P_n} &= n \cdot M_G - (n-1) \cdot M_{H_2O} \\ MM_i^{D_nPO} &= n \cdot (M_G - M_{H_2O}) + M_{PO} \end{aligned} \tag{23}$$

In the above expressions, M_G, M_{H_2O} and M_{PO} denote the molecular weights of a glucose molecule, a water molecule and a polyol molecule, respectively. Note that, contrary to radical polymerization systems, the calculation of the molar mass of the different species, present in this system, by a typical expression of the type: $MM_i = \sum n \cdot D_n \cdot M_{mu}$, would not be exact, due to the existence of different types of end-group and different amounts

of hydroxyl groups on the sugar molecules as well as due to the relatively low degrees of polymerization of this system, in comparison to a classical radical polymerization system. Hence, any expression of the average molecular weights, based on such an approach (i.e., that is unavoidable in the case of the commonly employed deterministic modeling techniques), can only be approximate. This problem does not exist in the case of the MC formulation where the detailed chain length and structure of the participating molecules are available throughout the course of the reaction.

The kinetic MC algorithm also provides the ability to track the evolution of the complete molecular weight distribution (MWD) developments of the macromolecular species, in contrast to the moments formulation. For the reconstruction of the complete MWD by the MC algorithm, the molar mass domain of the different saccharides must initially be discretized in a number of discretization bins, β_i. In the present work, the following discretization rule is adopted:

$$\beta_i = M_{min} \cdot 2^{(i-1)/q} \quad ; \quad i = 1, .., N_e \tag{24}$$

where M_{min} denotes the minimum considered value of the molar mass and q is a discretization parameter. The total number of discretization bins, N_e, can be calculated as a function of the length of the considered molecular weight domain, $[M_{min}, M_{max}]$, and of the parameter, q, according to the expression:

$$N_e = Int\left(1 + q \cdot \frac{\ln\left(M_{max}/M_{min}\right)}{\ln 2}\right) + 1 \tag{25}$$

where 'Int' denotes the integer part of the corresponding value. In the present work, the considered molecular weight domain extended from $M_{min} = 100$ g mol^{-1} to $M_{max} = 2 \cdot 10^4$ g mol^{-1} and the value of the parameter q was set to 3.2. Finally, another advantage of this approach is that there is no requirement for a closure technique.

3.3. Tracking the Structural Characteristics of the Sugar Molecules

Both the method of moments and the MC method rely on the calculation and tracking of the structural characteristics of the different saccharides, as presented previously in Section 2.2. This becomes evident by the form of the respective moment rate functions (Equations (A10)–(A14)) and instantaneous rates (Table 2) of the two methods. According to the description of these characteristics, per type of molecule, given previously in Table 1, it is possible to derive generic expressions for the calculation of the number of hydroxyl groups and glycosidic bonds for each saccharide within each modeling approach. Accordingly, although the number of anomeric hydroxyl groups is explicitly defined for every type of saccharide (i.e., equal to 1 only for the reducing saccharides and 0 for all the rest), the number of susceptible hydroxyl groups needs to be defined in terms of the DP of each type of sugar. In the present modeling work, this has been achieved by the use of the following expression:

$$OH_s^{X_n} = a_X \cdot n + b_X \tag{26}$$

where $OH_s^{X_n}$ denotes the number of susceptible hydroxyl groups per molecule of type X_n, n being its respective DP, and a_X and b_X being its characteristic coefficients. The values of these coefficients are given in Table 3. Note that, the implementation of this generic expression provides flexibility to this modeling framework and facilitates its eventual implementation to similar systems containing other forms of saccharides (e.g., sucrose, fructose, etc.). However, it should be emphasized that these coefficients do not constitute additional tunable parameters of the model as their values are explicitly defined by the structures of the corresponding saccharides, without them being subject to any form of adjustment or tuning.

Table 3. Values of the coefficients a and b, used for the calculation of the susceptible hydroxyl groups of each type of sugar molecule.

Type of Sugar Molecule	a	b
P_n	3	1
D_n	3	2
D_nPO	3	p
P_nAG	3	3
P_nHMF	3	1

According to the above, the calculation of the total concentration of susceptible hydroxyl groups of the molecules of type X_n, as encountered in the moment rate functions (Equations (A10)–(A14)), will be directly calculated by:

$$[OH_s^{X_n}] = (a_X \cdot n + b_X) \cdot [X_n] \tag{27}$$

In the same way, the total quantity of the same susceptible hydroxyl groups, required for the calculation of the MC instantaneous rates (Table 2), will be calculated as:

$$OH_s^{X_n} = \sum_{n=1}^{\infty} (a_X \cdot n + b_X) \cdot X_n \tag{28}$$

Note that, for the respective calculation for the non-macromolecular species, such as AG, PO and HMF, it suffices to set $n = 0$ in the above expressions.

3.4. Kinetic Rate Constants

The rate constants of the different reactions of the adopted kinetic scheme, representing the principal parameters of the proposed model, need typically to be determined on the basis of available experimental data. These 17 parameters in total (i.e., k_{A1}-k_{A6}, k_{A1r}-k_{A6r}, k_{D1}-k_{D4} and k_{D1r}) can be classified into two main categories, i.e., the parameters of the polycondensation reactions, leading to the formation of a bond with the parallel release of water, and those of the hydrolysis reactions, leading to the scission of the formed bonds. Within each of the above two categories, one could further distinguish the internal ring-closure reactions and the degradation reactions from the rest of the reactions that take place between two different saccharides. These categories have already been identified in the presentation of the postulated kinetic scheme, in Equations (1)–(11). This significantly reduces the considered lumped *reaction events* and their corresponding kinetic rate constants, provided that a global rate constant is considered for each category.

The determination of all 17 parameters would certainly add flexibility to the model and, eventually, a higher prediction accuracy since more degrees of freedom would be available for fitting the experimental data. On the other hand, the consideration of a reduced set of rate constants, on the basis of the aforementioned lumped reaction events (or categories), seems to be more realistic from a chemical viewpoint. For example, it would be natural to assume that the rate constants of the reactions (1) and (3) should not be significantly different, for the same type of bond. Note that, the consideration of individual formation and/or hydrolysis rates of the different types of bonds (i.e., 1-1, 1-2, 1-3, 1-4 1-6, in position α or β), in terms of steric hindrance effects, would be absolutely relevant and supported by reported data [15,17,20,22]. However, this distinction is not possible in the proposed modeling framework, under the method of moments or the kinetic MC formulation, as the types of bonds are not monitored during the reactions. Such a consideration would only be possible within a topological MC modeling approach, which would provide the possibility to record and follow the structural characteristics of the saccharides in more detail, as has been shown in other polymerization systems [40].

In the present work, the assumption that the reduced set of five rate constants is sufficient to describe the evolution of the system has been adopted and tested on the basis

of the available experimental data. Accordingly, the considered rate parameters have been reduced to: $k_A(= k_{Ai}, i = 1:6)$, $k_{Ar}(= k_{Ari}, i = 1:6)$, k_{D1}, k_{D1r} and k_{D2}. Finally, considering the degradation reactions (10) and (11), their respective kinetic rate constants have been considered unidentifiable. This is due to the fact that the average molar mass of the degradation products (Humins) has been considered equal to that of HMF [25], as well to the fact that the available experimental data did not contain any information allowing us to quantify them individually.

The parametric identification procedure of the above five rate constants was carried out manually, given their low number and the stochastic nature of the MC algorithm, starting from reported values of similar reacting systems [22]. This procedure was repeated for each reaction temperature for which experimental data were available (i.e., at 160 °C, 170 °C, 180 °C and 190 °C). Finally, the values of the pre-exponential constants and of the activation energies of Arrhenius-type expressions were determined via linear regression. These values are reported in Table 4, along with the expression allowing the calculation of the water evaporation rate (Equation (17)).

Table 4. Model parameters.

Parameter	Value	Units
k_A	$2.77 \cdot 10^6 \cdot exp(-79,800/R/T)$	L mol^{-1} min^{-1}
k_{D1}	$1.17 \cdot 10^4 \cdot exp(-63,900/R/T)$	min^{-1}
k_{D2}	$0.423 \cdot exp(-17,900/R/T)$	min^{-1}
k_{Ar}	$5.79 \cdot 10^8 \cdot exp(-83,100/R/T)$	L mol^{-1} min^{-1}
k_{D1r}	$0.514 \cdot exp(-43,400/R/T)$	L mol^{-1} min^{-1}
$k_W \cdot A$	$0.435 \cdot exp(-15,300/R/T)$	mol min^{-1}

R = 8.3141 J mol^{-1} K^{-1}.

Note that, all available experimental data were obtained using a constant concentration of the same acid catalyst (cf. Section 5). In this respect, it would be meaningless to include a term, in the kinetic rate expressions, accounting for the catalyst concentration, since the determination of its value would be without statistical significance. A comparison with the relevant literature [22], shows that the obtained parameter values are comparative to the reported ones. For example, the values of k_{D1}, k_{D2} and k_{Ar} are in the same order of magnitude with the respective reported values while the value of k_A is about one order of magnitude lower. However, this comparison can only be used to provide a general idea of the positioning of the estimated values with respect to reported ones, since the kinetic scheme that is adopted in this work is not directly comparable with any other reported work. It should also be noted that, due to the absence of corroborating experimental observations of diffusion-controlled phenomena [41,42], both in this study and in the relevant literature, no such effects have been considered in the developed model. In any case, should the need appear to include such phenomena, this would be straightforward, considering the form of the developed model.

4. Experimental

A series of polymerization experiments was carried out by the company ROQUETTE, under different experimental conditions, and the generated data were used for the calibration and the validation of the developed mathematical model. These experiments were carried out in a vacuum-tight thermo-microbalance analyzer, NETZSCH TG 209 F1, under four different reaction temperatures in the range of 160 °C to 190 °C. The pressure during the reactions was kept constant at $2 \cdot 10^4$ Pa in order to control the humidity level of the reaction medium, thus favoring the polycondensation reactions over their hydrolysis counterparts. The initial medium composition, in all tested temperatures, was composed of 90.1 wt% of maltose disaccharide (1,4-*O*-α-D-glucopyranosyl-D-glucose), 9.0 wt% of the polyol maltitol (4-*O*-α-D-glucopyranosyl-D-glucitol) and 0.9 wt% of citric

acid (2-hydroxypropane-1,2,3-tricarboxylic acid), which served as catalyst. The overall initial mass, for all the experiments, was approximately 0.05 g.

For each reaction temperature, several polymerization experiments were carried out with different duration in order to monitor the evolution of the conversion and molar mass indexes. In this respect, after the end of each polymerization, the reaction medium was analyzed by size exclusion chromatography (SEC), in a column equipped with a refractive index detector, while its calibration was carried out on the basis of pullulans and maltooligosaccharides of known molar mass. All the tested conditions, in terms of the reaction temperature and pressure, as well as in terms of the initial syrup composition, are completely relevant to the industrial production practice.

5. Model Results and Discussion

Due to the aforementioned limitations of the method of moments, mainly related to the moment closure problem, it was considered that the most fitted approach for the modeling of this system was that of the kinetic Monte Carlo algorithm, as described in Section 3.2. Accordingly, the model predictions presented in this section were generated solely via the implementation of this method. Following the experimental conditions (see Section 4), the initial sample of the MC simulations was composed of polyol molecules and disaccharides. A typical size of this sample, for the simulations presented here, was equivalent to $3 \cdot 10^5$ glucose units (i.e., distributed on the initially formed disaccharides) and $1.5 \cdot 10^4$ polyol molecules. This sample size, that was determined via the procedure described in [38], was sufficient for the generation of all the results presented in this section on the basis of a single simulation run. Finally, the program was developed in Matlab and the corresponding simulation time was of the order of 1 min, on a 3.6 GHz personal computer, without any code parallelization.

Figure 1 shows the comparison of the predictions of the model on the temporal evolution of the number- and weight-average molecular weights of the produced sugars with the respective experimental data, for the reactions carried out at 160 °C. The kinetic MC algorithm is capable of simulating the overall behavior of the mixture with very good accuracy, except the final experimental measurements that are slightly under-predicted. Note, that a single reduced set of values for the kinetic rate constants was used during the simulation of the system under the different reaction conditions (cf. Section 3.4).

The same comparison for the rest of the tested reaction temperatures, namely for the experiments run at 170 °C, 180 °C and 190 °C, is shown in Figure 2. The observed increase of both average molecular weight indexes, with increasing temperature, was mainly due to the decrease of the rates of hydrolysis induced by the decreased humidity of the reacting mixture. The MC algorithm displays again a very good capacity in simulating the evolution of the system under different temperatures but presents the same under-prediction, with respect to the final experimental measurements. However, the fact that the duration of the polymerization reactions varied with the reaction temperature, reduces the probability of this fact being an indication of a subsequent increase of the experimental molecular weights that was not captured by the model predictions and strengthens the possibility that this deviation is simply part of the typically expected error between experimental data and modeling predictions (i.e., including experimental error and model uncertainties). Note that, the curves corresponding to the predictions of the model are not entirely smooth, which is characteristic of the results of the stochastic nature of the MC algorithm [39]. Note also that the number-average molecular weight of the produced polysaccharides, after 80 min of reaction at 190 °C, reached a value close to 1200 g mol^{-1}, which corresponds to an average DP of more than seven glucose units.

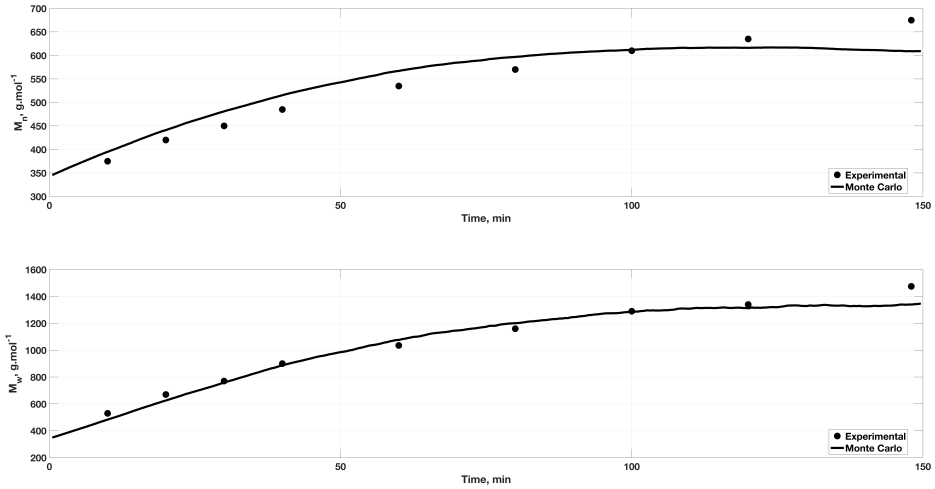

Figure 1. Comparison between model predictions (solid curves) and experimental data (filled dots) on the temporal evolution of the (**top**) number-average molecular weight, and (**bottom**) weight-average molecular weight of the produced polysaccharides, for the polymerization carried out at 160 °C.

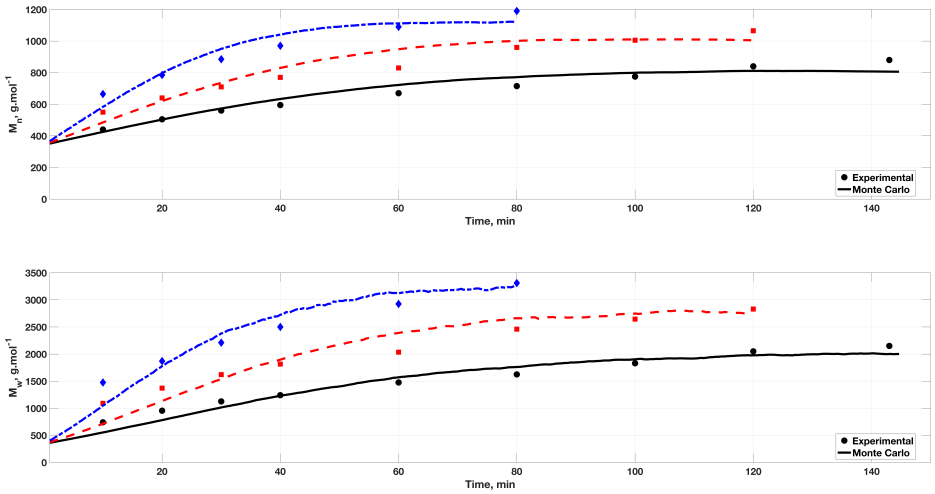

Figure 2. Comparisonbetween model predictions (curves) and experimental data (points) on the temporal evolution of the (**top**) number-average molecular weight, and (**bottom**) weight-average molecular weight of the produced polysaccharides (170 °C: black solid curves and filled dots, 180 °C: red dashed curves and filled squares, 190 °C: blue dash-dot curves and filled diamonds).

As discussed in Section 3.2, the proposed kinetic MC modeling framework allows for the monitoring of individual indexes and characteristics of interest of the sugars participating in the reaction. For example, Figure 3 shows the temporal evolution of the conversion of the disaccharide molecules, as well as that of the hydroxyl groups of all saccharides. More specifically, the conversion of the anomeric and susceptible hydroxyl groups are depicted separately in red and blue curves, respectively. This figure shows that the anomeric hydroxyl groups were consumed more rapidly than the susceptible ones, which can be explained by the fact that the vast majority of chemical reactions of the postulated kinetic scheme describes the consumption of equal amounts of susceptible and anomeric hydroxyl groups for the formation of a glycosidic intermolecular or intramolecular bond. Since the initial amount of susceptible hydroxyl groups was roughly four times higher than that of anomeric ones, it is normal that, in relative terms (i.e., in terms of a conversion ratio), the anomeric hydroxyl groups were consumed more rapidly along the polycondensation

reactions. The only exceptions to the above rule are the reaction of creation of 1-1 glycosidic bonds (reaction (2)), which results to the consumption of two anomeric hydroxyl groups, and the reaction of spontaneous HMF creation (reaction (9)), which consumes three susceptible hydroxyl groups and only one anomeric group. However, their relevant extent was not significant enough to change the overall trend, observed in Figure 3. The same figure also shows that the disaccharides, which represented 90.1 wt% of the initial mixture, were rapidly consumed until an equilibrium was reached at around 95% of their conversion. Their consumption may lead to the formation of either monosaccharides or polysaccharides, via hydrolysis or polycondensation reactions, respectively.

To further investigate these two potential routes, the evolution of the quantities of DP1, DP3 and DP4 sugars is depicted in Figure 4. From these curves, it becomes evident that, during the initial stages of the reaction, both the hydrolysis and the polycondensation of maltose proceeded in parallel. However, their respective rates were different. In fact, the formation of glucose, during these initial stages of the reaction at 160 °C, by the hydrolysis of maltose, prevailed that of the polycondensation of maltose to DP3 and DP4 sugars, which is also consistent with the rate constant values given in Table 4. However, as the quantity of formed glucose increased, so did their respective rate of polymerization, thus leading to a peak of the DP1 quantity curve, after approximately 45 min of reaction, and to a subsequent decrease during the rest of the polymerization. It is also seen that the quantity of formed sugars of DP4 increased with a higher rate than that of DP3 saccharides, probably due to the fact that, notably during the initial stages of the reaction, the molecules of maltose formed glycosidic bonds primarily among them (i.e., given their vast majority in the mixture), thus leading to the direct formation of DP4 sugars without forming the intermediate DP3 molecules. At the same time, the quantity of saccharides of DP3 displayed a delayed increase, with respect to that of the DP4 sugars, as the formation of a minimum quantity of glucose is a prerequisite for their synthesis via the reaction between DP1 and DP2 sugars.

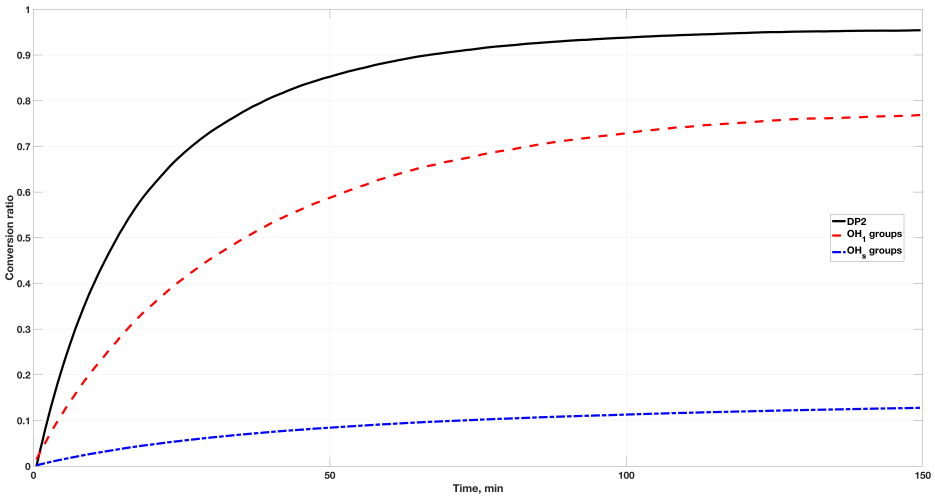

Figure 3. Temporal evolution of the conversion of the disaccharides (black solid curve), anomeric hydroxyl groups (red dashed curve) and hydroxyl groups susceptible to create a bond with the C1 carbocation (blue dash-dot curve), during the reaction carried out at 160 °C.

After the initial peak and the subsequent stage of quantity decrease, the slopes of all curves reveal that the system gradually reached equilibrium at different rates and after a varying reaction duration for the different types of sugar molecules. The overall evolution of the curves is consistent with the respective evolution of the DP2 and OH_1 curves, presented in Figure 3. Accordingly, the fact that the rate of conversion of the anomeric hydroxyl groups was slower than that of the disaccharides, right from the start of the reaction, is probably due to the fact that, in parallel to their consumption, there was a significant rate of formation of OH_1, via the hydrolysis of maltose.

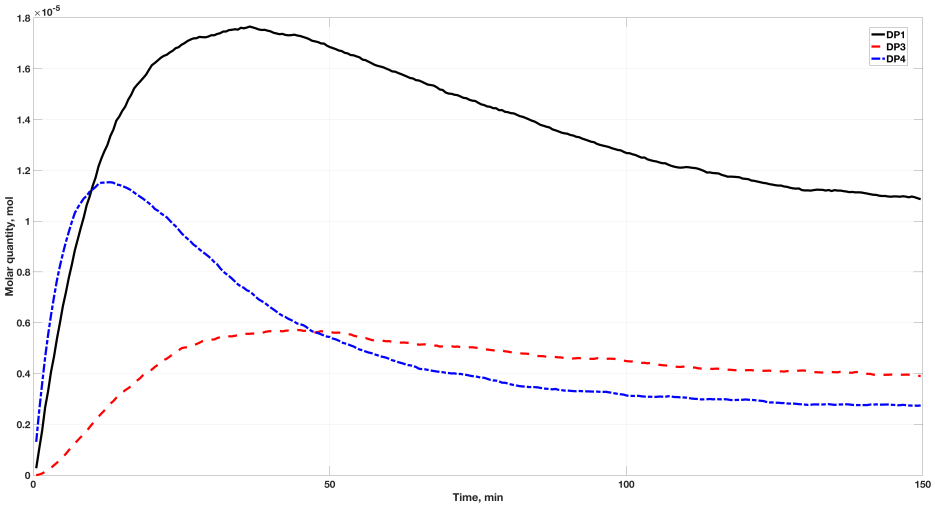

Figure 4. Temporal evolution of the quantities of the monosaccharides (black solid curve), saccharides of DP3 (red dashed curve) and saccharides of DP4 (blue dash-dot curve), during the reaction carried out at 160 °C.

The implementation of the MC method, in contrast to the method of moments, provides the additional advantage of tracking the analytical chain-length and structural characteristics of the sugar molecules participating in the reacting mixture. In this respect, it is possible to infer directly the MWD of the complete population of saccharides, at any given moment of the reaction. As example, Figure 5 depicts the MWD of the saccharides, at two different instances of the reaction at 160 °C, namely at the very beginning (i.e., after 10 min) and close to the end (i.e., after 1 h) of the reaction, for which experimental data were available. Both curves show clearly that the model possesses the capacity to follow the overall evolution of the MWD, mainly in terms of the relevant position of the different peaks. However, some peaks of the experimental spectra are over-predicted, especially at the very early stages of the reaction. This disagreement is more pronounced on the second peak of the spectrum, corresponding to the saccharides of DP2. At the same time, it is important to note that the MC method reconstructed the MWD on the basis of the molar mass of the different sugar molecules, which are, by the nature of the system, distinct discrete values. This is clearly visible in the form the MWD of the MC method that displays individual peaks, especially in the low-DP region of the figures where the discretization bins were narrow enough to contain individual saccharides (see Section 3.2). The peak values, calculated by the MC method, are marked by the filled blue circles on the graphs, while the connecting dashed-line curves correspond to a shape-preserving piecewise cubic interpolation between consecutive peaks. On the other hand, the experimental GPC curves display the typical continuous form that may also be subject to the commonly encountered resolution artifacts [43,44]. In any case, the overall areas covered by both experimental and MC spectra were consistent with each other.

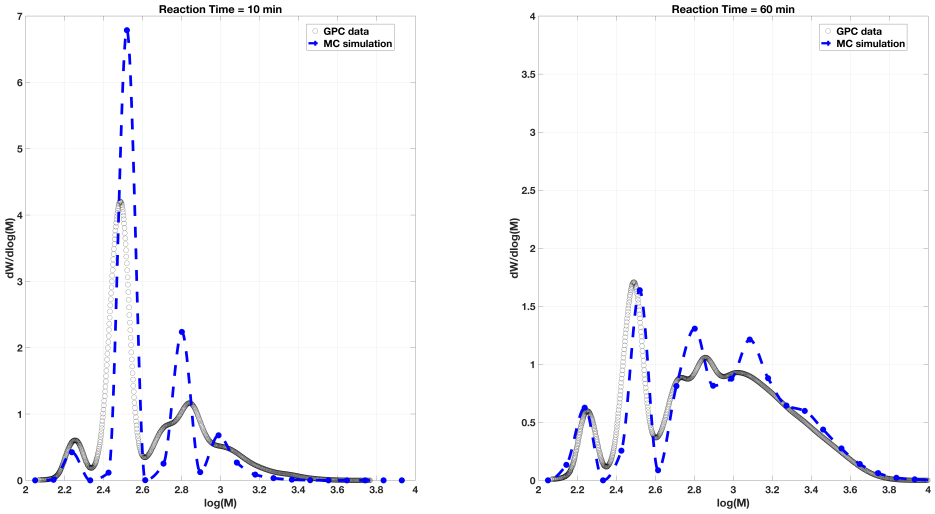

Figure 5. Comparison between the experimental GPC curves and the respective model predictions of the MWD of the sugars that are present in the reacting mixture at 160 °C, after (**left**): 10 min and (**right**) 1 h of reaction.

Finally, Figure 6 shows the comparison between the model predictions and the GPC experimental data of the MWD of the sugars obtained at the end of the reaction, at all four reaction temperatures. It is seen that, in all four cases, the peaks of the distributions corresponding to the low-DP sugars are significantly decreased, with respect to the beginning of the reaction, in parallel to the respective increase of the peaks at the higher-DP region. At the same time, these peaks are less distinct from one another and present a rather continuous multimodal character. This is mainly attributed to the fact that, as the value of the molar mass increases, the relative distance between the adjacent peaks of individual polysaccharides decreases, an effect that is more pronounced by the logarithmic scale of the horizontal axis. In terms of the MC predicted spectra, this effect is also reflected in the discretization rule of the molar mass domain (see Section 3.2). At the same time, the observed increase in the surface occupied by the higher-DP saccharides, with the reaction temperature, is also consistent with the effect observed in Figure 2.

Note that, the peaks observed mainly at temperatures above 170 °C, which are positioned at a value of $log(M)$ around 3.6–3.8, correspond to polysaccharides of a DP in the range of 30–40 glucose units. In fact, at this temperature, although the vast majority of the polysaccharides (i.e., around 87% according to the MC model) displayed a DP < 10 glucose units, which is consistent with the evolution of the average molecular weights shown in Figure 2, there existed also a significant amount of polysaccharides with much higher DP, reaching at values even above 40 glucose units. These polysaccharides would be impossible to simulate via a modeling approach similar to those presented in the introduction of this work, which further supports and demonstrates the interest and the predictive capacity of the proposed modeling framework.

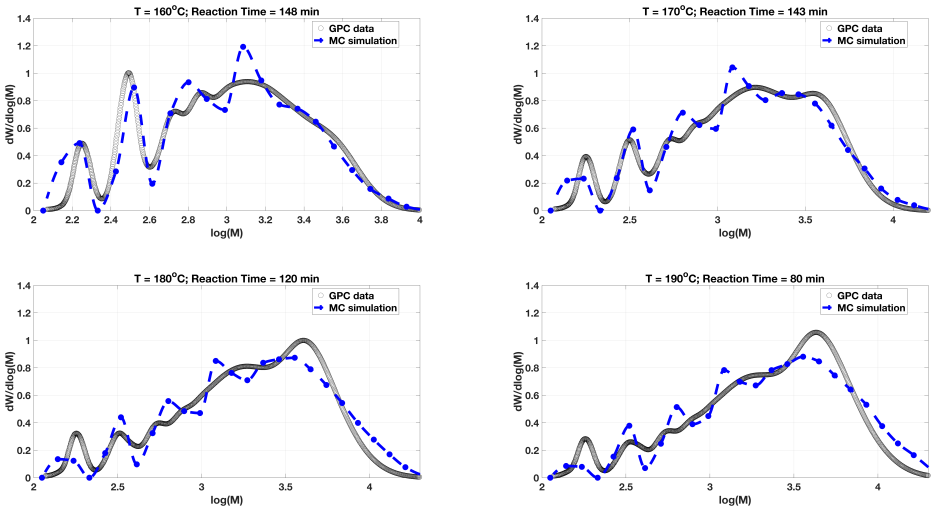

Figure 6. Comparison between the experimental GPC curves (black open circles) and the respective MC model predictions (blue dashed curves) of the MWD of the sugars, at the end of the reaction, at (**top left**): 160 °C, (**top right**) 170 °C, (**bottom left**): 180 °C and (**bottom right**) 190 °C.

6. Conclusions

In the present work, a novel kinetic modeling framework was proposed for the system of polycondensation of sugars, in the presence of polyols and under strict control of the humidity of the mixture, in order to limit the hydrolysis reactions. The developed model was based on an extended and generalized kinetic scheme, which was established following a classical polymerization paradigm in order to allow for the consideration of the synthesis of polysaccharides of high degrees of polymerization. Accordingly, the different species were identified in terms of the number of their constituting glucose units, as well as in terms of other structural characteristics, such as their number of hydroxyl groups, either in anomeric position or any other position, and the existence of intramolecular bonds. For the formulation of the mathematical model equations, two different approaches were implemented, namely a deterministic one in terms of the method of moments and a stochastic kinetic Monte Carlo approach.

Through the derivation of the equations of the method of moments, it became evident that it does not consist of a viable modeling approach for this system, mainly due to its limitation with respect to the well-known moment closure problem, that appears in several terms, as well as due to its incapacity to predict the complete molecular weight distribution developments. However, in a more general consideration, the benefits of the method in terms of the direct relation of several properties and indexes of interest of the system with different moments were clearly presented. Via the present work, the implementation of this technique to several terms appearing in the rate functions of the polysaccharides, that are not commonly encountered in classical radical polymerization systems, was also demonstrated.

The predictions of the kinetic MC algorithm were compared against a series of experimental data, generated at four different reaction temperatures in the range of 160 °C to 190 °C. These comparisons demonstrated the capacity of the proposed model to predict, with very good accuracy, the evolution of the average molecular weights and the complete molecular weight distributions of the produced saccharides, even though a reduced set of only five kinetic rate constants was adopted. In addition to the comparisons with the experimental data, the model was employed to generate the evolution of several indexes of the polymerization, in an attempt to better illustrate the course of the reactions and the dominant reaction routes along the duration of the experiments.

Author Contributions: Conceptualization, all; methodology and model developments, D.M.; experimental analyses and data acquisition, B.B.; writing—original draft preparation, D.M.; writing—review and editing, all; funding acquisition, B.B. All authors have read and agreed to the published version of the manuscript.

Funding: This research was funded by ROQUETTE.

Institutional Review Board Statement: Not applicable.

Informed Consent Statement: Not applicable.

Data Availability Statement: Restrictions apply to the availability of these data. Data was obtained from ROQUETTE and are available from the authors with the permission of ROQUETTE.

Conflicts of Interest: The authors declare no conflict of interest.

Abbreviations

The following abbreviations are used in this manuscript:

DP	Degree of Polymerization
GPC	Gel-Permeation Chromatography
MC	Monte Carlo
MWD	Molecular Weight Distribution

Appendix A. Model Equations

Appendix A.1. Rate Functions of the Macromolecular Species

The net formation rates of all the macromolecular species that participate in the different chemical reactions can be established, on the basis of the postulated general kinetic scheme (Equations (1)–(11)), as follows:

- Non-Reducing sugar molecules of size n, D_n

$$\begin{aligned} r_{D_n} = &+k_{A2}\sum_{m=1}^{n-1}[P_m]\cdot[P_{n-m}] - k_{A2r}\cdot[H_2O]\cdot[D_n] \\ &- k_{A3}\cdot[OH_s^{D_n}]\cdot\sum_{m=1}^{\infty}[P_m] + k_{A3}\sum_{m=1}^{n-1}[OH_s^{D_m}]\cdot[P_{n-m}] \\ &- \left(k_{A3r}\cdot[B^{D_n}] - \sum_{m=n+1}^{\infty}[D_m]\right)\cdot[H_2O] \end{aligned} \tag{A1}$$

- Non-Reducing sugar molecules of size n, containing a polyol unit, D_nPO

$$\begin{aligned} r_{D_nPO} = &+k_{A4}\cdot[OH_s^{PO}]\cdot[P_n] - k_{A4r}\cdot[H_2O]\cdot[D_nPO] \\ &+ k_{A3}\cdot\left(\sum_{m=1}^{n-1}[OH_s^{D_mPO}]\cdot[P_{n-m}] - [OH_s^{D_nPO}]\cdot\sum_{m=1}^{\infty}[P_m]\right) \\ &+ k_{A3r}\cdot[H_2O]\cdot\left(\sum_{m=n+1}^{\infty}[D_mPO] - [B^{D_nPO}]\right) \end{aligned} \tag{A2}$$

- Non-Reducing sugar molecules of size n, containing a 1-6-anhydrosugar D_nAG

$$\begin{aligned} r_{D_nAG} = &+k_{A5} \cdot [OH_s^{AG}] \cdot [P_n] - k_{A5r} \cdot [H_2O] \cdot [D_nAG] \\ &+ k_{D1} \cdot [P_{n+1}] - k_{D1r} \cdot [H_2O] \cdot [D_nAG] \\ &+ k_{A3} \cdot \left(\sum_{m=1}^{n-1} [OH_s^{D_mAG}] \cdot [P_{n-m}] - [OH_s^{D_nAG}] \cdot \sum_{m=1}^{\infty} [P_m] \right) \\ &+ k_{A3r} \cdot [H_2O] \cdot \left(\sum_{m=n+1}^{\infty} [D_mAG] - [B^{D_nAG}] \right) \end{aligned} \tag{A3}$$

- Non-Reducing sugar molecules of size n, containing an HMF molecule D_nHMF

$$\begin{aligned} r_{D_nHMF} = &+k_{A6} \cdot [OH_s^{HMF}] \cdot [P_n] - k_{A6r} \cdot [H_2O] \cdot [D_nHMF] \\ &+ k_{A3} \cdot \left(\sum_{m=1}^{n-1} [OH_s^{D_mHMF}] \cdot [P_{n-m}] - [OH_s^{D_nHMF}] \cdot \sum_{m=1}^{\infty} [P_m] \right) \\ &+ k_{A3r} \cdot [H_2O] \cdot \left(\sum_{m=n+1}^{\infty} [D_mHMF] - [B^{D_nHMF}] \right) \end{aligned} \tag{A4}$$

Finally, the rate function corresponding to the glucose molecules, P_1, that appear in some of the above expressions, can be directly obtained by the respective rate function of the reducing sugar molecules (Equation (12)):

$$r_{P_1} = r_{P_n} \cdot \delta(n-1) \tag{A5}$$

Appendix A.2. Rate Functions of the Non-Macromolecular Species

The net formation rates of the non-macromolecular species are established similarly, on the basis of the postulated kinetic scheme (Equations (1)–(11)):

1-6-anhydrosugar molecules, AG

$$\begin{aligned} r_{AG} = &-(3 \cdot k_{A5} \cdot \sum_{n=1}^{\infty} P_n + k_{D1r} \cdot [H_2O]) \cdot [AG] + k_{D1} \cdot [P_1] \\ &+ k_{A5r} \cdot [H_2O] \cdot \sum_{n=1}^{\infty} D_nAG \end{aligned} \tag{A6}$$

HMF molecules, HMF

$$\begin{aligned} r_{HMF} = &-(k_{A6} \cdot \sum_{n=1}^{\infty} P_n + k_{D4}) \cdot [HMF] + k_{D2} \cdot [P_1] + \\ &k_{A6r} \cdot [H_2O] \cdot \sum_{n=1}^{\infty} D_nHMF \end{aligned} \tag{A7}$$

Humins, H

$$r_H = k_{D3} \cdot \sum_{n=1}^{\infty} P_n + k_{D4} \cdot [HMF] \tag{A8}$$

Water molecules, H_2O

$$\begin{aligned} r_{H_2O} = {} & k_{A1} \cdot \sum_{n=1}^{\infty} P_n \cdot \sum_{m=1}^{\infty} [OH_s^{P_m}] - k_{A1r} \cdot [H_2O] \cdot \sum_{n=1}^{\infty} [B^{P_n}] \\ & + k_{A2} \cdot [OH_1^P]^2 + k_{A3} \cdot \sum_{n=1}^{\infty} P_n \cdot \sum_{m=1}^{\infty} \left([OH_s^{D_m}] + [OH_s^{D_m X}] \right) \\ & - k_{A2r} \cdot [H_2O] \cdot \sum_{n=1}^{\infty} [D_n] - k_{A3r} \cdot [H_2O] \cdot \sum_{n=1}^{\infty} \left([B^{D_n}] + [B^{D_n X}] \right) \\ & + (k_{A4} \cdot [OH_s^{PO}] + k_{A5} \cdot [OH_s^{AG}] + k_{A6} \cdot [OH_s^{HMF}]) \cdot \sum_{n=1}^{\infty} P_n \\ & - (k_{A4r} \cdot \sum_{n=1}^{\infty} [D_n PO] + k_{A5r} \cdot \sum_{n=1}^{\infty} [D_n AG] + k_{A6r} \cdot \sum_{n=1}^{\infty} [D_n HMF]) \cdot [H_2O] \\ & + 3 \cdot (k_{D2} + k_{D3}) \cdot [P_1] + k_{D1} \cdot \sum_{n=1}^{\infty} [P_n] - k_{D1r} \cdot [H_2O] \cdot \left(\sum_{n=1}^{\infty} [D_n AG] + [AG] \right) \end{aligned} \tag{A9}$$

Appendix A.3. Moment Rate Functions

In accordance to the definition given in Equation (18), the moments λ_k, ψ_k, ξ_k, ϕ_k and ω_k have been defined for the macromolecular species P_n, D_nPO, D_n, D_nAG and D_nHMF, respectively. Next, on the basis of the previously defined rate functions (Equations (A1)–(A4)), the following rate functions can be established for the leading moments of the number-chain-length distributions of the above macromolecular species:

$$\begin{aligned} r_{\lambda_k} = {} & -k_{A1}(\lambda_k \cdot (a_P \cdot \lambda_1 + b_P \cdot \lambda_0) + \lambda_0 \cdot (a_P \cdot \lambda_{k+1} + b_P \cdot \lambda_k)) \\ & + k_{A1r} \cdot [H_2O] \left(-(\lambda_{k+1} - \lambda_k) + 2 \cdot \sum_{m=0}^{k} \left(\binom{k}{m} \frac{B_m}{k-m+1} \cdot (\lambda_{k-m+1} - \lambda_0) \right) \right) \\ & + k_{A1} \cdot \left(a_P \cdot \sum_{m=0}^{k} \binom{k}{m} \lambda_{m+1} \cdot \lambda_{k-m} + b_P \cdot \sum_{m=0}^{k} \cdot \binom{k}{m} \lambda_m \cdot \lambda_{k-m} \right) \\ & - k_{A3} \cdot \lambda_k \cdot (a_D \cdot \xi_1 + a_{DAG} \cdot \phi_1 + a_{DPO} \cdot \psi_1 + a_{DHMF} \cdot \omega_1 \\ & + b_D \cdot \xi_0 + b_{DAG} \cdot \phi_0 + b_{DPO} \cdot \psi_0 + b_{DHMF} \cdot \omega_0) - 2 \cdot k_{A2} \cdot \lambda_k \cdot \lambda_0 \\ & + k_{A3r} \cdot [H_2O] \cdot \sum_{m=0}^{k} \left(\binom{k}{m} \frac{B_m}{k-m+1} \cdot (\mu_{k-m+1} - \mu_0) \right) \\ & + k_{A2r} \cdot [H_2O] \cdot \sum_{m=0}^{k} \left(\binom{k}{m} \frac{B_m}{k-m+1} \cdot \xi_{k-m} \right) \\ & - (k_{A4} \cdot p \cdot [PO] + k_{A5} \cdot 3 \cdot [AG] + k_{A6} \cdot [HMF]) \cdot \lambda_k \\ & + (k_{A4r} \cdot \psi_k + k_{A5r} \cdot \phi_k + k_{A6r} \cdot \omega_k) \cdot [H_2O] \\ & - (k_{D2} + k_{D3}) \cdot [P_1] - k_{D1} \cdot \lambda_k + k_{D1r} \cdot [H_2O] \cdot \sum_{i=0}^{k} \binom{k}{i} \phi_i \\ & + k_{D1r} \cdot [H_2O] \cdot [DAG] \end{aligned} \tag{A10}$$

- Moments of the non-reducing sugar molecules of size n, ξ_k

$$\begin{aligned} r_{\xi_k} = &+k_{A2}\sum_{m=0}^{k}\left(\binom{k}{m}\lambda_{k-m}\cdot\lambda_m\right) - k_{A2r}\cdot[H_2O]\cdot\xi_k \\ &+k_{A3}\left(a_D\cdot\sum_{m=0}^{k}\binom{k}{m}\xi_{m+1}\cdot\lambda_{k-m} + b_D\cdot\binom{k}{m}\xi_m\cdot\lambda_{k-m}\right) \\ &-k_{A3}\cdot\lambda_0\cdot(a_D\cdot\xi_{k+1}+b_D\cdot\xi_k) \\ &-k_{A3r}\cdot[H_2O]\cdot(\xi_{k+1}-\xi_k) + k_{A3r}\cdot[H_2O]\cdot\sum_{m=0}^{k}\left(\binom{k}{m}\frac{B_m}{k-m+1}\cdot(\xi_{k-m+1}-\xi_0)\right) \end{aligned} \tag{A11}$$

- Moments of the non-reducing sugar molecules of size n, containing a polyol unit, ψ_k

$$\begin{aligned} r_{\psi_k} = &+k_{A4}\cdot p\cdot[PO]\cdot\lambda_k - k_{A4r}\cdot[H_2O]\cdot\psi_k \\ &+k_{A3}\cdot\left(a_{DPO}\cdot\sum_{m=0}^{k}\binom{k}{m}\psi_{m+1}\cdot\lambda_{k-m} + b_{DPO}\cdot\binom{k}{m}\psi_m\cdot\lambda_{k-m}\right) \\ &-k_{A3}\cdot(\lambda_0\cdot(a_{DPO}\cdot\psi_{k+1}+b_{DPO}\cdot\psi_k)) \\ &+k_{A3r}\cdot[H_2O]\cdot\left(\sum_{m=0}^{k}\left(\binom{k}{m}\frac{B_m}{k-m+1}\cdot(\psi_{k-m+1}-\psi_0)\right) - (\psi_{k+1}-\psi_k)\right) \end{aligned} \tag{A12}$$

- Moments of the non-reducing sugar molecules of size n, containing a 1-6-anhydrosugar, ϕ_k

$$\begin{aligned} r_{\phi_k} = &+k_{A5}\cdot 3\cdot[AG]\cdot\lambda_k - k_{A5r}\cdot[H_2O]\cdot\phi_k \\ &+k_{D1}\cdot\sum_{i=0}^{k}\left(\binom{k}{i}\cdot(-1)^{k-i}\cdot(\lambda_i-[P_1])\right) - k_{D1r}\cdot[H_2O]\cdot\phi_k \\ &+k_{A3}\cdot\left(a_{DAG}\cdot\sum_{m=0}^{k}\binom{k}{m}\phi_{m+1}\cdot\lambda_{k-m} + b_{DAG}\cdot\sum_{m=0}^{k}\binom{k}{m}\phi_m\cdot\lambda_{k-m}\right) \\ &-k_{A3}\cdot(\lambda_0\cdot(a_{DAG}\cdot\phi_{k+1}+b_{DAG}\cdot\phi_k)) \\ &+k_{A3r}\cdot[H_2O]\cdot\left(\sum_{m=0}^{k}\left(\binom{k}{m}\frac{B_m}{k-m+1}\cdot(\phi_{k-m+1}-\phi_0)\right) - (\phi_{k+1}-\phi_k)\right) \end{aligned} \tag{A13}$$

- Moments of the non-reducing sugar molecules of size n, containing an HMF molecule, ω_k

$$\begin{aligned} r_{\omega_k} = &+k_{A6}\cdot[HMF]\cdot\lambda_k - k_{A6r}\cdot[H_2O]\cdot\omega_k \\ &+k_{A3}\cdot\left(a_{DHMF}\cdot\sum_{m=0}^{k}\binom{k}{m}\omega_{m+1}\cdot\lambda_{k-m} + b_{DHMF}\cdot\sum_{m=0}^{k}\binom{k}{m}\omega_m\cdot\lambda_{k-m}\right) \\ &-k_{A3}\cdot(\lambda_0\cdot(a_{DHMF}\cdot\omega_{k+1}+b_{DHMF}\cdot\omega_k)) \\ &+k_{A3r}\cdot[H_2O]\cdot\left(\sum_{m=0}^{k}\left(\binom{k}{m}\frac{B_m}{k-m+1}\cdot(\omega_{k-m+1}-\omega_0)\right) - (\omega_{k+1}-\omega_k)\right) \end{aligned} \tag{A14}$$

In the above expressions, the Bernoulli numbers are defined as:

$$B_j = \left[1,\ -\frac{1}{2},\ \frac{1}{6},\ 0,...\right] \quad ; \quad j = 0,1,2,3... \tag{A15}$$

According to the definition of the moments of the different species, the rate functions of the non-macromolecular species (Equations (A6)–(A9)) can be readily transformed, to eliminate the infinite summation terms.

Polyol molecules, PO

$$r_{PO} = -k_{A4} \cdot p \cdot [PO] \cdot \lambda_0 + k_{A4r} \cdot [H_2O] \cdot \psi_0 \tag{A16}$$

1-6-anhydrosugar molecules, AG

$$r_{AG} = -(3 \cdot k_{A5} \cdot \lambda_0 + k_{D1r} \cdot [H_2O]) \cdot [AG] + k_{D1} \cdot [P_1] + k_{A5r} \cdot [H_2O] \cdot \phi_0 \tag{A17}$$

HMF molecules, HMF

$$r_{HMF} = -(k_{A6} \cdot \lambda_0 + k_{D4}) \cdot [HMF] + k_{D2} \cdot [P_1] + k_{A6r} \cdot [H_2O] \cdot \omega_0 \tag{A18}$$

Humins, H

$$r_H = k_{D3} \cdot \lambda_0 + k_{D4} \cdot [HMF] \tag{A19}$$

Water molecules, H_2O

$$\begin{aligned} r_{H_2O} = {} & k_{A1} \cdot \lambda_0 \cdot (3 \cdot \lambda_1 + \lambda_0)) - k_{A1r} \cdot [H_2O](\lambda_1 - \lambda_0)) \\ & + k_{A3} \cdot \lambda_0 \cdot (a_D \cdot \xi_1 + a_{DAG} \cdot \phi_1 + a_{DPO} \cdot \psi_1 + a_{DHMF} \cdot \omega_1 \\ & + b_D \cdot \xi_0 + b_{DAG} \cdot \phi_0 + b_{DPO} \cdot \psi_0 + b_{DHMF} \cdot \omega_0) + k_{A2} \cdot \lambda_0^2 \\ & - k_{A2r} \cdot [H_2O] \cdot \xi_0 - k_{A3r} \cdot [H_2O] \cdot (\mu_1 - \mu_0) \\ & + (k_{A4} \cdot p \cdot [PO] + k_{A5} \cdot 3 \cdot [AG] + k_{A6} \cdot [HMF]) \cdot \lambda_0 \\ & - (k_{A4r} \cdot \psi_0 + k_{A5r} \cdot \phi_0 + k_{A6r} \cdot \omega_0) \cdot [H_2O] \\ & + 3 \cdot (k_{D2} + k_{D3}) \cdot [P_1] + k_{D1} \cdot \lambda_0 - k_{D1r} \cdot [H_2O] \cdot \phi_0 + [AG]) \end{aligned} \tag{A20}$$

References

1. Qian, X. Mechanisms and energetics for acid catalyzed β-D-glucose conversion to 5-hydroxymethylfurfurl. *J. Phys. Chem. A* **2011**, *115*, 11740–11748. doi:10.1021/jp2041982.
2. Hu, X.; Lievens, C.; Li, C.Z. Acid-catalyzed conversion of xylose in methanol-rich medium as part of biorefinery. *ChemSusChem* **2012**, *5*, 1427–1434. doi:10.1002/cssc.201100745.
3. Alonso, D.M.; Wettstein, S.G.; Dumesic, J.A. Bimetallic catalysts for upgrading of biomass to fuels and chemicals. *Chem. Soc. Rev.* **2012**, *41*, 8075–8098. doi:10.1039/c2cs35188a.
4. Yang, G.; Pidko, E.A.; Hensen, E.J. Mechanism of Bronsted acid-catalyzed conversion of carbohydrates. *J. Catal.* **2012**, *295*, 122–132. doi:10.1016/j.jcat.2012.08.002.
5. Caes, B.R.; Teixeira, R.E.; Knapp, K.G.; Raines, R.T. Biomass to Furanics: Renewable Routes to Chemicals and Fuels. *ACS Sustain. Chem. Eng.* **2015**, *3*, 2591–2605. doi:10.1021/acssuschemeng.5b00473.
6. Liu, L.; Li, Z.; Hou, W.; Shen, H. Direct conversion of lignocellulose to levulinic acid catalyzed by ionic liquid. *Carbohydr. Polym.* **2018**, *181*, 778–784. doi:10.1016/j.carbpol.2017.11.078.
7. Caratzoulas, S.; Davis, M.E.; Gorte, R.J.; Gounder, R.; Lobo, R.F.; Nikolakis, V.; Sandler, S.I.; Snyder, M.A.; Tsapatsis, M.; Vlachos, D.G. Challenges of and Insights into Acid-Catalyzed Transformations of Sugars. *J. Phys. Chem. C* **2014**, *118*, 22815–22833. doi:10.1021/jp504358d.
8. SriBala, G.; Vinu, R. Unified kinetic model for cellulose deconstruction via acid hydrolysis. *Ind. Eng. Chem. Res.* **2014**, *53*, 8714–8725. doi:10.1021/ie5007905.
9. Pascu, E.; Mora, P.T. Polycindensation of D-Glucose and other simple sugars in presence of acids. *J. Am. Chem. Soc.* **1950**, *72*, 1045. doi:10.1021/ja01158a529.
10. Mora, P.T.; Wood, J.W. Synthetic Polysaccharides. I. Polycondensation of Glucose. *J. Polym. Sci.* **1958**, *80*, 685–692.
11. Durand, H.W.; Dull, M.F.; Tipson, R.S. Polymerization of α-D-Glucose in the Solid State, in the Presence of Metaboric Acid. *J. Am. Chem. Soc.* **1958**, *80*, 3691–3697. doi:10.1021/ja01547a055.
12. Rennhard, H. Polysaccharides and Their Preparation. U.S. Patent No.3.766.165, 25 May 1972.
13. Pfizer Inc. Saccharide Polycondensation. GB1422294A, 5 April 1974.
14. Hu, X.; Kadarwati, S.; Wang, S.; Song, Y.; Hasan, M.D.; Li, C.Z. Biomass-derived sugars and furans: Which polymerize more during their hydrolysis? *Fuel Process. Technol.* **2015**, *137*, 212–219. doi:10.1016/j.fuproc.2015.04.024.
15. Long, Y.; Yu, Y.; Song, B.; Wu, H. Polymerization of glucose during acid-catalyzed pyrolysis at low temperatures. *Fuel* **2018**, *230*, 83–88. doi:10.1016/j.fuel.2018.05.022.

16. Xu, Q.; Hu, X.; Shao, Y.; Sun, K.; Jia, P.; Zhang, L.; Liu, Q.; Wang, Y.; Hu, S.; Xiang, J. Structural differences of the soluble oligomers and insoluble polymers from acid-catalyzed conversion of sugars with varied structures. *Carbohydr. Polym.* **2019**, *216*, 167–179. doi:10.1016/j.carbpol.2019.04.012.
17. Long, Y.; Yu, Y.; Wu, H. Mechanistic insights into the primary reactions during acid-catalysed pyrolysis of levoglucosan at 80–140 °C. *Fuel* **2020**, *268*. doi:10.1016/j.fuel.2020.117390.
18. Saeman, J.F. Kinetics of Wood Saccharification-Hydrolysis of Cellulose and Decomposition of Sugars in Dilute Acid at High Temperature. *Ind. Eng. Chem.* **1945**, *37*, 43–52. doi:10.1021/ie50421a009.
19. XIang, Q.; Kim, J.S.; Lee, Y.Y. A comprehensive Kinetic Model for Dilute-Acid Hydrolysis of Cellulose. *Appl. Biochem. Biotechnol.* **2003**, *105–108*, 337–352.
20. Girisuta, B.; Janssen, L.P.; Heeres, H.J. Green chemicals: A kinetic study on the conversion of glucose to levulinic acid. *Chem. Eng. Res. Des.* **2006**, *84*, 339–349. doi:10.1205/cherd05038.
21. Jing, Q.; Lü, X. Kinetics of Non-catalyzed Decomposition of Glucose in High-temperature Liquid Water. *Chin. J. Chem. Eng.* **2008**, *16*, 890–894. doi:10.1016/S1004-9541(09)60012-4.
22. Pilath, H.M.; Nimlos, M.R.; Mittal, A.; Himmel, M.E.; Johnson, D.K. Glucose reversion reaction kinetics. *J. Agric. Food Chem.* **2010**, *58*, 6131–6140. doi:10.1021/jf903598w.
23. Kupiainen, L.; Ahola, J.; Tanskanen, J. Kinetics of glucose decomposition in formic acid. *Chem. Eng. Res. Des.* **2011**, *89*, 2706–2713. doi:10.1016/j.cherd.2011.06.005.
24. Tan-Soetedjo, J.N.; Van De Bovenkamp, H.H.; Abdilla, R.M.; Rasrendra, C.B.; Van Ginkel, J.; Heeres, H.J. Experimental and Kinetic Modeling Studies on the Conversion of Sucrose to Levulinic Acid and 5-Hydroxymethylfurfural Using Sulfuric Acid in Water. *Ind. Eng. Chem. Res.* **2017**, *56*, 13228–13239. doi:10.1021/acs.iecr.7b01611.
25. Sumerskii, I.V.; Krutov, S.M.; Zarubin, M.Y. Humin-Like substances formed under the conditions of industrial hydrolysis of wood. *Rus. J. Appl. Chem.* **2010**, *83*, 320–327. doi:10.1134/S1070427210020266.
26. Verros, G.D. Calculation of molecular weight distribution in non-linear free radical copolymerization. *Polymer* **2003**, *44*, 7021–7032. doi:10.1016/j.polymer.2003.08.029.
27. Kiparissides, C. Challenges in particulate polymerization reactor modeling and optimization: A population balance perspective. *J. Process Control* **2006**, *16*. doi:10.1016/j.jprocont.2005.06.004.
28. Konstadinidis, K.; Achilias, D.S.; Kiparissides, C. Development of a unified mathematical framework for modelling molecular and structural changes in free-radical homopolymerization reactions. *Polymer* **1992**, *33*, 5019–5031. doi:10.1016/0032-3861(92)90053-Y.
29. Hulburt, H.; Katz, S. Some problems in particle technology. *Chem. Eng. Sci.* **1964**, *19*, 555–574. doi:10.1016/0009-2509(64)85047-8.
30. Zabisky, R.C.; Chan, W.M.; Gloor, P.E.; Hamielec, A.E. A kinetic model for olefin polymerization in high-pressure tubular reactors: A review and update. *Polymer* **1992**, *33*, 2243–2262. doi:10.1016/0032-3861(92)90514-W.
31. Lee, K.H.; Marano, J.P. Free-Radical Polymerization: Sensitivity of Conversion and Molecular Weights to Reactor Conditions. *ACS Symp. Ser. Polym. React Process.* **1979**, 221–251. doi:10.1021/bk-1979-0104.ch010.
32. Lim, C.; Nebus, J. *Vorticity, Statistical Mechanics, and Monte Carlo Simulation*; Springer Science & Business Media: New York, NY, USA, 2007.
33. Dagpunar, J.S. *Simulation and Monte Carlo: With Applications in Finance and MCMC*; John Wiley & Sons: Hoboken, NJ, USA, 2007.
34. Liu, J.S. *Monte Carlo Strategies in Scientific Computing*; Springer Science & Business Media: New York, NY, USA, 2008.
35. Rubinstein, R.Y.; Kroese, D.P. *Simulation and the Monte Carlo Method*; John Wiley & Sons: Hoboken, NJ, USA, 2016; Volume 10.
36. Gillespie, D.T. A general method for numerically simulating the stochastic time evolution of coupled chemical reactions. *J. Comput. Phys.* **1976**, *22*, 403–434.
37. Tobita, H. Molecular weight distribution in free radical polymerization with long-chain branching. *J. Polym. Sci. Part B Polym. Phys.* **1993**, *31*, 1363–1371. doi:10.1002/polb.1993.090311011.
38. Meimaroglou, D.; Krallis, A.; Saliakas, V.; Kiparissides, C. Prediction of the bivariate molecular weight-Long chain branching distribution in highly branched polymerization systems using Monte Carlo and sectional grid methods. *Macromolecules* **2007**, *40*, 2224–2234.
39. Meimaroglou, D.; Kiparissides, C. Review of Monte Carlo Methods for the Prediction of Distributed Molecular and Morphological Polymer Properties. *Ind. Eng. Chem. Res.* **2014**, *53*, 8963–8979. doi:10.1021/ie4033044.
40. Meimaroglou, D.; Kiparissides, C. A novel stochastic approach for the prediction of the exact topological characteristics and rheological properties of highly-branched polymer chains. *Macromolecules* **2010**, *43*, 5820–5832.
41. Keramopoulos, A.; Kiparissides, C. Development of a comprehensive model for diffusion-controlled free-radical copolymerization reactions. *Macromolecules* **2002**, *35*. doi:10.1021/ma010999q.
42. Achilias, D.S. A review of modeling of diffusion controlled polymerization reactions. *Macromol. Theory Simul.* **2007**, *16*. doi:10.1002/mats.200700003.
43. Duerksen, J.H.; Hamielec, A.E. Molecular Weight Distribution. Part III. Gel Permeation Chromatography, Methods of Correcting for Imperfect Resolution. *J. Polym. Sci. Part C Polym. Symp.* **1968**, *21*, 83–103.
44. Duerksen, J.H.; Hamielec, A.E. Polymer reactors and molecular weight distribution. Part VII. Further development of gel permeation chromatography. *J. Polym. Sci. Part C Polym. Symp.* **1968**, *12*, 2225–2255. doi:10.1002/polc.5070210110.

3. A Trade-Off Between Knowledge and Data

Not to unlearn what you have learned is the most necessary kind of learning...

Antisthenes

3.1 Application of an Artificial Neural Network to a physicochemical process

Over the last several years, a significant shift is observed in the business model and manufacturing paradigm of an ever-increasing number of companies, developing their activities in various sectors. This shift is primarily based on a more efficient collection, transfer and exploitation of information, taking advantage of the parallel exponential growth of the relevant technologies on data acquisition, storage and transfer. This fourth industrial revolution, as is one of the terms most commonly used to describe this new *modus operandi*, is thus using the connectivity of objects (i.e., the so-called Internet Of Things, IOT) as means to harvest more information, faster - even in real-time - and in a more reliable way in order to extract the knowledge that is contained therewith.

This procedure contains several steps, namely those of data collection, of their statistical visualization (descriptive analysis), of the identification of patterns within these data (predictive analysis) and, finally, of the decision making (prescriptive analysis). Many fields of scientific research have naturally spawn off these steps, focusing on the development of specific techniques and methods that can best meet the needs and the objectives of each of the above analyses. The fields of statistics, data science and mathematical modeling are principally concerned by these developments. As such, and in specific association primarily to the step of predictive analysis, data-driven modeling techniques have found an excellent field of growth and application.

As described previously, in the General Introduction (Chapter 1) of this report, data-driven modeling methods are focused on creating links between data, without them being able to assign the forms of these links, or even their very existence, to specific laws or phenomena that would allow their rationalization. In other words, these methods will adapt their responses according to what they have 'seen' in the data, without providing additional information on how or why. For example, given a set of values for the measured concentration of a reactant and the respective reaction rate, a data-driven model will describe that there is a power-law relationship between the two. However, the notions of the kinetic rate constant or reaction order will be 'hidden' within the parameters of the model. This is a typical example of a very simple modeling problem that can be formulated under numerous approaches.

The simplest approach, that is widely used in engineering, is the commonly employed linear regression, where the parameters, a and b, of an expression of the type $y = a\,x + b$ are identified on the basis of the available data using analytical or iterative approaches. In the previous example, x and y would refer to the logarithms of the reactant concentration and the reaction rate, respectively. Should the problem be extended to include data of additional properties (also known as features), such as the concentration of another reactant for example, a similar approach can be implemented in the form of a multivariate linear regression problem (also known as multilinear regression). This is the typical case of any experimental design strategy where the response(s) of the developed model are calculated by polynomial expressions, containing linear, quadratic and/or interaction terms between the considered features (or factors).

These modeling approaches are trivial in problems with a relatively limited number of features and/or when a minimum knowledge about the effects of these features on the response(s) (i.e., about the form of the sought response surface(e)) exist. However, in cases where the feature space becomes very high, or in cases where the commonly adopted forms of the mathematical expressions of the model fail to describe the observed effects, more advanced data-driven methods are required. Machine learning (ML) techniques provide this alternative through a plethora of tools and methods that can be proven extremely powerful, even in describing very complex response

surfaces. These tools can be implemented not only to problems where the values of both features and responses are available (i.e., supervised ML - see Chapter 5 of this report), but also to problems where only the values of the features are known.

One of the most powerful and most widespread techniques of this family is that of artificial neural networks (ANN). ANNs can create a mathematical expression for describing the relationship between the input(s) and output(s) of a given system that will be complicated enough to describe the corresponding response surface, no matter how complex. The fact that the form of this expression does not have to be imposed *a priori*, but is constructed by the algorithm during a 'learning phase', provides significant flexibility to this method in terms of its spectrum of applications.

In the following article, the development of a data-driven modeling framework, in terms of two consecutive ANNs, is presented for the modeling of a photocatalytic process for the degradation of a water contaminant. The main interest of this work relies in the deployment of a data-driven technique to describe a process for which the available knowledge and resources, at the time of the study, were not sufficient to allow for the development of a knowledge-based mathematical model. In addition, it is demonstrated how the implementation of an integrated two-step modeling approach, in terms of two distinct stages of the process, allowed the direct connection of the conditions of the first to the outcome of the second. These stages are respectively the synthesis of the photocatalyst and the photodegradation process. Despite the fact that they are completely detached and independent in practice, an underlying connection exists between them as the characteristics of the photocatalyst, which are determined in the first step of the process, will display an effect on its final photodegradation performance, as measured in the second step of the process. At the final part of the study, the developed model was also coupled with an evolutionary optimization algorithm for the identification of the optimal photocatalyst synthesis and photodegradation conditions that would result in a maximum degradation of the contaminant.

Contents lists available at ScienceDirect

Chemical Engineering Research and Design

journal homepage: www.elsevier.com/locate/cherd

Modeling and optimization of a photocatalytic process: Degradation of endocrine disruptor compounds by Ag/ZnO

Alma Berenice Jasso-Salcedo[a,1], *Sandrine Hoppe*[b], *Fernand Pla*[b], *Vladimir Alonso Escobar-Barrios*[c], *Mauricio Camargo*[d], *Dimitrios Meimaroglou*[b,*]

[a] *Instituto Potosino de Investigación Científica y Tecnológica, División Ciencias Ambientales, Camino a la Presa de San José 2055, Col. Lomas 4a Sección, C.P. 78216 San Luis Potosí, S.L.P., México*
[b] *CNRS, Laboratoire Réactions et Génie des Procédés, Université de Lorraine UMR 7274, Nancy F-54001, France*
[c] *Instituto Potosino de Investigación Científica y Tecnológica, División de Materiales Avanzados, Camino a la Presa de San José 2055, Col. Lomas 4a Sección, C.P. 78216 San Luis Potosí, S.L.P., México*
[d] *Université de Lorraine, ERPI, Equipe de Recherche sur les Processus Innovatifs, EA 6737, Nancy F-54001, France*

ARTICLE INFO

Article history:
Received 12 April 2017
Received in revised form 15 September 2017
Accepted 9 October 2017
Available online 18 October 2017

Keywords:
Artificial neural networks
Optimization
Photocatalysis
Bisphenol-A

ABSTRACT

Artificial neural network (ANN) modeling was applied to study the photocatalytic degradation of bisphenol-A. The operating conditions of the Ag/ZnO photocatalyst synthesis and its performance were simultaneously modeled and subsequently optimized to target the highest efficiency in terms of the degradation reaction rate. Two ANN models were developed to simulate the stages of the photocatalyst synthesis and photodegradation performance, respectively. A direct dependence between the two networks was also established, thus making it possible to directly relate the degradation rate of the contaminant, not only to the photodegradation conditions, but also to the photocatalyst synthesis conditions. In this respect, an optimization study was carried out, by means of an evolutionary algorithm, in order to identify the optimal synthesis and photodegradation conditions that would result in the degradation of a maximal amount of the contaminant. Through this integrated approach it was demonstrated that neural network models can be proven valuable tools in the evaluation, simulation and, ultimately, the optimization of different stages of complex photocatalytic processes towards the maximization of the efficiency of the synthesized photocatalyst.

1. Introduction

Endocrine-disrupting compounds (EDCs) is a class of chemical substances that pollute water and other environmental resources. They are responsible for adverse developmental, reproductive, neurological and immune side-effects on both humans and wildlife as they interfere with the organism's endocrine system. Bisphenol-A (BPA) is an EDC that was used initially (i.e., in the 1930's) as an estrogenic drug for birth control and later as a monomer in the synthesis of polycarbonate as well as an additive in the synthesis of polyvinylchloride, polyesters, epoxy resins, lacquer coatings, etc. It is these latter applications that have facilitated the extensive, worldwide spread of this contaminant, presently detected in various aqueous media including fresh and marine surface waters and groundwater (Flint et al., 2012; Klečka et al., 2009).

* *Corresponding author*.
E-mail address: dimitrios.meimaroglou@univ-lorraine.fr (D. Meimaroglou).
[1] Present address: Department of Materials and Environmental Chemistry, Arrhenius Laboratory, Stockholm University, SE-106 91 Stockholm, Sweden.
https://doi.org/10.1016/j.cherd.2017.10.012

Among the several studies on the removal of EDCs and pharmaceuticals from drinking water, sunlight-induced photocatalytic degradation is an attractive approach that has gained significant attention over the last years (Bohdziewicz et al., 2016; Esplugas et al., 2007; Fernández et al., 2014; Sin et al., 2012; Sornalingam et al., 2016; Tijani et al., 2013). Yet, despite the undisputed advantages of the process, such as its clean – non-chemical nature and its relatively low cost, heterogeneous photocatalysis is a complex process whose efficiency is related to a number of factors associated with the catalyst properties (e.g., crystal structure, morphology, surface area, defect sites, polarity, active surface sites and reactive charges life-time) and the photocatalytic reaction conditions (e.g., pH, contaminant concentration, catalyst dose, light intensity). Hence, the control of the photocatalytic performance of UV/Metal Oxide systems is not a trivial problem since it requires an optimal combination of the above mentioned material and process characteristics and conditions. In this respect, the development of an accurate robust mathematical model of the process becomes of profound importance to the study and implementation of this decontamination technique.

Traditional modeling approaches of such systems are based on kinetic models that simulate the contaminant degradation curves on the basis of a commonly adopted first-order kinetics equation (Amani-Ghadim and Seyed Dorraji, 2015; Rosenfeldt and Linden, 2004; Wang et al., 2009). On the other hand, alternative modeling methodologies (e.g., empirical models or response surface methodologies) (Asl et al., 2012; Babaei et al., 2011; Kiattisaksiri et al., 2015; Lee and Hamid, 2015; Merabet et al., 2016) are constantly gaining ground in the area, mainly due to the complex nature of the photodegradation processes and the lack of thorough understanding of all the mechanisms involved, which inhibits the development of generalized powerful mechanistic models. Among these alternatives, artificial neural network models display an evergrowing presence in the most recent relevant studies.

Artificial neural networks are powerful tools that can be implemented on a set of raw experimental data to establish non-linear mathematical relations between the input/output of the process. They belong to the general class of 'data-driven models' (DDM), which attempt to create connections between the input variables and the responses of a system, without requiring any prior knowledge on the underlying physical phenomena (Solomatine et al., 2009). Other advantages of this class of models are their ability to extract and recognize patterns in data, as well as their rather quick and simple development and implementation to completely different processes.

Under the condition of existence of a sufficient number of experimental data, ANN models can be proven quite efficient and accurate, both in correlating the existing data as well as in predicting the system behavior (within the limits of the explored experimental space), while they can also be easily customized to different systems. They are commonly developed with the aid of specifically designed software or software package toolboxes (e.g., the ANN toolbox of Matlab®), which are simple to use and quite flexible in terms of the customization of the model structure and characteristics (Sivanandam et al., 2006).

A review of the implementation of ANN on heterogeneous photocatalytic water and wastewater treatment processes was published by Khataee and Kasiri (2010). The accuracy of ANN models was also assessed in a recent study by Amani-Ghadim and Seyed Dorraji (2015), who compared three different model types, namely a kinetic model, an empirical model and an ANN model on the photodegradation of Acid blue 9 using UV/ZnO. In this study, the authors investigated the effect of different factors (i.e., contaminant initial concentration, ZnO content, light intensity, pH and time) on the photodegradation efficiency and concluded that ANN modeling allows an accurate description of the photocatalytic process without the necessity to resort to complex mathematical descriptions of the kinetics.

Traditionally, ANN models have been applied to photocatalytic degradation processes in order to study the effect of a variety of reaction conditions on the photocatalytic performance by means of percentage of degradation or removal efficiency. It is only recently that the apparent reaction rate constant of a first-order photocatalytic degradation curve was considered as the simulated response of the developed ANN model (Behnajady and Eskandarloo, 2015; Delnavaz, 2015). The characteristics of a series of similar recent studies are summarized in Table 1.

As can be seen, ANN models can be used to assess the effect of numerous important factors of the process, such as light intensity, organic/inorganic ions concentration and oxygen dose, which influence the photocatalytic performance but are rarely considered in kinetic models. For instance, Vaez et al. (2015) studied the effect of anions naturally present in wastewater (i.e., sulfate SO_4^{2-}, chloride Cl^-, bicarbonate HCO_3^- and carbonate CO_3^{2-}) and peroxide, on the photodegradation of Acid Red 73 on UV/TiO_2 nanoparticles immobilized on sackcloth fiber. In another noteworthy example, Tanasa et al. (2013) successfully studied the effect of both photocatalyst properties (i.e., crystallite size, surface area and absorption edge) and reaction conditions (i.e., dye initial concentration, time and catalyst dose) on the color removal of Eosin Y in UV/ZnO/SnO_2 systems.

In the present work, a novel modeling framework is proposed for the study of a photocatalytic degradation process of a water contaminant. In this respect, the two major stages of the photocatalytic process, namely the photocatalyst synthesis and the contaminant degradation experiments, are decoupled in order to separately assess the effects of the factors affecting these two process stages on the overall photocatalytic efficiency of the synthesized photocatalyst. Two artificial neural networks are developed for the modeling of these two stages, linked together by the fact that the output of the ANN model on the photocatalyst synthesis is, at the same time, an input for the ANN model on the photodegradation experiments. In a subsequent optimization analysis, the two models are separately optimized in the inverse order (i.e., starting from the model on the photodegradation tests), thus connecting the photodegradation efficiency (i.e., related to the objective function of the first optimization study on the second ANN model) with the photocatalyst synthesis conditions (i.e., optimal decision variables of the second optimization study on the first ANN model).

The system under study concerns the use of silver-modified ZnO particles (Ag/ZnO) as effective catalysts for the photodegradation of BPA in water. ZnO, charged with silver nanoparticles (AgNPs), is a prominent photocatalyst that has been employed in several contaminant photodegradation studies due to its decreased charge-carriers recombination rate, increased photostability and efficiency (Georgekutty et al., 2008; Wang et al., 2011; Xie et al., 2010). The detailed characteristics of the experimental system have been extensively presented in a recent publication (Jasso-Salcedo et al., 2016) and will not be the subject of the present work. To the best of the authors' knowledge, this is the first time that a two-stage, de-coupled ANN modelling framework is proposed for the study and, subsequently, the optimization of the photocatalytic degradation of an endocrine disrupting contaminant. The proposed approach allows for the evaluation of the effects of the factors of the two principal stages of the photodegradation process (i.e., the catalyst synthesis and the degradation experiments) on the final photodegradation efficiency, by distinguishing these two stages without completely isolating them from the overall process.

2. Methodology

2.1. Data collection

2.1.1. Preparation of Ag/ZnO

The Ag/ZnO photocatalyst was prepared by photodeposition (PD) and impregnation (IMP) methods (Jasso-Salcedo et al., 2014). For both methods, a suspension containing ZnO and stabilized silver nanoparticles (AgNPs) was adjusted at desired initial pH values using 0.1N HCl and/or 0.5 N NaOH. The suspension was stirred under UV irradiation or in darkness, for PD and IMP methods, respectively. Then the sample was submitted to centrifugation/re-dispersion cycles in distilled water and ethanol solutions several times to remove the free AgNPs (i.e., not attached to the ZnO surface). The actual weight per-

Table 1 – Neural network modeling studies of the photocatalytic performance on the degradation of water contaminants.

Photocatalyst	Model contaminant	ANN topology (In:Hid:Out)	Data number	Input/factors	Output/response	References
ZnO	Acid Blue 9	5:9:1	152	AB9, pH, ZnO, UV intensity	Degradation efficiency (%)	Amani-Ghadim and Seyed Dorraji (2015)
ZnO/Montmorillonite K10	Disperse Red 54 (DR54)	5:10:1	N/A	DR54, ZnO/MMT, time	Decolorization efficiency (%)	Kiransan et al. (2015)
ZnO/Montmorillonite K10	Basic yellow 28 (BY28)	3:14:1	N/A	BY28, ZnO/MMT dosage, UV radiation time	Decolorization efficiency (%)	Kıransan et al. (2015)
TiO_2	Acid Red 27	4:8:1	56	TiO_2, AR27, pH, UV intensity	Reaction rate constant (Kap)	Behnajady and Eskandarloo (2015)
TiO_2-lLight expanded clay aggregates	Phenol	5:6:4:2	325	Reaction time, Phenol, pH, TiO_2, UV intensity	Photocatalytic reactor efficiency (%) and kinetic constant (Kapp)	Delnavaz (2015)
TiO_2/sackcloth fibre	Acid Red 73	5: 15:1	300	pH, time, anion, H_2O_2, AR73 concentration	Photocatalytic efficiency (%)	Vaez et al. (2015)
SnO_2/Fe_3O_4	Phenol red	4:20:30:20:1	30	SnO_2/Fe_3O_4, phenol red, stirring intensity, UV intensity	Dye removal (%)	Sargolzaei et al. (2015)
TiO_2/ZrO_2	Carbamazepine (CBZ)	4:5:1	130	TiO_2/ZrO_2, pH, reaction time, CBZ	CBZ removal (%)	Das et al. (2014)
TiO_2	Chromium (Cr(VI))	4:4:1	558	Cr(VI), pH, TiO_2, irradiation time	Photocatalytic reduction Cr(VI) (%)	Sabonian and Behnajady (2014)
TiO_2	*N*,*N*-Diethyl-*m*-toluamide (DEET)	3:13:1	17	TiO_2, DEET, UV intensity	Photocatalytic oxidation (%)	Antonopoulou and Konstantinou (2013)
TiO_2	Total phenolic compounds (TPh)	3:12:1	17	TiO_2, TPh, UV intensity	Photocatalytic oxidation of TPh (%)	Antonopoulou et al. (2012)
TiO_2	17α-Ethynylestradiol (EE2)	5:13:1	222	Reaction time, TiO_2, EE2, water dissolved organic carbon, water conductivity	EE2 conversion (%)	Frontistis et al. (2012)
TiO_2	4-Nitrophenol (4-NP)	4:14:1	147	Nano TiO_2, time, UV intensity, 4-NP	Removal (%)	Ghanbary et al. (2012)
TiO2	Reactive black 5 (RB5)	4:10:1	N/A	pH, TiO_2 dose, RB5, time	Photocatalytic efficiency (%)	Dutta et al. (2010)

centage of AgNPs that were finally attached to the ZnO surface was calculated by the following expression:

$$W_{Ag}\% = \frac{W_{Ag}}{W_{Ag} + W_{Zn}} \times 100 \quad (1)$$

where the quantities of Ag and Zn were obtained from elemental quantification using inductively coupled plasma spectrometry (ICP-OES, 730-ES, Varian Inc.) at 328 nm and 213.9 nm, respectively. Before the analysis, the samples were submitted to acid digestion (69% Nitric acid), diluted with DI H_2O and filtered (0.45 μm).

2.1.2. *Photocatalysis experiments*

An aqueous solution of BPA and photocatalyst was mechanically stirred for 10 min in darkness and then irradiated at different wavelengths, namely at 254, 302 or 365 nm using a UV lamp (3UV-38, UVP Inc.) and at 450 nm using a fluorescent lamp (F8T5/CW, Hampton Bay). The experiments were carried out in a dark box, with the lamp placed at a distance of 8 cm above the sample, at room temperature and without external oxygen supply (Jasso-Salcedo et al., 2014). Samples were then collected at regular time intervals and centrifuged at 3000 rpm for 10 min to recover the photocatalyst powder. The liquid samples were filtered (0.45 μm) before liquid chromatography (HPLC 1200 Series, Agilent Technologies) analysis.

The apparent kinetic rate constant of the BPA degradation was obtained as follows: the experimental data (i.e, BPA con-

centration vs time plots) were initially approximated by an exponential decay function, as shown in Eq. (2):

$$C_N = a\exp(bt)\,;\, b < 0 \quad (2)$$

where C_N denotes the normalized BPA concentration (C/C_0). A least squares regression provided the values of a and b for each experiment. In order to associate the BPA degradation curves with a rate constant, the differential form of Eq. (2) was then transformed into a typical rate function of order n:

$$r = \left(-\frac{dC_N}{dt}\right) = k_{app} \times C_N^n \quad (3)$$

In the above equation, k_{app} and n are the apparent kinetic rate constant and the order of the reaction, respectively and r denotes the rate of the reaction. The values of k_{app} and n can be estimated by substituting Eq. (2) into Eq. (3):

$$\begin{cases} n = 1 \\ k_{app} = -b \end{cases}$$

The first order rate of the BPA degradation was also confirmed by plotting $ln(r)$ vs $ln(C_N)$ and estimating the regression parameters of the produced straight line, according to the linearized form of Eq. (3):

$$\ln(r) = \ln(k_{app}) + n\ln(C_N) \quad (4)$$

Note that the value of the correlation coefficient, R, of this linear regression is given for each experiment in Table 5, along with the values of the experimental measurements.

2.2. *Artificial neural network modeling*

A neural network is a cluster of processing nodes (i.e., neurons) arranged in several layers and interconnected in a variety of topologies, following the paradigm of the functionality of the human brain. The successful development and implementation of an ANN model relies onto three principal conditions, each one with its own significance for the accuracy and efficiency of the developed model:

- Correct identification of the input and output variables of the system, also called factors and responses, respectively. The selection of the principal factors (i.e., the ones with the greatest effect on the targeted response) from all possible candidates is a procedure that requires a minimum knowledge of the actual process. Its importance lies in the fact that the number and nature of the selected factors will affect, on the one hand, the number of required experimental data (i.e., the more factors considered, the greater the number of data required for an accurate model development), and on the other hand, will define whether important effects on the measured response have been omitted. In the case where prior knowledge on the process is completely absent, a small number of exploratory experiments can be carried out.
- Definition of the experimental space and execution of a set of experiments for the acquisition of data. Given that the main factors of the process have been correctly identified and under the assumption that there exists a correlation between these factors and the targeted response of the system, an ANN model can identify this correlation on the basis of a set of experimental data. Evidently, the ability of the ANN to successfully correlate the input(s) (i.e., factors) and output(s) (i.e., response(s)) is directly proportional to the number of available data. On the other hand, the number of experiments that can be carried out is always subject to feasibility constraints (e.g., time and/or cost limitations, etc.) that may dictate the studied process. Hence, the implementation of an experimental design strategy can become invaluable during this second stage of the model development procedure. The Design of Experiments (DoE) approach enables to obtain a maximum amount of information from a given predefined experimental effort. Typical DoE strategies include full- or fractional-factorial designs, central composite designs, Box–Behnken designs, Plackett– Burman (PB) designs, D-optimal and E-optimal designs, etc. (Ferreira et al., 2007; Georgakis, 2013; Heiligers, 1994; Witek-Krowiak et al., 2014).
- Identification of the topology of the ANN: the structure of the network, in terms of the number and size of the hidden layers, as well as its characteristics (i.e., training algorithm, type of transfer functions, etc.), display a significant effect on the accuracy of the model. To identify these parameters, most studies follow a trial and error procedure where different topologies of the ANN are tested until satisfactory

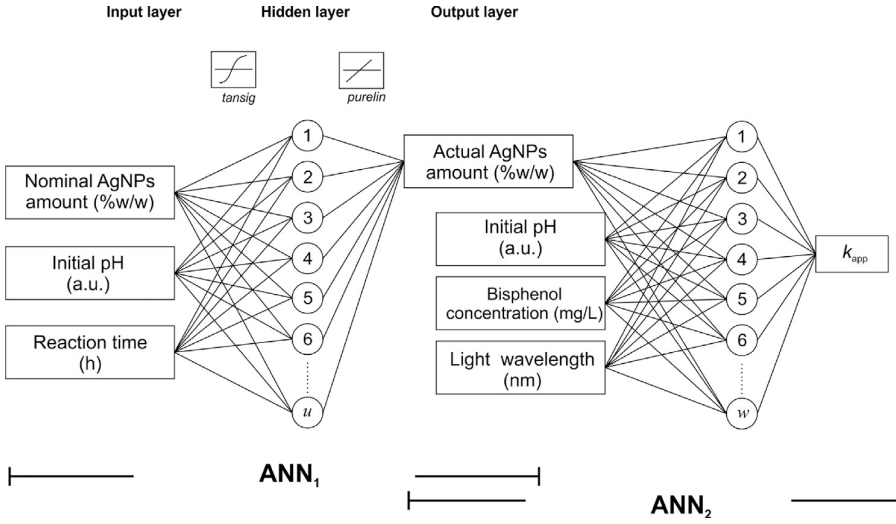

Scheme 1 – Description of the input/output characteristics and connecting points of the two ANN models.

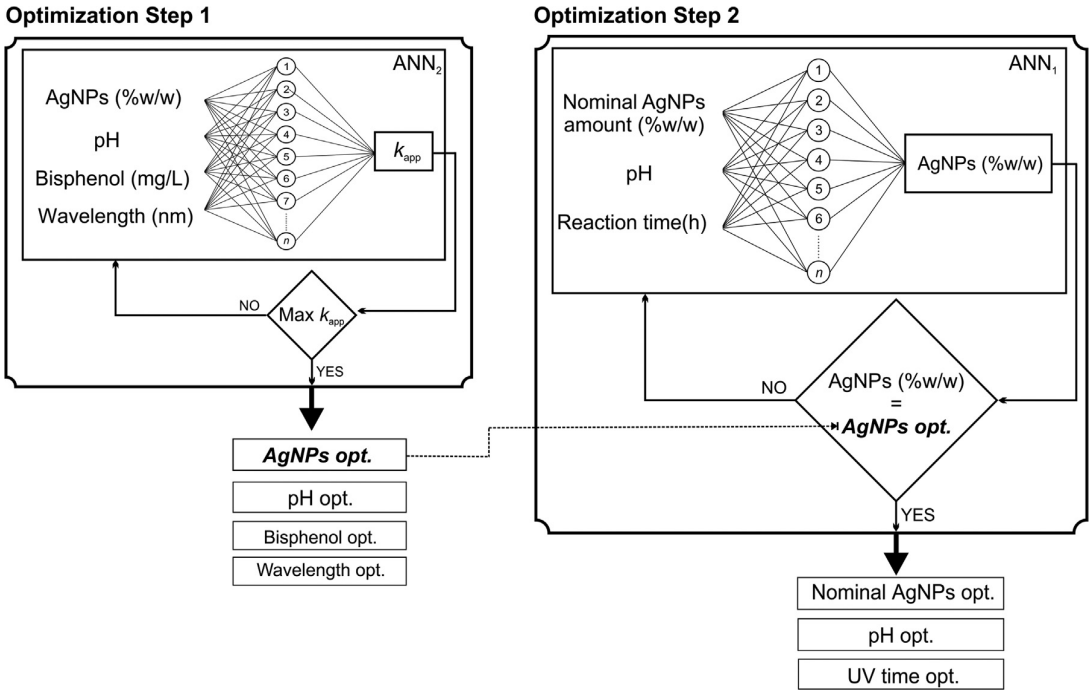

Scheme 2 – Methodology used on the evolutionary algorithm—ANN coupled optimization approach on this study.

accuracy has been achieved. Note that the random initialization of the values of the network parameters (e.g., the neuron's weights) as well as of the data separation (c.f. next paragraph) must be taken into account during this procedure.

Once the experimental data have been acquired and the factors/responses and architecture of the ANN model have been defined, the development of the model proceeds via a series of subsequent training (i.e., parametric identification) steps. In general, the accuracy of such models is assessed in terms of different statistical magnitudes, such as the Mean Square Error, MSE, or the correlation coefficient, R, calculated on the basis of the comparison of the model responses and the respective experimental targets. These latter are divided into three distinct subsets that serve for the training, validation and testing of the network, respectively. The training data set is used for the identification of the model parameters while the test data set is used to assess the accuracy of the model on a set of data different than the ones used for the training and validation processes. The validation data set is used to avoid overfitting phenomena by monitoring the error (i.e., on this data set) throughout the training process. This error normally decreases along with the training set error. An increase on the validation error for a number of sequential epochs (i.e., training *passes* of the network) is an indication of overfitting that triggers the stopping of the training process, returning the network (i.e., the values of weights and biases) corresponding to the minimum value of the validation error. In the present work, the number of sequential epochs of increasing validation error before stopping the training of the network was set to seven.

Among the various types of existing ANNs, the most commonly encountered in physicochemical process modeling is the feed-forward (i.e., the responses of each layer are used as inputs of the next layer) back-propagation (i.e., the mea-

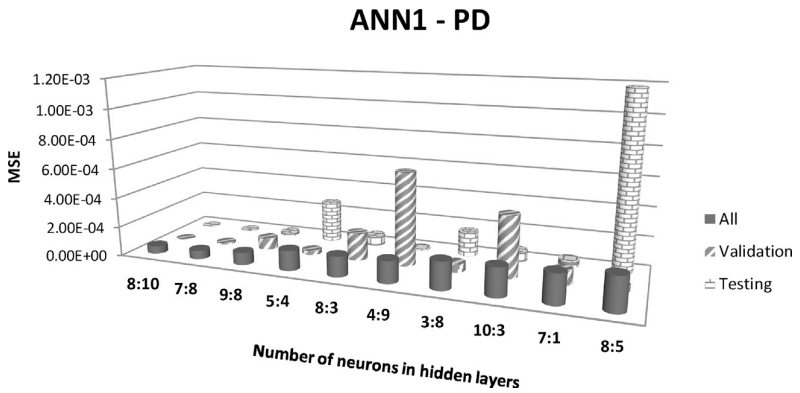

Fig. 1 – MSE for all data, validation and test datasets as function of neurons in the hidden layer on the network topology for the developed ANN1 model (photodeposition method).

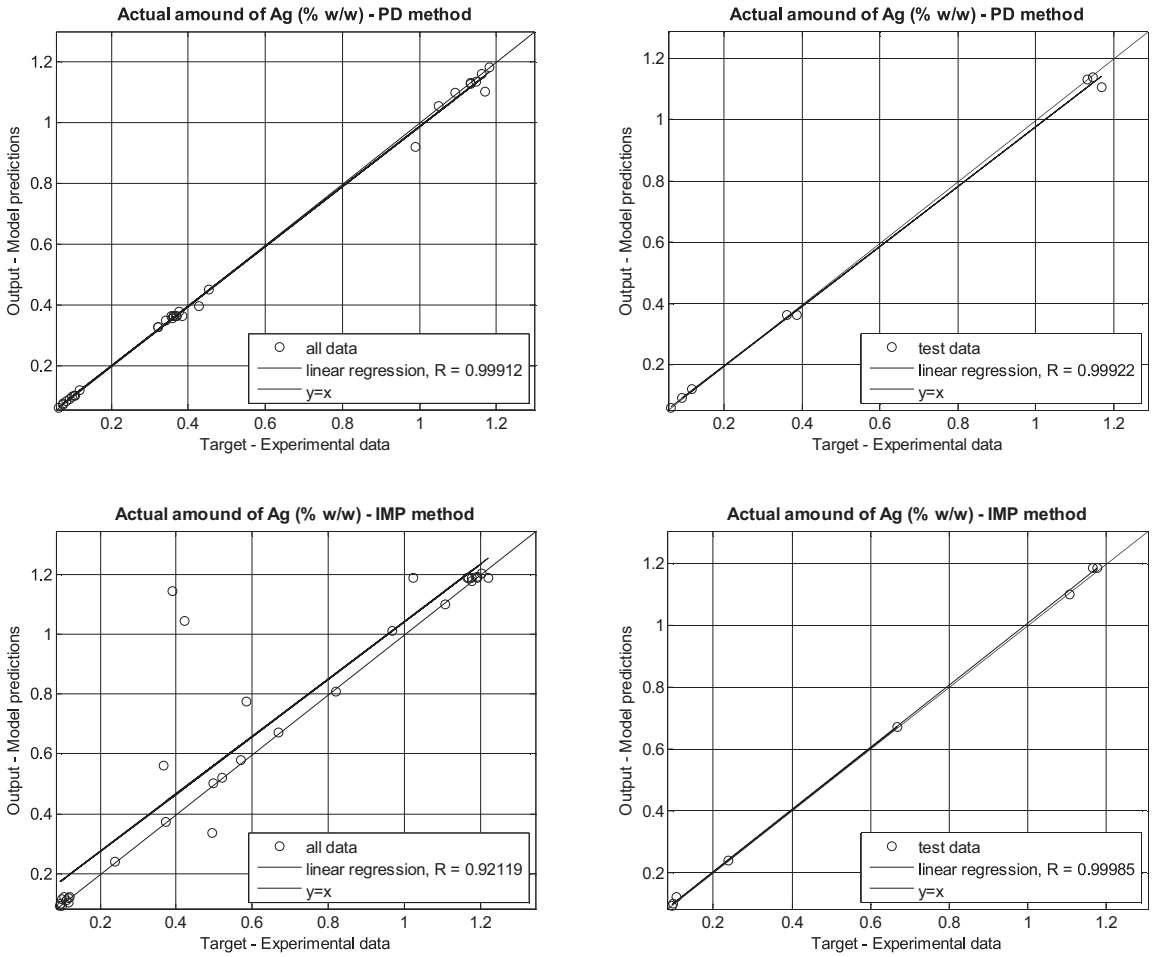

Fig. 2 – Regression plots of the experimental data (all data and test data sets) versus model predicted values for the developed neural network models ANN_1-PD (top) and ANN_1-IMP (bottom).

sured error at the output layer is back transferred to re-adjust the model parameter values) network, while the sigmoidal (e.g., logarithmic sigmoidal or tangent hyperbolic sigmoidal) and linear transfer functions are widely applied on the hidden and output layers, respectively (Cheng and Titterington, 1994; Haykin, 1994; Meireles et al., 2003; Sivanandam et al., 2006). Additional details on the principles and the characteristics of neural networks can be found in the relevant literature (Cheng and Titterington, 1994; Haykin, 1994; Meireles et al., 2003; Sivanandam et al., 2006).

Photocatalytic processes are greatly influenced by both catalyst properties and reaction conditions. These effects are traditionally studied separately (see Table 1), probably due to the complexity of assessing them simultaneously in a single study. An exception to this rule is the work of Tanasa et al. (2013), who studied the system of Eosin Y dye photocatalytic degradation using ZnO/SnO_2, taking into account the effects of crystallite size, surface area, absorption edge, catalyst dose and total organic carbon values in their model that was developed on the basis of a set of 547 experimental data. In addition, another commonly adopted practice is the consideration of the irradiation time as a factor in the modeling of the percentage of contaminant degradation (i.e., response). Given that the percentage of contaminant degradation will normally increase with the reaction time, this approach finally leads to a rather obvious correlation that, in turn, may come in the cost of missing other important effects of different factors.

In the present work, a model development is presented that does not comply with the above commonly adopted approaches. In order to combine the effects of both important stages of the photocatalytic process, namely the catalyst synthesis and the photodegradation experiments, a two-stage decoupled ANN model is developed where the response of the first network becomes a factor for the second network. Thus, in the first stage of the model, the effects of three operating conditions of the synthesis of Ag/ZnO (i.e., nominal silver concentration, pH and reaction time, which were identified in Jasso-Salcedo et al. (2014) as the most significant parameters of the process) on the actual amount of Ag attached on the surface of ZnO of the synthesized photocatalyst were assessed in terms of an initial neural network, henceforth called ANN_1. In the second stage of this modelling framework, the effect of the actual amount of Ag attached on the surface of ZnO, pH of the medium, initial contaminant concentration and wavelength of light on the photodegradation performance of the photocatalyst were assessed in terms of a second neural network, ANN_2. A direct dependence between the two networks was established by directly introducing the response of ANN_1 as a factor of ANN_2. The photodegradation performance (i.e., the response of ANN_2) was evaluated in terms of an apparent kinetic rate constant, k_{app}, of the degradation reaction of BPA. This way, the photocatalyst synthesis conditions were directly associated to its final photodegradation performance, taking simultaneously into account the effects of the

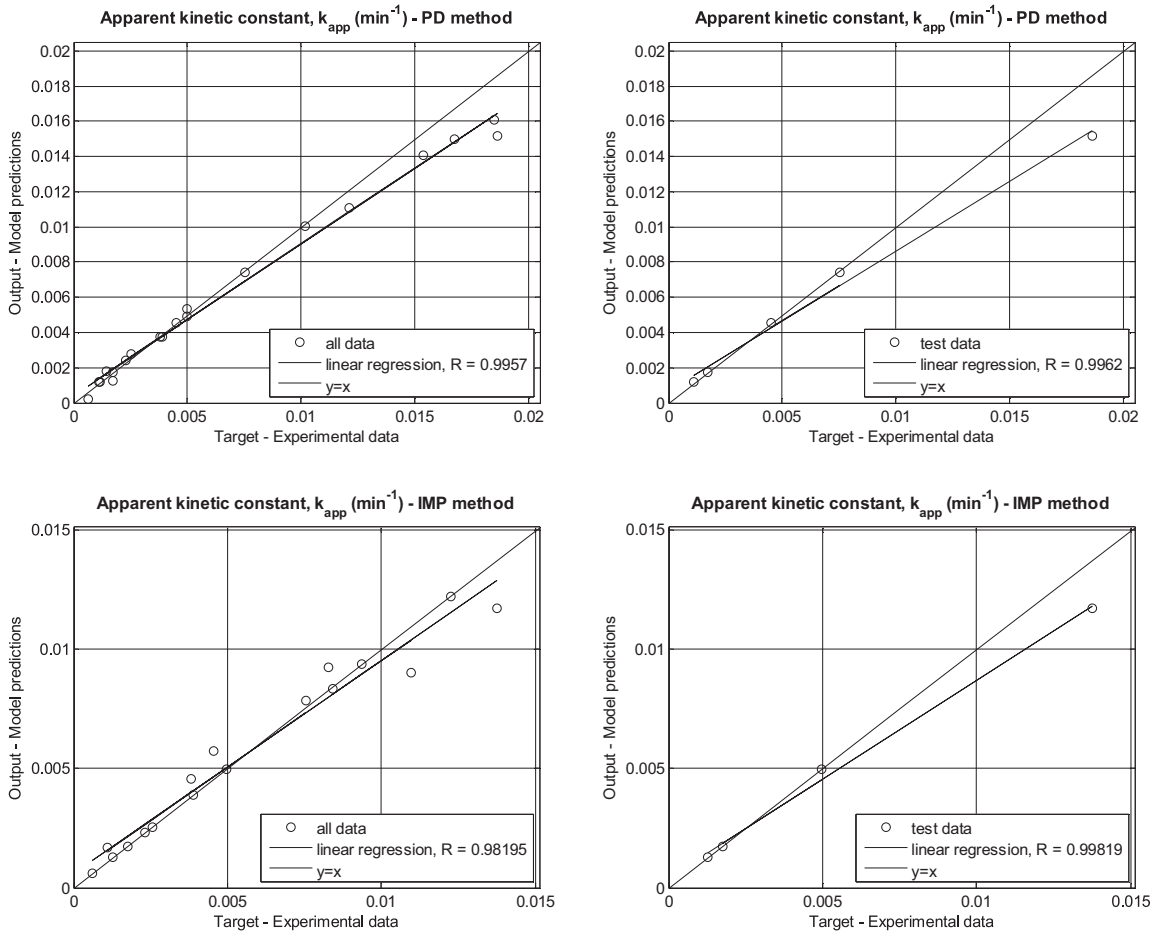

Fig. 3 – Regression plots of the experimental data (all data and test data sets) versus model predicted values for the developed neural network models ANN_2-PD (top) and ANN_2-IMP (bottom).

Table 2 – Experimental range of the Ag/ZnO photocatalyst synthesis conditions.

Input variables	Photodeposition	Impregnation
Nominal amount AgNPs (% w/w)	0.1–1	0.1–5
Initial pH	7–11	7–11
Time (h)	0.5–1	2–5

Table 3 – Experimental range of the photodegradation test conditions.

Input variables	
Initial pH	2.8–10.5
Actual amount AgNPs (%w/w)	0–1.2
Bisphenol-A (mg/L)	10–40
Wavelength (nm)	254, 302, 365 and 450

photodegradation conditions. Note that, since the evaluation of the performance of the photocatalyst was based on the rate of degradation of the contaminant, there was no need to consider the irradiation time among the factors of the photodegradation process, which was kept constant for all experiments and equal to 120 min.

The experimental ranges of all factors of the two sub-models (i.e., ANN_1 and ANN_2) are given in Tables 2 and 3, respectively. Note that for the modification experiments of ZnO, a central composite design was employed. The photocatalyst concentration used for the degradation tests was set to 1 g/L. A general schematic of the proposed modeling framework is shown in Scheme 1.

2.2.1. *Neural network structure*

A multi-layer feedforward network with Levenberg–Marquardt learning algorithm was used in this study. The experimental data corresponding to each model were randomly divided into training, validation and testing subsets (50%, 25% and 25% of data, respectively). All data were normalized in the range [−1:1] prior to their introduction into the models.

The topology of the network models, denoted as (In:Hid:Out), corresponds to the numbers of neurons in the input, hidden and output layers, respectively. Several configurations of the network were tested to determine the best number of neurons in the hidden layer(s), based on the values of the MSE of the data sets. The MSE value between the ANN model predictions and the experimental data is typically calculated by the expression:

$$MSE = \frac{\sum_{j=1}^{N}\left(y_j^{mod} - y_j^{exp}\right)^2}{N} \quad (5)$$

where the exponents 'mod' and 'exp' denote the outputs of the model (i.e., the responses) and the experiment (i.e., the targets), respectively and N is the total number of experimental data. Note that, in the present work, log-sigmoidal and lin-

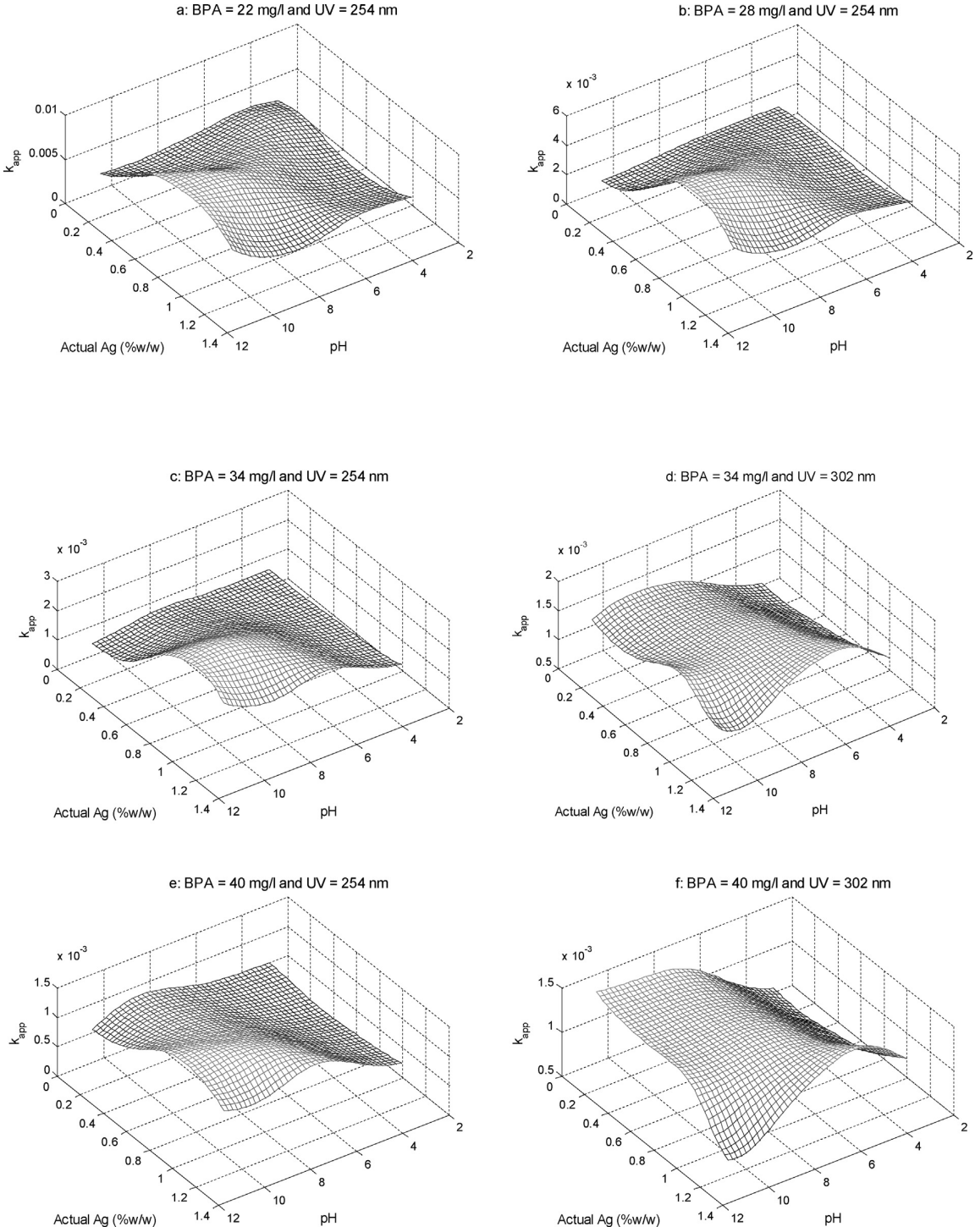

Fig. 4 – Effect of pH and actual silver content (% w/w) on the apparent degradation rate constant under different conditions of BPA content and UV wavelength, as simulated by the ANN_2-PD model.

ear transfer functions were used for hidden and output layers, respectively. The Neural Network Toolbox of the commercial software package MATLAB 8.3.0.532 (academic license) was used for the development of the models.

2.3. *Optimization study*

An ultimate purpose of process models, especially data-driven models, is their implementation in an optimization study in order to identify the combination of the different process conditions that will result to the desired properties/performance of the product/process under study. Among the plethora of different mathematical methods and techniques that have been developed for the treatment of optimization problems, evolutionary algorithms constitute a powerful approach with specific advantages and disadvantages.

In general, an evolutionary algorithm (EA) is based on the principle of the continuous improvement of a criterion (i.e., the optimization criterion) of the individuals of a population. The initial population is composed of a large set of randomly

Table 4 – Experimental conditions for the synthesis of Ag/ZnO photocatalyst and actual amount of Ag attached to the ZnO surface as measured experimentally and predicted theoretically by the ANN_1 models.

Nominal Ag %w/w	pH	Reaction time (min)	Attached Ag %w/w (experimental)	Attached Ag %w/w (ANN_1 model)	Nominal Ag %w/w	pH	Reaction time (min)	Attached Ag %w/w (experimental)	Attached Ag %w/w (ANN_1 model)
Photodeposition method					Impregnation method				
0.3573	7	30	0.320	0.327	0.1072	7	60	0.100	0.116
0.3573	7	60	0.342	0.348	0.1072	7	120	0.106	0.121
0.1073	7	30	0.082	0.084	0.1072	7	300	0.094	0.094
0.1073	7	60	0.107	0.102	1.0623	7	60	1.179	1.179
1.0623	7	30	0.991	0.920	1.0623	7	120	1.203	1.203
1.0623	7	60	1.093	1.099	1.0623	7	300	0.820	0.807
0.3573	9	30	0.358	0.356	5.095	7	60	0.521	0.522
0.3573	9	60	0.375	0.378	5.095	7	120	0.585	0.773
0.1073	9	30	0.062	0.062	5.095	7	300	0.668	0.671
0.1073	9	60	0.074	0.075	0.1072	9	60	0.099	0.093
1.0623	9	30	1.170	1.104	0.1072	9	120	0.110	0.110
1.0623	9	60	1.132	1.130	0.1072	9	300	0.096	0.100
0.3573	11	30	0.454	0.451	1.0623	9	60	0.970	1.012
0.3573	11	60	0.426	0.397	1.0623	9	120	1.192	1.188
0.1073	11	30	0.091	0.092	1.0623	9	300	1.194	1.193
0.1073	11	60	0.116	0.121	5.095	9	60	0.423	1.044
1.0623	11	30	1.183	1.182	5.095	9	120	0.494	0.336
1.0623	11	60	1.147	1.137	5.095	9	300	0.571	0.580
0.3573	7	45	0.320	0.325	0.1072	11	60	0.116	0.105
0.1073	9	45	0.074	0.071	0.1072	11	120	0.121	0.121
1.0623	9	45	1.132	1.132	0.1072	11	300	0.116	0.120
0.3573	9	45	0.362	0.365	1.0623	11	60	0.239	0.239
0.1073	7	45	0.096	0.096	1.0623	11	120	0.366	0.561
0.1073	11	45	0.103	0.102	1.0623	11	300	1.108	1.101
1.0623	7	45	1.050	1.054	5.095	11	60	0.374	0.375
1.0623	11	45	1.162	1.161	5.095	11	120	0.389	1.144
0.3573	9	45	0.371	0.365	5.095	11	300	0.498	0.503
0.3573	9	45	0.368	0.365	1.0623	9	120	1.169	1.188
0.3573	9	45	0.385	0.365	1.0623	9	120	1.223	1.188
0.3573	9	45	0.357	0.365	1.0623	9	120	1.023	1.188
0.3573	9	45	0.362	0.365	1.0623	9	120	1.179	1.188
					1.0623	9	120	1.167	1.188

selected individuals (e.g. experimental conditions), which are characterized by a measured property or model response (e.g., the degradation efficiency corresponding to each of these experiments). The population is classified from the best individual to the worst, according to its corresponding value of the criterion and depending on whether the problem is a minimization or a maximization one, and is subsequently subjected to a series of cycles of improvement of this criterion. The best individuals are combined to generate new ones that might perform better, while the worst individuals are removed from the population after each cycle and the procedure continues until the population has "evolved" to such a point where the desired convergence to an optimal has been achieved. Detailed information on the theoretical basis of EAs for mono- and multi-objective optimization, applied on physicochemical processes, can be found in the relevant literature (Camargo et al., 2011; Fonteix et al., 1995; Viennet et al., 1996; Xi et al., 2013). EAs have also been successfully implemented in the optimization study of the degradation of phenol by a combined photocatalysis/electro-Fenton system (Khataee et al., 2014).

In the present work, an optimization study, on the basis of an EA, was also carried out in order to identify the optimal catalyst synthesis and photodegradation conditions that would result to the highest photodegradation rate of BPA. In accordance to the two-stage structure of the model, the optimization was also carried out in two consecutive steps, following an *inverse direction*. In this respect, an initial optimization problem was solved on the basis of ANN_2 in order to identify the different photodegradation conditions that would result to a maximum degradation rate of BPA. Among these conditions, the pH, BPA concentration and light wavelength can be directly set to their optimized values, according to the results of this first optimization study. On the other hand, the actual silver content of the photocatalyst depends on the conditions of the photocatalyst synthesis process. Hence, a second optimization problem was subsequently solved, via the implementation of an EA on the basis of ANN_1, in order to identify the photocatalyst synthesis conditions that would result in the optimal amount of attached AgNPs on the ZnO surface , as defined by the output of the first optimization run. Thus, both important stages of the overall process (i.e., the synthesis of the photocatalyst and its subsequent use in the photodegradation experiments) were taken into account and their optimal conditions were identified in view of a maximal photodegradation rate of BPA. The overall optimization approach is schematically depicted in Scheme 2.

3. Results and discussion

The development of the two ANN sub-models was based on a total of 63 experiments for ANN_1 and 27 experiments for ANN_2, divided into the two methods of the photocatalyst synthesis (i.e., PD and IMP methods) as shown in Tables 4 and 5. On the basis of these experimental data, the identification of the optimal network topologies initially took place and sub-

Table 5 – Experimental conditions of bisphenol-A degradation and apparent kinetic rate constant k_{app} used on the ANN_2 model.

pH	Actual amount Ag (%w/w)	BPA (mg/L)	Wavelength (nm)	R[a]	Reaction order *n*	k_{app} experimental	k_{app} predicted (ANN_2 models)	
[b]Pure ZnO photocatalyst							*ANN_2-PD*	*ANN_2-IMP*
10.5	0	10	302	0.973	0.887	4.53E – 03	4.53E – 03	5.74E – 03
10.5	0	10	450	0.988	0.999	6.23E – 04	2.27E – 04	6.23E – 04
7.5	0	10	254	0.992	1.161	2.55E – 03	2.79E – 03	2.55E – 03
2.81	0	10	254	0.999	1.019	3.83E – 03	3.78E – 03	4.59E – 03
4.27	0	10	254	0.999	0.999	3.89E – 03	3.78E – 03	3.89E – 03
9.38	0	10	254	0.986	1.001	4.97E – 03	4.92E – 03	4.97E – 03
10.5	0	10	254	0.999	1.022	7.55E – 03	7.44E – 03	7.87E – 03
7.25	0	20	254	0.999	1.031	1.75E – 03	1.73E – 03	1.75E – 03
8.53	0	20	302	0.990	1.013	1.10E – 03	1.21E – 03	1.67E – 03
8.53	0	20	365	0.999	0.992	2.31E – 03	2.41E – 03	2.31E – 03
Photodeposition method							*ANN_2-PD*	
10.5	1.093	10	254	0.999	1.018	1.02E – 02	1.01E – 02	
10.5	1.093	10	302	0.999	1.006	1.86E – 02	1.52E – 02	
10.5	1.093	10	365	0.990	1.002	1.54E – 02	1.41E – 02	
10.5	1.093	20	254	0.999	1.022	4.97E – 03	5.33E – 03	
7.51	1.093	40	254	0.982	0.970	1.73E – 03	1.24E – 03	
10.5	1.147	10	254	0.999	1.024	1.21E – 02	1.11E – 02	
10.5	1.147	10	302	0.999	1.011	1.85E – 02	1.61E – 02	
10.5	1.147	10	365	0.999	1.008	1.02E – 02	1.01E – 02	
10.5	1.147	10	450	0.999	1.046	1.86E – 02	1.52E – 02	
7.2	1.147	40	254	0.999	0.956	1.54E – 02	1.41E – 02	
Impregnation method							*ANN_2-IMP*	
10.5	1.203	10	254	0.999	1.007	8.28E – 03	9.25E – 03	
10.5	1.203	10	302	0.999	0.995	9.37E – 03	9.37E – 03	
10.5	1.203	10	365	0.999	0.993	1.10E – 02	9.02E – 03	
10.5	0.366	10	254	0.999	1.006	8.42E – 03	8.36E – 03	
10.5	0.366	10	302	0.999	0.992	1.22E – 02	1.22E – 02	
10.5	0.366	10	365	0.999	1.006	1.37E – 02	1.17E – 02	
10.5	0.366	10	450	0.999	1.009	1.28E – 03	1.28E – 03	

[a] Correlation coefficient of the linear regression of the experimental data, as explained in Section 2.1.
[b] Common experiments, used for the development of both PD and IMP ANN_2 models.

sequently the ANN models were tested and validated before their implementation into the optimization study.

3.1. *Selection of optimal network topology*

The selection of the network topology was based on a typical trial and error approach where the number of neurons of the hidden layer(s) was varied in the range 1–20 (i.e., for a single hidden layer) and 1:1–10:10 (i.e., for two hidden layers) and the accuracy of the developed model was assessed in terms of the MSE values between the model predictions and the experimental data. An example of the results obtained by this procedure is shown in Fig. 1 for the ANN_1 model and the PD method. In this Figure, the ten best (i.e., corresponding to the lowest MSE values) network configurations are shown in a MSE-increasing order. Note that the errors corresponding to all data, validation and testing data sets are shown in order to verify the consistency of the model performance vis-à-vis the different data sets. Each network topology was run 50 times (i.e., 50 different ANNs with the same topology were developed and evaluated) and the average value of MSE was used for comparison, in order to avoid random correlation effects.

The numerical data corresponding to Fig. 1, as well as the data corresponding to the other three models (i.e., ANN_1-IMP, ANN_2-PD and ANN_2-IMP) are given in Table S.1 of Supplementary material. The network topologies that were retained according to this procedure are shown in Table 6.

Table 6 – Network topology of the developed models.

	Photodeposition—PD	Impregnation—IMP
ANN_1	3:8:10:1	4:9:8:1
ANN_2	3:10:10:1	4:8:10:1

3.2. *Evaluation of the ANN models*

Neural network models are typically assessed, in terms of their accuracy in simulating the experimental data, by plotting the model response with respect to the experimental measurements. A comparison of the points of such plots with the diagonal (i.e., the linear curve corresponding to $y = x$) reveals the accuracy of the developed model. Figs. 2 and 3 depict such plots for the ANN_1 and ANN_2 models, respectively. In these plots, the all data and test data sets are shown in order to reveal the accuracy of the model with respect to all available data, including the training data for which a higher accuracy is expected, as well as with respect only to the test data, which represent a subset of the available data that has not been used during the model training process. The value of the correlation coefficient, R, of the linear regression of the data is also shown on the plots. It can be seen that the ANN_1 model exhibits higher accuracy than the ANN_2 model, which seems to under-predict the experimental values at the high-values domain of k_{app} but, in general, remains quite accurate as well. This can be partially attributed to the smaller size of available experimental data for the second model. The val-

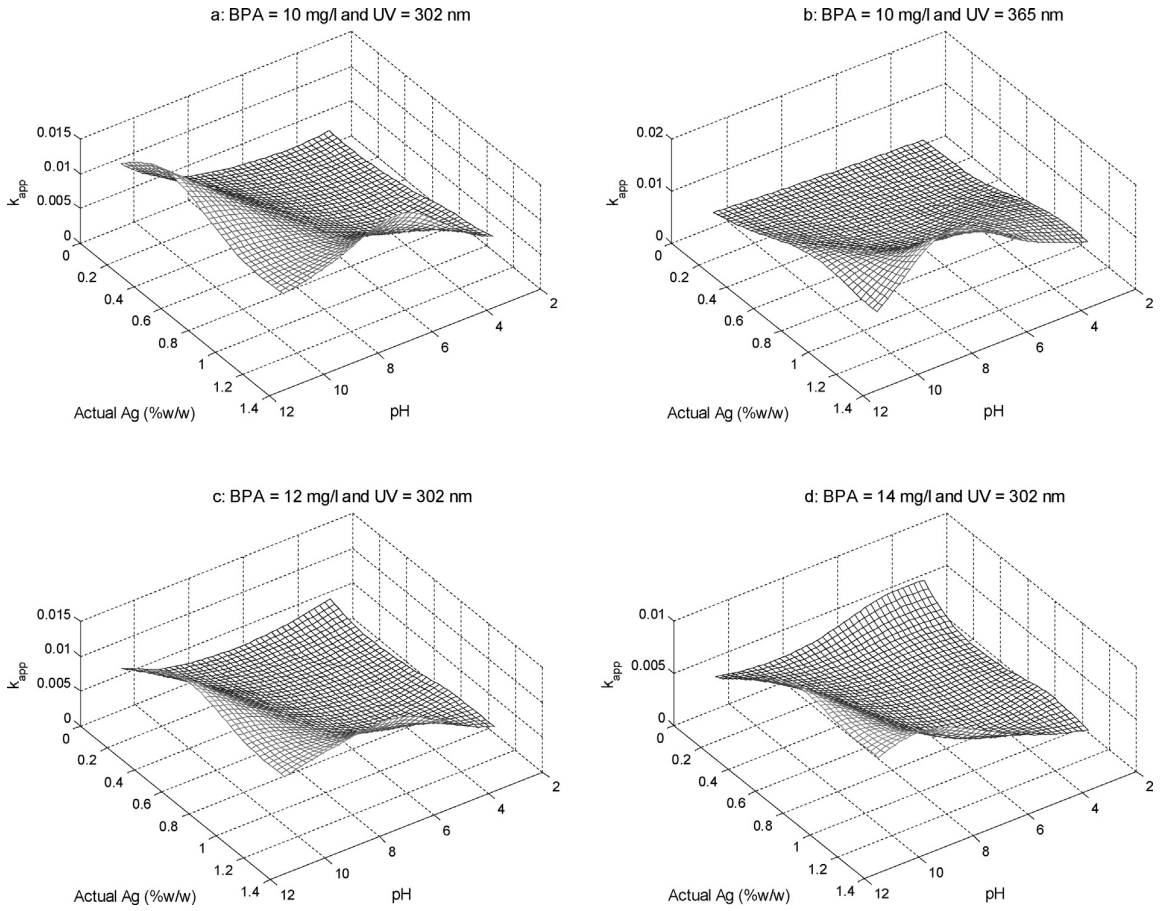

Fig. 5 – Effect of pH and actual silver content (% w/w) on the apparent degradation rate constant under different conditions of BPA content and UV wavelength, as simulated by the ANN_2-IMP model.

Table 7 – Results of the first optimization step on the maximization of k_{app}.

Optimal photodegradation conditions for the photodeposition method ($k_{app,max} = 0.0383\ min^{-1}$)			
Actual amount Ag, %w/w	pH (initial value)	BPA concentration, mg/L	Wavelength, nm
1.10	6.7	10.8	330
Optimal photodegradation conditions for the impregnation method ($k_{app,max} = 0.0167\ min^{-1}$)			
Actual amount Ag, %w/w	pH (initial value)	BPA concentration, mg/L	Wavelength, nm
0.78	10.1	10.2	358

ues of the experimental data used for the development of the models and the respective model predictions are also given in Tables 4 and 5. Note that, for the training of the models of the photodegradation experiments, ANN_2, the target values of the experimental apparent rate constant were transformed to their log values, in order to avoid a variation over several orders of magnitude. Nevertheless, in all graphical and numerical results presented in this paper, the original non-transformed values are shown for reasons of simplicity.

3.3. *Analysis of the model results*

Once the ANN models have been successfully developed and validated, they can be directly implemented, using input values that do not necessarily correspond to the experimentally tested conditions, in order to assess the effect of the different conditions of each sub-process (i.e., the catalyst synthesis and the degradation tests) to the respective response of interest (i.e., the actual amount of attached Ag on the photocatalyst and the apparent degradation rate constant, respectively). In this respect, Fig. 4a–f shows the effect of pH and actual silver content on the degradation rate of BPA, under different conditions of BPA amount and light wavelength, as produced by the ANN_2-PD model. An initial observation is that the response surfaces are highly irregular, not displaying a clear increasing or decreasing effect. It should be noted at this point that the presented curves can only serve to acquire a general idea about the different trends that the model might display with respect to the variation of certain inputs. They cannot be used to identify specific points or values with accuracy since the viewpoint angle and the graphical interpolation used for their creation may lead to errors.

Concerning the effect of pH, it can be seen that, as pH increases the values of k_{app} initially increase, reaching a maximum within the range of pH values 6–9, and then decrease. This effect is particularly obvious in Fig. 4d–f. The pH is an

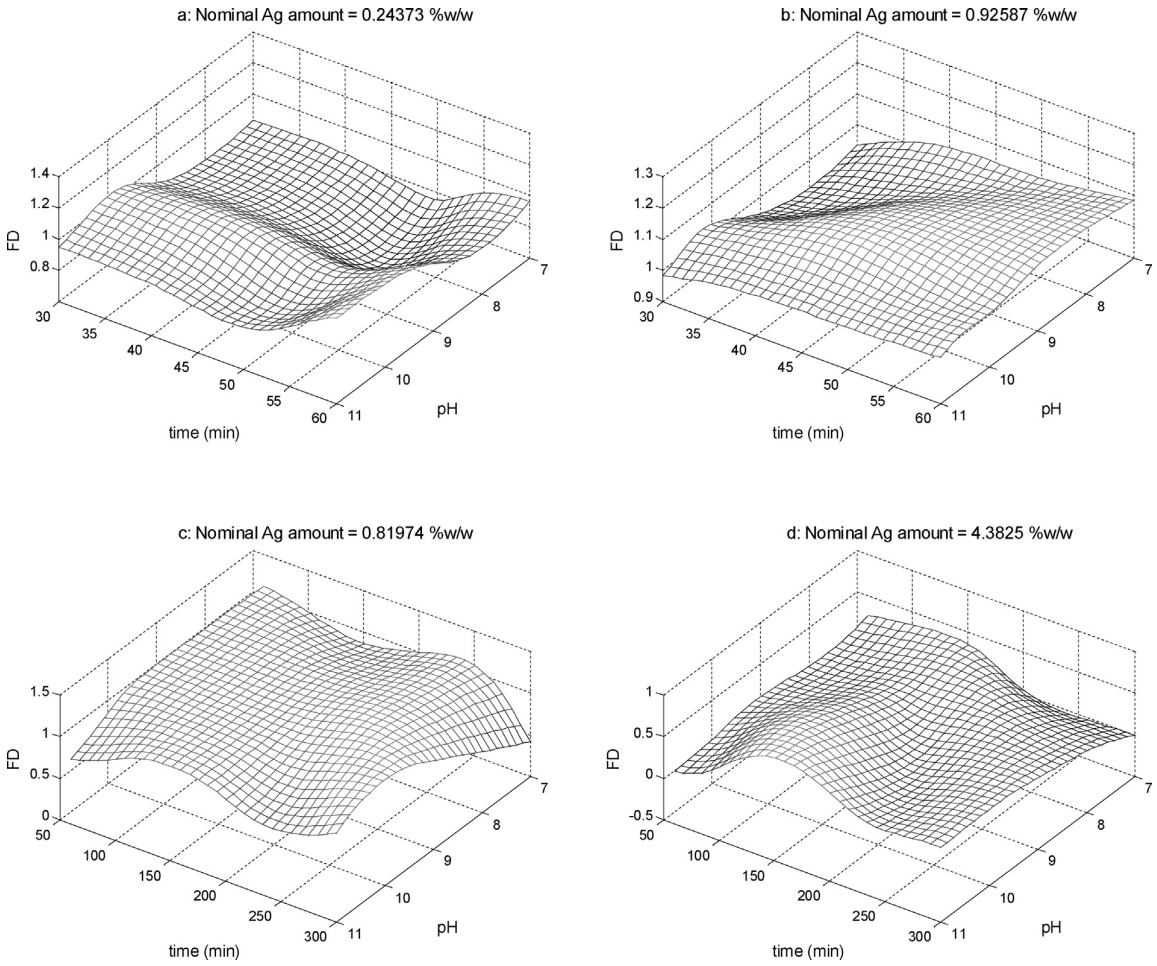

Fig. 6 – Effect of pH and reaction time on the functionalization degree (i.e., the ratio of actual to nominal amount of Ag) under different values of nominal Ag amount as simulated by the ANN_1-PD (a, b) and ANN_1-IMP (d, c) models.

important factor in photocatalysis since it affects the surface charges of both the photocatalyst and the contaminant as follows. In the vicinity above neutral $pH_{PZC} = 8.3$ (i.e., value of neutral surface charges for ZnO), hydroxyl-compounds of zinc such as $ZnOH^+$, $Zn(OH)_2$, and $Zn(OH)_3^-$ are formed in the solution and they interact with the undissociated BPA ($HO–C_{15}H_{14}–OH$) toward its oxidation. Below this value, an increase in the hydroxyl ion (^-OH) concentration and, subsequently, to the hydroxyl radical ($^\bullet OH$) concentration leads to the oxidation of BPA. Comparable results have been reported on the degradation efficiency of BPA by pure ZnO by Rahman et al. (2005), who reported 80% degradation efficiency of 100 mg/L of BPA in the pH range of 2–8.5, and a significant decrease to 60% at pH 11. Also, Clament Sagaya Selvam et al. (2013) reported the complete degradation of 200 mg/L of BPA at pH 8 and a subsequent decrease of the degradation efficiency at pH values above 9.

On the other hand, the effects of BPA concentration and UV wavelength are not so evident. Nevertheless, the initial contaminant concentration seems to display an inversely proportional effect on the values of k_{app}, since they seem to be decreasing at higher BPA concentrations. This effect can be partially explained by an absorbance of the UV light (at 255 and 277 nm) by BPA molecules. This way, the activation of the photocatalyst surface is reduced thus producing a *screening effect* of the BPA molecules towards the UV light penetration.

A similar effect for all factors can be observed for the impregnation model, ANN_2-IMP, as well. Four representative surfaces are shown in Fig. 5a–d, under different conditions of BPA content and light wavelength. As can be seen, the value of k_{app} displays once more a maximum around the middle of the pH and BPA concentration domains and decreases with increasing BPA concentration.

Concerning the first model, ANN_1, a similar analysis can be made on the effects of the catalyst synthesis conditions on the overall functionalization degree, FD, defined as the ratio of the actual amount of silver on the catalyst particles over the nominal amount of silver used during the catalyst synthesis. In Fig. 6a and b, two surface plots, similar to the ones previously depicted for ANN_2, are shown corresponding to the photodeposition method and to two different values of nominal amount of silver. The corresponding plots for the impregnation method are depicted in Fig. 6c and d. As can be seen, there is no significant variation of FD with respect to pH and time when the photodeposition method is implemented. On the other hand, the reaction time seems to have an overall positive effect on the FD values and to display a maximum around 150 min, when the impregnation method is used.

The effect of pH seems to vary with the time of reaction and the nominal AG amount, especially for the photodeposition method. At the same time, an excess nominal amount of silver does not seem to display a positive effect on the functionalization degree when the impregnation method is implemented,

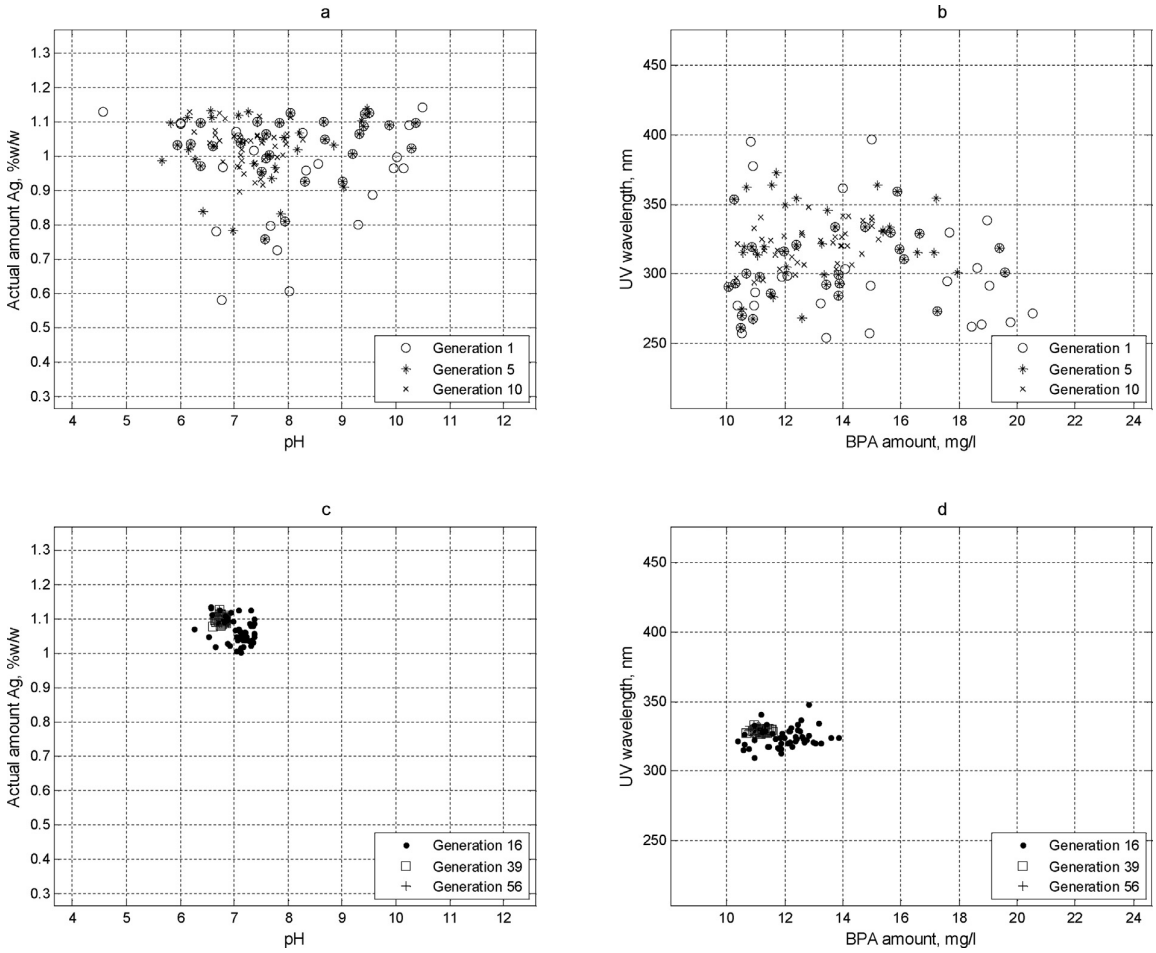

Fig. 7 – Presentation of the 50 optimal conditions in terms of the actual amount of Ag and pH (a, c) and the UV wavelength and the BPA amount (b, d), as predicted by the EA optimization on the basis of the ANN_2-PD model after 1, 5 and 10 generations (a, b) as well as after 16, 39 and 56 generations (c, d).

Table 8 – Results of the 2nd optimization step on the synthesis of a photocatalyst with a desired content of AgNPs.

Optimal photocatalyst synthesis conditions for the photodeposition method (actual Ag %w/w = 1.10)		
Nominal amount Ag, %w/w	pH	Time, min
1.00	9.5	48
Optimal photocatalyst synthesis conditions for the impregnation method (actual Ag %w/w = 0.78)		
Nominal amount Ag, %w/w	pH	Time, min
0.69	8.5	214

which is particularly obvious in Fig. 6d. It should be noted at this point that the experimental values of FD that are higher than 1 are due to experimental sampling and titration errors, as explained in Jasso-Salcedo et al. (2014). As a consequence it is normal that the developed neural network model, which was trained on the basis of these experimental values, provides responses that result in values of FD higher than 1.

3.4. *Optimization step 1—apparent kinetic rate constant, k_{app}*

Given the nature of the photodegradation process and the definition of the output of the process on the basis of the apparent kinetic rate constant of a first-order degradation reaction, it becomes evident that the desired value of this constant is the maximal possible value it could attain, as this will lead to a faster degradation of a maximum amount of BPA. Hence, the first step of the optimization study, on the basis of ANN_2, was the solution of a maximization problem in terms of the conditions of the photodegradation process, namely the actual amount of attached AgNPs, the pH, the BPA concentration and the light wavelength. The deployment of an EA for the solution of this problem for both methods of photocatalyst synthesis resulted in the sets of optimal conditions shown in Table 7. Note that, for the EA algorithm, the following parameters were used: the size of the population was set to 1000 individuals, the survival rate was set to 70% and the mutation rate to 10%. The program was entirely written and run on MATLAB (version 8.3.0.532; academic license) while the convergence of the algorithm was tested in terms of a tolerance in the relative difference between the best and worst criterion values of each generation, set in the order of 1%.The CPU time required for every optimization run was in the order of 30 s on a 2 × 2.4 GHz Intel® Xeon® Workstation.

In order to follow the evolution of the optimization and to verify its convergence around one (or more) optimal(s), one can plot the positions of a number of 'best' (i.e., top ranked) individuals, corresponding to an equal number of optimal conditions, along different generations of the opti-

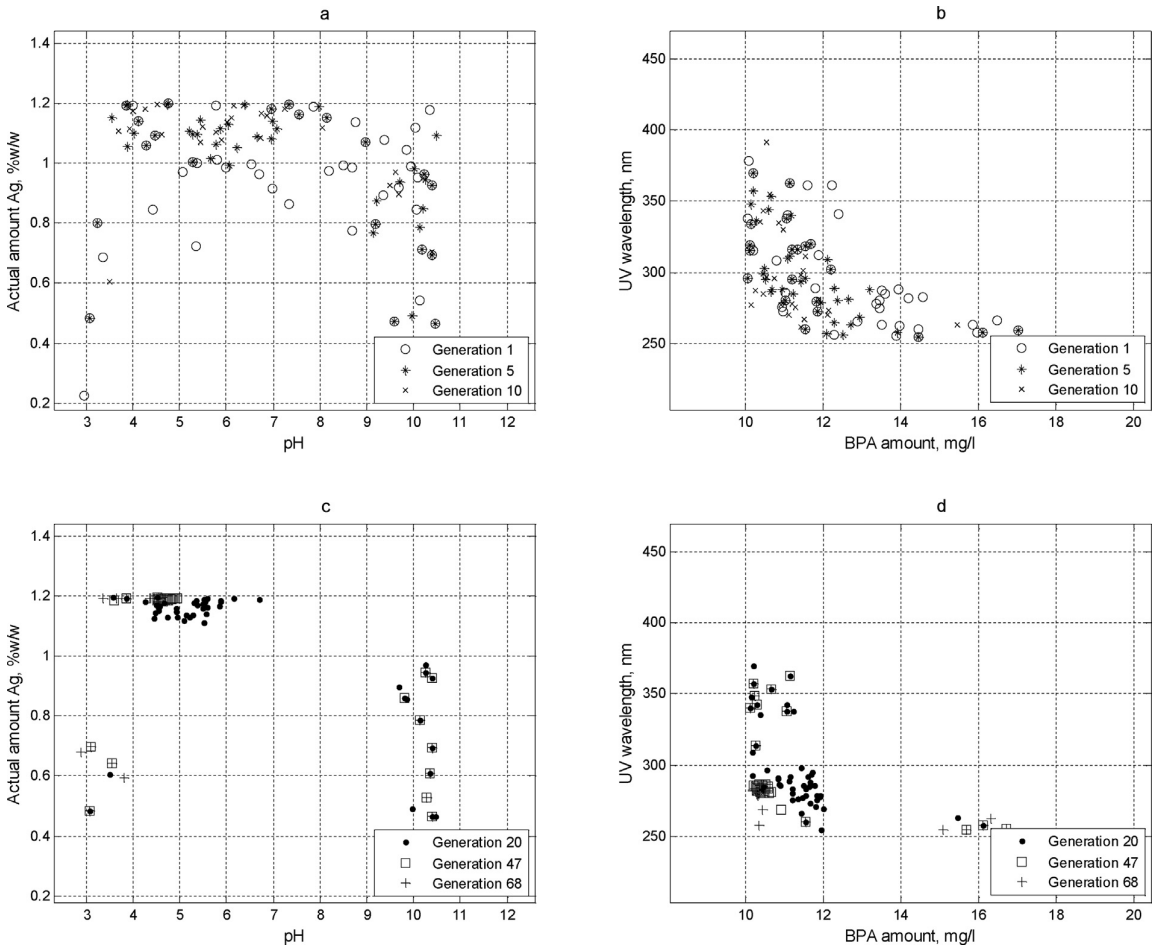

Fig. 8 – Presentation of the 50 optimal conditions in terms of the actual amount of Ag and pH (a, c) and the UV wavelength and the BPA amount (b, d), as predicted by the EA optimization on the basis of the ANN_2-IMP model after 1, 5 and 10 generations (a, b) as well as after 20, 47 and 68 generations (c, d).

mization procedure. In Fig. 7a–d, a set of 50 optimal conditions is depicted, as calculated by the EA optimization of the ANN_2-PD model.

Since there are four different factors for this model, two plots are produced for each generation, one corresponding to the optimal values of the actual amount of silver and pH and another corresponding to the optimal values of the UV wavelength and the initial BPA amount. The same figures have been plotted for three different generations at the early stages of the optimization (i.e., generations 1, 2 and 10, cf. Fig. 7a and b) as well as for three generations at the middle and final stages of the optimization (i.e., generations 16, 39 and 56, cf. Fig. 7c and d). This illustration reveals the convergence of the optimization around a unique set of optimal conditions (cf. Table 7). In this specific case, the convergence was achieved after 56 iterations, according to the convergence criterion defined earlier in this Section. Note that the predicted optimal value of k_{app} is significantly increased with respect to the experimentally measured values.

Fig. 8a–d presents the corresponding plots of the same optimization problem but for the impregnation method (i.e., on the basis of ANN_2-IMP). In this case, several local maxima seem to exist so the optimization does not converge around one single set of optimal conditions. The conditions reported in Table 7 are the ones that lead to the maximum attaint value of the apparent rate constant and correspond to the set of points located on the right in Fig. 8c and on the top left in Fig. 8d. In any case, this method seems to lead to significantly lower optimal values of the rate constant, in comparison to the photodeposition method.

3.5. *Optimization step 2—actual amount of silver in the ZnO photocatalyst*

On the basis of the optimal amount of AgNPs defined by the previous optimization step, a second optimization run was carried out in order to define the conditions that would result in the synthesis of a photocatalyst with this optimal amount of silver nanoparticles. So, in this case, the goal was to minimize the objective function defined by the absolute difference between the model response (i.e., the actual Ag amount) and the desired Ag amount, as this was defined in the previous optimization step. This second step of the optimization study was based on ANN_1 and the results of the EA that was deployed for the solution of this problem are shown in Table 8. In both cases, the error between the desired and attained value was inferior to 0.01%, significantly lower than the associated experimental error of the measurements.

The respective 2D plots of the evolution of the 50 optimal conditions in terms of the model factors are presented in Figs. 9 a–d and 10 a–d, for the photodeposition and the impregnation methods respectively. Note that, as the number of factors

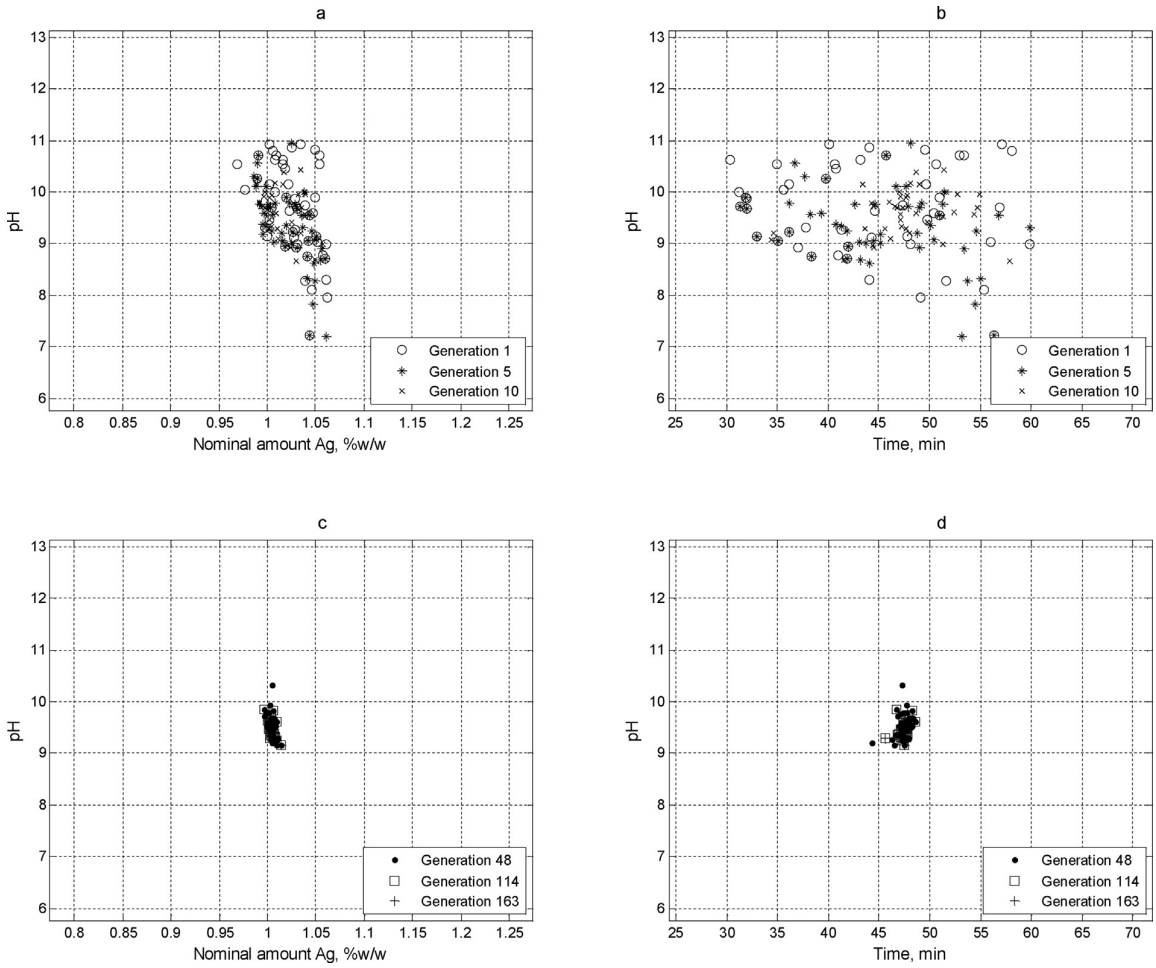

Fig. 9 – Presentation of the 50 optimal conditions in terms of the nominal amount of Ag and pH (a, c) and the reaction time and pH (b, d), as predicted by the EA optimization on the basis of the ANN_1-PD model after 1, 5 and 10 generations (a, b) as well as after 48, 114 and 163 generations (c, d).

is limited to three in this case, both couples that are used in the plots contain pH as one of the factors.

The results of these optimization runs are quite similar to the first optimization runs as, once again, the impregnation method seems to provide several alternatives as local minima, especially in terms of the value of the pH, as becomes evident in Fig. 10a and c. The photodeposition method, on the other hand, has a clear minimum of the objective function that is identified by the EA algorithm already somewhere between the 10th and 48th iteration, despite the fact that the algorithm requires more than 160 iterations to meet the convergence criterion. Finally, a paradox is observed in both optimization results since the optimal nominal amount of Ag is lower than the desired actual amount of Ag. Once again, this is due to the fact that the models have been trained with experimental data containing such discrepancies, which are caused by the experimental error associated with the experimental protocol and the analytical method (Jasso-Salcedo et al., 2014). This should not be interpreted as an error associated with the modeling framework or the optimization approach.

4. Conclusions

In the present work, a modeling framework on the basis of artificial neural networks was presented for the simulation of the effects of two important stages of a photocatalytic process, namely the catalyst synthesis and the photodegradation experiments, on the final photodegradation performance of the synthesized photocatalyst. In this respect, a two-stage ANN model was developed, connected by means of introducing the response of the first model as a factor to the second model. The developed models were subsequently introduced in an optimization study, carried out with the aid of an evolutionary algorithm and comprised also of two steps. Through this integrated approach, it has been possible to study simultaneously the effects of a series of important conditions associated with two totally distinct stages of the process and to connect the initial photocatalyst synthesis conditions with its final photodegradation performance.

By means of the developed models, the effects of pH, nominal amount of silver nanoparticles introduced in the suspension and reaction time were assessed in terms of their effects on the actual amount of silver nanoparticles that are finally retained on the ZnO surface. At the same time, this amount of attached silver along with the pH, the light wavelength and the initial contaminant amount present in the photodegradation experiments were studied in terms of their effect on the photodegradation performance of the synthesized photocatalyst. This performance was associated with an apparent rate constant, thus eliminating the time from the factors of the photodegradation tests.

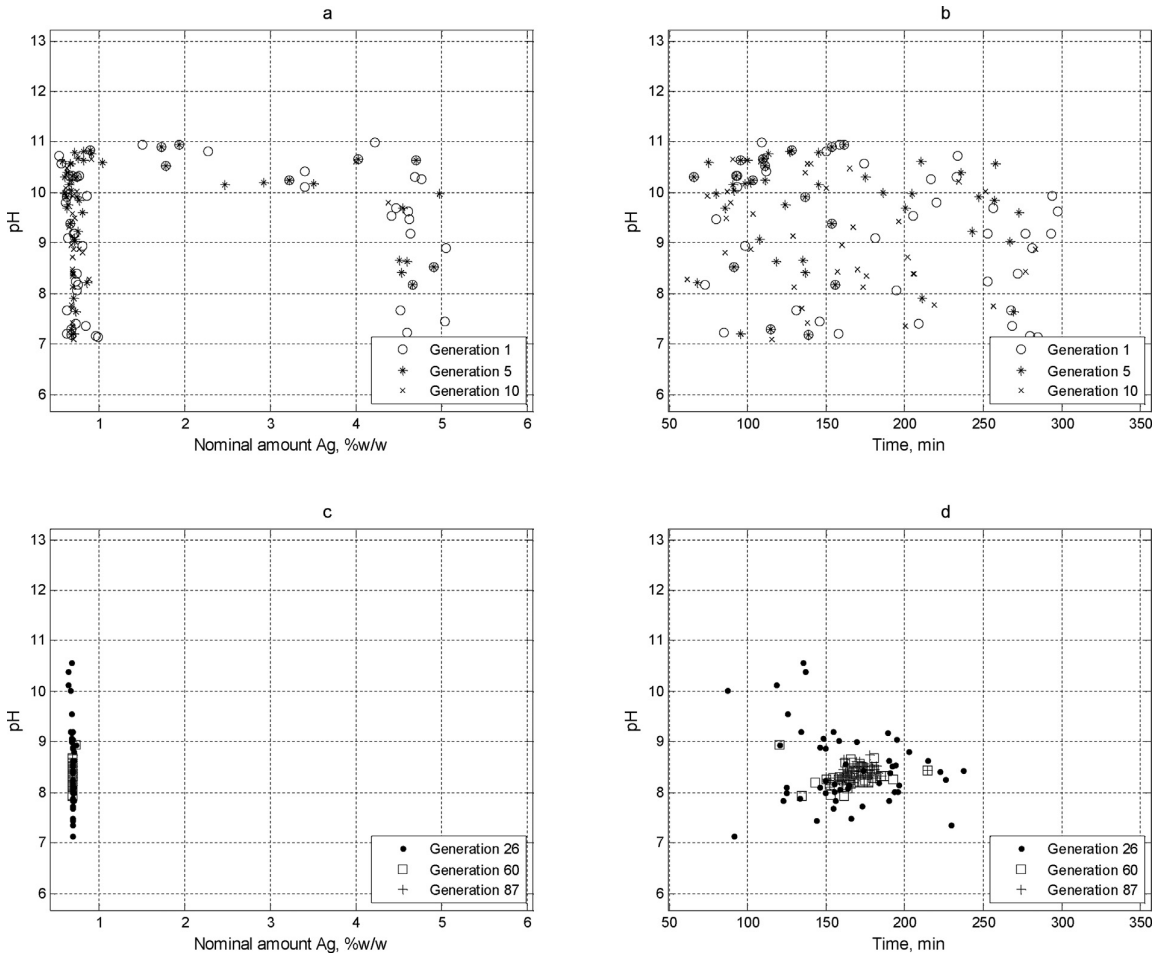

Fig. 10 – Presentation of the 50 optimal conditions in terms of the nominal amount of Ag and pH (a, c) and the reaction time and pH (b, d), as predicted by the EA optimization on the basis of the ANN_1-IMP model after 1, 5 and 10 generations (a, b) as well as after 26, 60 and 87 generations (c, d).

The decoupling of these two processes that was proposed in this study allowed a better understanding of the nature of the indisputable indirect bond that exists between them. In this respect, it has been shown that an intermediate quality criterion of the photocatalyst, namely the actual amount of silver attached to the ZnO surface that, in turn, can only be controlled by the photocatalyst synthesis conditions, displays a direct effect on its photodegradation performance. Finally, by investigating two different methods of the photocatalyst synthesis, namely a photodeposition and an impregnation method, the study has also demonstrated that it can display an important effect on the final photodegradation efficiency of the photocatalyst.

Acknowledgements

This work was supported by CONACYT and the French Ministry of Education and Research (scholarship PCP/RUI-004-12 granted to AB Jasso-Salcedo).

Appendix A. Supplementary data

Supplementary data associated with this article can be found, in the online version, at https://doi.org/10.1016/j.cherd.2017.10.012.

References

Amani-Ghadim, A.R., Seyed Dorraji, M.S., 2015. Modeling of photocatalyatic process on synthesized ZnO nanoparticles: kinetic model development and artificial neural networks. Appl. Catal. B: Environ. 163, 539–546.

Antonopoulou, M., Konstantinou, I., 2013. Optimization and modeling of the photocatalytic degradation of the insect repellent DEET in aqueous TiO_2 suspensions. CLEAN: Soil Air Water 41, 593–600.

Antonopoulou, M., Papadopoulos, V., Konstantinou, I., 2012. Photocatalytic oxidation of treated municipal wastewaters for the removal of phenolic compounds: optimization and modeling using response surface methodology (RSM) and artificial neural networks (ANNs). J. Chem. Technol. Biotechnol. 87, 1385–1395.

Asl, S.K., Sadrnezhaad, S.K., Rad, M.K., Üner, D., 2012. Comparative photodecolorization of red dye by anatase, rutile (TiO_2): and wurtzite (ZnO) using response surface methodology. Turk. J. Chem. 36, 121–135.

Babaei, A., Mesdaghiniai, A., Haghighi, N.J., Nabizadeh, R., Mahvi, A., 2011. Modeling of nonylphenol degradation by photo-nanocatalytic process via multivariate approach. J. Hazard. Mater. 185, 1273–1279.

Behnajady, M.A., Eskandarloo, H., 2015. Preparation of TiO_2 nanoparticles by the sol–gel method under different pH conditions and modeling of photocatalytic activity by artificial neural network. Res. Chem. Intermed. 41, 2001–2017.

Bohdziewicz, J., Kudlek, E., Dudziak, M., 2016. Influence of the catalyst type (TiO_2 and ZnO) on the photocatalytic oxidation

of pharmaceuticals in the aquatic environment. Desalin. Water Treat. 57, 1552–1563.
Camargo, M., Morel, L., Fonteix, C., Hoppe, S., Hu, G.H., Renaud, J., 2011. Development of new concepts for the control of polymerization processes: multiobjective optimization and decision engineering. II. Application of a Choquet integral to an emulsion copolymerization process. J. Appl. Polym. Sci. 120, 3421–3434.
Cheng, B., Titterington, D.M., 1994. Neural networks: a review from a statistical perspective. Stat. Sci. 9, 49–54.
Clament Sagaya Selvam, N., Judith Vijaya, J., John Kennedy, L., 2013. Comparative studies on influence of morphology and La doping on structural, optical, and photocatalytic properties of zinc oxide nanostructures. J. Colloid Interface Sci. 407, 215–224.
Das, L., Maity, U., Kumar Basu, J., 2014. The photocatalytic degradation of carbamazepine and prediction by artificial neural networks. Process Saf. Environ. Prot. 92, 888–895.
Delnavaz, M., 2015. Application of artificial neural networks for prediction of photocatalytic reactor. Water Environ. Res. 87, 113–122.
Dutta, S., Parsons, S.A., Bhattacharjee, C., Bandhyopadhyay, S., Datta, S., 2010. Development of an artificial neural network model for adsorption and photocatalysis of reactive dye on TiO_2 surface. Expert Syst. Appl. 37, 8634–8638.
Esplugas, S., Bila, D.M., Krause, L.G.T., Dezotti, M., 2007. Ozonation and advanced oxidation technologies to remove endocrine disrupting chemicals (EDCs) and pharmaceuticals and personal care products (PPCPs) in water effluents. J. Hazard. Mater. 149, 631–642.
Fernández, R.L., McDonald, J.A., Khan, S.J., Le-Clech, P., 2014. Removal of pharmaceuticals and endocrine disrupting chemicals by a submerged membrane photocatalysis reactor (MPR). Sep. Purif. Technol. 127, 131–139.
Ferreira, S.L.C., Bruns, R.E., Ferreira, H.S., Matos, G.D., David, J.M., Brandão, G.C., da Silva, E.G.P., Portugal, L.A., dos Reis, P.S., Souza, A.S., dos Santos, W.N.L., 2007. Box–Behnken design: an alternative for the optimization of analytical methods. Anal. Chim. Acta 597, 179–186.
Flint, S., Markle, T., Thompson, S., Wallace, E., 2012. Bisphenol A exposure, effects, and policy: a wildlife perspective. J. Environ. Manage. 104, 19–34.
Fonteix, C., Bicking, F., Perrin, E., Marc, I., 1995. Haploid and diploid algorithms, a new approach for global optimization: compared performances. Int. J. Syst. Sci. 26, 1919–1933.
Frontistis, Z., Daskalaki, V.M., Hapeshi, E., Drosou, C., Fatta-Kassinos, D., Xekoukoulotakis, N.P., Mantzavinos, D., 2012. Photocatalytic (UV-A/TiO_2) degradation of 17α-ethynylestradiol in environmental matrices: experimental studies and artificial neural network modeling. J. Photochem. Photobiol. A: Chem. 240, 33–41.
Georgakis, C., 2013. Design of dynamic experiments: a data-driven methodology for the optimization of time-varying processes. Ind. Eng. Chem. Res. 52, 12369–12382.
Georgekutty, R., Seery, M.K., Pillai, S.C., 2008. A highly efficient Ag–ZnO photocatalyst: synthesis, properties, and mechanism. J. Phys. Chem. C 112, 13563–13570.
Ghanbary, F., Modirshahla, N., Khosravi, M., Behnajady, M.A., 2012. Synthesis of TiO_2 nanoparticles in different thermal conditions and modeling its photocatalytic activity with artificial neural network. J. Environ. Sci. 24, 750–756.
Haykin, S., 1994. Neural Networks: A Comprehensive Foundation, vol. 2. Macmillan.
Heiligers, B., 1994. E-optimal designs in weighted polynomial regression. Ann. Stat., 917–929.
Jasso-Salcedo, A.B., Meimaroglou, D., Hoppe, S., Pla, F., Escobar-Barrios, V.A., 2016. Surface modification and immobilization in poly(acrylic acid) of Ag/ZnO for photocatalytic degradation of endocrine-disrupting compounds. J. Appl. Polym. Sci. 133.
Jasso-Salcedo, A.B., Palestino, G., Escobar-Barrios, V.A., 2014. Effect of Ag, pH, and time on the preparation of Ag-functionalized zinc oxide nanoagglomerates as photocatalysts. J. Catal. 318, 170–178.
Khataee, A.R., Fathinia, M., Zarei, M., Izadkhah, B., Joo, S.W., 2014. Modeling and optimization of photocatalytic/photoassisted-electro-Fenton like degradation of phenol using a neural network coupled with genetic algorithm. J. Ind. Eng. Chem. 20, 1852–1860.
Khataee, A.R., Kasiri, M.B., 2010. Artificial neural networks modeling of contaminated water treatment processes by homogeneous and heterogeneous nanocatalysis. J. Mol. Catal. A: Chem. 331, 86–100.
Kiattisaksiri, P., Khamdahsag, P., Khemthong, P., Pimpha, N., Grisdanurak, N., 2015. Photocatalytic degradation of 2,4-dichlorophenol over Fe–ZnO catalyst under visible light. Korean J. Chem. Eng. 32, 1578–1585.
Kiransan, M., Khataee, A., Karaca, S., Sheydaei, M., 2015. Artificial neural network modeling of photocatalytic removal of a disperse dye using synthesized of ZnO nanoparticles on montmorillonite. Spectrochim. Acta A: Mol. Biomol. Spectrosctrosc. 140, 465–473.
Kıransan, M., Khataee, A., Karaca, S., Sheydaei, M., 2015. Synthesis of zinc oxide nanoparticles on montmorillonite for photocatalytic degradation of basic Yellow 28: effect of parameters and neural network modeling. Curr. Nanosci. 11, 343–353.
Klečka, G.M., Staples, C.A., Clark, K.E., van der Hoeven, N., Thomas, D.E., Hentges, S.G., 2009. Exposure analysis of bisphenol A in surface water systems in North America and Europe. Environ. Sci. Technol. 43, 6145–6150.
Lee, K.M., Hamid, S.B.A., 2015. Simple response surface methodology: investigation on advance photocatalytic oxidation of 4-chlorophenoxyacetic acid using UV-active ZnO photocatalyst. Materials 8, 339–354.
Meireles, M.R., Almeida, P.E., Simoes, M.G., 2003. A comprehensive review for industrial applicability of artificial neural networks. IEEE Trans. Ind. Electron. 50, 585–601.
Merabet, S., Assadi, A.A., Bouzaza, A., Wolbert, D., 2016. Photocatalytic degradation of indole-4-methylphenol mixture in an aqueous solution: optimization and statistical analysis. Desalin. Water Treat. 57, 17039–17050.
Rahman, M.A., Kaneco, S., Suzuki, T., Katsumata, H., Ohta, K., 2005. Optimized conditions for the solar photocatalytic degradation of bisphenol a in water using zinc oxide. Annal. Chim. 95, 715–719.
Rosenfeldt, E.J., Linden, K.G., 2004. Degradation of endocrine disrupting chemicals bisphenol A, ethinyl estradiol, and estradiol during UV photolysis and advanced oxidation processes. Environ. Sci. Technol. 38, 5476–5483.
Sabonian, M., Behnajady, M.A., 2014. Artificial neural network modeling of Cr(VI) photocatalytic reduction with TiO_2-P25 nanoparticles using the results obtained from response surface methodology optimization. Desalin. Water Treat., 1–11.
Sargolzaei, J., Hedayati Moghaddam, A., Nouri, A., Shayegan, J., 2015. Modeling the removal of phenol dyes using a photocatalytic reactor with SnO2/Fe3O4 nanoparticles by intelligent system. J. Disper. Sci. Technol. 36 (4), 540–548.
Sin, J.-C., Lam, S.-M., Mohamed, A.R., Lee, K.-T., 2012. Degrading endocrine disrupting chemicals from wastewater by TiO_2 photocatalysis: a review. Int. J. Photoenergy 2012, Article ID 185159, 23 pages.
Sivanandam, S., Sumathi, S., Deepa, S., 2006. Introduction to Neural Networks Using MATLAB 6.0: Tata. McGraw-Hill Education.
Solomatine, D., See, L.M., Abrahart, R.J., 2009. Data-driven modelling: concepts, approaches and experiences. In: Practical Hydroinformatics. Springer, Berlin, Heidelberg, pp. 17–30.
Sornalingam, K., McDonagh, A., Zhou, J.L., 2016. Photodegradation of estrogenic endocrine disrupting steroidal hormones in aqueous systems: progress and future challenges. Sci. Total Environ. 550, 209–224.

Tanasa, D.E., Piuleac, C.G., Curteanu, S., Popovici, E., 2013. Photodegradation process of Eosin Y using ZnO/SnO_2 nanocomposites as photocatalysts: experimental study and neural network modeling. J. Mater. Sci. 48, 8029–8040.

Tijani, J.O., Fatoba, O.O., Petrik, L.F., 2013. A review of pharmaceuticals and endocrine-disrupting compounds: sources, effects, removal, and detections. Water Air Soil Pollut. 224, 1–29.

Vaez, M., Omidkhah, M., Alijani, S., Zarringhalam Moghaddam, A., Sadrameli, M., Gholipour Zanjani, N., 2015. Evaluation of photocatalytic activity of immobilized titania nanoparticles by support vector machine and artificial neural network. Can. J. Chem. Eng. 93, 1009–1016.

Viennet, R., Fonteix, C., Marc, I., 1996. New multicriteria optimization method based on the use of a diploid genetic algorithm: example of an industrial problem. In: European Conference, Springer, pp. 120–127.

Wang, J., Fan, X.M., Tian, K., Zhou, Z.W., Wang, Y., 2011. Largely improved photocatalytic properties of Ag/tetrapod-like ZnO nanocompounds prepared with different PEG contents. Appl. Surf. Sci. 257, 7763–7770.

Wang, R., Ren, D., Xia, S., Zhang, Y., Zhao, J., 2009. Photocatalytic degradation of bisphenol A (BPA) using immobilized TiO_2 and UV illumination in a horizontal circulating bed photocatalytic reactor (HCBPR). J. Hazard. Mater. 169, 926–932.

Witek-Krowiak, A., Chojnacka, K., Podstawczyk, D., Dawiec, A., Pokomeda, K., 2014. Application of response surface methodology and artificial neural network methods in modelling and optimization of biosorption process. Bioresour. Technol. 160, 150–160.

Xi, J., Xue, Y., Xu, Y., Shen, Y., 2013. Artificial neural network modeling and optimization of ultrahigh pressure extraction of green tea polyphenols. Food Chem. 141, 320–326.

Xie, W., Li, Y., Sun, W., Huang, J., Xie, H., Zhao, X., 2010. Surface modification of ZnO with Ag improves its photocatalytic efficiency and photostability. J. Photochem. Photobiol. A: Chem. 216, 149–155.

4. Polymer Recycling

The greatest threat to our planet is the belief that someone else will save it...

R. Swan

4.1 The role of modeling towards the development of sustainable polymer processes

The two previous chapters were primarily focused on the methodological approach of the different applications, in terms of the implemented modeling technique (or combination of techniques). In this sense, the principal advantages and drawbacks of the different modeling approaches were illustrated through a series of studies. In this section, the focus is placed on the nature and the characteristics of the applications. In fact, a single application is presented here, which is part of a long-lasting study that is still under development, concerning the polymerization of styrene in the presence of used tire particles [1].

The main objective of this study is to respond to a major environmental problem of modern society, related to the over-accumulation of used tires of light and/or heavy vehicles, through the synthesis of materials with interesting mechanical properties. The idea is based on creating an analog of the commercial thermoplastic high-impact polystyrene (HIPS), by substituting the dispersed rubber phase within the matrix of polystyrene (PS) with particles of used tire rubber (also known as Ground Tire Rubber, GTR). To this end, GTR, which is commercially obtained directly in the form of micrometric powder, free of the fabric and metallic parts of automotive tires, needs to be dispersed in the matrix of PS during the synthesis of this latter. This can be achieved via *in situ* polymerization of styrene in the presence of these particles, in view of promoting the direct

[1] At the time of the final publication of this HDR report, the presented manuscript was still under review by the journal "Chemical Engineering Science"

grafting of PS on GTR (i.e., the creation of covalent bonds between the growing PS chains and the particles of GTR).

The main factors controlling the final properties of the produced polymer are the PSD of the GTR particles and the relative ratio of grafting reactions over the respective homopolymerization reactions of styrene that inevitably take place in the reacting mixture, around the particles and in parallel to the grafting reactions. The level to which the PSD can be controlled is somewhat limited, due to relevant technological constraints of the available grinding techniques. As a result, the average particle size of GTR is in the order of several hundreds micrometers.

Regarding the kinetic developments, the situation becomes even more complex since, in contrast to the pure polybutadiene rubber that is used in the production of HIPS, the particles of GTR are composed of a mixture of different elastomers (i.e., commonly between three to five elastomers at different proportions) and additives that are typically included in the composition of the tires to infer to them better traction, higher resistance and increased longevity. In addition, this composition will vary depending on the source and the type of the tires.

As expected, the different elastomers of the GTR particles will not display the same affinity towards the radicals that are present during the polymerization of styrene, which may affect the course of the grafting reactions. In addition, some of the additives, as is the case of carbon black, a typical reinforcing filler that is commonly introduced in rubber formulations, possess chemical groups susceptible to react with other species that participate in the polymerization (i.e., styrene or the initiator agent), thus inducing an accelerating, retarding or even inhibiting effect on the course of the polymerization.

This system has made the subject of several studies in LRGP, that have been primarily carried out within the framework of two consecutive PhD dissertations [36, 37]. It is worth noting at this point, that the above described grafting polymerization system is only the first stage of a series of subsequent thermomechanical modification steps of the polymer obtained from the reactor, in order to produce a final product with enhanced mechanical properties. The rest of the process being limited, in terms of eventual communication actions, due to a pending patent submission,

the reported studies concern solely the grafting polymerization stage.

Accordingly, an experimental study has been carried out using differential scanning calorimetry, in an attempt to shed more light to the kinetic developments taking place in the mixture, under different GTR loading, initiator content and reaction temperatures [38]. This study has clearly shown that, depending on the type of initiator agent that is used to initiate the polymerization, the relative extent of grafting reactions, as well as that of side-reactions with the participation of carbon black, may vary significantly. As a continuation to this experimental study, a phenomenological modeling framework was recently developed to describe the observed phenomena. This modeling study, that is presented in this section, is based on a styrene homopolymerization kinetic model, that is used as initial validation point and reference for the extension to the grafting reactions. The developed kinetic model is initially compared against reported experimental data, derived from various sources, to verify its validity on the styrene polymerization system in the absence of GTR. At a second stage, a series of additional chemical reactions are introduced in the proposed kinetic scheme to describe the observed behavior of the system in the presence of GTR. For the tuning and validation of this part of the model, the experimental data that were generated in the framework of the aforementioned DSC study [38] are used.

The proposed modeling framework for this extremely complex reactive system is novel and succeeds in describing with good accuracy the evolution of the monomer conversion under different reaction conditions, in terms of the GTR content, the initiator concentration and the reaction temperature. However, the available data were not sufficient to allow for a more profound study, notably concerning the behavior of the system under a wider range of GTR compositions, as well concerning the molecular weight developments of the produced polymer. Accordingly, another study is currently underway, within the framework of a project funded by the Carnot Institute (cf. Chapter 5 and Appenddix **??**), that will allow the substantial enrichment of the experimental data. This project will also include the development of a complementary data-driven model, that will be combined with the existing phenomenological one in view of extending the predictive capacity of the new hybrid model in terms of the properties of the produced polymer.

A kinetic modeling framework for the peroxide-initiated radical polymerization of styrene in the presence of rubber particles from recycled tires

Dimitrios Meimaroglou*, Daniela Florez[1], Guo-Hua Hu

Laboratoire Réactions et Génie des Procédés,Université de Lorraine,CNRS, LRGP, F-54000 Nancy, France

Abstract

A novel modeling framework is presented for the peroxide-initiated radical polymerization of styrene, in the presence of ground-tire rubber particles. The model takes into account the previously observed effects of the rubber particles, and their highly-reactive additives, on the course of the polymerization. To this end, a generalized kinetic mechanism is proposed, on the basis of a typical styrene homopolymerization scheme, including also a series of additional chemical reactions that are implemented to describe the deviation of the system from the respective homopolymerization case when ground-tire rubber is present in the mixture. This deviation is mainly manifested through an accelerated peroxide decomposition and significant retardation and inhibition of the reaction and displays a non-linear dependence on the contents of rubber particles and initiator. The proposed model succeeds in predicting this behavior under different reaction conditions, while its generality makes it

*Corresponding author

Email address: dimitrios.meimaroglou@univ-lorraine.fr (Dimitrios Meimaroglou)

[1]current address: 7 Le Beaulieu, les Voivres, 88240, France

suitable for implementation in other similar grafting polymerization systems.

Keywords: styrene, radical polymerization, ground-tire rubber, kinetic model, method of moments, peroxide

---

1. Introduction

Automobile tires constitute an irreplaceable product of modern everyday life and an example of continuous scientific research and advancements in terms of its durability and performance. At the same time, they also constitute a significant source of pollution since an important part of end-of-life tires (i.e., tires that can no longer be used on automobiles, even after retreading) end-up in land fills or are burnt for energy recovery. Hence, an increasing scientific interest is nowadays directed towards the exploitation of eventual solutions to this ecological problem [1, 2, 3]. This need is further amplified by the increasing global demand in reducing, reusing and recycling plastic waste, since a significant proportion of tires is composed of a mixture of elastomers (i.e., rubber) [4].

In this respect, a promising solution consists in mechanically grinding the rubber part of tires, after removal of tissue and metallic parts, to form a powder of micrometric particles that can be subsequently used as raw material for new products and applications. For example, this powder, which is commercially called Ground Tire Rubber, GTR, is often used to modify the mechanical properties of new polymeric materials. For instance, it can be employed as a filler of otherwise brittle polymers, such as polystyrene (PS) [5], to improve their stress cracking resistance and their impact strength [1, 6, 7].

The addition of pure rubber particles of nanometric size to the matrix of PS, a brittle thermoplastic commodity polymer of a very wide range of applications, is a well-established commercial process that imparts significant strength to the final polymeric product, commercially known as high-impact polystyrene (HIPS) [4, 5, 8]. Accordingly, an idea that has been followed by several research studies focuses on replacing the fresh rubber with GTR particles in an attempt to achieve a similar improvement in the mechanical properties of polystyrene [9, 10, 11]. This idea is even more interesting as it promotes, at the same time, the recycling of used tires within a general sustainability perspective.

However, a simple mixing of the two materials (i.e., of pure PS and GTR) does not result in the expected outcome as the two phases display low adhesion towards one another. Hence, the produced blend is highly heterogeneous, with respect to the dispersion of the GTR particles within the PS matrix, thus severely limiting the improvement of its stress cracking resistance. Several solutions have been proposed to overcome this low adhesion by targeting its main sources, including compatibilization techniques and surface modification treatments of GTR. Among them, a particularly interesting strategy is to render the two phases compatible by grafting the polymer directly onto the surface of the GTR particles via in-situ radical polymerization [1, 12, 11].

When particulate fillers are present in radical polymerization systems, they may often interact with other reactive species that are present in the mixture, thus affecting the kinetic developments and the overall course of the polymerization. The degree to which these effects may be more or less pronounced depends mainly on the filler's physicochemical characteristics as

well as on the nature of the system. As a result, the polymerization may be mildly or significantly accelerated or retarded, in terms of the evolution of the monomer conversion and/or the chain length characteristics, by the presence of a filler that displays strong interactions with other reactive components of the system (e.g., the monomer(s) or the initiator agent(s)) [4, 13, 14].

GTR has been shown to display such effects when present in radical polymerization systems. For example, when added to acrylate polymerization systems, such as methyl methacrylate (MMA), glycidyl methacrylate (GMA) and hydroxy ethyl methacrylate (HEMA), initiated using benzoyl-peroxide (BPO), an acceleration of the course of the polymerization was observed [13]. At the same time, the presence of GTR in the radical polymerization of styrene displayed an overall inhibition effect, when BPO was used as initiator, but when an azo-initiator, such as azobis(isobutyronitrile) (AIBN), was used instead of BPO, its impact was merely observed [11, 15]. Previous studies [13, 16, 17, 18, 19, 20, 21, 22] have pointed out that important interactions may take place between peroxide initiators and active groups that exist on the surface of carbon black (see Scheme 1), the most widespread reinforcing agent of rubber tires. However, these interactions may be of different nature and extent in different reactive systems. In this respect, the way in which GTR may affect the course of the polymerization, displaying an overall accelerating or inhibiting effect on different polymerization systems, has been attributed [13, 23] to the e-value of the monomers, which is characteristic of their polarity and reactivity, as defined in the original work of Alfrey and Price [24].

In an attempt to elucidate these effects, differential scanning calorimetry

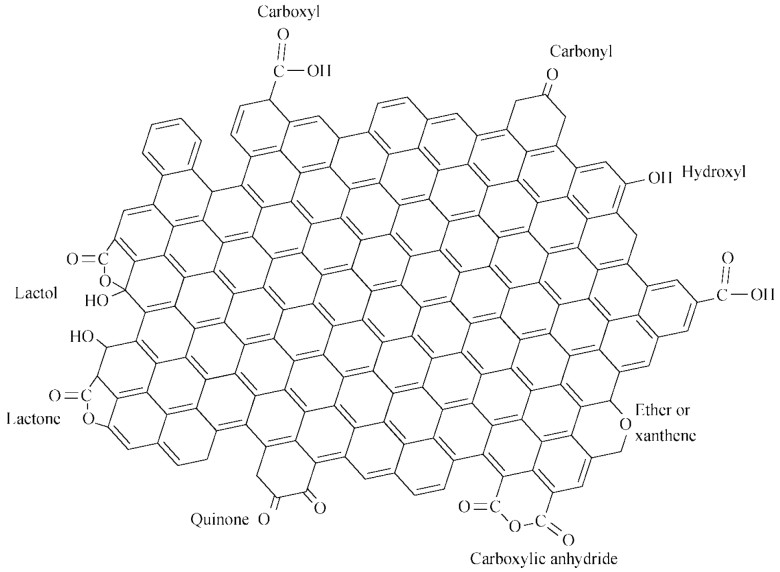

Scheme 1: Aromatic layer plane of carbon black with different functional groups [25].

(DSC) has been used, in the framework of a previous work, to study the bulk radical polymerization of styrene in the presence of different amounts of GTR [23]. The results of that study confirmed that the presence of GTR displays a significant inhibition effect on the course of the peroxide-initiated polymerization. They also revealed that these effects were more pronounced at GTR content of around 30% wt and that a further increase of its content did not necessarily aggravate the observed inhibition effects, thus suggesting the interplay of "coverage" or "masking" phenomena of the carbon black surface active groups. Finally, the findings of that study, including the calculation of the apparent activation energy of the polymerization under the different tested conditions, were also in line with a previously reported effect of accelerated decomposition of peroxide initiators, also induced by the

presence of carbon black [13, 16].

Following up on that experimental study, this work presents a comprehensive modeling framework for the radical bulk polymerization of styrene that is consistent with the observed evolution of the system, both in the absence and in the presence of GTR. The proposed model is based on an extended kinetic scheme that includes the typical chemical reactions that are commonly encountered in styrene homopolymerization studies, as well as chemical reactions that have been introduced to simulate the effects observed when GTR is added to the system. For the calibration and the validation of the model, a series of experimental data have been collected from different literature studies, initially corresponding only to the case of pure styrene homopolymerization. These data were then enriched with additional experimental data produced in the framework of this study, including DSC measurements [23] and bench-scale solution polymerization runs [26], both in the presence and in the absence of GTR.

The mathematical modeling of the radical polymerization of styrene has been extensively studied and several modeling frameworks have been proposed. The reported works of the group of Hamielec [27, 28, 29, 30], as well as the work of Mayo [31], were certainly pioneering in the domain and have set the grounds for later modeling developments. In the following years, the diffusion-controlled phenomena, governing the termination, propagation and initiation reactions, were also extensively analyzed and different models were proposed to describe them [32, 33, 34]. Among the relatively more recent studies, one can distinguish the works published by Penlidis [35, 36], Kotoulas et al. [37] and, more recently, Woloszyn [38, 39], since they present

accurate models combining thermal and chemical initiation mechanisms and diffusion phenomena, explore the cases of multifunctional initiators and focus on parametric identification problems.

Several studies are also reported for the modeling of styrene radical polymerization i0ncluding grafting mechanisms. A very early study, published by Manaresi et al. [40], presented a kinetic mechanism that included grafting reactions of styrene on pure 1,4-polybutadiene and a corresponding kinetic model. A series of relevant studies has also been published by Cameron and coworkers, extending over a long period of time and including different systems in terms of rubber polymers (e.g., polybutadiene and polyisoprene) and monomers (e.g., styrene and methyl-methacrylate) [12, 41, 42]. Similarly, Huang and Sundberg [43, 44, 45, 46] published a series of studies on the grafting mechanisms of different monomers (i.e., styrene, methyl acrylate and methyl methacrylate) on polybutadiene, in the presence of various initiators and on the basis of a detailed kinetic mechanism, including homopolymerization and grafting reactions. Meira and coworkers also presented detailed kinetic models on the production process of high-impact polystyrene (HIPS) [47, 8]. More recent modeling studies can also be found in the relevant literature, with slight modifications in terms of the reacting components and/or the process [48, 49, 50]. In certain cases, inhibition reactions were also included in the proposed kinetic mechanisms to account for the effect of impurities, or other additives, that could be present in the mixture and could lead to the termination of growing radicals [8]. However, to the best of the authors' knowledge, the presence of used tire rubber particles in the styrene radical polymerization system has not yet been addressed by any

modeling study. Note that, as mentioned above, GTR is a mixture of different rubbers and additives whose exact composition and structure are often unknown. This is a major difference with respect to the aforementionned works on well-identified elastomers. The present work is the first attempt to propose a complete kinetic modeling framework of this system, capable of describing the evolution of the polymerization both in the absence (i.e., homopolymerization case) and in the presence of used tire particles as well as the effects of the contents of the GTR and additives on the course of the polymerization.

2. Experimental

2.1. DSC experiments

All DSC measurements were carried out in a Q2000 calorimeter of TA Instruments, using hermetic aluminum pans, specifically adapted for volatile products. Two consecutive isothermal scans were performed with an intermediate cooling step down to 50 °C. All the reagents used, namely, styrene monomer (with a purity $\geq$ 99.5% and stabilized with $\sim$ 0.005% of 4-tert-butylcatechol) and BPO (75%, remainder water), were purchased from Sigma-Aldrich and used without further purification. Commercial GTR, in the form of powder, was obtained from DeltaGom France and was used without purification. The relevant details about the sample preparation process, the scanning and recording details, as well as the exploitation of the recorded data, can be found elsewhere [23].

2.2. Bench-scale polymerization experiments

Isothermal solution homopolymerization of styrene, in toluene, was carried out in an agitated batch reactor of total volume capacity of 1 liter [26]. Styrene was purified, prior to the polymerization, by filtration in an aluminum oxide (Al_2O_3) column. The initial mass of toluene in the system was equal to that of styrene in all experiments. Polymerizations were performed at 80 °C and 90 °C. BPO was previously dissolved in the solvent and the mixture was introduced in the reactor and purged with nitrogen atmosphere during 20 minutes under permanent agitation. Subsequently, the monomer was added and the medium was heated to the reaction temperature at 2 °C /min. The total reaction time was 4 to 6 h, under permanent stirring at 300 rpm. The degree of monomer conversion was measured by gravimetry and the number- and weight-average molecular weights were determined by size exclusion chromatography (SEC), using a refractive index Obtilab REX (RI) detector and a multi-angle light scattering MALS WYATT mini dawn TREOS detector, in combination with three separation columns PLgel with pore sizes of 100 Å, 1000 Å and 10^5 Å. Measurements were carried out at a flow rate of 1 mL/min in THF at 40 °C, at a concentration of about 6 to 8 mg/mL.

3. Polymerization kinetic mechanism

The following kinetic scheme was employed to account for all possible reactions taking place in the system, both in the absence and in the presence of GTR:

- Chemical initiation

- Thermal decomposition of initiator:

$$I \xrightarrow{k_d, f_1} 2PR \tag{1}$$

- Decomposition of initiator induced by carbon black:

$$I + CB \xrightarrow{k_{dCB}, f_2} PRl \tag{2}$$

- Free radical initiation:

$$M + PR \xrightarrow{k_I} R_1 \tag{3}$$

- Formation of grafted primary radicals:

$$G + PR \xrightarrow{k_{IG}} GPR \tag{4}$$

- Grafted radical initiation:

$$M + GPR \xrightarrow{k_{pG}} GR_1 \tag{5}$$

- Initiation of reduced-activity free radicals:

$$M + PRl \xrightarrow{\alpha \cdot k_I} P_1 \tag{6}$$

- Initiation of reduced-activity grafted radicals:

$$G + PRl \xrightarrow{\alpha \cdot k_{IG}} GP_1 \tag{7}$$

- Thermal initiation

  - Diels-Alder dimerization of styrene:

$$2M \underset{k_{-1}}{\overset{k_1}{\leftrightarrow}} AH \tag{8}$$

- Initiation from Diels-Alder adduct (AH):

$$AH + M \xrightarrow{k_2} AR + MR \tag{9}$$

- Initiation from 1-phenyltetralyl radical (AR):

$$AR + M \xrightarrow{k_A} R_3 \tag{10}$$

- Initiation from styryl radical (MR):

$$MR + M \xrightarrow{k_B} R_2 \tag{11}$$

- Trimerization reaction of Diels-Alder adduct:

$$AH + M \xrightarrow{k_C} D_3 \tag{12}$$

- Propagation:

  - of free radicals:

$$M + R_n \xrightarrow{k_p} R_{n+1} \tag{13}$$

  - of grafted radicals:

$$M + GR_n \xrightarrow{k_{pG}} GR_{n+1} \tag{14}$$

  - of reduced-activity free radicals:

$$M + P_n \xrightarrow{\alpha \cdot k_p} P_{n+1} \tag{15}$$

  - of reduced-activity grafted radicals:

$$M + GP_n \xrightarrow{\alpha \cdot k_{pG}} GP_{n+1} \tag{16}$$

- Transfer:
  - to monomer from free radicals:

$$M + R_n \xrightarrow{k_{fm}} D_n + R_1 \tag{17}$$

  - to adduct from free radicals:

$$AH + R_n \xrightarrow{k_{fAH}} D_n + AR \tag{18}$$

  - to monomer from grafted radicals:

$$M + GR_n \xrightarrow{k_{fmG}} GD_n + R_1 \tag{19}$$

  - to adduct from grafted radicals:

$$AH + GR_n \xrightarrow{k_{fAHG}} GD_n + AR \tag{20}$$

  - to GTR from free radicals:

$$G + R_n \xrightarrow{k_{fG}} D_n + GPR \tag{21}$$

  - to primary-radicals from free radicals

$$R_n + PR \xrightarrow{k_{tPR}} D_n \tag{22}$$

  - to primary-radicals from grafted radicals

$$GR_n + PR \xrightarrow{k_{tPRG}} GD_n \tag{23}$$

- Scission (induced by primary-radicals):

  - of free polymer

$$PR + D_n \xrightarrow{k_s} R_m + D_{n-m} \tag{24}$$

  - of grafted polymer

$$PR + GD_n \xrightarrow{k_{sG}} R_m + GD_{n-m} \tag{25}$$

- Termination:

  - by combination of free radicals

$$R_n + R_m \xrightarrow{k_{tc}} D_{n+m} \tag{26}$$

  - by disproportionation of free radicals

$$R_n + R_m \xrightarrow{k_{td}} D_n + D_m \tag{27}$$

  - by combination between free and grafted radicals

$$R_n + GR_m \xrightarrow{k_{tcG}} GD_{n+m} \tag{28}$$

  - by disproportionation between free and grafted radicals

$$R_n + GR_m \xrightarrow{k_{tdG}} D_n + GD_m \tag{29}$$

  - between free and reduced-activity radicals

$$R_n + P_m \xrightarrow{\alpha \cdot k_{tc/td}} D_{n+m}/D_n + D_m \tag{30}$$

  - between grafted and reduced-activity radicals

$$GR_n + P_m \xrightarrow{\alpha \cdot k_{tcG/tdG}} GD_{n+m}/GD_n + D_m \tag{31}$$

– between free and reduced-activity grafted radicals

$$R_n + GP_m \xrightarrow{\alpha \cdot k_{tcG/tdG}} GD_{n+m}/D_n + GD_m \tag{32}$$

– between reduced-activity radicals

$$P_n + P_m \xrightarrow{\alpha^2 \cdot k_{tc/td}} D_{n+m}/D_n + D_m \tag{33}$$

- Radical deactivation by carbon black:

  – of primary-radicals

$$PR/GPR + CB \xrightarrow{k_{dea}} DPR \tag{34}$$

  – of MR radicals

$$MR + CB \xrightarrow{k_{dea}} D_1 \tag{35}$$

  – of AR radicals

$$AR + CB \xrightarrow{k_{dea}} D_2 \tag{36}$$

  – of free radicals

$$CB + R_n \xrightarrow{k_{dea}} D_n \tag{37}$$

  – of grafted radicals

$$CB + GR_n \xrightarrow{k_{deaG}} GD_n \tag{38}$$

  – of reduced-activity free radicals

$$CB + P_n \xrightarrow{\alpha \cdot k_{dea}} D_n \tag{39}$$

  – of reduced-activity grafted radicals

$$CB + GP_n \xrightarrow{\alpha \cdot k_{deaG}} GD_n \tag{40}$$

All symbols are described in the Nomenclature (section 7). The postulated kinetic scheme contains all the chemical reactions that are commonly encountered in studies of the radical polymerization of styrene, including both chemical and thermal initiation mechanisms (i.e., reactions (1), (3), (8)-(12)), propagation, transfer and termination reactions (i.e., reactions (13), (17)-(18), (22), and (26)-(27)), as well as scission reactions by primary radicals (i.e., reaction (24)), as reported in some studies [38, 39]. Note that, a much simpler thermal initiation mechanism has been proposed by Hui and Hamielec [29], employing a single kinetic chemical reaction. Although this mechanism is attractive and has been adopted by several subsequent studies, it limits the flexibility of the model in terms of its possibility to track the intermediate species, such as the Diels-Alder adduct, which may participate in other reactions (e.g., transfer reactions). Thus, the complete thermal initiation mechanism, reported in Kotoulas et al. [37] and in other similar modeling studies [38, 39], has been adopted in this work.

In addition to the above, a series of additional chemical reactions are included in this general kinetic scheme to simulate the kinetic developments taking place in the system in the presence of GTR. These have been employed in accordance to the effects observed previously and reported in the literature [13, 23]. More specifically, these effects can be broadly classified into two general categories. The first one includes the grafting reactions, describing the formation of radicals on the surface of the GTR particles and their subsequent participation in the polymerization reactions (i.e., reactions (4)-(5), (7), (14), (16), (19)-(21), (23), (25), (28)-(29), (31)-(32), (34), (38) and (40)). The second category includes the reactions of catalyzed decomposition of the initiator (i.e., reaction (2)) and radical deactivation (i.e, reactions

(34)-(40)), both induced by the presence of carbon black in the formulation of GTR. The observed retardation effect, also attributed to the presence of carbon black [13, 17, 16], has been included in the kinetic scheme by the fact that the carbon black-induced initiation leads to the formation of radicals of reduced activity with respect to the radicals formed by the classical chemical and thermal initiation mechanisms. These are denoted as PRl, Pn and GPn, for the primary-radicals, the free radicals and the grafted ones, respectively.

Accordingly, the overall inhibition/retardation effect of carbon black is taken into account by considering that its presence will either lead to complete or partial deactivation of primary radicals. In this sense, the consideration of additional chemical reactions for the deactivation of reduced-activity primary radicals has been considered redundant in terms of its effect on the overall course of the polymerization and has not been included in the kinetic scheme. Note that, the two aforementioned general categories, grafting and catalyzed initiator decomposition, are not independent of one another as some reactions of the proposed kinetic scheme belong to both of them (e.g., reactions (7) and (31)).

From the above, it becomes obvious that the postulated kinetic scheme displays a general form, allowing the incorporation of different effects and observed phenomena. In the case of the absence of GTR, the kinetic scheme reduces to the typical homopolymerization case. This is taken into account in the proposed model by setting the quantity of GTR equal to zero, without the necessity to modify any other parameter or equation of the model. A global set of kinetic rate constants has been identified and employed for the simulation of all tested cases and conditions, either in the presence of GTR or for the pure homopolymerization system. Two different peroxide initiators have been tested, namely dicumyl peroxide (DCP) and BPO. DCP has been implemented in order to compare the results of the model with reported homopolymerization data [37]. On the other

hand, BPO has been shown to display more interesting behavior in terms of its interactions with carbon black and, as such, has been extensively tested by the present model.

To avoid the multiplication of the parameters of the model, the reduced activity of the carbon black-initiated radicals has been taken into account by a correcting coefficient, α. Accordingly, the kinetic rate constant of a chemical reaction containing reduced-activity radicals has been considered equal to the rate constant of the respective reaction of normal-activity radicals, multiplied by α. In the case of reactions between reduced-activity radicals, the respective rate constant has been multiplied by α^2. Details about the parameters of the model are given later in section 4.5. Note also that some of the postulated chemical reactions have been denoted in a condensed form to avoid redundant repetitions. This is, for example, the case with the termination reactions including grafted and/or reduced-activity radicals, where the combination and disproportionation reactions have been condensed in a single chemical reaction (i.e., Eqs. (30)-(32)).

4. Model developments

On the basis of the postulated general kinetic scheme (i.e., reactions (1)-(40)), the net rates of production of the different species that are present in the reacting mixture can be established. They are divided into the rates of the macromolecular and the non-macromolecular species. The first category includes the free, grafted and reduced-activity radicals as well as the free and grafted polymer chains, while the second category includes all the remaining species, such as initiator agents, styrene, GTR, carbon black, primary radicals, AH adduct and AR and MR radicals. Note that, in this study, GTR has been considered as a non-macromolecular species, despite its macromolecular nature. In fact, in the framework of the present kinetic model, GTR participates in the kinetic developments by its chemical groups

that are exposed to the rest of the reacting species and are prone to react. As such, it is not the macromolecular character of the different elastomers, that are present in the formulation of GTR, that constitutes an element of interest for the model, but rather the quantity of these groups. This quantity is denoted in the model equations by G and details on its calculation are given later in the text (see Eq.(65) in section 4.4).

Finally, it should be noted that the present approach is based on the assumptions of i) chain-length independent rate constants for all the reactions and ii) homogeneous reacting mixture. In fact, the majority of previous modeling studies of the system of rubber-grafting polymerization have treated the system as homogeneous, with some exceptions where a heterogeneous approach was implemented mainly to describe the phase-inversion stage of the formation of HIPS [8, 49]. The consideration of mass transfer and diffusion phenomena within the structure of GTR is expected to provide a more realistic representation of the system, notably at high GTR loading, as well as a more plausible concentration profile of the different species at the grafting sites. However, this would further complicate the model and increase its number of parameters. It would also necessitate accurate relevant measurements that, for the moment, are not reported for this system. In this respect and considering the nature of the systems and the conditions studied in this work, the aforementioned diffusional limitations, beyond the point to which the difference in the kinetic rate constants between grafting and homopolymerization reactions can capture, have been considered negligible.

4.1. Rate functions of the macromolecular species

In this section, the development of the net rate of production of only one macromolecular species is presented, namely that of the free radicals of size 'n', R_n, while the rest of the rate functions are presented in detail in Appendix A:

$$
\begin{aligned}
r_{R_n} = & \left(k_I \cdot [PR] \cdot [M] + k_{fm} \cdot [M] \cdot \sum_{k=1}^{\infty} [R_k] \right) \cdot \delta(n-1) \\
& + k_A \cdot [AR] \cdot [M] \cdot \delta(n-3) + k_B \cdot [MR] \cdot [M] \cdot \delta(n-2) \\
& + k_p \cdot [M] \cdot ([R_{n-1}] - [R_n]) - (k_{fm} \cdot [M] + k_{fAH} \cdot [AH]) \cdot [R_n] \\
& + k_s \cdot [PR] \cdot \sum_{k=n+1}^{\infty} [D_k] - (k_{tc} + k_{td}) \cdot [R_n] \cdot \sum_{k=1}^{\infty} [R_k] \\
& - k_{tPR} \cdot [PR] \cdot [R_n] + \left(k_{fmG} \cdot [M] \cdot \sum_{k=1}^{\infty} [GR_k] \right) \cdot \delta(n-1) \\
& - k_{fG} \cdot [G] \cdot [R_n] + k_{sG} \cdot [PR] \cdot \sum_{k=n+1}^{\infty} [GD_k] \\
& - (k_{tcG} + k_{tdG}) \cdot [R_n] \cdot \sum_{k=1}^{\infty} [GR_k] - k_{dea} \cdot [CB] \cdot [R_n] \\
& - \alpha \cdot [R_n] \cdot \left((k_{tc} + k_{td}) \cdot \sum_{k=1}^{\infty} [P_k] + (k_{tcG} + k_{tdG}) \cdot \sum_{k=1}^{\infty} [GP_k] \right)
\end{aligned}
\tag{41}
$$

In the above equation, the rate of production of R_n, r_{R_n} is expressed in units of molar concentration over time (i.e., $mol.l^{-1}.min^{-1}$), while the molar concentrations of the different species (i.e., in $mol.l^{-1}$) are denoted with the use of brackets [ ]. Also, $\delta(n-1)$ is the Kroenecker's delta, given by:

$$
\delta(n-i) = \begin{cases} 1 & \text{for n = i} \\ 0 & \text{for n} \neq \text{i} \end{cases} \tag{42}
$$

4.2. Method of Moments

Since the rate functions of the macromolecular species (Eq.(41) and Eqs.(A.1)-(A.5)) are described with respect to their chain length, the resulting system of differential equations (see Eqs.(62)-(63)) will be of size equal to the considered

maximum chain-length. In this respect, one of the most commonly employed techniques to reduce the size of the system and the associated computational effort is the method of moments [51]. It is a widely-used technique that is based on the statistical representation of the average molecular properties of the macromolecular species in terms of the leading moments of their number-chain-length distribution. Accordingly, one can define the moment of order k, for the free radicals, R_n, as:

$$\lambda_k = \sum_{n=1}^{\infty} n^k R_n \tag{43}$$

The moments for the rest of the macromolecular species can be defined accordingly. Following the above definition, the rate function of the free radicals (Eq.(41)) can be readily transformed to express the rate function of their leading moments:

$$\begin{aligned} r_{\lambda_k} &= k_I \cdot [PR] \cdot [M] + k_{fm} \cdot [M] \cdot \lambda_0 \\ &+ 3^k \cdot k_A \cdot [AR] \cdot [M] + 2^k \cdot k_B \cdot [MR] \cdot [M] \\ &+ k_p \cdot [M] \cdot \left(\sum_{r=0}^{k} \binom{k}{r} \lambda_r - \lambda_k \right) - (k_{fm} \cdot [M] + k_{fAH} \cdot [AH]) \cdot \lambda_k \\ &+ k_s \cdot [PR] \cdot T_1 - (k_{tc} + k_{td}) \cdot \lambda_k \cdot \lambda_0 - k_{tPR} \cdot [PR] \cdot \lambda_k \\ &+ k_{fmG} \cdot [M] \cdot \nu_0 - k_{fG} \cdot [G] \cdot \lambda_k + k_{sG} \cdot [PR] \cdot T_{1G} - (k_{tcG} + k_{tdG}) \cdot \lambda_k \cdot \nu_0 \\ &- k_{dea} \cdot [CB] \cdot \lambda_k - \alpha \cdot \lambda_k \cdot ((k_{tc} + k_{td}) \cdot \theta_0 + (k_{tcG} + k_{tdG}) \cdot \omega_0) \end{aligned} \tag{44}$$

In the above expression, $\binom{k}{r}$ denotes the binomial coefficients and T_1 and T_{1G}

are given by:

$$T_1 = \sum_{m=0}^{k} \frac{B_m}{k-m+1} \left(\mu_{k-m+1} - \mu_0\right) \qquad ; \qquad T_{1G} = \sum_{m=0}^{k} \frac{B_m}{k-m+1} \left(\xi_{k-m+1} - \xi_0\right) \tag{45}$$

with the Bernoulli numbers defined as:

$$B = \left[1,\ -\frac{1}{2},\ \frac{1}{6},\ 0, ...\right] \tag{46}$$

The notation of the different moment species is defined in the Nomenclature section and the corresponding rate functions are detailed in Appendix A (Eqs.(A.6)-(A.10)).

4.3. Rate functions of the non-macromolecular species

The net production rates of the non-macromolecular species of interest can be defined on the basis of their participation in the different chemical reactions of the postulated general kinetic scheme (Eqs.(1)-(40)):

- Styrene monomer, M

$$\begin{aligned} r_M = &- \left(k_I \cdot [PR] + (k_p + k_{fM}) \cdot \lambda_0\right) \cdot [M] \\ &- \left((k_2 + k_C) \cdot [AH] + k_A \cdot [AR] + k_B \cdot [MR]\right) \cdot [M] \\ &- \left(k_{pG} \cdot ([GPR] + \nu_0) + k_{fmG} \cdot \nu_0\right) \cdot [M] \\ &- 2 \cdot k_1 \cdot [M]^2 + 2 \cdot k_{-1} \cdot [AH] - \alpha \cdot k_I \cdot [PRl] \cdot [M] \\ &- \alpha \cdot \left(k_p \cdot \theta_0 + k_{pG} \cdot \omega_0\right) \cdot [M] \end{aligned} \tag{47}$$

- Ground Tire Rubber, G

$$r_G = - \left(k_{IG} \cdot ([PR] + \alpha \cdot\ [PRl]) + k_{fG} \cdot \lambda_0\right) \cdot [G] \tag{48}$$

- Carbon Black, CB

$$\begin{aligned} r_{CB} = &- \left(k_{dCB} \cdot [I] + k_{dea} \cdot (\lambda_0 + \alpha \cdot \theta_0) + k_{deaG} \cdot (\nu_0 + \alpha \cdot \omega_0)\right) \cdot [CB] \\ &- k_{dea} \cdot ([PR] + [GPR] + [AR] + [MR]) \cdot [CB] \end{aligned} \tag{49}$$

- Initiator, I

$$r_I = - \left(k_d + k_{dCB} \cdot [CB]\right) \cdot [I] \tag{50}$$

- Diels-Alder adduct, AH

$$\begin{aligned} r_{AH} = &\, k_1 \cdot [M]^2 - \left(k_{-1} + (k_2 + k_C) \cdot [M]\right) \cdot [AH] \\ &- (k_{fAH} \cdot \lambda_0 + k_{fAHG} \cdot \nu_0) \cdot [AH] \end{aligned} \tag{51}$$

- Styryl radicals, MR

$$r_{MR} = k_2 \cdot [AH] \cdot [M] - k_B \cdot [M] \cdot [MR] - k_{dea} \cdot [MR] \cdot [CB] \tag{52}$$

- 1-Phenyl tetraryl radicals, AR

$$\begin{aligned} r_{MR} = &\, k_i \cdot [AH] \cdot [M] - k_A \cdot [M] \cdot [AR] \\ &+ (k_{fA} \cdot \lambda_0 + k_{fAG} \cdot \nu_0) \cdot [AH] - k_{dea} \cdot [AR] \cdot [CB] \end{aligned} \tag{53}$$

- Primary radicals, PR

$$\begin{aligned} r_{PR} = &\, 2 \cdot f_1 \cdot k_d \cdot [I] - k_I \cdot [M] \cdot [PR] \\ &- k_{IG} \cdot [G] \cdot [PR] - (k_s \cdot \mu_0 + k_{sG} \cdot \xi_0) \cdot [PR] \\ &- (k_{tPR} \cdot \lambda_0 + k_{tPRG} \cdot \nu_0 + k_{dea} \cdot [CB]) \cdot [PR] \end{aligned} \tag{54}$$

- Grafted primary radicals, GPR

$$\begin{aligned} r_{GPR} = &\, k_{IG} \cdot [G] \cdot [PR] - k_{pG} \cdot [M] \cdot [GPR] + k_{fG} \cdot [G] \cdot \lambda_0 \\ &- k_{dea} \cdot [CB] \cdot [GPR] \end{aligned} \tag{55}$$

- Reduced-activity primary radicals, PRl

$$r_{PRl} = f_2 \cdot k_{dCB} \cdot [CB] \cdot [I] - \alpha \cdot (k_I \cdot [M] + k_{IG} \cdot [G]) \cdot [PRl] \tag{56}$$

- Deactivated primary radicals, DPR

$$r_{DPR} = k_{dea} \cdot [CB] \cdot ([PR] + [GPR]) \tag{57}$$

It should be noted that the deactivated primary radicals, DPR, do not participate in any other reaction and, thus, the rate function of their concentration (Eq.(57)) serves only in the overall mass balance check. For the calculation of the evolution of the concentration of the different primary radical species (i.e., PR, GPR and PRl), as well as for the Diels-Alder adduct, AH, the quasi-steady-state assumption (Q.S.S.A.) has been employed, leading to the following expressions:

- Diels-Alder adduct, AH

$$[AH] = \frac{k_1 \cdot [M]^2}{k_{-1} + (k_i + k_C) \cdot [M] + k_{fAH} \cdot \lambda_0 + k_{fAHG} \cdot \nu_0} \tag{58}$$

- Primary radicals, PR

$$[PR] = \frac{2 \cdot f_1 \cdot k_d \cdot [I]}{k_I \cdot [M] + k_{IG} \cdot [G] + k_s \cdot \mu_0 + k_{sG} \cdot \xi_0 + k_{tPR} \cdot \lambda_0 + k_{tPRG} \cdot \nu_0 + k_{dea} \cdot [CB]} \tag{59}$$

- Grafted primary radicals, GPR

$$[GPR] = \frac{k_{IG} \cdot [G] \cdot [PR] + k_{fG} \cdot [G] \cdot \lambda_0}{k_{pG} \cdot [M] + k_{dea} \cdot [CB]} \tag{60}$$

- Reduced-activity primary radicals, PRl

$$[PRl] = \frac{f_2 \cdot k_{dCB} \cdot [CB] \cdot [I]}{\alpha \cdot (k_I \cdot [M] + k_{IG} \cdot [G])} \tag{61}$$

4.4. Reactor design equations

The reactor design equations, for a batch polymerization system, can be directly derived for all the species of interest (i.e., non-macromolecular species and leading moments of the macromolecular species), on the basis of the established rate functions. In this respect, the resulting system of ordinary differential equations (ODEs) will be of the form:

$$\frac{dn_S}{dt} = r_S \cdot V \tag{62}$$

where S denotes the different species of interest and V is the volume of the reacting mixture, which also varies according to:

$$\frac{dV}{dt} = r_M \cdot \left(\frac{1}{d_M} - \frac{1}{d_P} \right) \cdot M_0 \cdot V \tag{63}$$

where M_0 is the molecular weight of styrene and d_M and d_P are the respective densities of styrene and polystyrene in $g.mol^{-1}$, calculated by the following expressions [37]:

$$d_m = 9.236 \cdot 10^{-1} - 0.887 \cdot T(^{\circ}C) \qquad ; \qquad d_p = 1.085 - 0.605 \cdot T(^{\circ}C) \tag{64}$$

The above system of ODEs is completed by the algebraic equations for the calculation of the concentrations of AH, PR, GPR and PRl (Eqs.(58)-(61)). For the determination of the initial concentration of G, corresponding to the available reaction sites on the accessible internal and external surface of the GTR particles, the following approach has been adopted: the composition of GTR, in terms of the type and weight fraction of elastomers, as provided by the supplier, has been considered in order to calculate a theoretical estimation of the molar quantity of double bonds. This quantity has also been found to coincide with the experimental

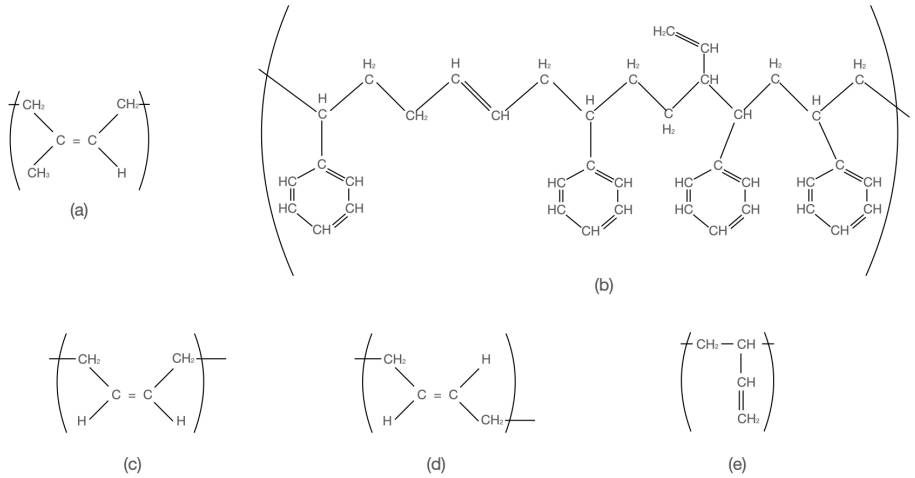

Scheme 2: Chemical structure of (a)*cis*-Polysioprene, (b)Styrene-Butadiene Rubber, (c)*cis*-1,4-Polybutadiene, (d)*trans*-1,4-Polybutadiene, (c)Vinyl-1,2-polybutadiene.

determination of the concentration of double bonds of the elastomer chains of GTR, which was carried out according to the standard test method for iodine value of drying oils and fatty acids (ASTM D-1959). Both experimental and theoretical values were found to be of the order of $3.5 \cdot 10^{-3}$ mol of double bonds per gram of GTR. The composition of GTR is shown in Table 1 while the chemical structures of the most commonly encountered elastomers in GTR are given in Scheme 2. The calculated value of double bonds was multiplied by an efficiency factor in the model (i.e., parameter f_{GTR}) to transform it to available reaction sites, prone to react. Finally, to account for the exposure and coverage of these possible reaction sites on GTR, the initial concentration of G was calculated according to the following expression:

$$[G]_0 = \frac{\left(\frac{GRat}{GRat_c}\right)^6}{1+\left(\frac{GRat}{GRat_c}\right)^6} \cdot [M_{DB}] \cdot f_{GTR} \qquad ; \qquad GRat = \frac{W_{GTR}}{W_{GTR}+W_{St}} \qquad (65)$$

In the above expression, $Grat$ and $Grat_c$ denote the actual mass fraction of GTR in the mixture and a critical value of this mass fraction, respectively. M_{DB} is the calculated molar concentration of double bonds of GTR according to the procedure described previously.

According to the relative literature, there exist two principal mechanisms for the grafting reactions, namely the addition of radicals to the unsaturated double bonds of the elastomers of GTR and the mechanism of hydrogen abstraction by the radicals [4, 11, 12, 41, 52, 42]. The extent to which grafting by any of these two mechanisms will take place is primarily dictated by the type of radicals and elastomers as well as by the position of the double bonds (i.e., as pendant side-chain groups or within the main backbone of the elastomer, see also Scheme 2). The same factors affect also the competition between homopolymerization and grafting reactions. In this respect, and given that GTR is composed of a mixture of different elastomers, as shown in Table 1, the calculation, in the model, of the quantity of sites of GTR that are prone to participate in grafting reactions has been based on the above simplified and generalized approach. Thus, the initial calculation of the amount of double bonds of GTR allows the consideration of the actual composition and characteristics of GTR, while the implementation of the parameter f_{GTR} provides a degree of liberty and includes the aforementioned variations. In addition, the first term of Eq.(65) was introduced to account for the coverage and masking effects that have been observed for different GTR contents [23]. In fact, the sigmoidal curve, resulting from the application of Eq.(65), allows for the consideration of a critical GTR concentration, beyond which the observed

Table 1: Formulation of GTR.

Elastomer	Weigh fraction
Styrene-butadiene rubber	0.4
Polyisoprene	0.3
Polybutadiene	0.2
Butadiene-acrylonitrile rubber	0.05
Isobutylene-isoprene rubber	0.05

effects are gradually attenuated. The previous experimental study of Florez et al. [23] has shown that this critical concentration should be below 50% of GTR and the parametric estimation of the model proposed in this work has resulted in a value equal to 0.43 for this parameter, as shown in Table 2, which is in accordance with the previous findings. Finally, the initial concentration of carbon black, in the model, was considered equal to a fixed percentage of $[G]_0$, set to 30% in this study.

4.5. Kinetic rate constants

The values of the model parameters were estimated in a two-step process, on the basis of reported values (when available). More specifically, in the first step, the kinetic rate constants of the reactions corresponding only to the pure homopolymerization case (i.e., in the absence of GTR) were estimated on the basis of the available homopolymerization data. Among them, the values of $k_{d,DCP}$, $k_{d,BPO}$, k_{-1}, k_1/k_{-1}, k_2 and k_{tc} were taken directly from the relevant literature [37, 53], as shown in Table 2. The values of k_p, k_C, k_{fAH} and k_{fm}, were tuned via the implementation of the Nedler-Mead optimization algorithm of Lagarias et al. [54], from the optimization toolbox of Matlab, using all the available homopolymerization data, presented in this work (see Figures 1-4). This concerned

both pre-exponential factors and activation energies, simultaneously. The values of these parameters were then kept constant throughout the rest of the estimation process. In addition to the parameters defined in Table 2, the commonly adopted assumption of $k_A = k_B = k_I = k_p$ has been adopted.

The second step of the estimation process concerned only the model parameters of the reactions related to the presence of GTR in the system. However, given the fact that, in the framework of this work, the only relevant available data concerned the temporal evolution of monomer conversion, the proposed kinetic model has been reduced accordingly. In this respect, only the chemical reactions of the proposed general kinetic scheme that are directly associated with the evolution of monomer conversion, in the presence of GTR, were considered in the parametric estimation process (see Table 2). The kinetic rate constants of the rest of the reactions involving GTR and carbon-black were set to zero. In fact, it would be meaningless to attempt to estimate at this point the complete set of rate constants solely on the basis of monomer conversion measurements. A new study has been launched aiming to acquire additional experimental data on molar mass and grafting efficiency indexes, which will allow the estimation of all the kinetic constants of the model. Until then, and in the absence of relevant data in the literature, the present work aims to demonstrate that the proposed unified modeling framework is capable of predicting the behavior of the system, as observed through the currently available data, both in the absence and in the presence of GTR. In addition, it presents a general kinetic scheme that can be implemented for the modeling of other polymerization systems in the presence of GTR.

Accordingly, the parameters presented in Table 2, besides the previously estimated ones on the basis of the homopolymerization data, were estimated via the Nedler-Mead algorithm using the DSC data of Florez et al. [23]. More particularly, an initial set of values was estimated on the basis of the DSC data at 90°C and

then another one at 120°C. From the values of the parameters obtained for the two above temperatures, the pre-exponential factor and the activation energy of k_{dCB}, as well as the linear correlation parameters (i.e., with respect to temperature) of k_{pG}/k_p and k_{IG}/k_p were determined via linear regression. On the other hand, the values of k_{tcG}/k_{tc}, k_{dea}/k_p and k_{deaG}/k_{dea} were kept fixed, as they did not display significant variation with temperature. Finally, all the parameters, related to the copolymerization system, were fine-tuned to their final values in an ultimate optimization step using all available DSC data (i.e., at 85°C, 90°C and 120°C). Note that, the implementation of ratio-coefficients of the rate constants of reactions involving GTR over their homopolymerization counterparts was made in an attempt to constrain the number of parameters of the model.

The final set of estimated parameter values, as presented in Table 2, has been kept constant and unchanged for all the simulations presented in this work, both in the absence and in the presence of GTR. However, the efficiency factor of the initiator decomposition (Eq.(1)), f_1, was set to a higher value for the simulations of the DSC data, in order to compensate the expected differences between the experimental systems in terms of the level of impurities and homogeneity (see Table 2). Finally, some rate constants of reactions related to the pure homopolymerization case (e.g., termination by disproportionation, Eq.(27), transfer to primary radicals, Eq.(22), as well as scission reactions, Eq.(24), which are expected to have an impact only when the polymerization is kept to relatively high temperatures for long periods of time [39]), were also set to zero, in accordance with reported studies and/or with the generated data. The same was done for their copolymerization counterparts. These parameters are not reported in Table 2.

The proposed model also takes into account the diffusion controlled phenomena affecting the reactions of termination, propagation and initiation, also known as the gel-, glass- and cage-effects, respectively. To this end, the model originally

proposed by Marten and Hamielec [32] was employed. The equations of this model are omitted here but can be found in the original study, as well in more recent studies that have adopted it [39], while the values of its parameters are given in Table 2. Note that, the model of Marten and Hamielec [32] was adopted in its complete form, including all the above diffusion-controlled phenomena, for the sake of completeness and generality in the applicability of the presented kinetic model.

Table 2: Model parameters

Parameter	Value	Units	Reference
$k_{d,DCP}$	$5.500 \cdot 10^{17} \cdot exp(-36650/R/T)$	min^{-1}	[37]
$k_{d,BPO}$	$2.289 \cdot 10^{14} \cdot exp(-27233/R/T)$	min^{-1}	[53]
k_p	$1.149 \cdot 10^{9} \cdot exp(-7513/R/T)$	$l.mol^{-1}.min^{-1}$	This work
k_{-1}	$6.840 \cdot 10^{3} \cdot exp(-13533/R/T)$	min^{-1}	[37]
k_1/k_{-1}	$6.400 \cdot 10^{4} \cdot exp(-12907/R/T)$	$l.mol^{-1}$	[37]
k_2	$9.800 \cdot 10^{7} \cdot exp(-23883/R/T)$	$l.mol^{-1}.min^{-1}$	[37]
k_C	$2.360 \cdot 10^{6} \cdot exp(-21346/R/T)$	$l.mol^{-1}.min^{-1}$	This work
k_{fm}	$1.032 \cdot 10^{7} \cdot exp(-10545/R/T)$	$l.mol^{-1}.min^{-1}$	This work
k_{fAH}	$7.360 \cdot 10^{7} \cdot exp(-30800/R/T)$	$l.mol^{-1}.min^{-1}$	This work
k_{tc}	$7.530 \cdot 10^{10} \cdot exp(-1677/R/T)$	$l.mol^{-1}.min^{-1}$	[37]
k_{dCB}	$2.147 \cdot 10^{-1} \cdot exp(-1478.7/R/T)$	$l.mol^{-1}.min^{-1}$	This work
$log(k_{pG}/k_p)$	$5.34 \cdot 10^{-2} \cdot T(^{\circ}C) - 5.1574$	-	This work
$log(k_{IG}/k_p)$	$7.52 \cdot 10^{-2} \cdot T(^{\circ}C) - 7.1353$	-	This work
k_{tcG}/k_{tc}	9.823	-	This work
k_{dea}/k_p	0.310	-	This work
k_{deaG}/k_{dea}	3.770	-	This work
α	$3.70 \cdot 10^{-6}$	-	This work
f_1	0.65 (0.83 for DSC data)	-	This work
f_2	0.40	-	This work
f_{GTR}	0.53	-	This work
$GRat_c$	0.43	-	This work
$a_m; a_p$	$1.4 \cdot 10^{-3}; 4.8 \cdot 10^{-4}$	K^{-1}; K^{-1}	[39], this work
$\delta; \sigma$	$3.8 \cdot 10^{-9}; 3.7 \cdot 10^{-9}$	$m; m$	This work
$j_c; \delta_c$	$175; 5.0 \cdot 10^{-4}$	$-; l.g^{-1}$	[39], this work
$A_{cr}; E_{cr}/R$	$9.0; 1960^{31}$	$g^{1/2}.mol^{-1/2}; K$	This work
$A_{crm}; E_{crm}$	$0.231; 1670$	$-; cal.mol^{-1}$	[39], this work
$A; B; C/B; n$	$0.4315; 0.7; 0.9; 2.5$	$-; -; -; -$	This work

$R = 1.9872\ cal.mol^{-1}.K^{-1}$

5. Model results and discussion

The model has been initially validated against reported data for the pure styrene hopolymerization system, in the absence of GTR. Different data sources and polymerization conditions have been tested to assure its generality and robustness. Monomer conversion and average molecular weight predictions have been compared to their respective experimental data, either as specific point predictions or as complete temporal evolution profiles, depending on the availability of the data. In all presented cases, the predictions of the model are plotted as curves and the experimental data as discrete points.

In this respect, Figure 1 compares the experimental data for the temporal evolution of monomer conversion and average molecular weights, reported in Villalobos et al. [53], with the respective predictions of the model. It is seen that the model succeeds in following with great accuracy the evolution of all three experimental data sets. Note that the same set of data has also been used previously as reference for the validity of other reported models [39].

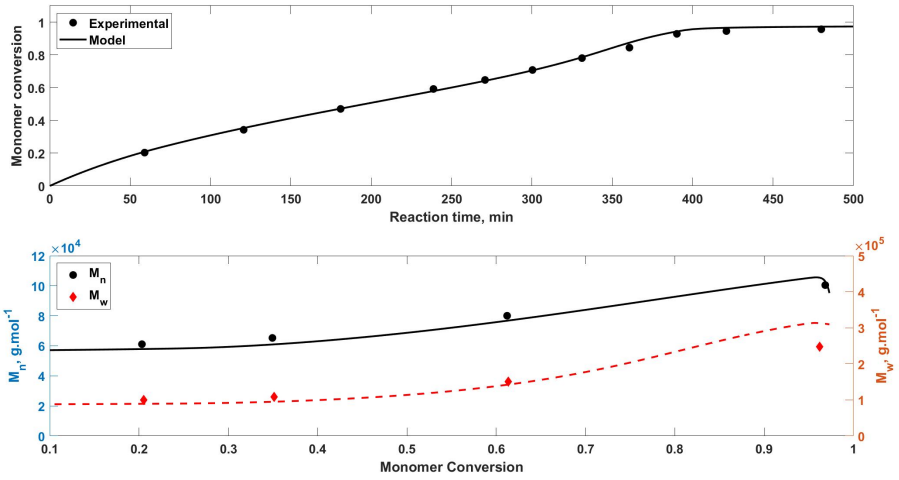

Figure 1: Comparison between model predictions and reported experimental data [53]; upper Figure: time evolution of monomer conversion; lower Figure: time evolution of number-average (left y axis, filled circles and solid curve) and weight-average (right y axis, filled diamonds and dashed curve) molecular weights. (T = 90 °C; BPO 0.01 $mol.l^{-1}$; $f_1 = 0.65$).

Similarly, another set of data that can be used as a reference point, is the one presented in the work of Kotoulas et al. [37], as it covers a wide range of temperatures and, thus, incorporates the significance of the thermal initiation mechanism. The comparison of these data, for four different reaction temperatures (i.e., from 120 °C to 150°C), with the respective predictions of the model developed in this work, are shown in Figure 2. As can be seen, the model succeeds in following with high accuracy all the monomer conversion time-histories as well as the molecular weights at the highest temperatures, but under-predicts the average molecular weights at high monomer conversions, notably for temperatures $\leq$ 130 °C. The observed disagreement may be related to the incapacity of the employed gel-effect model to accurately describe the related phenomena, as also evidenced by the

fact that this disagreement is principally located in the conversion range where diffusion-controlled phenomena become very important, marked by the characteristic s-shape of the curves at these temperatures. In fact, in the original work of Kotoulas et al. [37], a more comprehensive model has been employed for the description of the diffusion-controlled phenomena [33], instead of the one selected here [32]. In any case, the selected gel-effect model was considered to be sufficient to describe the observed behavior of the rest of the tested data.

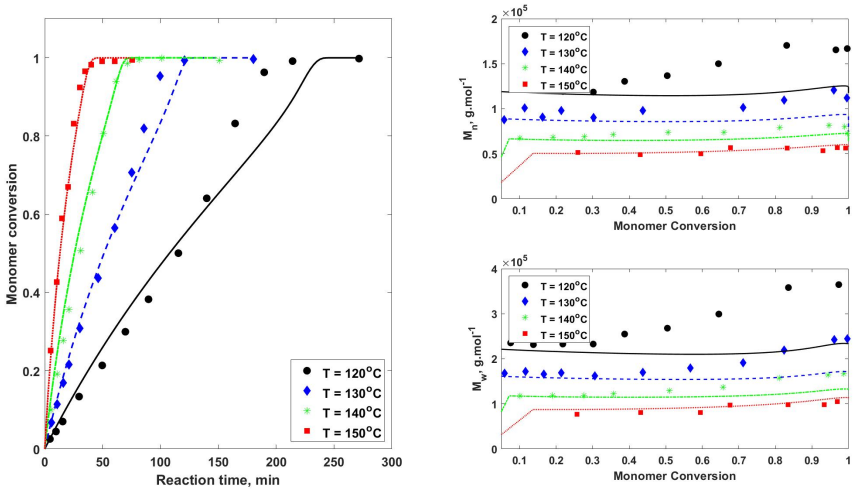

Figure 2: Comparison between model predictions and reported experimental data for different reaction temperatures [37]; left Figure: time evolution of monomer conversion; upper right Figure: evolution of number-average molecular weight with respect to the monomer conversion; lower right Figure: evolution of weight-average molecular weight with respect to the monomer conversion. (Filled circles and solid curves: T= 120 °C; filled diamonds and dashed curves: T= 130 °C; stars and dash/point curves: T= 140 °C; filled squares and point curves: T= 150 °C; DCP 4000 ppm; $f_1 = 0.65$).

The model has also been tested on solution polymerization experiments, carried out in a bench-scale reactor, as described in Section 2.2. These experiments

were realized within the framework of a study that was focused on the final average molecular weight of the produced polystyrene [26]. As such, not enough intermediate data were recorded to allow the tracking of the complete temporal evolution of the course of the polymerization. Nonetheless, the comparison with the model predictions, depicted in Figure 3, provides evidence that the model remains coherent in this solution polymerization case as well, under two different polymerization temperatures.

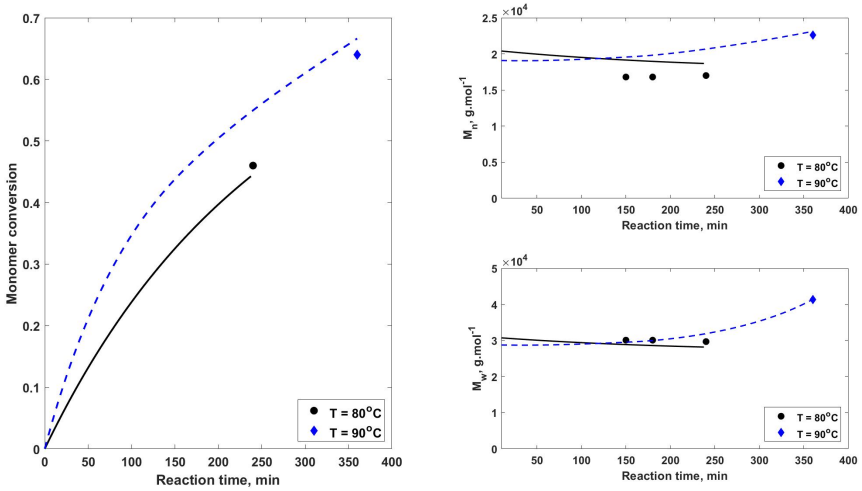

Figure 3: Comparison between model predictions and experimental data of a solution polymerization system [26]; left Figure: time evolution of monomer conversion; upper right Figure: time evolution of number-average molecular weight; lower right Figure: time evolution of weight-average molecular weight. (Filled circles and solid curves: T= 80 °C; filled diamonds and dashed curves: T= 90 °C; BPO 0.8 $\%wt$; $f_1 = 0.65$).

The last set of data of pure styrene homopolymerization, on which the model has been tested, is the DSC data set that has been produced and reported in the framework of our previous study [23]. This comparison is shown in Figure 4, where the conversion-time histories are plotted for three different reaction temperatures,

namely at 85 °C, 90 °C and 120 °C. In all three cases, the model succeeds in tracking both the initial stages of the reaction as well as the onset of the gel- and glass-effect stages that are clearly distinct on the curves of the two lowest reaction temperatures (i.e., marked by the characteristic S-shape of the curves).

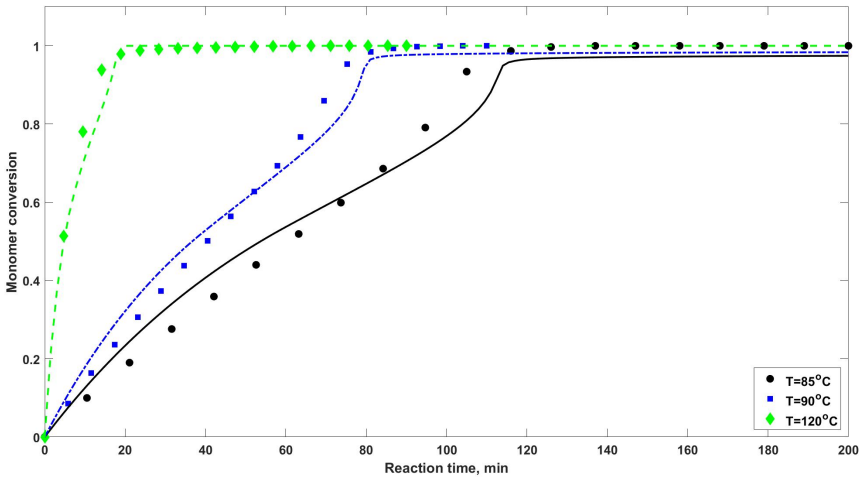

Figure 4: Comparison between model predictions and experimental DSC data of the homopolymerization system [23]. (filled circles and solid curves: T= 85 °C; filled squares and dot/dashed curves: T= 90 °C; filled diamonds and dashed curves: T= 120 °C; BPO/St 4.6 $\%wt$).

Subsequently, the model has been calibrated and tested over a range of DSC data, all produced in the framework of the previously reported experimental DSC study of Florez et al. [23], in the presence of GTR. The first comparison, shown in Figure 5, concerns the evolution of monomer conversion under different GTR contents and for a given ratio of BPO initiator to styrene. The case of a pure homopolymerization, under the same initiator content, is also included to demonstrate the effect of GTR content on the course of the polymerization. All cases are isothermal at 90 °C. The observed effects of accelerated reaction during the

first stage of the polymerization, which is particularly evident in the case of 30% GTR content, and the overall inhibition, in terms of the final monomer conversion, that is proportional to the content of GTR, are both well-captured by the model and coherent to the experimental data. This is due to the inclusion, in the adopted general kinetic scheme, of the reactions of accelerated decomposition of BPO for the production of radicals of reduced activity (Eq.(2)) and the reactions of deactivation of the radicals (Eqs.(34)-(40)), induced by carbon black [23].

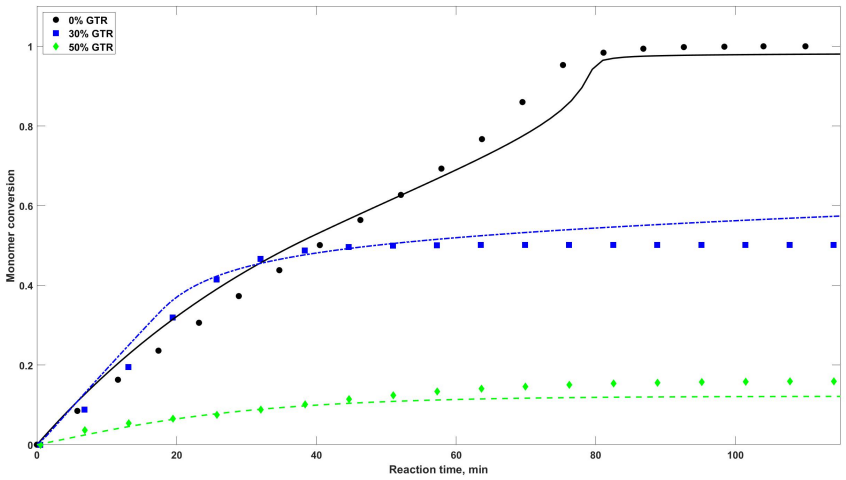

Figure 5: Effect of the GTR content on the evolution of monomer conversion, during the isothermal BPO-initiated polymerization of styrene in the presence of GTR particles [26]. (Filled circles and solid curves: pure homopolymerization; filled squares and dot/dashed curves: 30% GTR; filled diamonds and dashed curves: 50% GTR; T= 90 °C; BPO/St 4.6 $\%wt$).

In Figure 6, the evolution of styrene conversion is plotted for two different initiator contents at a given GTR content of 50%. The respective homopolymer case is also shown on the same plot, to emphasize the difference between the effect of GTR content and that of initiator content on the course of the polymerization. In

fact, it is seen that, even a very significant increase of the BPO content, from 4.6% to 9.6%, with respect to the mass of styrene, has a minor positive impact on the evolution and final value of monomer conversion, in comparison to the inhibition induced by the presence of GTR in the mixture. In all cases, the proposed model predicts these effects with very good accuracy.

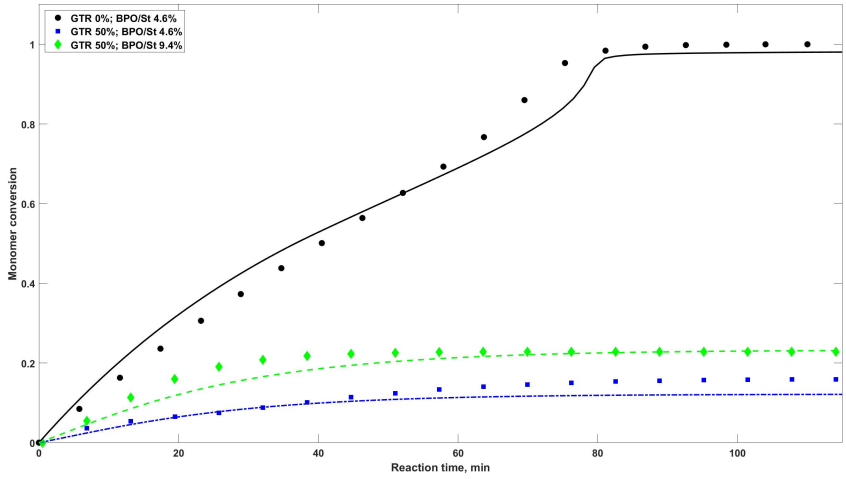

Figure 6: Effect of the initiator content on the evolution of monomer conversion, during the isothermal BPO-initiated polymerization of styrene in the presence of GTR particles [26]. (Filled circles and solid curves: BPO/St 4.6 $\%wt$ with 0% GTR; filled squares and dot/dashed curves: BPO/St 4.6 $\%wt$ with 50% GTR; filled diamonds and dashed curves: BPO/St 9.4 $\%wt$ for 50% GTR; T= 90 °C).

In an attempt to clarify the observed inhibition, the developed model was employed to generate the evolution of additional indicators with time, under the same conditions. Accordingly, the temporal trajectories of monomer conversion, BPO quantity, total radical concentration and ratio of reduced-activity primary radical generation by the decomposition of BPO are shown in Figures (7) and (8). More precisely, Figure (7) shows, on the left, the evolution of monomer

conversion for the three copolymer cases of GTR and BPO contents that have been presented previously in Figures (6) and (5), but for longer simulation times than the experimental ones. On the right, the respective evolution of the initiator content is presented for the same cases. From these plots, it becomes evident that, at high GTR content of 50%, the monomer conversion becomes quickly limited by the rapid consumption of the peroxide initiator, while at a lower GTR content of 30%, the consumption of BPO is significantly slower allowing the system to reach higher values of monomer conversion, which is limited asymptotically at ∼60%, after 800 minutes of reaction.

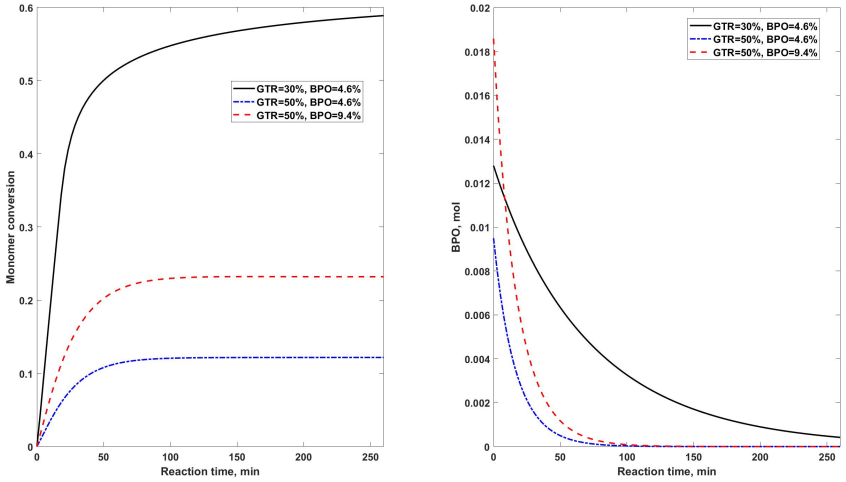

Figure 7: Evolution of monomer conversion (left Figure) and BPO content (right Figure) with reaction time, for different initial content of GTR and BPO. (Solid curves: BPO/St 4.6 %wt with 30% GTR; dashed curves: BPO/St 4.6 %wt with 50% GTR; dotted curves: BPO/St 9.4 %wt for 50% GTR; T= 90 °C).

Figure (8), shows, on the left, the temporal variation of the total radical quantity (i.e., $\lambda_0 + \nu_0 + \theta_0 + \omega_0$) for the same cases. The observed peaks, which are typical of radical polymerization systems, are completely consistent with the

monomer conversion trajectories, since the two cases corresponding to the higher GTR content display more pronounced peaks, that are narrower and are positioned earlier than the 30% GTR case. At the same time, between the two cases of 50% GTR content, the one with the higher initial BPO content displays a taller and broader peak, thus explaining the achievement of higher monomer conversion than the respective case of equal GTR content but lower BPO initial concentration. This is due to the fact that, in the case of 9.4% BPO content, the polymerization takes place at a higher rate, as evidenced by the height of the respective peak, and for longer reaction time, as evidenced by the larger width of the same peak, as well as by the respective BPO consumption curve (see right Fig.(7)). Finally, the right Figure (8) plots the evolution of the fraction of the reduced-activity primary radicals over the total amount of radicals produced by the decomposition of BPO (see Eqs.(34) and (35)). It is seen that, in both cases of 50% GTR content, the production of reduced-activity primary radicals is favored over the production of normal primary-radicals (i.e., the ratio is constantly higher than 0.5), which is consistent with the observed inhibition. At the same time, the higher BPO content slightly favors the normal-activity radicals, which is again pertinent with the higher monomer conversion achieved. On the other hand, in the 30% GTR content case, the reactions proceed with a very low percentage of reduced-activity radicals, due to the low GTR content, thus leading to higher polymerization rate and monomer conversion.

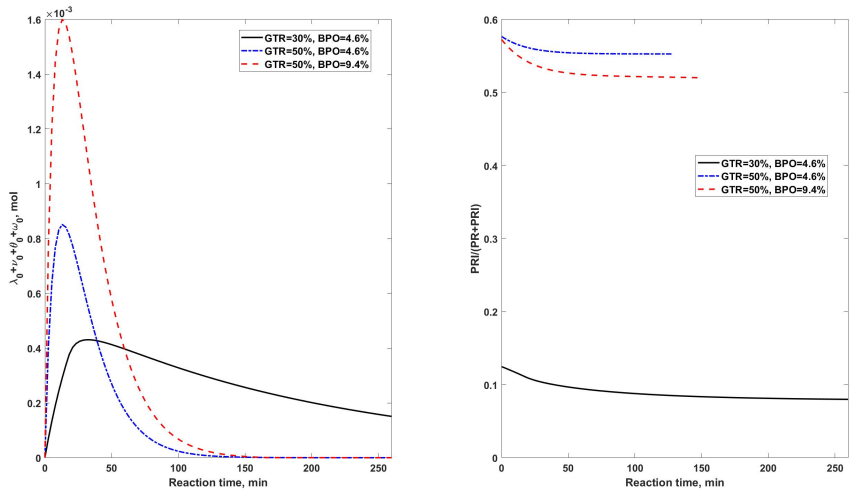

Figure 8: left Figure: Evolution of the total quantity of radicals in the system with reaction time, for different initial contents of GTR and BPO; right Figure: Temporal evolution of the fraction of reduced-activity primary radicals, produced by the decomposition of BPO, for different initial contents of GTR and BPO. (Solid curves: BPO/St 4.6 %wt with 30% GTR; dashed curves: BPO/St 4.6 %wt with 50% GTR; dotted curves: BPO/St 9.4 %wt for 50% GTR; T= 90 °C).

To further investigate the effect of GTR content on the evolution of the polymerization, a series of simulations were carried out for varying GTR content, at conditions different than the realized DSC experiments. Figure 9 shows the effect of the initial GTR content on the final values (i.e., after 120 min of reaction) of four different quantities, namely the monomer conversion, number average molecular weight, M_n, of the free and the grafted polymer and grafting efficiency. The overall trend of the final monomer conversion is pertinent to the previous observations since it gradually decreases with increasing initial GTR content, as shown in the top Figure. The same behavior is observed for M_n of the free polymer, which seems to gradually decrease in parallel to the monomer conversion, as one would

expect. At the same time, the grafting efficiency, defined as the ratio of the mass of grafted polymer over the total mass of polymer formed in the system, displays an inverse effect of gradual increase along with the increase of the initial GTR content, as shown in the bottom Figure. However, the final number average molecular weight of the formed grafted polymer seems to be unaffected by the initial GTR content, keeping a relatively constant value close to the respective value of the free polymer, as shown by the ratio of the final M_n of the grafted polymer over that of the free polymer, plotted on the right y-axis of the middle Figure. All these effects show that, as the initial amount of GTR increases, GTR-participating reactions are clearly favored in the system, leading to increased inhibition that lowers the monomer conversion and the free polymer molecular weight. At the same time, the grafting reactions are favored thus leading to the formation of more active sites on the particles of GTR and to a higher grafting efficiency. Nonetheless, although the ratio of the grafted polymer radicals over the free ones increases proportionally to the initial GTR content, their rate of polymerization remains comparable in this temperature, as a result of the respective propagation and termination rates. In this sense, free and grafted polymer chains will grow to reach comparative average chain lengths in this temperature, even though their relative population might vary significantly with the initial GTR content. Note that the conditions of the simulations presented in this figure have been selected in order to have a maximum coverage of the monomer conversion and grafting efficiency domains.

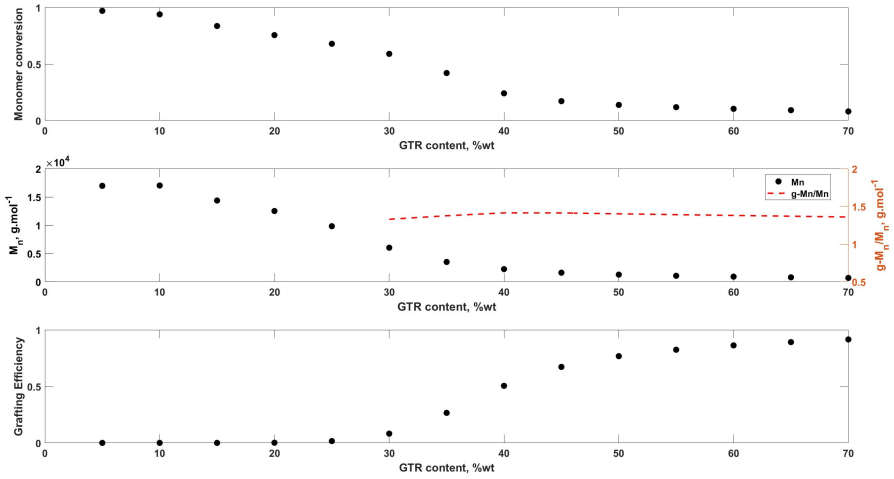

Figure 9: top Figure: Effect of the initial GTR content on final monomer conversion; middle Figure: effect of the initial GTR content on the final number average molecular weight of the free polymer (left y axis) and on the ratio of the final number average molecular weight of the grafted polymer over that of the free polymer (right y axis) ; bottom Figure: effect of the initial GTR content on the final grafting efficiency. (BPO/St 8 $\%wt$; T= 110 °C; reaction time = 120 min).

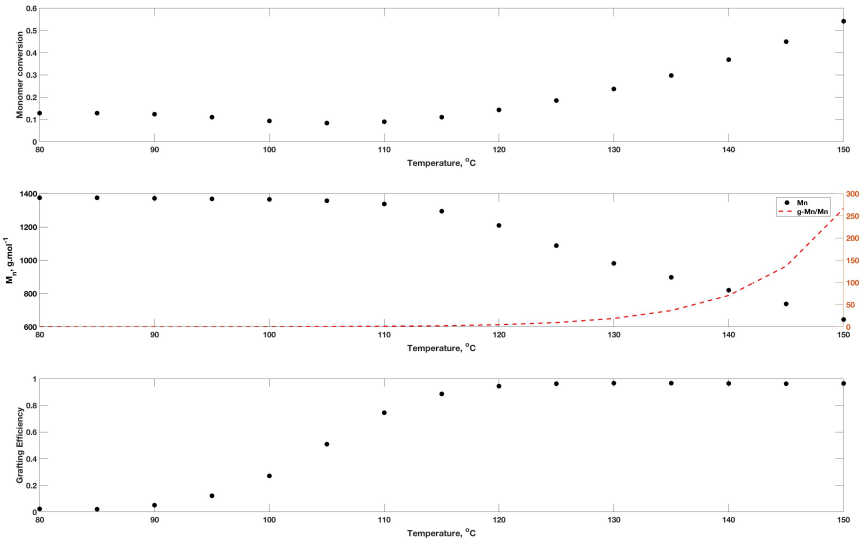

Figure 10: top Figure: Effect of the reaction temperature on the final monomer conversion; middle Figure: effect of the reaction temperature on the final number average molecular weight of the free polymer (left y axis) and on the ratio of the final number average molecular weight of the grafted polymer over that of the free polymer (right y axis); bottom Figure: effect of the reaction temperature on the final grafting efficiency . (BPO/St 5 $\%wt$ for 50% GTR; reaction time = 120 min).

In Figure 10, the variation of the same quantities is plotted with respect to the reaction temperature, for constant GTR and BPO contents (i.e., BPO/St = 5 $\%wt$ and 50% GTR). In this case, a different behavior is observed as the final (i.e., after 120 min of reaction) monomer conversion and M_n initially remain relatively constant, for temperatures lower than 100-110 °C, and then display a rather rapid increase (for monomer conversion) and decrease (for M_n), respectively. At the same time, the ratio of the final M_n of the grafted polymer over that of the free polymer displays a behavior similar to the one of monomer conversion, while the final grafting efficiency increases rapidly and reaches a value close to

100%, already at a temperature of about 120 °C. In fact, at lower temperatures, the mild increase of the rate of radical production with temperature seems to be counterbalanced by the parallel increase of the rates of radical termination and deactivation, thus limiting the monomer conversion and molecular weight at a constant level. However, as the temperature rises to values higher than 100-110 °C, the rate of creation of new radicals, both by the very rapid decomposition of the initiator and the thermal initiation mechanism, increases exponentially. Monomer propagation rates also increase. At the same time, the increase in the radical deactivation rate becomes limited by the saturation of the active sites of carbon black, thus allowing the system to reach high monomer conversion rates very rapidly, before complete consumption of the initiator. The increased number of radicals also contributes to the decrease of M_n. On the other hand, as the rate of propagation of the grafted radicals becomes significantly more important than the relative propagation rate of the free polymer (cf. Table 2), the respective average molecular weight constantly increases and so does the grafting efficiency as well. As a result, at very high temperatures and for the given GTR and BPO contents, the polymerization seems to take place principally on the grafted chains instead of the free radicals.

Figures 9 and 10 provide insights about the trends of the plotted magnitudes that are useful mainly within the perspective of a qualitative analysis. Note, however, that, as mentioned previously in section 4.5, the parametric estimation of the constants related to the grafting mechanisms, affecting the values of molecular weights and grafting efficiency in a copolymerization system, has been carried out solely on the basis of monomer conversion data (i.e., the only available data). As such, the actual values predicted by the model for the molecular weights, in the presence of GTR, should be considered with caution. In fact, the experimental measurement of the molecular weight of the free polymer and of the grafting effi-

ciency, requires an initial step of separation of the free polymer (and the remaining monomer) from the grafted polymer and the GTR particles. This step is typically carried out via solvent extraction. Then, the molecular weight can be determined by size exclusion chromatography while grafting efficiency can be calculated by gravimetric analysis [11, 26]. In this work, given that all copolymerization experiments were carried out at milligram scale during the DSC experiments, such analyses were not carried out. On the other hand, the molar mass of the grafted polymer cannot be experimentally measured by the above procedure, since the remaining mixture of GTR and grafted polymer is insoluble. In this respect, a kinetic model that can accurately predict the evolution of the polymerization under varying conditions, becomes of even greater importance in the analysis and understanding of such systems.

Finally, the predictions of the model have been tested against experimental DSC data for different reaction temperatures, as shown in Figure 11. More specifically, the evolution of monomer conversion under varying GTR and BPO contents is compared to the model predictions for two additional temperatures (i.e., besides the temperature considered in Figures 4-6, equal to 90°C), namely at 85°C and 120°C. The comparison further validates the capacity of the proposed model to capture the behavior of the system, in the presence of GTR, under different conditions and up to relatively high temperatures.

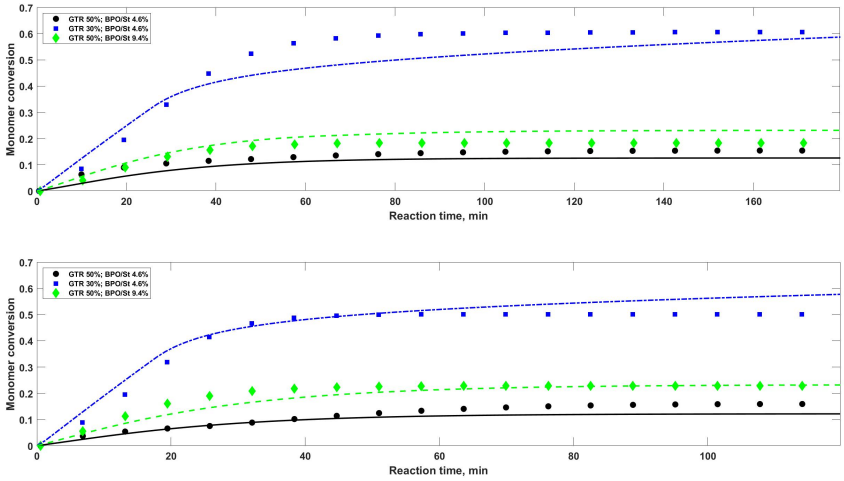

Figure 11: Evolution of monomer conversion, during the isothermal BPO-initiated polymerization of styrene in the presence of GTR particles, under different temperatures [23]. Upper Figure: T = 85 °C; lower Figure: T = 120 °C. (Filled circles and solid curves: BPO/St 4.6 %wt with 50% GTR; filled squares and dot/dashed curves: BPO/St 4.6 %wt with 30% GTR; filled diamonds and dashed curves: BPO/St 9.4 %wt with 50% GTR).

6. Conclusions

The radical polymerization of styrene in the presence of ground-tire rubber particles is a system that displays significant deviation from the respective pure styrene homopolymerization case, when a peroxide initiator is used. This deviation has been attributed to various factors, notably associated with the presence of highly-reacting additives in the formulation of GTR, such as carbon black, and with its three-dimensional network structure [23]. In this respect, a unified mathematical modeling framework, capable of predicting the behavior of the system both in the absence and in the presence of GTR and under different conditions in terms of GTR content, initiator content and reaction temperature, would be

extremely valuable to the relative research in this field.

The modeling framework proposed in this work attempted to respond to this exact need. In this sense, a general and comprehensive kinetic scheme was proposed to describe all the kinetic developments taking place in the system, on the basis of previously established models on styrene polymerization. A series of additional chemical reactions were included to account for the accelerated decomposition of peroxide radicals as well as for the grafting and the deactivation (partial and total) of the chain radicals. The diffusion-controlled phenomena were also incorporated in the model.

The proposed model was capable of describing the available polymerization data with high accuracy and of capturing the effects of the GTR and initiator content under different polymerization temperatures. Additional simulation runs were implemented to further illustrate the predicted effects of the different reaction conditions on the monomer conversion, molecular weight and grafting efficiency developments. The generality of the kinetic scheme of the proposed framework allows further development and validation in the light of new data for the polymerization system under study, and makes it suitable for implementation in other similar systems employing different monomers and/or initiators.

7. Acknowledgements

The authors acknowledge the valuable contribution of Dr. Alexandros Kiparissides, from the University College London (UCL), on the parametric estimation of the model.

Nomenclature

Greek Characters

α Reduced-mobility multiplicative coefficient

α_m Monomer thermal expansion coefficient (K^{-1})

α_p Polystyrene thermal expansion coefficient (K^{-1})

δ Average chain root mean square end-to-end distance (m)

δ_c Segmental diffusion parameter for styrene ($l.g^{-1}$)

λ_k Moment of the number-chain-length distribution of the free radicals, of order k ($mol.l^{-1}$)

μ_k Moment of the number-chain-length distribution of the free polymers, of order k ($mol.l^{-1}$)

ν_k Moment of the number-chain-length distribution of the grafted radicals, of order k ($mol.l^{-1}$)

ω_k Moment of the number-chain-length distribution of the reduced-activity grafted radicals, of order k ($mol.l^{-1}$)

σ Lennard Jones diameter (m)

θ_k Moment of the number-chain-length distribution of the reduced-activity free radicals, of order k ($mol.l^{-1}$)

ξ_k Moment of the number-chain-length distribution of the grafted polymers, of order k ($mol.l^{-1}$)

Symbols

A Adjustable parameter for the onset of the 2^{nd} stage of gel-effect

AH Diels-Alder adduct

AR 1-Phenyltetraryl radical

B Adjustable parameter for the onset of the 3^{rd} stage of gel-effect

C Adjustable parameter for the onset of the 4^{th} stage of gel-effect

CB Carbon black

D_n Polymer of chain length 'n'

DPR Deactivated primary-radical

f_1 Efficiency factor of chemical initiation

f_2 Efficiency factor of CB-induced initiation

f_{GTR} Efficiency factor of the GTR double bonds

GD_n Grafted polymer of chain length 'n'

GP_n Reduced-activity grafted radical of chain length 'n'

GPR Grafted primary-radical

GR_n Grafted radical of chain length 'n'

$GRat_c$ Critical value of mass fraction of GTR in the reacting mixture

I Initiator agent

j_c Average number of monomer units between chain entaglements (m

k kinetic rate constant (units: mol; l; min)

M Monomer, styrene

M_0 Molecular mass of styrene ($g.mol^{-1}$)

M_{DB} Initial molar concentration of double bonds of GTR ($mol.l^{-1}$)

MR Styryl radical

n_S Molar quantity of species S (mol)

P_n Reduced-activity free radical of chain length 'n'

PR Free primary radical

PRl Reduced-activity primary-radical

R_n Free radical of chain length 'n'

r_X Net formation rate of species X ($mol.min^{-1}.l^{-1}$)

V Volume of the reacting mixture (l)

GRat Mass fraction of GTR in the reacting mixture

Subscripts of the kinetic constants

-1 Diels-Alder dimerization inverse reaction

1 Diels-Alder dimerization forward reaction

2 Thermal initiation reaction from AH

A Thermal initiation reaction from AR

B Thermal initiation reaction from MR

C Trimerization reaction

d	Initiator decomposition reaction
dCB	CB-induced decomposition reaction
dea	Radical deactivation reaction
fx	Transfer reaction to species 'x'
I	Initiation reaction
p	Propagation reaction
S	Scission reaction
tc	Termination by combination reaction
td	Termination by dispropportionation reaction
tPR	Transfer reaction to primary-radicals
xG	Grafting reaction analogous to the respective free radical mechanism 'x'

References

[1] S. Ramarad, M. Khalid, C. T. Ratnam, A. L. Chuah, W. Rashmi, Waste tire rubber in polymer blends: A review on the evolution, properties and future, Progress in Materials Science 72 (2015) 100–140. doi:10.1016/j.pmatsci.2015.02.004.

[2] D. Dobrotă, G. Dobrotă, An innovative method in the regeneration of waste rubber and the sustainable development, Journal of Cleaner Production 172 (2018) 3591–3599. doi:10.1016/j.jclepro.2017.03.022.

[3] H. L. Liu, X. P. Wang, D. M. Jia, Recycling of waste rubber powder by mechano-chemical modification, Journal of Cleaner Production 245 (2020). doi:10.1016/j.jclepro.2019.118716.

[4] J. E. Mark, B. Erman, M. C. Roland, The Science and Technology of Rubber, volume 1, 4th ed., Elsevier, Oxford, 2013. doi:10.1017/CBO9781107415324.004.

[5] D. Priddy, Styrene Polymers, volume 4, 2001. doi:10.1002/0471440264.pst354.

[6] D. Tuchman, S. L. Rosen, the Mechanical Properties of Plastics Containing Cryogenically Ground Tire, Journal of Elastomers and Plastics 10 (1978) 115–128.

[7] J. Karger-Kocsis, L. Mészáros, T. Bárány, Ground tyre rubber (GTR) in thermoplastics, thermosets, and rubbers, volume 48, 2013. doi:10.1007/s10853-012-6564-2.

[8] G. R. Meira, C. V. Luciani, D. A. Estenoz, Continuous Bulk Process for the Production of High-Impact Polystyrene: Recent Developments in Mod-

eling and Control, Macromolecular Reaction Engineering 1 (2007) 25–39. doi:10.1002/mren.200600010.

[9] R. P. Burford, M. Pittolo, Rubber-crumb modified polystyrene. Part 2: Fracture toughness, Journal of Materials Science 21 (1986) 2308–2314.

[10] M. Pittolo, R. P. Burford, Rubber-crumb modified polystyrene. Part 1: Tensile properties, Journal of Materials Science 21 (1986) 1769–1774. doi:10.1007/bf01114738.

[11] S. Coiai, E. Passaglia, F. Ciardelli, D. Tirelli, F. Peruzzotti, E. Resmini, Modification of cross-linked rubber particles by free radical polymerization, Macromolecular Symposia 234 (2006) 193–202. doi:10.1002/masy.200650225.

[12] A. Brydon, G. M. Burnett, G. G. Cameron, Free-Radical Grafting of Monomers To Polydienes - I. Effect of Reaction Conditions on Grafting of Styrene To Polybutadiene., J Polym Sci Part A-1 Polym Chem 11 (1973) 3255–3269.

[13] R. Xiong, Studies in polymer composites based on carbon containing pulverized rubber materials, Doctor of philosophy in chemical engineering, Illinois Institute of Technology, 2010.

[14] E. L. Rodriguez, The effect of free radical initiators and fillers on the cure of unsaturated polyester resins, Polymer Engineering & Science 31 (1991) 1022–1028. doi:10.1002/pen.760311405.

[15] K. Fujiki, N. Tsubokawa, Y. Sone, Radical Grafting from Carbon Black. Graft Polymerization of Vinyl Monomers Initiated by Azo Groups Introduced onto Carbon Black Surface, Polymer Journal 22 (1990) 661–670.

[16] G. Kraus, T. Gruver, J., K. W. Rollmann, Polymerization by Carbon Blacks, Journal of Polymer Science XXXVI (1959) 564–565.

[17] K. Ohkita, N. Tsubokawa, E. Saitoh, M. Noda, N. Takashina, The free radical polymerization of vinyl monomers in the presence of carbon black, Carbon 13 (1975) 443–448. doi:10.1016/0008-6223(75)90017-2.

[18] K. Ohkita, N. Tsubokawa, E. Saitoh, The competitive reactions of initiator fragments and growing polymer chains against the surface of carbon black, Carbon 16 (1978) 41–45. doi:10.1016/0008-6223(78)90114-8.

[19] J. Yan, X. Miao, Q. Zhang, X. Cui, J. Li, H. Wang, One-Step Preparation of Black Polystyrene Particles via In Situ Suspension Polymerization, Polymer Engineering and Science (2011) 294–301. doi:10.1002/pen.

[20] J. Yan, W. Chunlei, Y. Gao, Z. Zheng, Z. Cheng, X. Cui, H. Wang, Experimental Investigation on the Role of PVA in Eliminating Inhibition Phenomenon of Carbon Black During the Synthesis of Polystyrene/Carbon Black Composite Particles, Polymer Engineering and Science (2012). doi:10.1002/pen.

[21] N. Tsubokawa, K. Fujiki, Y. Sone, Radical Grafting from Carbon Black. Graft Polymerization of Vinyl Monomers Initiated by Peroxyester Groups Introduced, Polymer Journal 20 (1988) 213–220.

[22] J. Ueda, H. Yamaguchi, K. Shirai, T. Yamauchi, N. Tsubokawa, Radical Polymerization of Vinyl Monomers in the Presence of Carbon Black Initiated by 2,2'-Azobisisobutyronitrile and Benzoyl Peroxide in Ionic Liquid, Journal of Applied Polymer Science 107 (2008) 3300–3305. doi:10.1002/app.27448.

[23] D. Florez, S. Hoppe, G. H. Hu, D. Meimaroglou, Radical bulk polymerization of styrene in the presence of rubber particles from recycled tires: a kinetic study using DSC, Journal of Thermal Analysis and Calorimetry (2020). doi:10.1007/s10973-020-09701-z.

[24] T. Alfrey, C. C. Price, Relative reactivities in vinyl copolymerization, Journal of Polymer Science 2 (1947) 101–106. doi:10.1002/pol.1947.120020112.

[25] M.-J. Wang, C. A. Gray, S. R. Reznek, K. Mahmud, Y. Kutsovsky, Vol. 9 Carbon Black, 2005.

[26] D. C. Florez Parra, Effects of the presence of recycled tire powders on the kinetics of the radical polymerization of styrene and the properties of the resulting materials, Ph.D. thesis, University of Lorraine, 2019.

[27] A. E. Hamielec, J. W. Hodgins, K. Tebbens, Polymer Reactors and Molecular Weight Distribution: Part II. Free Radical Polymerization in a Batch Reactor, AIChE Journal 13 (1967) 1087–1091. doi:10.1002/app.1969.070130705.

[28] J. H. Duerksen, A. E. Hamielec, J. W. Hodgins, Polymer reactors and molecular weight distribution: Part I. Free radical polymerization in a continuous stirred-tank reactor, AIChE Journal 13 (1967) 1081–1086. doi:10.1002/aic.690130609.

[29] A. W. Hui, A. E. Hamielec, Thermal polymerization of styrene at high conversions and temperatures. An experimental study, Journal of Applied Polymer Science 16 (1972) 749–769. doi:10.1002/app.1972.070160319.

[30] A. Husain, A. E. Hamielec, Thermal polymerization of styrene, Journal of Applied Polymer Science 22 (1978) 1207–1223. doi:10.1002/app.1978.070220505.

[31] F. R. Mayo, The dimerization of styrene, Journal of the American Chemical Society 90 (1968) 1289–1295.

[32] F. L. Marten, A. E. Hamielec, High-Conversion Diffusion-Controlled Polymerization of Styrene. I, Journal of Applied Polymer Science 27 (1982) 489–505.

[33] D. S. Achillas, C. Kiparissides, Development of a General Mathematical Framework for Modeling Diffusion-Controlled Free-Radical Polymerization Reactions, Macromolecules 25 (1992) 3739–3750. doi:10.1021/ma00040a021.

[34] N. Tefera, G. Weickert, K. R. Westerterp, Modeling of free radical polymerization up to high conversion. II. Development of a mathematical model, Journal of Applied Polymer Science 63 (1997) 1663–1680.

[35] J. Gao, K. D. Hungenberg, A. Penlidis, Process modelling and optimization of styrene polymerization, Macromolecular Symposia 206 (2004) 509–522. doi:10.1002/masy.200450239.

[36] M. J. Scorah, R. Dhib, A. Penlidis, Modelling of free radical polymerization of styrene and methyl methacrylate by a tetrafunctional initiator, Chemical Engineering Science 61 (2006) 4827–4859. doi:10.1016/j.ces.2006.03.018.

[37] C. Kotoulas, A. Krallis, P. Pladis, C. Kiparissides, A comprehensive kinetic model for the combined chemical and thermal polymerization of styrene up to high conversions, Macromolecular Chemistry and Physics 204 (2003) 1305–1314. doi:10.1002/macp.200390104.

[38] J. D. Woloszyn, K. B. Mcauley, Application of Parameter Selection and Estimation Techniques in a Thermal Styrene Polymerization Model, Macromolecular Reaction Engineering 5 (2011) 453–466. doi:10.1002/mren.201100021.

[39] J. D. Woloszyn, P. Hesse, K. D. Hungenberg, K. B. Mcauley, Parameter selection and estimation techniques in a styrene polymerization model, Macromolecular Reaction Engineering 7 (2013) 293–310. doi:10.1002/mren.201200074.

[40] P. Manaresi, V. Passalacqua, F. Pilati, Kinetics of graft polymerization of styrene on cis-1,4-polybutadiene, Polymer 16 (1975) 520–526. doi:10.1016/0032-3861(75)90011-7.

[41] A. Brydon, G. M. Burnett, G. G. Cameron, Free-Radical Grafting of Monomers To Polydienes - 2. Kinetics and Mechanism of Styrene Grafting To Polybutadiene., J Polym Sci Part A-1 Polym Chem 12 (1974) 1011–1021.

[42] G. G. Cameron, M. Y. Qureshi, Free Radical Grafting of Monomers To Polydienes - 3. Kinetics and Mechanism of Styrene Grafting To Polyisoprene., Journal of polymer science. Part A-1, Polymer chemistry 18 (1980) 2143–2153. doi:10.1002/pol.1980.170181102.

[43] N. J. Huang, D. C. Sundberg, Fundamental studies of grafting reactions in free radical copolymerization. I. A detailed kinetic model for solution polymerization, Journal of Polymer Science Part A: Polymer Chemistry 33 (1995) 2533–2549. doi:10.1002/pola.1995.080331502.

[44] N. J. Huang, D. C. Sundberg, Fundamental studies of grafting reactions in free radical copolymerization. IV. Grafting of styrene, acrylate, and methacrylate monomers onto vinyl-polybutadiene using benzoyl peroxide and AIBN initiators in solution polymerization., Journal of Polymer Science Part A: Polymer Chemistry 33 (1995) 2587–2603. doi:10.1002/pola.1995.080331505.

[45] N. J. Huang, D. C. Sundberg, Fundamental studies of grafting reactions in free

radical copolymerization. II. Grafting of styrene, acrylate, and methacrylate monomers onto cis-polybutadiene using AIBN initiator in solution polymerization, Journal of Polymer Science Part A: Polymer Chemistry 33 (1995) 2551–2570. doi:10.1002/pola.1995.080331503.

[46] N. J. Huang, D. C. Sundberg, Fundamental studies of grafting reactions in free radical copolymerization. III. Grafting of styrene, acrylate, and methacrylate monomers onto cis-polybutadiene using benzoyl peroxide initiator in solution polymerization, Journal of Polymer Science Part A: Polymer Chemistry 33 (1995) 2571–2586. doi:10.1002/pola.1995.080331504.

[47] D. A. Estenoz, G. R. Meira, N. Gomez, , O. H. M., Mathematical model of a continuous industrial high-impact polystyrene process, AIChE Journal 44 (1998) 427–441. doi:10.1002/aic.690440219.

[48] J. L. White, A. Sasaki, Free radical graft polymerization, Polymer - Plastics Technology and Engineering 42 (2003) 711–735. doi:10.1081/PPT-120024992.

[49] D. Elizarrarás, G. Morales, R. Díaz De León, C. Luciani, D. Estenoz, A mathematical model of the bulk copolymerization of styrene and acrylonitrile in the presence of polystyrene-block-polybutadiene, Macromolecular Theory and Simulations 17 (2008) 180–197. doi:10.1002/mats.200800004.

[50] C. Gutierrez, D. A. Estenoz, L. M. Gugliotta, J. R. Vega, G. R. Meira, Solution and Quasi-Bulk Copolymerizations of Styrene and Methyl Methacrylate in the Presence of Polybutadiene: Mathematical Model, Journal of Applied Polymer Science 117 (2010) 899–919. doi:10.1002/app.31403.

[51] K. Konstadinidis, D. S. Achilias, C. Kiparissides, Development of a unified mathematical framework for modelling molecular and structural changes in

free-radical homopolymerization reactions, Polymer 33 (1992) 5019–5031. doi:10.1016/0032-3861(92)90053-Y.

[52] G. G. Cameron, M. Y. Qureshi, Free Radical Grafting of Monomers To Polydienes - 4. Kinetics and Mechanism of Methyl Methacrylate Grafting To Polybutadiene., Journal of polymer science. Part A-1, Polymer chemistry 18 (1980) 3149–3161. doi:10.1002/pol.1980.170181102.

[53] M. A. Villalobos, A. E. Hamielec, P. E. Wood, Bulk and suspension polymerization of styrene in the presence of n-pentane. An evaluation of monofunctional and bifunctional initiation, Journal of Applied Polymer Science 50 (1993) 327–343. doi:10.1002/app.1993.070500214.

[54] J. C. Lagarias, J. A. Reeds, M. H. Wright, P. E. Wright, Convergence Properties of the Nelder-Mead Simplex Method in Low Dimensions, SIAM Journal of Optimization 9 (1998) 112–147.

[55] R. C. Zabisky, W. M. Chan, P. E. Gloor, A. E. Hamielec, A kinetic model for olefin polymerization in high-pressure tubular reactors: a review and update, Polymer 33 (1992) 2243–2262. doi:10.1016/0032-3861(92)90514-W.

Appendix A. Model Equations

Appendix A.1. Rate functions of the macromolecular species

The net formation rates of all the macromolecular species that participate in the different chemical reactions can be established, on the basis of the postulated general kinetic scheme (Eqs.(1)-(40)), as follows:

- Free polymer, D_n

$$
\begin{aligned}
r_{D_n} &= k_C \cdot [AH] \cdot [M] \cdot \delta(n-3) + (k_{fm} \cdot [M] + k_{fAH} \cdot [AH]) \cdot [R_n] \\
&+ k_s \cdot [PR] \cdot \left(\sum_{k=n+1}^{\infty} [D_k] - (n-1) \cdot [D_n] \right) + k_{tPR} \cdot [PR] \cdot [R_n] \\
&+ \frac{1}{2} k_{tc} \cdot \sum_{k=1}^{n-1} [R_k] \cdot [R_{n-k}] + k_{td} \cdot [R_n] \cdot \sum_{k=1}^{\infty} [R_k] + k_{fG} \cdot [G] \cdot [R_n] \\
&+ k_{tdG} \cdot [R_n] \cdot \sum_{k=1}^{\infty} [GR_k] + k_{dea} \cdot [CB] \cdot ([R_n] + \alpha \cdot [P_n]) \\
&+ \alpha \cdot \left(\frac{1}{2} k_{tc} \cdot \left(\alpha \cdot \sum_{k=1}^{n-1} [P_k] \cdot [P_{n-k}] + 2 \cdot \sum_{k=1}^{n-1} [R_k] \cdot [P_{n-k}] \right) \right) \\
&+ \alpha \cdot k_{td} \cdot \left(\alpha \cdot [P_n] \cdot \sum_{k=1}^{\infty} [P_k] + [R_n] \cdot \sum_{k=1}^{\infty} [P_k] + [P_n] \cdot \sum_{k=1}^{\infty} [R_k] \right) \\
&+ \alpha \cdot k_{tdG} \cdot \left(([R_n] + \alpha \cdot [P_n]) \cdot \sum_{k=1}^{\infty} [GP_k] + [P_n] \cdot \sum_{k=1}^{\infty} [GR_k] \right) \\
&+ k_{dea} \cdot [CB] \cdot ([MR] \cdot \delta(n-1) + [AR] \cdot \delta(n-2))
\end{aligned}
\tag{A.1}
$$

- Grafted radicals, GR_n

$$\begin{aligned} r_{GR_n} = &(k_pG \cdot [GPR] \cdot [M]) \cdot \delta(n-1) + k_pG \cdot [M] \cdot ([GR_{n-1}] - [GR_n]) \\ &- (k_{fmG} \cdot [M] + k_{fAHG} \cdot [AH]) \cdot [GR_n] \\ &- (k_{tcG} + k_{tdG}) \cdot [GR_n] \cdot \left(\sum_{k=1}^{\infty} [R_k] + \alpha \cdot \sum_{k=1}^{\infty} [P_k] \right) \\ &- k_{tPRG} \cdot [PR] \cdot [GR_n] - k_{deaG} \cdot [CB] \cdot [GR_n] \end{aligned} \tag{A.2}$$

- Grafted polymer, GD_n

$$\begin{aligned} r_{GD_n} = &(k_{fmG} \cdot [M] + k_{fAHG} \cdot [AH]) \cdot [GR_n] \\ &+ k_{tcG} \cdot \sum_{k=1}^{n-1} [R_k] \cdot [GR_{n-k}] + k_{tdG} \cdot [GR_n] \cdot \sum_{k=1}^{\infty} [R_k] \\ &+ k_{tPRG} \cdot [PR] \cdot [GR_n] + k_{deaG} \cdot [CB] \cdot ([GR_n] + \alpha \cdot [GP_n]) \\ &+ \alpha \cdot k_{tcG} \cdot \left(\sum_{k=1}^{n-1} [GR_k] \cdot [P_{n-k}] + \sum_{k=1}^{n-1} [R_k] \cdot [GP_{n-k}] + \alpha \cdot \sum_{k=1}^{n-1} [P_k] \cdot [GP_{n-k}] \right) \\ &+ \alpha \cdot k_{tdG} \cdot \left(\alpha \cdot [GP_n] \cdot \sum_{k=1}^{\infty} [P_k] + [GP_n] \cdot \sum_{k=1}^{\infty} [R_k] + [GR_n] \cdot \sum_{k=1}^{\infty} [P_k] \right) \end{aligned} \tag{A.3}$$

- Reduced-activity free radicals, P_n

$$\begin{aligned} r_{P_n} = &(\alpha \cdot k_I \cdot [M] \cdot [PRl]) \cdot \delta(n-1) \\ &+ \alpha \cdot k_p \cdot [M] \cdot ([P_{n-1}] - [P_n]) - \alpha^2 \cdot (k_{tc} + k_{td}) \cdot [P_n] \cdot \sum_{k=1}^{\infty} [P_k] \\ &- \alpha \cdot \left((k_{tc} + k_{td}) \cdot \sum_{k=1}^{\infty} [R_k] + (k_{tcG} + k_{tdG}) \cdot \left(\sum_{k=1}^{\infty} [GR_k] + \alpha \cdot \sum_{k=1}^{\infty} [GP_k] \right) \right) \cdot [P_n] \\ &- \alpha \cdot \ k_{dea} \cdot [P_n] \cdot [CB] \end{aligned} \tag{A.4}$$

- Reduced-activity grafted radicals, GP_n

$$r_{GP_n} = (\alpha \cdot k_{IG} \cdot [G] \cdot [PRl]) \cdot \delta(n-1) + \alpha \cdot k_{pG} \cdot [M] \cdot ([GP_{n-1}] - [GP_n]) - \alpha \cdot \left((k_{tcG} + k_{tdG}) \cdot \left(\sum_{k=1}^{\infty} [R_k] + \alpha \cdot \sum_{k=1}^{\infty} [P_k] \right) \right) \cdot [GP_n] - \alpha \cdot \ k_{deaG} \cdot [GP_n] \cdot [CB] \tag{A.5}$$

Note that the rate function for the free radicals has already been presented in section 4 (Eq.(41)).

Appendix A.2. Moment rate functions

In accordance to the definition given in Eq.(43), the moments μ_k, ν_k, ξ_k, θ_k and ω_k have been defined for the macromolecular species D_n, GR_n, GD_n, P_n and GP_n, respectively. Next, on the basis of the previously defined rate functions (Eqs.(A.1)-(A.5)) and according to the procedure followed previously for R_n (Eq.(44)), the following rate functions can be established for the leading moments of the number-chain-length distributions of the above macromolecular species:

- Moments of the free polymer, μ_k

$$\begin{aligned} r_{\mu_k} = {} & 3^k \cdot k_C \cdot [AH] \cdot [M] + (k_{fm} \cdot [M] + k_{fAH} \cdot [AH]) \cdot \lambda_k \\ & + k_s \cdot [PR] \cdot (T_1 - (\mu_{k+1} - \mu_k)) + k_{tPR} \cdot [PR] \cdot \lambda_k \\ & + \frac{1}{2} k_{tc} \cdot \sum_{r=0}^{k} \binom{k}{r} \lambda_r \cdot \lambda_{k-r} + k_{td} \cdot \lambda_k \cdot \lambda_0 \\ & + k_{fG} \cdot [G] \cdot \lambda_k + k_{tdG} \cdot \lambda_k \cdot \nu_0 + k_{dea} \cdot [CB] \cdot (\lambda_k + \alpha \cdot \theta_k) \\ & + \alpha \cdot \left(\frac{1}{2} k_{tc} \cdot \left(\alpha \cdot \sum_{r=0}^{k} \binom{k}{r} \theta_r \cdot \theta_{k-r} + 2 \cdot \sum_{r=0}^{k} \binom{k}{r} \lambda_r \cdot \theta_{k-r} \right) \right) \\ & + \alpha \cdot k_{td} \cdot (\alpha \cdot \theta_k \cdot \theta_0 + \lambda_k \cdot \theta_0 + \theta_k \cdot \lambda_0) + \alpha \cdot k_{tdG} \cdot ((\lambda_k + \alpha \cdot \theta_k) \cdot \omega_0 + \theta_k \cdot \nu_0) \\ & + k_{dea} \cdot [CB] \cdot ([MR] + 2 \cdot [AR]) \end{aligned} \tag{A.6}$$

- Moments of the grafted radicals, ν_k

$$\begin{aligned} r_{\nu_k} &= k_pG \cdot [GPR] \cdot [M] + k_pG \cdot [M] \cdot \left(\sum_{r=0}^{k} \binom{k}{r} \nu_r - \nu_k \right) - k_{tPRG} \cdot [PR] \cdot \nu_k \\ &- (k_{fmG} \cdot [M] + k_{fAHG} \cdot [AH]) \cdot \nu_k - (k_{tcG} + k_{tdG}) \cdot \nu_k \cdot (\lambda_0 + \alpha \cdot \theta_0) \\ &- k_{deaG} \cdot [CB] \cdot \nu_k \end{aligned} \tag{A.7}$$

- Moments of the grafted polymer, ξ_k

$$\begin{aligned} r_{\xi_k} &= (k_{fmG} \cdot [M] + k_{fAHG} \cdot [AH]) \cdot \nu_k + k_{tdG} \cdot \nu_k \cdot \lambda_0 \\ &+ k_{tcG} \cdot \sum_{r=0}^{k} \binom{k}{r} \lambda_r \cdot \nu_{k-r} + k_{tPRG} \cdot [PR] \cdot \nu_k \\ &+ k_{deaG} \cdot [CB] \cdot (\nu_k + \alpha \cdot \omega_k) + \alpha \cdot k_{tdG} \cdot (\alpha\omega_k \cdot \theta_0 + \omega_k \cdot \lambda_0 + \nu_k \cdot \theta_0) \\ &+ \alpha \cdot k_{tcG} \cdot \left(\sum_{r=0}^{k} \binom{k}{r} \nu_r \cdot \theta_{k-r} + \sum_{r=0}^{k} \binom{k}{r} \lambda_r \cdot \omega_{k-r} + \alpha \cdot \sum_{r=0}^{k} \binom{k}{r} \theta_r \cdot \omega_{k-r} \right) \end{aligned} \tag{A.8}$$

- Moments of the reduced-activity free radicals, θ_k

$$\begin{aligned} r_{\theta_k} &= \alpha \cdot [M] \cdot \left(k_I \cdot [PRl] + k_p \cdot \left(\sum_{r=0}^{k} \binom{k}{r} \theta_r - \theta_k \right) \right) \\ &- \alpha \cdot ((k_{tc} + k_{td}) \cdot (\alpha \cdot \theta_0 + \lambda_0) + (k_{tcG} + k_{tdG}) \cdot (\nu_0 + \alpha \cdot \omega_0)) \cdot \theta_k \\ &- \alpha \cdot \ k_{dea} \cdot \theta_k \cdot [CB] \end{aligned} \tag{A.9}$$

- Moments of the reduced-activity grafted radicals, ω_k

$$\begin{aligned} r_{\omega_k} &= \alpha \cdot \left(k_{IG} \cdot [G] \cdot [PRl] + k_{pG} \cdot [M] \cdot \left(\sum_{r=0}^{k} \binom{k}{r} \omega_r - \omega_k \right) \right) \\ &- \alpha \cdot \omega_k \cdot ((k_{tcG} + k_{tdG}) \cdot (\lambda_0 + \alpha \cdot \theta_0)) - \alpha \cdot \ k_{deaG} \cdot \omega_k \cdot [CB] \end{aligned} \tag{A.10}$$

The definitions of the terms T_1 and T_{1G} are given in Eq.(45). Note that, some terms of the above rate functions create a dependency of a moment of order k on a moment of order k+1 (i.e., the so-called moment-closure problem). To overcome this problem and *close* the mass balances of the system, the following closure technique has been adopted in this study, on the basis of an assumed log-normal distribution [55]:

$$\Phi_3 = \Phi_0 \cdot \left(\frac{\Phi_2}{\Phi_1}\right)^3 \tag{A.11}$$

where Φ_k denotes the moment of order k of any of the macromolecular species of the system. The above expression provided satisfactory mass balance closure (i.e., $\geq 99.9\%$) for all the tested systems and conditions.

Appendix A.3. Calculation of properties

The implementation of the method of moments provides a straightforward calculation of many average properties of interest of the various macromolecular species of the system. In this respect, the number- and weight-average molecular weights of the free polymer, D_n, will be directly calculated by:

$$M_n = \frac{\mu_1}{\mu_0} \cdot M_0 \quad ; \quad M_w = \frac{\mu_2}{\mu_1} \cdot M_0 \tag{A.12}$$

Accordingly, the respective properties of any of the macromolecular species, that are present in the reacting mixture, can be calculated at any instant of the polymerization.

5. Concluding Remarks and Future Perspectives

Time will eventually provide all the answers, without even needing to ask...

Euripides

5.1 General conclusions

The work presented in this report concerned the development of mathematical models for physicochemical systems, and more specifically, for problems related to the field of polymers. A major emphasis has been placed on applications in the domain of polymer reaction engineering, where the goal is to predict the properties of the produced (co)polymers as a function of the synthesis conditions and recipe. These properties of interest may refer to different scales of the system (i.e., polymeric particles or the macromolecular chains) and to various levels of detailed information, ranging from simple average properties to complex multivariate distributions or even to the detailed topological architectures of the (co)polymer chains.

Even in the case where the domain of application is strictly and explicitly defined, a plethora of different modeling techniques and approaches are presented as eventual candidates, each one with its own strengths and weaknesses. This fact can produce confusion or frustration, leading eventually to a selection that is either random or based on the researcher's previous experience. As such, it is less likely that the most-fitting modeling strategy will be employed, in terms of its efficiency or even its capacity to produce the desired level of information. In the worst case scenario, a poor selection and implementation of the modeling approach can even result in misleading or erroneous conclusions.

This work was directly confronted with this dilemma, through the demonstration of a series of case studies. Through the articulation of the different sections, an attempt was made to demonstrate the capabilities and the drawbacks of different classes of modeling approaches, as well as to illustrate some characteristic applications of interest in the domain of polymer science. Accordingly, a very large part of the report has been devoted to modeling applications on the basis of a stochastic MC algorithm. Through the different case studies that were presented, it was shown how this method is specifically suitable to problems dealing with high dimensionality, in terms of monitoring different properties of interest within a population of entities.

More specifically, the development of MC algorithms for the modeling of the detailed molecular and/or topological properties of highly branched polymers, copolymers and multi-functional biopolymers was presented via three different case studies. In addition, a comparison with an alternative deterministic modeling approach, the method of moments, which finds widespread applicability in numerous modeling studies of polymer systems, was used to demonstrate two extreme scenarios. The first one concerned an application, namely that of the copolymerization system of acrylic acid, where this alternative was proven more efficient in cases where the detailed distributed properties of the produced copolymer were not of immediate interest, as for example in the case of a routine simulation of the process to check the average molecular weight profiles. This application showed clearly that the implementation of sophisticated algorithms is not necessarily required or justified in all cases. The other scenario that was demonstrated through the other two case studies concerned the cases where such alternatives are proven less adequate or even insufficient to respond to specific objectives of the modeling study. These objectives may be related to the sought level of detail in the responses of the model, as was the case of the modeling of the topology of LDPE, or simply to the characteristics of the system that render the model equations of the moments very difficult - if not impossible - to solve, as was the case in the modeling of the polycondensation of sugars.

At a second stage, the dilemma between knowledge-based and data-driven approaches was addressed through the presentation of a case study on a process of photodegradation of water

contaminants, for which the level of available knowledge and resources was not sufficient to allow the adoption of a knowledge-based modeling strategy. In this sense, the development of two consecutive interconnected artificial neural networks allowed the association of the conditions prevailing during the process of the synthesis of the photocatalyst with its final photodegradation performance, despite the fact that these two processes are completely dissociated in experimental practice. This case study displayed a characteristic example of an application in which the decisive factors in the selection of the most adapted modeling strategy were the complexity of the process in combination with the desired objective of the study, under the constraints related to the lack of the capacity to describe in detail the prevailing phenomena of the process.

Besides addressing the subject of selection of the most suitable modeling strategy for different problem formulations, another issue addressed in this report, through the presented applications, was that of the nature and the characteristics of the systems under study. The presented modeling strategies have been tested, throughout these years, onto several systems, such as different polymerization systems for the production of synthetic (co)polymers, biodegradable polymers and biopolymers (cf. Appendix **??**). The case studies presented here were selected as the most representative ones, mainly in terms of the associated modeling complexity, that allowed a clearer demonstration of the capacity and the advantages of the adopted modeling strategies. At the same time, the respective application domains displayed increased industrial and/or environmental interest.

5.2 Perspectives for future developments

The envisaged perspectives of this work can be considered as natural extensions of the principal directions that were adopted in the presentation of this report, and of the main issues that were addressed herein. In this sense, the development of stochastic MC algorithms for the modeling of complex systems, characterized by high dimensionality, is an action that will be further pursued and developed for different systems.

In fact, the previous relative applications have clearly shown how this technique can provide an efficient tool for the modeling of structurally complex systems to a level of detail that is, for the

moment, unreachable by alternative deterministic techniques. The pioneering work on the prediction of the topological characteristics of LDPE has set a new standard for the description of similar systems, thus paving the way for a whole new spectrum of applications and allowing the ultimate bridging between synthesis conditions and end-use functionalities of the produced polymers. An example of such an application concerns the ring-opening polymerization of polylactic acid (PLA), where the structure of the synthesized polymer can be tailored on the basis of the functionality of the molecule that is used as co-initiator. An initial kinetic MC application to the system has already been developed [39] and will be further extended to include multifunctional co-initiator systems.

Another example of such an application, which is currently underway, concerns the extension of the modeling framework of the polycondensation of sugars, presented in the last section of Chapter 2, towards a topological formulation. The work presented in the aforementioned article showed how a kinetic MC algorithm could overcome the limitations imposed by classical modeling approaches of the system, where the maximum considered DP of the polysaccharides was significantly limited (i.e., DP<=6). However, as mentioned in the article, this kinetic MC framework does not allow the consideration of individual bond formation rates, depending on the relative position of the hydroxyl group (i.e., positions 1, 2, 3, 4 or 6) reacting with the carbocation at the C1 carbon atom of the reducing saccharide. This effect can present limitations when simulating saccharide syrups of variable initial compositions. A kinetic-topological MC modeling approach can overcome such limitations, since the exact structural information of every glucose unit of the different saccharides will be monitored in detail. Other examples where a topological stochastic modeling approach could present major advantages, in comparison to the existing modeling approaches, concern the systems of enzymatic hydrolysis of biomass or other similar saccharide molecules as well as biological systems containing bacterial cultures, proteins, etc.

In parallel to the above developments, a second axe that will be pursued concerns the implementation of advanced data-driven techniques, belonging to the family of machine learning methods, in the general framework of artificial intelligence (AI) applications. Some of these techniques, such as artificial neural networks, are certainly not new in the field of chemical engineering as their

implementation to similar problems dates back to the late 80's, with the first applications concerning mainly the domains of process control and fault diagnosis [40, 41]. However, the numerous recent developments, both in terms of the characteristics and functionalities of these techniques, as well as in terms of the accessible computer power, have brought about a new wave of applications with significantly improved efficiency and predictive accuracy [42]. At the same time, the panel of machine learning methods has become very large and, in contrary to other fields of research, such as computer science, robotics, and signal processing, their exploitation in the field of chemical engineering remains rather limited.

Besides the typical regression problems, as the one presented in Section 3.1, machine learning methods can be very efficiently applied on problems of classification and clustering. In a classification problem, the objective is to classify the list of responses (also known as labels) into different classes, in contrast to regression problems where a specific value is attributed to each response of the model. On the other hand, in clustering, one tries to group the inputs into different clusters, without even having any prior knowledge or access to the number or size of these clusters. Typical examples of these two categories, in chemical engineering, are problems related to dimensionality reduction (clustering), quality control (classification) and process monitoring and fault diagnosis (both) [42].

In general, machine learning techniques are broadly classified into four major categories, namely the supervised learning, non-supervised learning, semi-supervised learning, and reinforcement learning methods, depending mainly on the structure of the data set with respect to the availability of measured responses (or labeled data). In other words, in supervised learning, the algorithm is given a set of complete examples (e.g., historical data), including input and their respective labels, and it then tries to predict the labels of new input on the basis of the patterns identified within the given examples. Regression and classification problems fall within this category. In unsupervised learning, the algorithm is not given the 'right answer' and it needs to explore the data in order to find some structure that makes sense. This category includes mainly clustering techniques. Semisupervised learning techniques are an intermediate of the above two extremes,

in the sense that the data set contains both labeled and unlabeled data, the former being often significantly fewer than the latter. Finally, reinforcement learning techniques are mostly related to decision-making problems, via a learning procedure that is based on trial and error, and find widespread applicability in the domain of automation.

Besides their undeniable power and capacities, it should be noted that these techniques suffer also from several limitations, especially associated with the availability and quality of data as well as their transparency and lack of understanding. In fact, the choice of a representative data set of "good" quality and "sufficient" quantity is crucial to the performance and the reliability of the developed model. In certain areas of science, such as computer vision and natural language processing, data is often abundant, publicly available and simple to acquire [43, 44]. As such, these areas have greatly benefited of significant AI-related research over the last decades. On the contrary, in chemical engineering, data is more expensive to generate and rarely publicly shared due to confidentiality and competitiveness reasons. In addition, the uncertainty related to some types of generated data can be extremely variable, thus creating additional drawbacks in their utilization.

To overcome these limitations, machine learning methods that are specifically adapted to limited-data problems, such as kernel methods, low-variance models with feature reduction capabilities, multi-process modeling and transfer learning have been developed [45, 46, 47, 48]. Furthermore, the implementation of business analysis and improvement statistical tools, such as Six Sigma methods, which can help identifying and eliminating causes of mistakes or defects in a process by analyzing its elements of critical importance, can greatly improve the anticipated data quality when applied "upstream" of a data-driven modeling implementation. In parallel, data sharing within the scientific community, which is intensively promoted over the last years by numerous funding organizations and research institutions, is expected to reduce the aforementioned availability limitation [49].

Machine learning techniques have also become the source of skepticism with a part of the scientific community still being reluctant to their acceptance and adoption. This is mainly driven by

the lack of credibility of these techniques, commonly expressed in terms of their interpretability, explainability, transparency, accountability, bias and privacy [50, 51]. The first three characteristics are typically related to the "black-box" nature of these methods, not allowing a direct rationalization and traceability of the reasons that lead the developed models to behave the way they do in their predictions, artificial neural networks being the most typical examples. In this respect, several tools and techniques, specifically dedicated to the task of decoding and rationalizing these methods, are gaining continuous attention of the research community in an attempt to ensure the consistency of their outcomes and increase the confidence on their implementation. Examples of such tools are the wiring of more transparent models directly into the connections of a neural network, in order to increase the external control over its procedures, or the perturbation of the inputs of a network and a parallel monitoring and analysis of the subsequent deviation of its responses, in order to identify and understand its activation flow [52]. At the same time, a greater contribution from expertise and knowledge-driven approaches (e.g., in hybrid models), as well as the implementation of posterior consistency checks, can also greatly contribute in the increase of the interpretability and the control of the way these tools work.

On the other hand, the issues of bias, privacy and accountability are rather related to the data-driven character of these techniques. The recent worldwide-known scandal of the implementation of AI methods, in combination with large data sets of personal information, for the manipulation of the behavior of human target groups is a typical example of the negative side of the use of these powerful techniques and a flagrant sign of the need for a more specific framework regarding their practice and accountability. In this sense, an increased awareness and related education could also greatly contribute to avoiding misuse of these tools.

A PhD dissertation has been recently launched, in October 2020, on the study of the application of machine learning methods for the modeling of physicochemical systems (cf. Table **??** in Appendix **??**). In the framework of this work, specific emphasis will be placed on product design problems, including polymer-related problems as the ones presented in this report. The objective of this PhD will be to further develop and enrich the relevant knowledge and understanding of

these techniques, with the largest possible coverage of their spectrum. At the same time, similar interrogations of adaptability and fitness of these techniques to different types of problems will guide this study. In this sense, several applications are already envisaged, including the system of the radical polymerization of styrene in the presence of GTR, as presented in Section 4.1, as well as an application related to working fluids for power and refrigeration applications, in combination with a computer-aided molecular design approach and in collaboration with two other research groups of LRGP.

From an application viewpoint, the above perspectives for future developments will retain a constant reference point to industrial and societal challenges. The research community has shifted towards a more sustainable and circular production paradigm, where any development must meet high standards of energetic and/or material consumption efficiency and life-cycle analysis. Along these developments, the domain of polymers has become an epicenter of advancements as the plastics and micro-plastics pollution problems have rightfully emerged as high-priority societal challenges. In this respect, the undertaken study on the recycling of used tires, presented in Section 4.1 will be further pursued. In parallel, the aforementioned applications on the systems of PLA, biomass hydrolysis, polycondensation of sugars and working fluids are some of the projects that are already in progress and that will be further developed, all of them presenting specific energetic, health and/or environmental characteristics of interest.

Summarizing, the objectives for future developments will be to continue addressing the issue of selection of a suitable modeling strategy according, each time, to the specific characteristics of the problem under study. In this sense, the developed modeling tools and the associated experience will be further exploited in more demanding applications (e.g., topological MC) and, in parallel, a widening towards new modeling techniques (e.g., machine learning) will be steadily and intensively pursued. All these, through different applications that respond to the modern industrial production paradigm and to the sustainability challenges of our times.

Supplemental Reference List

[1] Luc Pronzato and Eric Walter. *Identification of parametric models from experimental data*. Springer-Verla, London, 1997.

[2] H. M. Hulburt and S. Katz. Some problems in particle technology. A statistical mechanical formulation. *Chemical Engineering Science*, 19(8), 1964.

[3] Doraiswami Ramkrishna. The Status of Population Balances. *Reviews in Chemical Engineering*, 3(1), 1985.

[4] Doraiswami Ramkrishna and Meenesh R. Singh. Population balance modeling: Current status and future prospects, 2014.

[5] Costas Kiparissides. Challenges in particulate polymerization reactor modeling and optimization: A population balance perspective. *Journal of Process Control*, 16(3), 2006.

[6] Mohsen Shiea, Antonio Buffo, Marco Vanni, and Daniele Marchisio. Numerical Methods for the Solution of Population Balance Equations Coupled with Computational Fluid Dynamics, 2020.

[7] H. Zhao, A. Maisels, T. Matsoukas, and C. Zheng. Analysis of four Monte Carlo methods for the solution of population balances in dispersed systems. *Powder Technology*, 173(1), 2007.

[8] Xi Yu, Michael J Hounslow, and K Reynolds, Gavin. Accuracy and Optimal Sampling in Monte Carlo Solution of Population Balance Equations. *AIChE Journal*, 61(8):2394–2402, 2015.

[9] Zuwei Xu, Haibo Zhao, and Chuguang Zheng. Accelerating population balance-Monte Carlo simulation for coagulation dynamics from the Markov jump model, stochastic algorithm and GPU parallel computing. *Journal of Computational Physics*, 281:844–863, 2015.

[10] Stutee Bhoi and Debasis Sarkar. Hybrid finite volume and Monte Carlo method for solving multi-dimensional population balance equations in crystallization processes. *Chemical*

Engineering Science, 217, 2020.

[11] Ashok Das and Jitendra Kumar. Population balance modeling of volume and time dependent spray fluidized bed aggregation kernel using Monte Carlo simulation results. *Applied Mathematical Modelling*, 92, 2021.

[12] H. M. Vale and T. F. McKenna. Modeling particle size distribution in emulsion polymerization reactors. *Progress in Polymer Science (Oxford)*, 30(10):1019–1048, 2005.

[13] Costas Kotoulas and Costas Kiparissides. A generalized population balance model for the prediction of particle size distribution in suspension polymerization reactors. *Chemical Engineering Science*, 61(2), 2006.

[14] Alireza Hosseini, Ala Eldin Bouaswaig, and Sebastian Engell. Comparison of classical population balance models of emulsion polymerization with experimental results and a stochastic extension. *Chemical Engineering Science*, 72, 2012.

[15] Ehsan Vafa, Mohammad Shahrokhi, and Hossein Abedini. Solution of population balance equations in emulsion polymerization using method of moments. *Chemical Engineering Communications*, 200(1), 2013.

[16] Simone Castellano, Nida Sheibat-Othman, Daniele Marchisio, Antonio Buffo, and Sophie Charton. Description of droplet coalescence and breakup in emulsions through a homogeneous population balance model. *Chemical Engineering Journal*, 354, 2018.

[17] Behnam Khadem and Nida Sheibat-Othman. Modeling of double emulsions using population balance equations. *Chemical Engineering Journal*, 366, 2019.

[18] Behnam Khadem and Nida Sheibat-Othman. Modeling droplets swelling and escape in double emulsions using population balance equations. *Chemical Engineering Journal*, 382, 2020.

[19] Sanjeev Kumar and D. Ramkrishna. On the Solution of Population Balance Equations by Discretization. *Chemical Engineering Science*, 51(8), 1996.

[20] Sanjeev Kumar and D. Ramkrishna. On the solution of population balance equations by discretization - II. A moving pivot technique. *Chemical Engineering Science*, 51(8), 1996.

[21] Sanjeev Kumar and D. Ramkrishna. On the solution of population balance equations by

discretization - I. A fixed pivot technique. *Chemical Engineering Science*, 51(8), 1996.

[22] Sanjeev Kumar and D. Ramkrishna. On the solution of population balance equations by discretization - III. Nucleation, growth and aggregation of particles. *Chemical Engineering Science*, 52(24), 1997.

[23] A. I. Roussos, A. H. Alexopoulos, and C. Kiparissides. Part III: Dynamic evolution of the particle size distribution in batch and continuous particulate processes: A Galerkin on finite elements approach. *Chemical Engineering Science*, 60(24), 2005.

[24] Laura Müller, Axel Klar, and Florian Schneider. A numerical comparison of the method of moments for the population balance equation. *Mathematics and Computers in Simulation*, 165, 2019.

[25] Samer Alzyod and Sophie Charton. A meshless Radial Basis Method (RBM) for solving the detailed population balance equation. *Chemical Engineering Science*, 228, 2020.

[26] Kaiyuan Wang, Suyuan Yu, and Wei Peng. A new method for solving population balance equations using a radial basis function network. *Aerosol Science and Technology*, 54(6), 2020.

[27] Mahmoud Lotfi. Discontinuous Galerkin Spectral Element Method for Solving Population Balance Differential Equations. *International Journal of Mathematical Models and Methods in Applied Sciences*, 14, 2020.

[28] Chinmay Das, Nathanael J. Inkson, Daniel J. Read, Mark A. Kelmanson, and Tom C. B. McLeish. Computational linear rheology of general branch-on-branch polymers. *Journal of Rheology*, 50(2), 2006.

[29] Zuowei Wang, Xue Chen, and Ronald G. Larson. Comparing tube models for predicting the linear rheology of branched polymer melts. *Journal of Rheology*, 54(2), 2010.

[30] P. Pladis, D. Meimaroglou, and C. Kiparissides. Prediction of the Viscoelastic Behavior of Low-Density Polyethylene Produced in High-Pressure Tubular Reactors. *Macromolecular Reaction Engineering*, 9(3), 2015.

[31] Th J. van der Molen. Free Radical Bulk Polymerization of Ethylene at Low Temperatures. *J*

Polym Sci, Part C, Polym Symp, (42), 1973.

[32] Ram Kumar Agarwal, Jitka Horská, Jaroslav Stejskal, Otakar Quadrat, Pavel Kratochvíl, and Pavel Hudec. Distribution of molecular weights and branching of high-density polyethylene. *Journal of Applied Polymer Science*, 28(11), 1983.

[33] Costas Kiparissides, George Verros, and John F. MacGregor. Mathematical Modeling, Optimization, and Quality Control of High-Pressure Ethylene Polymerization Reactors. *Journal of Macromolecular Science, Part C*, 33(4):437–527, 1993.

[34] Dimitrios Meimaroglou and Costas Kiparissides. A novel stochastic approach for the prediction of the exact topological characteristics and rheological properties of highly-branched polymer chains. *Macromolecules*, 43(13):5820–5832, 2010.

[35] Dimitrios Meimaroglou, Prokopis Pladis, Apostolos Baltsas, and Costas Kiparissides. Prediction of the molecular and polymer solution properties of LDPE in a high-pressure tubular reactor using a novel Monte Carlo approach. *Chemical Engineering Science*, 66(8):1685–1696, 2011.

[36] Ning Yu. *Study of the kinetics of free radical polymerization of styrene in a three dimensional network and applications for used tire recycling*. PhD thesis, University of Lorraine, 2015.

[37] Daniela Carolina Florez Parra. *Effects of the presence of recycled tire powders on the kinetics of the radical polymerization of styrene and the properties of the resulting materials*. PhD thesis, University of Lorraine, 2019.

[38] Daniela Florez, Sandrine Hoppe, Guo Hua Hu, and Dimitrios Meimaroglou. Radical bulk polymerization of styrene in the presence of rubber particles from recycled tires: a kinetic study using DSC. *Journal of Thermal Analysis and Calorimetry*, 2020.

[39] D. Meimaroglou, P. Pladis, and C. Kiparissides. Dynamic Monte Carlo Simulation of the l,l-Lactide Ring-Opening Polymerization. *Macromolecular Reaction Engineering*, 11(1), 2017.

[40] J. C. Hoskins and D. M. Himmelblau. Artificial neural network models of knowledge representation in chemical engineering. *Computers and Chemical Engineering*, 12(9-10), 1988.

[41] G. Allen Pugh. Synthetic neural networks for process control. *Computers and Industrial*

Engineering, 17(1-4), 1989.

[42] Zhiqiang Ge, Zhihuan Song, Steven X. Ding, and Biao Huang. Data Mining and Analytics in the Process Industry: The Role of Machine Learning. *IEEE Access*, 5:20590–20616, 2017.

[43] *Artificial Intelligence Colloquium: Accelerating Chemistry with AI*, 2019.

[44] Tyler Stukenbroeker and Jonathan Clausen. Chapter 6 a prediction of future states: Ai-powered chemical innovation for defense applications. In *Machine Learning in Chemistry: The Impact of Artificial Intelligence*, pages 136–168. The Royal Society of Chemistry, 2020.

[45] Linkai Luo, Yuan Yao, Furong Gao, and Chunhui Zhao. Mixed-effects Gaussian process modeling approach with application in injection molding processes, 2017.

[46] Mojtaba Haghighatlari, Jie Li, Farnaz Heidar-Zadeh, Yuchen Liu, Xingyi Guan, and Teresa Head-Gordon. Learning to Make Chemical Predictions: The Interplay of Feature Representation, Data, and Machine Learning Methods. *Chem*, 6(7):1527–1542, 2020.

[47] Hironao Yamada, Chang Liu, Stephen Wu, Yukinori Koyama, Shenghong Ju, Junichiro Shiomi, Junko Morikawa, and Ryo Yoshida. Predicting Materials Properties with Little Data Using Shotgun Transfer Learning. *ACS Central Science*, 5(10):1717–1730, 2019.

[48] Andreas C. Geiger, Ziyi Cao, Zhengtian Song, James R. W. Ulcickas, and Garth J. Simpson. Chapter 18 autonomous science: Big data tools for small data problems in chemistry. In *Machine Learning in Chemistry: The Impact of Artificial Intelligence*, pages 450–487. The Royal Society of Chemistry, 2020.

[49] Wuxin Sha, Yan Li, Shun Tang, Jie Tian, Yuming Zhao, Yaqing Guo, Weixin Zhang, Xinfang Zhang, Songfeng Lu, Yuan-Cheng Cao, and Shijie Cheng. Machine learning in polymer informatics. *InfoMat*, (August 2020):1–9, 2021.

[50] Ribana Roscher, Bastian Bohn, Marco F. Duarte, and Jochen Garcke. Explainable Machine Learning for Scientific Insights and Discoveries. *IEEE Access*, 8:42200–42216, 2020.

[51] Serge Rebouillat, Benoit Steffenino, Mirosława Lapray, and Antoine Rebouillat. New AI-IP-EI Trilogy Opens Innovation to New Dimensions; Another Chip in "the Innovation Wall", What About Emotional Intelligence (EI)? *Intelligent Information Management*, 12(04):131–

182, 2020.

[52] Paul Voosen. The AI detectives. *Science (New York, N.Y.)*, 357(6346):22–27, 2017.